2026-03

# Mathematical Modeling and Optimal Control Strategies of Peste des Petits Ruminants Dynamics in Ethiopia

Yibekal, Walle


BAHIR DAR UNIVERSITY
COLLEGE OF SCIENCE
DEPARTMENT OF MATHEMATICS

---

# Mathematical Modeling and Optimal Control Strategies of Peste des Petits Ruminants Dynamics in Ethiopia

---

by
Yibekal Walle Dilie

March 30, 2026
Bahir Dar, Ethiopia

**BAHIR DAR UNIVERSITY**
**COLLEGE OF SCIENCE**
**DEPARTMENT OF MATHEMATICS**

# Mathematical Modeling and Optimal Control Strategies of Peste des Petits Ruminants Dynamics in Ethiopia

**By**
**Yibekal Walle Dilie**

*A Dissertation Submitted in Partial Fulfilment of the Requirements for the Doctor of Philosophy*

in Mathematics

Principal advisor: Joseph Y.T. Mugisha (PhD, Professor)
Makerere University, Uganda

Co-advisor: Dawit Melese Gebru (PhD, Associate Professor)
Bahir Dar University, Bahir Dar
Co-advisor: Haileyesus Tessema (PhD, Associate Professor)
Unversity of Gondar, Gondar

March 30, 2026
Bahir Dar, Ethiopia

# Declaration of Authorship

This is to certify that the dissertation titled "Mathematical Modeling and Optimal Control Strategies of Peste des Petits Ruminants Dynamics in Ethiopia", submitted in partial fulfillment of the requirements for the degree of Doctor of Philosophy in Mathematics, Department of Mathematics, Bahir Dar University, is a record of original work carried out by me and has never been submitted to this or any other institution to get any other degree or certificates. The assistance and help I received during the course of this investigation have been duly acknowledged.

| Yibekal Walle Dilie | _____ | _____ |
|---|---|---|
| Name of the candiadte | Signature | Date |

**BAHIR DAR UNIVERSITY**
**COLLEGE OF SCIENCE**
**DEPARTMENT OF MATHEMATICS**

## Approval of Dissertation for Defense

I hereby certify that I have supervised, read, and evaluated this dissertation titled "Mathematical Modeling and Optimal Control Strategies of Peste des Petits Ruminants Dynamics in Ethiopia" by Yibekal Wall Dilie prepared under my guidance. I recommend the dissertation be submitted for oral defense.

| | | |
|---|---|---|
| Prof. Joseph Y.T. Mugisha |  | |
| Advisor's name | Signature | Date |
| Dr. Dawit Melese Gebru |  | |
| Co-Advisor's name | Signature | Date |
| Dr. Haileyesus Tessema Alemneh |  | |
| Co-Advisor's name | Signature | Date |
| Dr. Hunegnaw Dessie | | |
| Department Head | Signature | Date |

**BAHIR DAR UNIVERSITY**
**COLLEGE OF SCIENCE**
**DEPARTMENT OF MATHEMATICS**

## Approval of Dissertation for Defense Result

As members of the Board of examiners, we examined this dissertation titled "Mathematical Modeling and Optimal Control Strategies of Peste des Petits Ruminants Dynamics in Ethiopia" by Yibekal Walle Dilie. We hereby certify that the dissertation is accepted for fulfilling the requirements for the award of the degree of Doctor of Philosophy in Mathematics.

| External examiner name | Signature | Date |
|---|---|---|
| Dr Anuraj Singh, ABV-IIITM Gwalior | 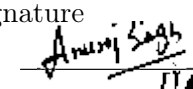 | 01/04/2026 |
| Prof. Legesse Lemecha Obsu | 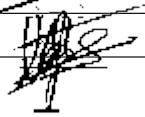 | 01/04/2026 |

| Internal examiner name | Signature | Date |
|---|---|---|
| Dr. Abdu Mohammed | | |
| | | |

| Chairperson's name | Signature | Date |
|---|---|---|
| | | |

# Dedication

This work is dedicated to my beloved mother, **Ehita Wubeneh**, whose unconditional love and prayers have been a constant source of strength and inspiration throughout my life. I also dedicate this dissertation to my dear wife, **Meaza Asfaw**, for her unwavering support, resilience in the face of challenges, and devoted care of our children during this journey. With deepest love, I further dedicate this dissertation to my sons, **Azarya Yibekal**, **Ananya Yibekal**, and **Misael Yibekal**, whose births during my PhD studies brought immense joy and inspiration into my life. Your presence gave me renewed strength and motivation to persevere. This achievement is as much yours as it is mine.

# *Acknowledgements*

I am profoundly grateful to the **Almighty God** for His unwavering grace and blessings. I also extend heartfelt thanks to the **Blessed Virgin Mary** for her loving support throughout my academic journey. My sincere appreciation goes to my supervisor, **Prof. Joseph Y.T. Mugisha**, for his insightful mentorship, guidance, and steadfast encouragement. I am equally thankful to my co-supervisor, **Dr. Dawit Melese**, whose constructive feedback and continuous support have been instrumental to the completion of this work. I also wish to acknowledge the second co-supervisor **Dr. Haileyesus Tessema** for his valuable advice throughout my doctoral studies. I am indebted to the **University of Gondar** for generously sponsoring my studies, and to **Bahir Dar University** for granting me admission and providing ongoing support. Finally, I offer my deepest gratitude to my family and friends for their unwavering encouragement and understanding during every stage of this journey.

To all who have contributed to my growth and success, I extend my heartfelt thanks.

## *Abstract*

Peste des petits ruminants (PPR) is a highly contagious viral disease that severely threatens the livelihoods and food security of smallholder farmers across Africa, the Middle East, and Asia, including Ethiopia, where persistent outbreaks undermine national eradication efforts. Despite ongoing vaccination and surveillance campaigns, the continued prevalence of PPR highlights critical gaps in understanding its transmission dynamics, particularly regarding the role of animal movement, restocking practices, and spatial spread factors that have been insufficiently modelled compared to other transboundary diseases. Furthermore, there is a notable lack of integrated cost-effectiveness analyses of intervention strategies and optimal control frameworks tailored to PPR. Addressing these gaps, this dissertation develops and analyses a suite of deterministic mathematical models, incorporating novel components such as imperfect vaccination, restocked subpopulations, spatial heterogeneity, and co-infection with Sheep and Goat Pox (SGP), using epidemiological data from the Ethiopian Ministry of Agriculture and World orgnazation of animal health (WOAH). Model parameters were carefully estimated despite data incompleteness, employing nonlinear least squares and sensitivity analyses. Through rigorous qualitative and quantitative analysis, including stability assessments, optimal control characterisation using Pontryagin's minimum principle, and comprehensive cost-effectiveness evaluations, this research reveals that combining vaccination with targeted biosecurity and movement control measures is the most effective and economically viable strategy for PPR eradication. Notably, the introduction of infected, restocked animals is shown to facilitate disease persistence, underscoring the need for integrated interventions beyond vaccination alone. The findings provide actionable recommendations for policymakers: prioritizing coordinated vaccination, movement restrictions, and enhanced biosecurity, supported by optimal allocation of limited veterinary resources. Overall, this dissertation advances the understanding of PPR dynamics and provides practical recommendations for improving disease control strategies in Ethiopia, thereby supporting national efforts toward the eradication of PPR.


**Keywords:** PPR, SGP, Mathematical Modeling, Optimal Control, Restocking, Cost-effectiveness, Vaccination, co-infection

# Contents

# List of Figures

# List of Tables

# List of Abbreviations

| | |
|---|---|
| **ACER** | Average Cost Effectiveness Ratio |
| **CaPV** | Capripox Virus |
| **CBPP** | Contagious Bovine Pleuropneumonia |
| **DFE** | Disease Free Equilibrium point |
| **EE** | Endemic Equilibrium |
| **ELISA** | Enzyme-linked immunoassay |
| **FAO** | Food and Agriculture Organization |
| **FAOSTAT** | Food and Agriculture Organization Statistical Database |
| **FMD** | Foot and Mouth Disease |
| **GDP** | Gross Domestic Product |
| **GSCE** | Global Strategy for the Control and Eradication |
| **MOA** | Ministry of Agriculture |
| **NAADSM** | North American Animal Disease Spread Model |
| **ODE** | Ordinary Differential Equation |
| **PMP** | Pontryagin's Minimum Principle |
| **PPR** | Peste des Petits Ruminanats |
| **RPV** | Rinderpest Virus |
| **RVF** | Rift Valley Fever |
| **SGP** | Sheep and Goat Pox |
| **WAHIS** | World Animal Health Information System |
| **WOAH(OIE)** | World Organisation for Animal Health(International des Epizooties) |

# List of Publications

1. Walle, Y., Mugisha, J.Y.T., Melese, D., & Tessema, H. (2025). The impact of movement and vaccination on Peste des Petits Ruminants disease spread between two different agroecological zones. Scientific African, 27, e02532. https://doi.org/10.1016/j.sciaf.2025.e02532

2. Walle, Y., Mugisha, J.Y.T., Melese, D., & Tessema, H. (2024). Modeling the Peste des Petits Ruminants (PPR) disease transmission dynamics with impacts of vaccination and restocking in small ruminant population in Amhara region, Ethiopia. Heliyon, 10(24). https://doi.org/10.1016/j.heliyon.2024.e41016

3. Walle, Y., Mugisha, J.Y.T., Melese, D., & Tessema, H. (2025). A Deterministic Optimal Control Model for PPR in Ethiopia: Assessing the Role of Infective Recruits and Cost-Effectiveness Strategies. Optimal Control, Applications and Methods. https://doi.org/10.1002/oca.70048

4. Walle, Y., Mugisha, J.Y.T., Melese, D., & Tessema, H. (2025). Model and control Co-infection of PPR with Sheep and Goat Pox (SGP). Egyptian Journal of Basic and Applied Sciences (Taylor and Francis-Under Review)

# Conference and Seminor Presentations

1. The $3^{rd}$ African Graduate Students Conference, Bahir Dar University, Bahir Dar, Ethiopia, 09-10 June 2023.
2. Seminar on "Mathematical Model and Optimal control for Peste Des Petits Ruminants (PPR) in Small Ruminant Population ", Bahir Dar University, Bahir Dar, Ethiopia, June 24, 2022.

# Chapter 1

# Introduction

This introduction establishes the scope of the research by outlining the epidemiological background of PPR, stating the core problem, defining the study's objectives, and presenting the organization of the dissertation.

## 1.1 Epidemiology of Peste des Petits Ruminants (PPR)

This section introduces the biological context of PPR, paying particular attention to the current situation in Ethiopia. The biological background of PPR is necessary to understand the reasoning behind the mathematical models formulated in this research.

### 1.1.1 Peste des Petits Ruminants (PPR)

PPR is an economically significant and highly contagious viral disease of small ruminants, caused by the *Peste des Petits Ruminants virus* (PPRV), a member of the genus *Morbillivirus*, within the family *Paramyxoviridae* (Ahaduzzaman, 2020). PPRV is closely related to other *Morbilliviruses*, including the bovine rinderpest virus, canine distemper virus, human measles virus, and morbilliviruses of marine mammals (Waret-Szkuta et al., 2008; Fournié et al., 2018; Balamurugan et al., 2014). Recognized as a notifiable transboundary disease by the World Organization for Animal Health (WOAH-OIE), PPR threatens livestock production, food security, and rural livelihoods, particularly in regions dependent on sheep and goat farming (Balamurugan et al., 2014). PPR has been prioritized for global eradication by 2030 under the joint efforts of FAO and OIE.

### 1.1.2 Clinical Signs and Transmission

PPR is clinically characterized by high fever (pyrexia), conjunctivitis, oculo-nasal discharges, necrotizing and erosive stomatitis, diarrhea, and bronchopneumonia, which can result in either death or recovery of the affected animal (Balamurugan et al., 2014). PPR is often confused with other diseases that present similar clinical signs and fever, particularly when it is newly introduced. Diseases with overlapping symptoms that require differential diagnosis include Bluetongue (BT), Contagious Ecthyma (Orf), Foot and Mouth Disease (FMD), Contagious Caprine Pleuropneumonia (CCPP), and Pasteurellosis. Additionally, mixed infections of PPR with goatpox, sheep pox, Orf, or BT may occur (Fournié et al., 2018). The disease is highly transmissible, with morbidity and mortality rates reaching nearly 100% in naive populations (Malik et al., 2011).

Transmission primarily occurs through close contact between infected animals, as the virus is shed in nasal and salivary secretions and excreted in feces. Aerosol transmission is also a significant route of infection (Fournié et al., 2018; Aetiology, 2020; Gopilo, 2005). Spread through ingestion and conjunctival penetration, by licking of bedding, feed and water troughs are also common. Furthermore, mixed populations sheep and goats, the introduction of new animals into a herd/flock, congregation of susceptible animals at grazing land and watering points and intensive type farming system facilitate the transmission of this highly contagious disease (Fournié et al., 2018). PPR virus (PPRV) is sensitive to environmental factors and does not survive long outside the host (Ahaduzzaman, 2020). There is no known carrier state for PPRV. The incubation period typically lasts 3 to 10 days, with death potentially occurring within 10 to 12 days post-infection due to severe dehydration and respiratory failure (Ahaduzzaman, 2020). Notably, infected animals can transmit the virus before the onset of clinical signs (Couacy-Hymann et al., 2007).

### 1.1.3 Diagnosis and Pathogenesis

Diagnosis of PPR is currently based on the detection of antibodies, antigens, or the viral genome. Serological detection, primarily through enzyme-linked immunosorbent assay (ELISA) kits, is widely utilized to identify antibodies in infected animals. This method is effective because animals infected with PPRV develop a sustained antibody response that persists for life (Munir, 2013). Techniques for antigen detection and viral genome detection are also employed for definitive diagnosis, providing reliable tools for early detection and confirmation of the disease.

PPRV enters the host through the epithelial lining of the oral cavity, respiratory tract, and digestive tract. The virus replicates in regional lymph nodes, leading to viremia and dissemination to other epithelial tissues, resulting in lesions and clinical signs. The severity of the disease is influenced by host factors such as age, breed, body condition, and innate immunity, as well as the virulence of the virus. Concurrent bacterial and parasitic infections may exacerbate the disease (Aetiology, 2020; Ahaduzzaman, 2020). In endemic regions, sheep and goats develop lifelong immunity following natural infection; however, naive animals maintain virus circulation, perpetuating the endemic state (Ahaduzzaman, 2020).

### 1.1.4 Geographical Distribution

PPR was first reported in 1942 in Ivory Coast, West Africa. Since then, the disease has spread far beyond its origin, with exponential dissemination over the past 15 years (WOAH, 2023; Fournié et al., 2018). PPR is now present in over 70 countries across Asia, Africa, and the Near and Middle East, having reached Europe in 2016 (Georgia). This situation has devastating consequences for families, communities, and nations.

PPR is endemic in most African and Asian countries, posing significant challenges to small ruminant production and food security. Globally, small ruminants, particularly sheep and goats, are essential for the livelihoods of over 300 million rural households. According to the Food and Agriculture Organization (FAO), the global population of small ruminants was approximately 2.5 billion in 2018, with 1.74 billion (69.6%) residing in PPR-endemic regions (Zhao et al., 2021).

Among these, 56.4% (982.3 million) are located in Asia, 43.6% (759.1 million) in Africa, and a negligible fraction (0.1%, or 1.57 million) in Europe.

The study by Zhao et al. (2021) indicates that between 2015 and 2019, a total of 12,757 PPR outbreaks were reported globally, with 75.1% (9,582 outbreaks) occurring in Asia and the Middle East, 24.8% (3,166 outbreaks) in Africa, and 0.1% (9 outbreaks) in Europe (Zhao et al., 2021). Among the affected countries, 22 reported more than 100 outbreaks during this period, including 15 in Africa and 7 in Asia. Notably, five countries-Benin (480 outbreaks), Afghanistan (824), Iran (3,710), Kuwait (761), and Turkey (402)-accounted for 48.4% of all reported outbreaks.

The global distribution of PPR outbreaks from 2015 to 2019 is illustrated in Figure 1.1. This map highlights the regional burden of the disease, with the highest concentration of outbreaks reported in Asia and Africa. The widespread distribution underscores the transboundary nature of PPR and the urgent need for coordinated global efforts to control and eradicate the disease.

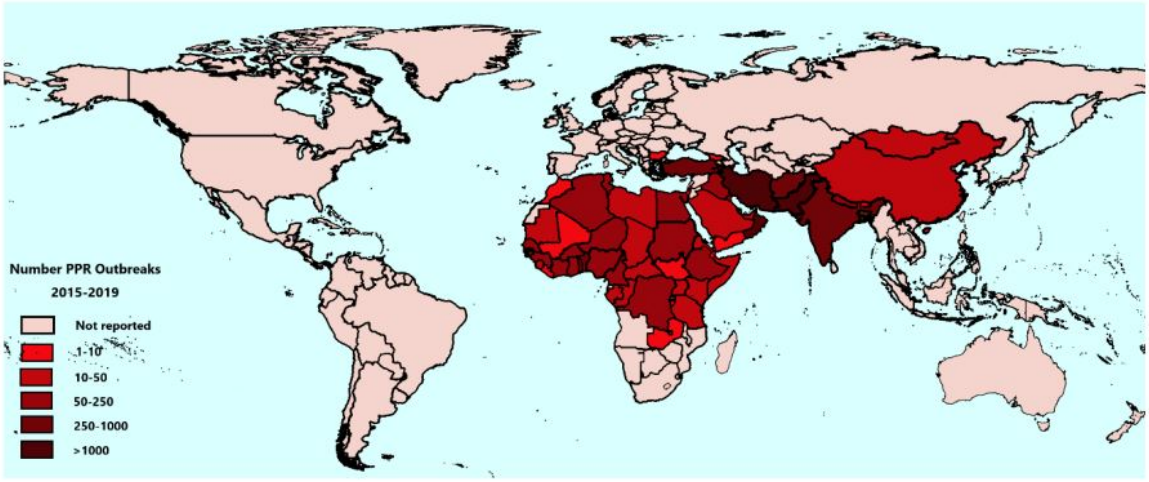


FIGURE 1.1: Global distribution of Peste des Petits Ruminants (PPR) outbreaks from 2015 to 2019. (Source: Zhao et al. (2021)).

The high number of outbreaks in endemic regions is attributed to factors such as poor vaccination coverage, extensive livestock movement, and limited access to veterinary services. The disease continues to threaten the livelihoods of smallholder farmers, disrupt livestock trade, and endanger wildlife conservation efforts (Zhao et al., 2021).

### 1.1.5 PPR Situation in Ethiopia

Ethiopia, which has the largest livestock population in Africa, is home to 40 million sheep and 51 million goats as of 2020 (Mekuriaw et al., 2021). These small ruminants play a vital role in the livelihoods of rural and pastoral communities, serving as a primary source of income, meat, milk, and other products. They are particularly important for marginalized and landless households, contributing to food security, cultural practices, and resilience against economic shocks. Additionally, small ruminants support the national economy by fulfilling domestic demand for meat consumption and generating export earnings (Fournié et al., 2018).

In Ethiopia, PPR was first suspected in 1977 in the Afar region and was later confirmed in 1991 (Fentie et al., 2018). Among PPR-endemic countries, Ethiopia ranks seventh in terms

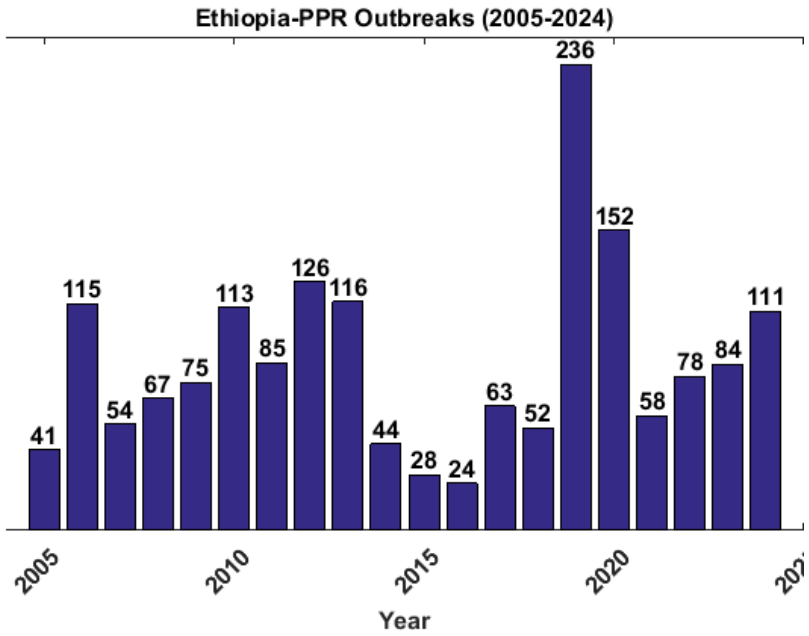


FIGURE 1.2: Outbreaks of PPR in Ethiopia (2005-2024)(Source: WOAH (2023))

of small ruminant population, further emphasizing the significance of this sector (Zhao et al., 2021). Over the past two decades, as shown in the bar graph in Figure 1.2, the OIE World Animal Health Information Database (WAHID) has recorded 1,722 outbreaks in Ethiopia, averaging 86 outbreaks per year. These outbreaks have affected 317,979 animals, resulting in 111,033 deaths, with annual averages of 15,899 cases and 5,552 deaths. A total of 34.6 million animals have been vaccinated during this period, averaging 1.73 million vaccinations annually (WOAH, 2023).

The widespread presence of Peste des Petits Ruminants (PPR) across Ethiopia is confirmed by the significant spatiotemporal heterogeneity illustrated in the 2021 outbreak data from the national Disease Outbreak and Vaccination Activity Report (DOVAR), shown in Figures 1.3A and 1.3B. A detailed analysis of these patterns is fundamental for transitioning from uniform campaigns to targeted, scheduled control programs.

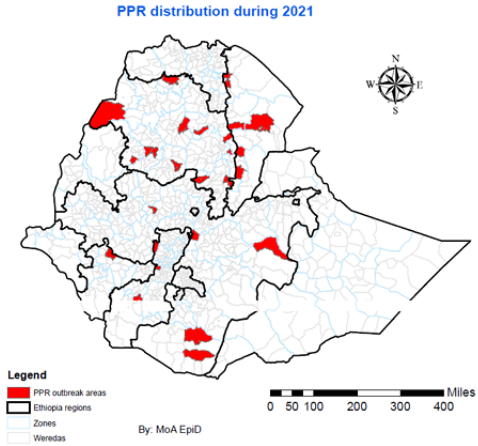


(A) Spatial pattern of 2021 PPR outbreake

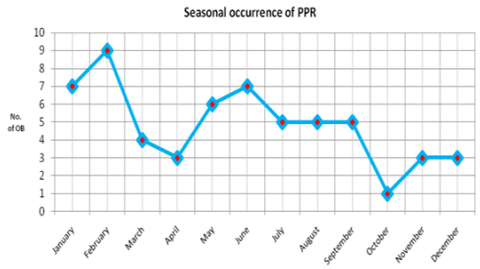


(B) Temporal pattern for 2021 PPR outbreake

FIGURE 1.3: Spatio-temporal pattern of 2021 PPR outbeake

### 1.1.6 Economic Impact

Outbreaks of PPR lead to significant economic losses, including reduced productivity, loss of animals, and increased costs for disease control and prevention. The annual global economic impact of PPR is estimated between USD 1.4 billion and USD 2.1 billion. In Ethiopia, PPR outbreaks reduce small ruminant production by 3.5%, resulting in significant economic losses, including a 0.34% contraction in GDP (USD 326 million) (Kotchofa et al., 2021). Livelihoods of rural farming households are disproportionately affected, as sheep and goats play a critical role in sustaining income and food security in developing countries (Fournié et al., 2018; Zhao et al., 2021).

A practical illustration of the economic burden of PPR is provided by an outbreak investigation in the Metema district of northwestern Ethiopia (Jemberu et al., 2022). The study reported animal-level morbidity and mortality rates of 51% and 22–25%, respectively, in small ruminants. This resulted in a mean flock-level financial loss of ETB 7,136–7,835 (USD 300–329), equivalent to approximately 14% of the average annual household income for affected farmers. With mortality accounting for over 70% of these losses, the impact on livelihoods was severe. A cost-benefit analysis from the same district suggests that vaccination, at a cost of ETB 3 per animal, is economically justified if a major outbreak occurs more than once every 13 years, a threshold that does not include the added value of herd immunity. While this case is specific to Metema, it exemplifies the profound economic burden that PPR outbreaks impose on smallholder producers, a reality faced by numerous districts across various regions of Ethiopia.

### 1.1.7 Control and Prevention

Small ruminants have a huge importance on livelihoods of population in many regions of the world. The benefits and profits accrued from controlling the disease may result in improved productivity, food security, income generation and social empowerment.

❶ **Vaccination:** Vaccines currently available for the control of PPR are live attenuated vaccines. They confer strong protection of the host against all strains of the disease following proper administration, with no side effect whatever the physiological status of the host (in particular no abortion).

Live-attenuated vaccines provide strong immunity, but maintaining the cold chain is challenging in tropical and subtropical countries (Sen et al., 2010). Sheep and goats vaccinated with an attenuated strain of PPR or that recover from PPR develop an active life-long immunity against the disease (Jilo, 2016). Mass vaccination campaigns are the cornerstone of PPR control and eradication efforts, but achieving high coverage is difficult due to logistical and economic constraints (Jones et al., 2016). Suboptimal vaccination coverage may allow virus persistence, necessitating new strategies for eradication.

❷ **Treatment:** Peste des petits ruminants (PPR) is a viral disease for which there is no specific cure. Nevertheless, supportive care and preventative measures are essential for effectively managing and controlling outbreaks (Balamurugan et al., 2014). Treatment primarily aims to alleviate symptoms and prevent secondary infections (WOAH, 2020).

Supportive care is crucial for infected animals and includes maintaining hydration, providing nutritional support, and managing secondary bacterial infections with appropriate antibiotics (WOAH, 2020; Fentie et al., 2018). Early detection and intervention can significantly enhance recovery rates among affected animals. However, the emphasis should remain on preventive strategies, as treatment options are limited and often ineffective once the disease progresses. The management of clinical cases of PPR, particularly during outbreaks in sheep and goats, is critical to minimizing economic losses for farmers (Wosu, 1989).

❸ **Bioseccurity Measures:** To control the spread of peste des petits ruminants (PPR), implementing robust biosecurity measures is essential. These measures include maintaining strict animal movement controls to prevent the introduction of infected animals into disease-free areas, conducting regular health checks and vaccinations for herds, and ensuring proper sanitation practices in livestock facilities. Furthermore, farmers should establish quarantine protocols for newly introduced animals and regularly disinfect equipment, vehicles, and clothing that may come into contact with infected livestock (WOAH, 2020; FAO, 2015; Ahaduzzaman, 2020). Enhancing community awareness about the disease and encouraging reporting of suspicious cases can also significantly mitigate risks associated with PPR outbreaks.

Despite these established control and prevention measures, the efficacy of the cornerstone strategy-mass vaccination as outlined in the Global Strategy for the Control and Eradication of PPR (GSCE)-is compromised by critical implementation gaps. Specifically, the reliance on achieving 70–80% coverage for herd immunity is frequently undermined by operational weaknesses such as non-risk-based campaign delivery, cold-chain failures, high animal mobility, and poor integration with complementary surveillance and biosecurity protocols. These systemic shortcomings reveal significant limitations in the current approach, leaving persistent vulnerabilities that hinder sustainable PPR control and the progression toward eradication as envisioned by the GSCE.

### 1.1.8 Risk Factors

Basic risk factors for the spread of peste des petits ruminants (PPR) include animal movement practices, such as transhumance and trade, which facilitate virus transmission between herds. In Africa, livestock movements are primarily driven by the need to access essential resources like grazing and water, leading animals to travel significant distances daily. This mixing of herds increases the risk of pathogen spread and disease emergence (Fèvre et al., 2006).

Restocking practices can introduce infected animals into disease-free areas, exacerbating outbreaks, particularly in regions with extensive production systems. Transboundary livestock movements further complicate control efforts (Zhao et al., 2021). In Ethiopia, for instance, the pastoral areas of Afar, Somali, and Oromia are known for significant livestock movement toward central highlands, where major markets and export facilities are located. Seasonal cross-border migrations in search of pasture and water also pose challenges to disease control (Fournié et al., 2018; Abraham et al., 1994).

Additionally, improper vaccine administration such as inadequate coverage and failure to maintain cold chain logistics contributes to increased susceptibility. Regions with high livestock density and poor biosecurity measures are particularly vulnerable. Other risk factors include insufficient veterinary infrastructure and inadequate surveillance systems. Environmental stressors, like drought, can weaken animal immunity, further increasing susceptibility to infection (FAO, 2015; Njeumi et al., 2015).

## 1.2 Statement of the Problem

Peste des petits ruminants (PPR) remains a significant transboundary animal disease in Ethiopia, with substantial morbidity, mortality, and economic losses among small ruminants. As detailed in the sections "PPR Situation in Ethiopia" and "Economic Impact," the national burden is quantitatively documented (outbreaks, cases, deaths, vaccinations) and economically devastating at both household and macroeconomic levels. Despite ongoing global and regional initiatives (FAO/WOAH)-including mass vaccination and surveillance-PPR continues to spread, undermining smallholder livelihoods and straining veterinary systems.

In Ethiopia, where the burden of PPR is particularly high, current control strategies face challenges arising from diverse risk factors, logistical constraints, variable coverage, and limited resources. While several epidemiological and statistical studies have explored PPR prevalence and distribution, there remains a lack of comprehensive, Ethiopia-focused mathematical modeling that rigorously integrates mobility- and geography-driven heterogeneity, evaluates the cost-effectiveness of realistic control portfolios, and accounts for reporting and operational constraints. In contrast to other transboundary diseases such as foot-and-mouth disease (FMD), the dynamics and control of PPR in Ethiopia are still insufficiently investigated from a systems and modeling perspective.

Mathematical modeling is invaluable for understanding infectious disease dynamics, simplifying experimental procedures, and supporting evidence-based policy. However, for PPR in Ethiopia, critical gaps remain, and they are challenging for analytical reasons:

- Integration of key risk factors (restocking, animal movement/transhumance and trade, spatial heterogeneity, highland–lowland interfaces) into dynamic, spatially explicit transmission models is limited.
- Comparative assessment of current control strategies (notably vaccination), including cost-effectiveness and sustainability, remains insufficient.
- There is a lack of studies employing optimal control under operational constraints to guide resource allocation and scheduling. Constrained optimal control can translate model insights into implementable, risk-based vaccination and surveillance plans.
- Co-dynamics with other small ruminant diseases (e.g., sheep and goat pox, SGP) and the potential for combined vaccination are not evaluated. Developing a joint PPR–SGP model could quantify epidemiologic interactions and assess whether integrated vaccination reduces burden and delivery costs compared to disease-specific campaigns.

Addressing these gaps requires grounding models in available quantitative evidence (WAHIS, DOVAR, outbreak investigations, vaccination records) while acknowledging data limitations (underreporting, delayed detection, variable coverage). Therefore, this study aims to systematically investigate the transmission dynamics of PPR in Ethiopia using a suite of mathematical models that incorporate risk factors and geographic targeting (pastoral areas and highland–lowland interfaces), evaluate current and integrated control strategies (including combined PPR–SGP vaccination) with cost-effectiveness analysis, and apply optimal control approaches under real-world constraints. By providing a rigorous, data-informed framework, this research seeks to support more effective, targeted, and economically efficient decision-making for PPR control and eradication at the national level.

### 1.2.1 General Objective

The general objective of this dissertation is to develop and analyze deterministic mathematical models that describe the transmission dynamics of peste des petits ruminants (PPR) in small ruminants and to evaluate the effectiveness of various intervention and control strategies in Ethiopia.

### 1.2.2 Specific Objectives

The specific objectives of the study are to:

❶ Construct mathematical models that incorporate vaccination and restocking to assess their impacts on the spread of PPR in small ruminant populations in Amhara region.

❷ Investigate the effects of animal movement and vaccination on PPR transmission dynamics across agroecological zones.

❸ Develop optimal control strategies for PPR management that emphasize cost-effectiveness and account for infective recruits in the population.

❹ Formulate a mathematical model to examine the transmission and control of PPR co-infection with Sheep and Goat Pox (SGP) under relevant intervention measures.

## 1.3 Significance of the Study

Peste des petits ruminants (PPR) poses a substantial threat to the livelihoods, food security, and socio-economic stability of millions of smallholder farmers and pastoralists, particularly in regions where outbreaks can lead to catastrophic losses. The global economic burden of PPR is estimated to be between US$1.4 billion and US$2.1 billion annually. In addition to direct losses of livestock, the disease exacerbates poverty, food insecurity, and migration, and can heighten social and economic instability.

This study is significant for the following reasons:

❍ It provides a rigorous mathematical framework to better understand the transmission dynamics of PPR, addressing key factors such as animal movement, restocking, vaccination, and co-infection with other diseases.

- The findings will inform veterinary health services and stakeholders in optimizing intervention strategies, enabling more cost-effective allocation of limited resources for PPR control and eradication.
- By evaluating the effectiveness of various control measures, the study offers evidence-based guidance for policy makers to develop and implement targeted public and animal health policies.
- The results contribute to the national and regional efforts to control and eradicate PPR, supporting the broader objectives of international organizations such as the OIE and FAO.
- The study advances methodological approaches in infectious disease modeling, providing a foundation for future research on PPR and other emerging diseases affecting small ruminants.
- Insights from this research can be used to design educational programs, workshops, and training initiatives aimed at improving disease awareness and management practices among farmers, veterinarians, and public health officials.

## 1.4 Organization of the Dissertation

This dissertation is structured as follows: Chapter 2 presents a comprehensive review of the literature regarding statistical studies and epidemiological models related to PPR, as well as mathematical models that incorporate optimal control strategies for infectious diseases similar to PPR. Chapter 3 introduces and analyzes a mathematical model describing the transmission dynamics of PPR, with particular emphasis on the roles of vaccination and restocking in small ruminant populations within the Amhara regional state of Ethiopia. In Chapter 4, optimal control approaches for managing PPR in the presence of infective recruits are developed and assessed, including a cost-effectiveness analysis to facilitate informed resource allocation. Chapter 5 examines the influence of animal movement and vaccination on the spatial spread of PPR across distinct agroecological zones, shedding light on regional disease dynamics. Chapter 6 extends the modeling framework to address deterministic optimal control in the context of co-infection with Sheep and Goat Pox (SGP), exploring integrated intervention strategies. Finally, Chapter 7 presents a synthesis of the principal findings, discusses their broader implications, and offers recommendations for future research directions in the control and eradication of PPR.

# Chapter 2

# Literature Review

The focus of this chapter is a critical review of the literature on mathematical modeling of infectious diseases, with emphasis on models applied to animal diseases and on statistical and mathematical studies of PPR. Mathematical models ranging from simple deterministic compartmental systems (e.g., SIR, SEIR) to stochastic, spatial, network, and agent-based frameworks are essential tools for describing transmission mechanisms, estimating key quantities such as transmission rates and reproduction numbers, and evaluating the likely impact and cost-effectiveness of control measures when experimental or large-scale trials are impractical. Originating with Bernoulli (Bernoulli, 1766) and formalized by Kermack–McKendrick (Kermack et al., 1927), these models have evolved to incorporate host demographics, latent periods, waning immunity, vectors, heterogeneous contact structures, and multispecies (One Health) interactions relevant to zoonoses.

In veterinary epidemiology, models have informed control policies for major livestock diseases (e.g., rinderpest (Mariner et al., 2005), FMD (Sseguya et al., 2022), RVF (Chamchod et al., 2014), CBPP (Aligaz et al., 2019), capripox (Chamchod, 2018)), and contemporary approaches increasingly combine optimal control theory, economic assessment, spatial heterogeneity, and agent-based simulation to design targeted, cost-effective interventions. Given PPR's high contagion, socio-economic importance in developing countries, and the presence of heterogenous production systems and animal movement patterns, integrating these modeling principles is crucial for robust inference and policy guidance. This chapter synthesizes statistical evidence and model-based studies relevant to PPR and related livestock diseases, highlighting gaps particularly the relative scarcity of optimal control and cost-effectiveness modeling for PPR and thereby motivating the development of new, targeted mathematical models in subsequent chapters.

## 2.1 Statistical Studies on PPR Disease

Several statistical studies have provided important insights into the epidemiology, risk factors, and control of PPR:

Balamurugan et al. (2014) presented a comprehensive review of the diagnosis and control of peste des petits ruminants (PPR), emphasizing recent advances in diagnostic techniques and vaccination strategies, as well as their economic implications. The authors underscored the necessity of robust diagnostic methods, timely vaccination, and effective outbreak management to mitigate economic losses among smallholder farmers. Furthermore, they highlighted the importance of quantifying economic impacts to guide research priorities and inform control programs.

Notably, the review recommended future analytical and epidemiological studies to better support evidence-based policy decisions for PPR control.

Wieland et al. (2020) presented an integrated framework for understanding the epidemiology and socio-economic impact of PPR through four key research components: assessing epidemiological patterns and socio-economic effects with attention to gender disparities; modeling control strategies to evaluate their effectiveness; developing gender-responsive vaccine delivery and diagnostic approaches to enhance vaccine accessibility; and building capacity and surveillance systems to strengthen the enabling environment for disease control.

Waret-Szkuta et al. (2008) provided a detailed analysis of a national serological survey conducted in Ethiopia in 1999, which remained one of the largest PPR surveys in Africa. The study analyzed 13,651 serum samples from seven of eleven regions using competitive enzyme-linked immunosorbent assay (cELISA), explored the spatial distribution of PPR, and identified risk factors for seropositivity. By calculating intragroup correlation coefficients for 43 administrative units (wereda), the authors revealed substantial heterogeneity in seroprevalence both between regions and within wereda, with prevalence estimates ranging from 0% to 52.5%. The practical implications of these findings were discussed with respect to PPR-endemic areas.

Fentie et al. (2018) conducted a sero-epidemiological investigation of PPR in small ruminants in the Amhara region of Ethiopia, employing both cross-sectional and retrospective study designs to estimate seroprevalence, identify risk factors, and map disease distribution. The study found that host and environmental factors-including species, sex, agro-ecology, and study location-were significantly associated with PPR seropositivity, and the data confirmed the widespread presence of the disease. The authors recommended implementing regular surveillance and vaccination programs as essential control measures.

Zhao et al. (2021) reported on global progress towards PPR eradication through vaccination, utilizing data from FAOSTAT, OIE's World Animal Health Information System, regional roadmap meetings, and country-level PPR Monitoring and Assessment Tool (PMAT) responses. Between 2015 and 2019, 12,757 PPR outbreaks were reported, predominantly in Asia and Africa. The number of outbreaks declined markedly following intensified vaccination campaigns, with 1,218 outbreaks in 2019 compared to 3,688 in 2015. Nevertheless, the authors emphasized the need for scientifically informed vaccination strategies, cross-border coordination, and enhanced surveillance and post-vaccination sero-monitoring to achieve effective control.

Collectively, these studies have advanced understanding of PPR epidemiology and control. However, most have not incorporated cost-effectiveness analyses, indicating an important area for future research.

## 2.2 Models with Optimal Control in Infectious Disease

In this section, we review mathematical models with optimal control applied to human, animal, and zoonotic infectious diseases that exhibit epidemiological similarities to Peste des Petits Ruminants (PPR). These diseases, such as measles, brucellosis, foot-and-mouth disease (FMD), rinderpest, Rift Valley fever (RVF), contagious bovine pleuropneumonia (CBPP), and capripoxvirus,

share key characteristics with PPR in terms of host-pathogen interactions, transmission dynamics, and control strategies. The studies summarized below provide important insights and methodological frameworks relevant to PPR modeling and control.

Rahmayani et al. (2021) developed a deterministic SEIR-V model to analyze measles transmission incorporating first and second dose vaccination, as well as treatment interventions. Utilizing incidence data from Jakarta, they estimated the basic reproduction number $\mathcal{R}_0 = 2.22$ and established the global stability of the disease-free equilibrium when $\mathcal{R}_0 < 1$. Optimal control analysis demonstrated that the combined implementation of first-dose vaccination $(u_1, u_2)$ and treatment $(u_4)$ most effectively minimized infection levels, reducing cases by $3.8 \times 10^5$ over a 60-month period. Cost-effectiveness analysis identified this combined strategy as having the lowest average cost-effectiveness ratio (ACER), making it the optimal intervention for measles control in Indonesia.

Nyerere et al. (2020b) investigated brucellosis, a zoonotic disease of significant public health and economic concern, through the development of a deterministic compartmental model featuring four control measures: (1) livestock vaccination, (2) gradual culling of seropositive animals, (3) environmental hygiene and sanitation, and (4) personal protection for humans. The primary objective was to minimize both brucellosis transmission and the costs associated with these interventions. By employing Pontryagin's maximum principle and conducting a cost-effectiveness analysis, the study demonstrated the positive impact of these strategies on brucellosis mitigation.

Sseguya et al. (2022) formulated a deterministic compartmental model to evaluate FMD control strategies across neighboring districts, incorporating both vaccination and movement restrictions. The study derived district-specific reproduction numbers ($\mathcal{R}_0$) and proved global stability of the disease-free equilibrium for $\mathcal{R}_0 < 1$. Optimal control analysis indicated that combined vaccination and movement restrictions were most effective in minimizing outbreaks; however, incremental cost-effectiveness analysis (ICER) identified vaccination alone as the optimal strategy, reducing implementation costs by 49.9% compared to movement restrictions alone. Numerical simulations, calibrated with 2015–2016 Ugandan outbreak data, underscored the limited efficacy of movement restrictions in the face of high cross-district transmission rates.

Mariner et al. (2005) developed a stochastic SEIR model to study the transmission dynamics of lineage-1 and lineage-2 rinderpest viruses in East African pastoral systems, integrating empirical data and participatory epidemiological information. The estimated basic reproduction number $\mathcal{R}_0$ was 4.4 for lineage-1 and 1.2–1.9 for lineage-2, with corresponding herd immunity thresholds of approximately 77% and 50%. The findings showed that small communities could sustain lineage-2 transmission over extended periods, highlighting the risk of eradication failure due to vaccination gaps. The study emphasized the necessity of epidemiologically targeted, high-coverage vaccination strategies for successful rinderpest eradication.

Chamchod et al. (2014) presented a deterministic compartmental model for Rift Valley fever (RVF) transmission, a zoonotic disease affecting various domestic ruminants. The model incorporated both host and vector populations, stratifying ruminants into susceptible $(S)$, infectious $(I)$, and recovered $(R)$ compartments, while categorizing female mosquitoes as uninfected $(U)$

or infectious ($V$). Applying optimal control theory and logistic growth for the ruminant population, the authors demonstrated through numerical simulations that immediate vaccination substantially reduces outbreak incidence and preserves livestock viability. Furthermore, the study provided valuable insights into the impact of seasonal transmission patterns on RVF control.

Aligaz et al. (2019) developed a mathematical model for the transmission dynamics of Contagious Bovine Pleuropneumonia (CBPP), considering both antibiotic treatment and vaccination. CBPP, caused by *Mycoplasma mycoides* subspecies *mycoides*, significantly impacts cattle and buffalo populations. The model comprised susceptible, vaccinated, exposed, infectious, persistently infected, and recovered compartments. The authors derived the control reproduction number $\mathcal{R}_c$ and proved that for $\mathcal{R}_c < 1$, the disease-free equilibrium is globally asymptotically stable, ensuring CBPP elimination. Conversely, for $\mathcal{R}_c > 1$, the endemic equilibrium is globally asymptotically stable, allowing the disease to persist. The analysis confirmed that appropriate application of intervention strategies can control the disease ($\mathcal{R}_c < 1$).

Chamchod (2018) constructed a mathematical model to capture the transmission dynamics of capripoxvirus (CaPV) among livestock, accounting for both direct and indirect transmission pathways. The model assessed multiple vaccination strategies and identified key determinants of outbreak severity and prevalence, including the vector-to-livestock ratio, infection probability, vaccination rates, waning immunity, and the timing of virus introduction. The optimal approach was to vaccinate newborns at maximum capacity throughout the control period, while moderately increasing vaccination rates among susceptible animals following an outbreak. Although designed for sheeppox and goatpox, the model is adaptable to other pox-like diseases, such as lumpy skin disease.

While additional literature exists on infectious disease models with optimal control, the studies highlighted above are particularly relevant due to their focus on diseases sharing epidemiological and control features with PPR. These models provide essential frameworks for the effective design, implementation, and analysis of control and prevention strategies for PPR and similar infectious diseases.

## 2.3 Mathematical Models of PPR

This section presents a review of mathematical modeling studies pertaining to Peste des Petits Ruminants (PPR). Although numerous statistical analyses of PPR have been conducted, there remains a notable paucity of mathematical modeling studies on PPR, especially when compared to similar transboundary animal diseases such as foot-and-mouth disease (FMD) and brucellosis. The existing body of work in this field is relatively limited, yet provides valuable insights into the transmission dynamics and control strategies for PPR. The principal mathematical modeling studies to date on PPR are summarized as follows:

Fathelrahman et al. (2021) conducted a comprehensive epidemiological and economic assessment of PPR eradication strategies in the United Arab Emirates using an adapted North American Animal Disease Spread Model (NAADSM). The study employed a seven-compartment disease progression framework comprising susceptible, latent, sub-clinically infectious, clinically

infectious, naturally immune, vaccine-immune, and disease-induced mortality states. Three distinct intervention scenarios were systematically evaluated: Scenario A examined the epidemiological consequences of mass vaccination cessation in conjunction with moderate movement restrictions; Scenario B assessed the combined effects of mass vaccination and stamping out protocols; and Scenario C investigated the impact of intensive ring vaccination coupled with strict movement control and stamping out. The findings indicated that Scenario C produced optimal outcomes, reducing outbreak duration by 57% (from 142 to 61 days) and infection incidence by 77% (from 12,417 to 2,856 cases), while simultaneously decreasing government expenditures by 43% relative to baseline interventions. This modeling approach provided quantitative evidence supporting the effectiveness of combined ring vaccination and movement restrictions, achieving a reduction in the basic reproduction number ($\mathcal{R}_0$) from 2.3 to 0.4, thereby aligning with the OIE's strategic framework for PPR eradication in the Middle Eastern context.

The study by Fournié et al. (2018) developed a dynamic metapopulation model to analyze PPR transmission in Ethiopia, integrating deterministic within-village dynamics with stochastic between-village spread. Using Approximate Bayesian Computation with Sequential Monte Carlo (ABC-SMC) methods, the authors estimated transmission parameters by fitting the model to a nationwide serological survey encompassing 11,457 samples. The analysis revealed distinct transmission patterns between pastoral (lowland) and sedentary (highland) production systems, with pastoral villages functioning as persistent reservoirs (between-village reproduction number $\mathcal{R}^b_{LL} = 1.49$). The study determined that maintaining 37% herd immunity in at least 70.7% of pastoral villages would suffice for PPR elimination; however, the high turnover rate in these populations necessitates annual vaccination coverage of 61.7%. This work established an important framework for integrating heterogeneous livestock production systems into disease transmission models and provided concrete thresholds for control programs targeting PPR eradication.

Savagar et al. (2023), building on the model of Fournié et al. (2018), developed an agent-based, stochastic SIR model to investigate the influence of heterogeneous mixing among small ruminant flocks on PPRV transmission and the effectiveness of vaccination strategies. The results indicated that the 70% vaccination coverage recommended by the Global Strategy for the Control and Eradication (GSCE) may be insufficient for eradication if high-risk populations are not specifically targeted. Persistent transmission was observed even at high coverage levels when vaccination efforts were primarily directed towards lower-risk groups. These findings underscore the importance of implementing risk-based, targeted vaccination strategies to optimize PPRV eradication efforts.

This dissertation develops deterministic compartmental models of PPR transmission, applying and adapting established methodological frameworks for model formulation, analysis, and parameter inference. Using these models, we evaluate the epidemiological impact and cost-effectiveness of candidate intervention strategies, and thereby provide evidence-based recommendations to improve PPR control and disease management in affected production systems.

# Chapter 3

# Modeling the PPR Disease Transmission Dynamics with Vaccination and Restocking in Small Ruminant Population in Amhara Region, Ethiopia

## 3.1 Introduction

Peste des Petits Ruminants (PPR) continues to pose a substantial threat to small ruminant populations and livelihoods in the Amhara region of Ethiopia, despite the availability of effective vaccines and ongoing control efforts. While vaccination remains the cornerstone of disease control, frequent restocking practices such as the introduction of animals of unknown health status following trade movements, markets, and festivals-present significant challenges to eradicating PPR. These activities risk introducing infected animals into otherwise disease-free herds, potentially undermining vaccination campaigns and facilitating persistent endemic transmission.

Although previous studies have emphasized the epidemiology, risk factors, and spatial distribution of PPR in Ethiopia, the specific influence of restocking on the effectiveness of vaccination and overall disease dynamics has not been thoroughly investigated using mathematical modeling approaches. To address this gap, this chapter develops a deterministic compartmental SVEIR model that explicitly incorporates both vaccination and restocked subpopulations. The model analyzes the impact of imperfect vaccination and the introduction of infected animals through restocking on the persistence and control of PPR.

Model parameters are estimated using recent outbreak data from January 2019 to Aug. 2022 in Amhara region, Ethiopia. Theoretical analysis, including the computation of the basic reproduction number and global stability assessment using the Lyapunov-LaSalle invariance principle, is complemented by numerical simulations and sensitivity analysis. The results demonstrate that even with high vaccine efficacy, restocking of infected animals can sustain endemic transmission, highlighting the necessity for additional control measures beyond vaccination, such as strict movement restrictions and enhanced biosecurity. These findings offer important insights for policymakers aiming to achieve regional and national PPR eradication targets.

## 3.2 Model Formulation

In this section, a nonlinear epidemic model with restocking effect is formulated. The population of small ruminants with homogeneity $N(t)$ is divided into susceptible (S(t)), vaccinated (V(t)), exposed (E(t)), infectious (I(t)), restocked (B(t)) and recovered (R(t)) compartments. Therefore the total population becomes

$$N(t) = S(t) + V(t) + E(t) + I(t) + B(t) + R(t)$$

The population of susceptible ruminants is generated through the birth of newborn animals (at the rate $\Lambda$). The susceptible population acquires PPR infection through effective contact with PPR-infected ruminants at a mass action incidence rate of $\beta SI$, where $\beta$ represents the disease transmission rate relative to infected ruminants in the $I(t)$ class. This population is reduced by vaccination at a rate of $\omega$ and by natural death at a rate of $\mu$. Additionally, the population is further increased through restocking from the market and other sources, with a fraction $\alpha_1$ of the restocked population $B$. Therefore, the dynamics of this class can be described by the following equation:

$$\frac{dS}{dt} = (1-\rho)\Lambda + \alpha_1 B(t) - \beta S(t)I(t) - (\mu+\omega)S(t) \tag{3.1}$$

To describe the vaccination class, we assume that a fraction of susceptible small ruminants receive vaccinations at a rate of $\omega$ and subsequently join the vaccinated class. In cases where vaccination delivery is inadequate, small ruminants may not only receive vaccinations but also lose their immunity. However, there is a probability that this immunization will reduce the likelihood of a successful infection by $\epsilon$. If $\epsilon = 0$, small ruminants are fully protected from PPR by the vaccine, whereas if $\epsilon = 1$, they are not protected at all. The natural death rate ($\mu$) lowers this population. A fraction of newborn animals denoted by $\rho\Lambda$ (where $0 \leq \rho \leq 1$) are successfully vaccinated and move to the vaccinated class.

$$\frac{dV}{dt} = \rho\Lambda + \omega S(t) - \epsilon\beta V(t)I(t) - \mu V(t). \tag{3.2}$$

The population in the exposed compartment is generated when susceptible ruminants become infected after interacting with PPRV-infected ruminants. The population is decreased by the transfer rate $\sigma$ to the infected class and by the natural death rate $\mu$. Additionally, a fraction $\alpha_2$ of the restocked population $B$ transitions into the latent compartment. Thus, we can describe the dynamics of this class using the following equation.

$$\frac{dE}{dt} = \alpha_2 B(t) + \beta I(t)(\epsilon V(t) + S(t)) - (\sigma+\mu)E(t). \tag{3.3}$$

The population of infected ruminants is reduced by the natural death rate $\mu$, the rate of death induced by the disease $\delta$, and the restocking process, where a fraction $\alpha_2$ of the population $B$ is added in unit time. Additionally, individuals from this class are transferred to the recovered class

at a rate of $\gamma$. Therefore, the dynamics of this class can be described by the following equation.

$$\frac{dI}{dt} = \alpha_3 B(t) + \sigma E(t) - (\mu + \delta + \gamma) I(t). \tag{3.4}$$

The restocked class $B$ is continuously replenished through various sources such as returns from markets, trading, loaning, giving animals, restocking programs, and other unknown origins. This recruitment process is represented by the recruitment rate $\kappa$, ensuring a constant influx of newly restocked animals. However, since the restocked animals come from different unknown origins without undergoing health guarantee or quarantine, there is a possibility of introducing infected individuals into the population. Hence, the restocked class $B$ may contain infected animals. On the other hand, the outflow from the restocked class is determined by the rates $\alpha_1$, $\alpha_2$, and $\alpha_3$, which represent the proportions of animals moving from the restocked class to the susceptible class $S$, the exposed class $E$, and the infected class $I$, respectively. Additionally, there is a natural death rate denoted as $\mu$ contributing to the outflow from the restocked class.

Taking these factors into account, we can describe the rate of change of the restocked class $B$ with respect to time using the following equation:

$$\frac{dB}{dt} = \kappa - (\alpha_1 + \alpha_2 + \alpha_3 + \mu) B(t). \tag{3.5}$$

Finally, the recovered class is generated by transfer rates $\gamma$ and is reduced by the natural death rate $\mu$. Thus, we obtain the following equation for this class.

$$\frac{dR}{dt} = \gamma I(t) - \mu R(t). \tag{3.6}$$

Based on the above assumptions of the model, Figure (3.1) depicts the transfer diagram between compartments.

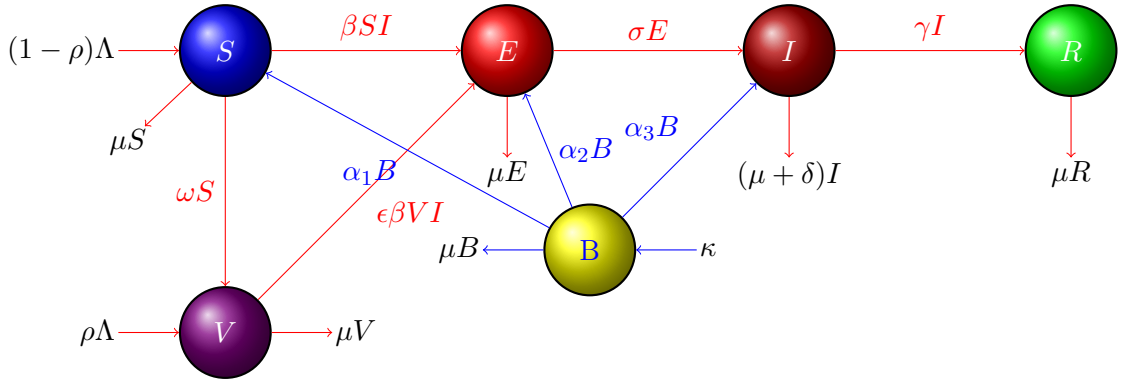


FIGURE 3.1: The Compartmental diagram for PPR disease transmission model model (3.7)

TABLE 3.1: Parameter description of model (3.7).

| Parameter | Description |
|---|---|
| $\Lambda$ | Small ruminants per capita birth rate |
| $\kappa$ | A constant flow rate of small ruminant into Restocked population |
| $\beta$ | Effective contact rate (PPR transmission rate) |
| $\mu$ | Natural mortality rate |
| $\omega$ | The rate at which susceptible individuals are vaccinated |
| $1-\epsilon$ | Vaccine efficancy |
| $\delta$ | Disease-induced mortality rate |
| $\sigma$ | The rate at which the exposed population becomes infective |
| $\gamma$ | Rates of natural recovery from infected class |
| $\rho$ | Fraction of recruited small ruminants that are vaccinated |
| $\alpha_1$ | The rate of flow from restocked class to susceptible class |
| $\alpha_2$ | The rate of flow from restocked class to exposed class |
| $\alpha_3$ | The rate of flow from restocked class to infected class |

Combining all the differential equations formulated in (3.1)-(3.6) gives the following system of equations

$$\begin{cases} \frac{dS}{dt} = (1-\rho)\Lambda + \alpha_1 B(t) - \beta S(t)I(t) - (\mu+\omega)S(t), \\ \frac{dV}{dt} = \rho\Lambda + \omega S(t) - \epsilon\beta V(t)I(t) - \mu V(t), \\ \frac{dE}{dt} = \alpha_2 B(t) + \beta I(t)(\epsilon V(t) + S(t)) - (\sigma+\mu)E(t), \\ \frac{dI}{dt} = \alpha_3 B(t) + \sigma E(t) - (\mu+\delta+\gamma)I(t), \\ \frac{dB}{dt} = \kappa - (\alpha_1+\alpha_2+\alpha_3+\mu)B(t), \\ \frac{dR}{dt} = \gamma I(t) - \mu R(t), \end{cases} \tag{3.7}$$

with intial condition

$$S(0) \geq 0, V(0) \geq 0, E(0) \geq 0, I(0) > 0, B(0) \geq 0, R(0) \geq 0.$$

where, we assume that $0 \leq \alpha_1 + \alpha_2 + \alpha_3 < 1$.

All parameters in the model (3.7) maintain non-negative, and their biological meanings are described in Table (3.1) so that the total host population remains bounded.

## 3.3 Model Analysis

### 3.3.1 Well-Posedness of the Model

In this section, it is essential to provide evidence of the existence of a solution that is not negative, as well as to establish the uniqueness and boundedness of the solution for the mathematical and epidemiological interpretation of the model (3.7).

The total population $N(t)$ at any time $t$, can be determined by adding all equations in (3.7), we obtain

$$\frac{dN}{dt} = \Lambda + \kappa - \mu N - \delta I \leq \Theta - \mu N, \tag{3.8}$$

where $\Theta = \Lambda + \kappa$ and solving the differential inequality (3.8) with initial condition $N(0) = N_0$ using 'Groonwall's Inequality' gives

$$N(t) \leq N_0 e^{-\mu t} + \frac{\Theta}{\mu}\left(1 - e^{-\mu t}\right),$$

then

$$\lim_{t\to\infty} sup(N(t)) \leq \frac{\Theta}{\mu}.$$

As a result, the total population $N(t)$ experiences fluctuations over time. When there is no disease or $\delta = 0$ (indicating the absence of disease-dependent mortality), the total population size $N(t)$ converges to $\frac{\Theta}{\mu}$. Since the spread of the disease within the population reduces $N(t)$, it can be inferred that $N(t)$ is within the range of $[0, \frac{\Theta}{\mu}]$. Therefore, the feasible region of the model (3.7) is defined as follows:

$$\Gamma = \left\{(S, V, E, I, B, R) \in \mathcal{R}_+^6 : N(t) \leq \frac{\Theta}{\mu}\right\}.$$

**Lemma 3.3.1.** *For any initial condition* $(S_0, V_0, E_0, I_0, B_0, R_0) \in \mathbf{R}_+^6$*, system* (3.7) *has a unique solution* $(S(t), V(t), E(t), I(t), B(t), R(t))$ *defined on* $[0, \infty)$ *satisfying the initial conditions and the properties:*

$$S(t), V(t), E(t), I(t), B(t), R(t) \geq 0, N(t) \leq \frac{\Theta}{\mu}.$$

**Proof** We first show the local existence and uniqueness of the solution.

Let $x(t) = (S(t), V(t), E(t), I(t), B(t), R(t))^T$ and write system (3.7) as

$$\frac{dx}{dt} = f(x), \quad x(0) = x_0 \in \mathbb{R}_+^6,$$

where $f : \mathbf{R}^6 \to \mathbf{R}^6$ is given by the right-hand sides. Each component of $f$ is a polynomial in the state variables; hence $f$ is continuously differentiable ($C^1$) on $\mathbf{R}^6$. A $C^1$ function is locally Lipschitz continuous. By the Picard–Lindelöf theorem, for every $x_0$ there exists a unique solution defined on a maximal interval $[0, t_{\max})$.

Next, we prove non-negativity and invariance of $\mathbf{R}+^6$ by apply the invariance theorem (Thieme, 2018)) to the closed set $D = \mathbf{R}+^6$. For $x \in \partial D$, a coordinate $x_i = 0$ must satisfy $f_i(x) \geq 0$ to guarantee that the flow does not leave $D$. We can easily verify this condition for each variable:

When $B = 0$:

$$f_5(x) = \frac{dB}{dt} = \kappa > 0$$

. When $S = 0$:

$$f_1(x) = \frac{dS}{dt} = (1 - \rho)\Lambda + \alpha_1 B \geq 0.$$

When $V = 0$:

$$f_2(x) = \frac{dV}{dt} = \rho\Lambda + \omega S \geq 0.$$

When $E = 0$:

$$f_3(x) = \frac{dE}{dt} = \alpha_2 B + \beta I(\varepsilon V + S) \geq 0.$$

When $I = 0$:

$$f_4(x) = \frac{dI}{dt} = \alpha_3 B + \sigma E \geq 0.$$

When $R = 0$:

$$f_6(x) = \frac{dR}{dt} = \gamma I \geq 0.$$

All inequalities hold because the other variables are non-negative on $D$. Consequently, the vector field $f$ points inward (or is tangent) on $\partial D$. By Thieme's theorem, $\mathbf{R}+^6$ is positively invariant: if $x_0 \in \mathbf{R}+^6$, then $x(t) \in \mathbf{R}+^6$ for all $t \in [0, t\text{max})$. Finally, we prove the boundedness of the solution. Let $x$ be a solution with values in $\mathcal{R}^6_+$, defined in the interval $[0, \infty)$. To show that $x$ is bounded on $[0, \infty)$, it suffices to observe that $N(t) \leq \frac{\Theta}{\mu}$ for all $0 \leq t < \infty$. Since $S, V, E, I, B$, and $R$ are nonnegative and sum up to $N$, they are bounded by $\frac{\Theta}{\mu}$. The claim is supported by Theorem A.1 in (Thieme, 2018).

**Remark 3.3.2.** *From Lemma 3.3.1, it follows that the biologically meaningful feasible region for system (3.7) is given by*

$$\Gamma = \left\{ (S(t), V(t), E(t), I(t), B(t), R(t)) \in \mathbf{R}^6_+ : N(t) = S + V + E + I + B + R \leq \frac{\Theta}{\mu} \right\}.$$

*This region $\Gamma$ is positively invariant with respect to the dynamics of (3.7): any solution starting in $\Gamma$ remains in $\Gamma$ for all $t \geq 0$. Consequently, the long-term behavior of the system can be analyzed within this compact, epidemiologically relevant domain.*

### 3.3.2 Existence and Stability Analysis of Equilibria

#### Case of No Infective Influx from Restocked Small Ruminants

Considering that there is no influx of infective restocked small ruminants, i.e., $\alpha_2 = \alpha_3 = 0$, and given that the state variable R does not impact the remaining equations, the system (3.7) can be reduced to the following five-dimensional system.

$$\begin{cases} \frac{dS}{dt} = (1-\rho)\Lambda + \alpha_1 B(t) - \beta S(t) I(t) - (\mu + \omega) S(t), \\ \frac{dV}{dt} = \rho\Lambda + \omega S(t) - \epsilon\beta V(t) I(t) - \mu V(t), \\ \frac{dE}{dt} = \beta I(t)(\epsilon V(t) + S(t)) - (\sigma + \mu) E(t), \\ \frac{dI}{dt} = \sigma E(t) - (\mu + \delta + \gamma) I(t), \\ \frac{dB}{dt} = \kappa - (\alpha_1 + \mu) B(t), \end{cases} \tag{3.9}$$

and

$$N_1(t) = S(t) + V(t) + E(t) + I(t) + B(t).$$

It is apparent that model (3.9) permits the existence of another biologically feasible region,

$$\Gamma_1 = \left\{ (S, V, E, I, B) \in \mathbf{R}_+^5 : S \geq 0, V \geq 0, E \geq 0, I \geq 0, B \geq 0, N_1 \leq \frac{\Theta}{\mu} \right\},$$

which is also positive-invariant and attracting such that model (3.9) is well-posed in $\Gamma_1$. Similar to the original model, but with a few minor modifications, the aforementioned result can be verified.

The PPR-disease free equilibrium state $\xi_0$, of the system (3.9) can be obtained as:

$$\xi_0 = (S_0, V_0, 0, 0, B_0) = \left( \frac{\Lambda(1-\rho) + \alpha_1 B_0}{\omega + \mu}, \frac{\Lambda\rho + \omega S_0}{\mu}, 0, 0, \frac{\kappa}{\alpha_1 + \mu} \right).$$

The local stability of $\xi_0$ can be determined by calculating the control reproduction number $\mathcal{R}_v$ using the method of the next-generation operator developed by Van den Driessche et al. (2002). The control reproduction number $\mathcal{R}_v$ serves as a threshold parameter that reflects the potential for disease spread under ongoing vaccination. It quantifies the expected number of new cases of PPR generated by a single infected small ruminant in a completely susceptible population within a region with a vaccination program. If $\mathcal{R}_v < 1$, the infection will die out. Conversely, if $\mathcal{R}_v > 1$, the disease will persist in the population. The control reproduction number of the system (3.9) is given as:

$$\mathcal{R}_v = \frac{\beta\sigma(\epsilon\rho\Lambda(\omega+\mu)(\alpha_1+\mu) + (\epsilon\omega+\mu)((1-\rho)\Lambda(\alpha_1+\mu) + \alpha_1\kappa))}{\mu(\alpha_1+\mu)(\omega+\mu)(\sigma+\mu)(\delta+\gamma+\mu)}. \tag{3.10}$$

A similar threshold quantity known as the basic reproduction number $\mathcal{R}_0$, is obtained by setting $\omega = 0$ and $\rho = 0$ in $\mathcal{R}_v$ and given by

$$\mathcal{R}_0 = \frac{\beta\sigma(\Lambda(\alpha_1+\mu) + \alpha_1\kappa)}{\mu(\alpha_1+\mu)(\sigma+\mu)(\delta+\gamma+\mu)}.$$

The quantity $\mathcal{R}_0$ (Van den Driessche et al., 2002) measures the expected number of secondary cases generated by an index case in an unvaccinated, equilibrium population $(\frac{\Theta}{\mu}, 0, 0, 0, \frac{\kappa}{\alpha_1+\mu})$. With this definition for $\mathcal{R}_0$, $\mathcal{R}_v$ can be expressed as

$$\mathcal{R}_v = \mathcal{R}_0 \frac{\epsilon\rho\Lambda(\omega+\mu)(\alpha_1+\mu) + (\epsilon\omega+\mu)((1-\rho)(\alpha_1+\mu)\Lambda + \alpha_1\kappa)}{(\omega+\mu)((\alpha_1+\mu)\Lambda + \alpha_1\kappa)}.$$

Furthermore, setting $\mathcal{R}_v = 1$ and solving for $\omega$ gives the threshold vaccination rate, $\omega_c$:

$$\omega_c = \frac{((\alpha_1+\mu)(1-(\epsilon\rho-\rho+1)\mathcal{R}_0)\Lambda + \kappa\alpha_1(1-\mathcal{R}_0))\mu}{((\alpha_1+\mu)\Lambda + \alpha_1\kappa)(\epsilon\mathcal{R}_0 - 1)}.$$

Biological $\omega_c$ represents the minimum vaccination rate required to drive the control reproduction number $\mathcal{R}_v$ below 1, thereby ensuring disease elimination. When the vaccination rate exceeds $\omega_c$, the combined effects of vaccination coverage and efficacy ($\epsilon$) are sufficient to reduce

secondary infections below replacement level, leading to epidemic control. Conversely, if $\omega < \omega_c$, the vaccination effort is insufficient to prevent sustained transmission.

**Remark 3.3.3.** *(i). By considering that $\omega \geq 0$ and $0 \leq \epsilon \leq 1$, we can establish the relationship $\mathcal{R}_0 \geq \mathcal{R}_v \geq \epsilon\mathcal{R}_0$. This implies that if $\epsilon\mathcal{R}_0 > 1$ (which is equivalent to $\epsilon > \frac{1}{\mathcal{R}_0} = \epsilon_c$), then $\mathcal{R}_v > 1$. Therefore, even with vaccination efforts, it is not possible to achieve $\mathcal{R}_v < 1$. The critical value for the reduction rate of infection due to vaccination is defined as $\epsilon_c$.*

*(ii). Note that $\mathcal{R}_v \leq \mathcal{R}_0$ holds true, with equality occurring only when $\omega = 0$ and $\rho = 0$. It is observed that in the case of imperfect vaccines, where $\omega > 0$ and $0 < \rho \leq 1$, the effect is a reduction in the reproduction number of the disease.*

**Theorem 3.3.4.** *The PPR disease-free equilibrium $\xi_0$ is locally asymptotic stable if $\mathcal{R}_v < 1$ but unstable for $\mathcal{R}_v > 1$.*

**Proof** To prove this theorem, we employ the linearization method. The Jacobian matrix of system (3.9) evaluated at the PPR disease free equilibrium state $\xi_0$ is as follows:

$$J(\xi_0) = \begin{bmatrix} -(\mu+\omega) & \omega_0 & 0 & -\beta S_0 & \alpha_1 \\ \omega & -\mu & 0 & -\epsilon\beta V_0 & 0 \\ 0 & 0 & -(\sigma+\mu) & \beta S_0 + \epsilon\beta V_0 & 0 \\ 0 & 0 & \sigma & -(\delta+\gamma+\mu) & 0 \\ 0 & 0 & 0 & 0 & -(\alpha_1+\mu) \end{bmatrix}.$$

We obtain the characteristic polynomial equation of the Jacobian matrix, which is given by

$$(\lambda+\mu)(\lambda+\omega+\mu)(\alpha_1+\lambda+\mu)(\lambda^2+b_1\lambda+b_0) = 0 \tag{3.11}$$

where

$$\begin{cases} b_1 = 2\mu+\delta+\gamma+\sigma, \\ b_0 = (\sigma+\mu)(\delta+\mu+\gamma)(1-\mathcal{R}_v). \end{cases} \tag{3.12}$$

Since all parameters in (3.11) are positive, some roots of the characteristic polynomial in (3.11) are $\lambda_1 = -\mu$, $\lambda_2 = -(\omega+\mu)$, and $\lambda_2 = -(\alpha_1+\mu)$, all of which have negative real parts. It should be noted that $b_1 > 0$ and $b_0 > 0$ only if $\mathcal{R}_v < 1$, as determined by the Routh-Hurwitz criterion in (Yang, 2002). According to this criterion, the other two roots of (3.11), $\lambda_4$ and $\lambda_5$, will also have negative real parts if both $b_0$ and $b_1$ in (3.12) are positive. Consequently, the PPR disease-free equilibrium state $\xi_0$ will be locally asymptotically stable if $\mathcal{R}_v < 1$.

**Theorem 3.3.5.** *If $\mathcal{R}_v \leq 1$, $\xi_0$ is globally asymptotically stable in $\Gamma_1$.*

**Proof** Following the same idea in (Wang et al., 2021), we take the candidate Lyapunov function $L(t) = E(t) + \left(\frac{\sigma+\mu}{\sigma}\right) I(t)$.

Now, calculate the time derivative of $L(t)$ along the solution of model (3.9), we find

$$\begin{aligned}
\frac{dL}{dt} &= \frac{dE}{dt} + \left(\frac{\sigma+\mu}{\sigma}\right)\frac{dI}{dt} \\
&= \beta I(\epsilon V + S) - (\sigma+\mu)E + \left(\frac{\sigma+\mu}{\sigma}\right)(\sigma E - (\mu+\delta+\gamma)I) \\
&= I\left(\beta(\epsilon V + S) - \frac{\sigma+\mu}{\sigma}(\delta+\gamma+\mu)\right), \quad \text{since,} \quad \epsilon V(t) + S(t) \leq \epsilon V_0 + S_0 \quad \text{for all} \quad t > 0, \\
&\leq \frac{(\sigma+\mu)(\delta+\gamma+\mu)}{\sigma} I\left(\frac{\beta\sigma(\epsilon V_0 + S_0)}{(\sigma+\mu)(\delta+\gamma+\mu)} - 1\right), \\
&= \frac{(\sigma+\mu)(\delta+\gamma+\mu)}{\sigma} I\left(\mathcal{R}_v - 1\right).
\end{aligned}$$

If $\mathcal{R}_v \leq 1$, then $L'(t) \leq 0$ for $(S, V, E, I, B) \in \Gamma_1$ sufficiently close to $(S_0, V_0, 0, 0, B_0)$ and $L'(t) = 0$ holds only when $I = 0$. Since $\{\xi_0\}$ is the largest invariant set in the subset of $\Gamma_1$ where $L'(t) = 0$. Its globally asymptotically stability follows from local stability of $\xi_0$ and Lasalle's invariance principle (LaSalle, 2012).

The endemic equilibrium of model (3.9) can be given:

$$\begin{cases}
S^* = \dfrac{(1-\rho)\Lambda + \alpha_1 B^*}{\beta I^* + \omega + \mu}, \\
V^* = \dfrac{\rho\Lambda + \omega S^*}{\epsilon\beta I^* + \mu}, \\
E^* = \dfrac{(\gamma+\delta+\mu)I^*}{\sigma}, \\
B^* = \dfrac{\kappa}{\mu+\alpha_1},
\end{cases} \tag{3.13}$$

and from equations (3.13) and model (3.9), $I^*$ is the positive root of the quadratic polynomial:

$$\mathcal{H}(I^*) = aI^{*2} + bI^* + c,$$

where

$$\begin{cases}
a = \epsilon\beta^2, \\
b = \beta(\epsilon(\omega+\mu)+\mu) - \dfrac{\epsilon\beta^2\sigma(\Lambda+\alpha_1 B^*)}{(\delta+\gamma+\mu)(\sigma+\mu)}, \\
c = \mu(\mu+\omega)(1-\mathcal{R}_v).
\end{cases} \tag{3.14}$$

According to Equation (3.14), it can be deduced that $a > 0$ and $c < 0$ if $\mathcal{R}_v > 1$. Consequently, the quadratic polynomial $\mathcal{H}(I^*)$ possesses two roots with opposite signs. Therefore, it can be concluded that the model (3.9) has a unique positive endemic equilibrium $\xi^* = (S^*, V^*, E^*, I^*, B^*)$ when $\mathcal{R}_v > 1$.

**Theorem 3.3.6.** *Model(3.9)has a unique endemic equilibrium $\xi^*$ if and only if $\mathcal{R}_v > 1$.*

**Theorem 3.3.7.** *The endemic equilibrium $\xi^*$ is locally asymptotically stable if $\mathcal{R}_v > 1$. In addition, the model (3.9) exhibits the forward bifurcation.*

**Proof** In line with Theorem 4.1 of (Carr, 2012), we employ center manifold theory (Castillo-Chavez et al., 2004). Now, let us express the system (3.9) in vector notation:

$$\frac{dx}{dt} = f(x)$$

where $x = (x_1, x_2, x_3, x_4, x_5) = (S, V, E, I, B)$ and $f = (f_1, f_2, f_3, f_4, f_5)$. Let $\beta$ be the bifurcation parameter, then system (3.9) becomes

$$\begin{cases} \frac{dx_1}{dt} = (1-\rho)\Lambda + \alpha_1 x_5 - \beta x_1 x_4 - (\mu+\omega)x_1, \\ \frac{dx_2}{dt} = \rho\Lambda + \omega x_1 - \epsilon\beta x_2 x_4 - \mu x - 2, \\ \frac{dx_3}{dt} = \beta x_4(\epsilon x_2 + x_1) - (\sigma+\mu)x_3, \\ \frac{dx_4}{dt} = \sigma x_3 - (\mu+\delta+\gamma)x_4, \\ \frac{dx_5}{dt} = \kappa - (\alpha_1+\mu)x_5, \end{cases} \tag{3.15}$$

with $\mathcal{R}_v = 1$ corresponding to $\beta = \beta^* = \frac{\mu(\omega+\mu)(\sigma+\mu)(\delta+\gamma+\mu)(\alpha_1+\mu)}{\sigma(\epsilon\rho\Lambda(\omega+\mu)(\alpha_1+\mu)+(\epsilon\omega+\mu)(\Lambda(1-\rho)(\alpha_1+\mu)+\alpha_1\kappa))}$. The Jacobian matrix of the system (3.9) at the PPR disease-free equilibrium point $\xi_0$ when $\beta = \beta^*$ is given by

$$J(\xi_0)|_{\beta=\beta^*} = \begin{bmatrix} -(\mu+\omega) & 0 & 0 & -\beta x_1^0 & \alpha_1 \\ \omega & -\mu & 0 & -\epsilon\beta x_2^0 & 0 \\ 0 & 0 & -(\sigma+\mu) & \frac{(\sigma+\mu)(\delta+\gamma+\mu)}{\sigma} & 0 \\ 0 & 0 & \sigma & -(\delta+\gamma+\mu) & 0 \\ 0 & 0 & 0 & 0 & -(\alpha_1+\mu) \end{bmatrix} \tag{3.16}$$

where $\xi_0 = (x_1^0, x_2^0, x_3^0, x_4^0, x_5^0)$ corresponding to $(S_0, V_0, E_0, I_0, B_0)$. We obtain the characteristic polynomial equation of the Jacobian matrix (3.16), which is given by

$$(2\mu+\delta+\gamma+\sigma+\lambda)(\mu+\omega+\lambda+\omega_0)(\mu+\lambda)(\alpha_1+\mu+\lambda)\lambda = 0. \tag{3.17}$$

It is clearly shown in (3.17) that 0 is a simple eigenvalue of $J(\xi_0)|_{\beta=\beta^*}$, and the other eigenvalues are real and negative ($\xi_0$ is a non-hyperbolic equilibrium). Hence, Theorem 4.1 in (Castillo-Chavez et al., 2004) can be used to analyse the dynamics of (3.9) near $\beta = \beta^*$. In particular, it will be used to show locally asymptotic stability of the endemic equilibrium of (3.9) for $\beta$ near $\beta^*$. It can be shown that a right eigenvector associated with zero eigenvalue is $u = (u_1, u_2, u_3, u_4, u_5)^T$,

where

$$\begin{cases} u_1 = -\dfrac{\beta x_1^0}{(\omega+\mu)}u_4, \\ u_2 = -\dfrac{\beta(\epsilon x_2^0(\mu+\omega)+\omega x_1^0)}{\mu(\omega+\mu)}u_4, \\ u_3 = \dfrac{\delta+\gamma+\mu}{\sigma}u_4, \\ u_4 = u_4, \\ u_5 = 0. \end{cases} \tag{3.18}$$

We can see in (3.18) that $u_1 < 0; u_2 < 0; u_3 > 0;$ and $u_4 > 0$. The left eigenvector $v = (v_1, v_2, v_3, v_4, v_5)$ of $J(\xi_0)|_{\beta=\beta^*}$ (associated with the zero eigenvalue) can be obtained as

$$\begin{cases} v_1 = 0, \\ v_2 = 0, \\ v_3 = v_3 > 0, \\ v_4 = \dfrac{\sigma+\mu}{\sigma}v_3 > 0, \\ v_5 = 0. \end{cases} \tag{3.19}$$

Here we have taken into account the expression for $\beta^*$, where $u_4$ and $v_3$ are calculated to ensure that the eigenvectors satisfy the condition $u.v = 1$. Based of this condition we have $u_4 v_3 = \frac{\sigma}{\delta+\gamma+2\mu}$.

Next, we will compute the values of $a$ and $b$ based on Theorem 4.1 of (Castillo-Chavez et al., 2004). From equation (3.19), since $v_1 = v_2 = v_5 = 0$, we only need to compute the partial derivatives of the $f_3$ and $f_4$ in (3.15) at the PPR disease-free equilibrium. For system (3.15) , the associated non-zero partial derivative of $f_3$ and $f_4$ at the PPR disease-free equilibrium is given by

$$\frac{\partial^2 f_3}{\partial x_4 \partial x_1} = \frac{\partial^2 f_3}{\partial x_1 \partial x_4} = \beta^*, \frac{\partial^2 f_3}{\partial x_4 \partial x_2} = \frac{\partial^2 f_3}{\partial x_2 \partial x_4} = \epsilon\beta^*$$

with

$$\frac{\partial^2 f_3}{\partial x_4 \partial \beta} = u_4 v_3(\epsilon x_2^0 + x_1^0)$$

where all partial derivatives of $f_3$ with respect to other variables and all partial derivatives of $f_4$ are zero.Then we have

$$\begin{aligned} a &= \sum_{k,i,j=1}^{4} v_k u_i u_j \frac{\partial^2 f_k}{\partial x_i \partial x_j} = 2v_3 u_4 \beta^*(u_1 + \epsilon u_2) < 0, \\ b &= \sum_{k,i=1}^{4} v_k u_i \frac{\partial^2 f_k}{\partial x_i \partial \beta^*} = v_3 u_4(\epsilon x_2^0 + x_1^0) > 0. \end{aligned} \tag{3.20}$$

Thus, the signs of $a$ and $b$ in (3.20) and according to item (iv) of Theorem 4.1 in (Castillo-Chavez et al., 2004), we can conclude that $\xi^*$ is locally asymptotically stable if $\mathcal{R}_v > 1$.

Furthermore, when the control reproduction number is equal to one, a change of stability occurs. Specifically, the PPR disease-free equilibrium becomes unstable, and a non-trivial (endemic) equilibrium arises and remains stable. Therefore, system (3.9) with parameter values outlined in Table (3.2) exhibits a forward bifurcation, as depicted in Figure (3.2), when $\mathcal{R}_v = 1$. The presence of a forward bifurcation in our model indicates that the basic reproduction number becomes the sole determinant for the eradication of PPR disease. As long as we can maintain a condition of $\mathcal{R}_v < 1$, PPR disease will always vanish from the small ruminant population.

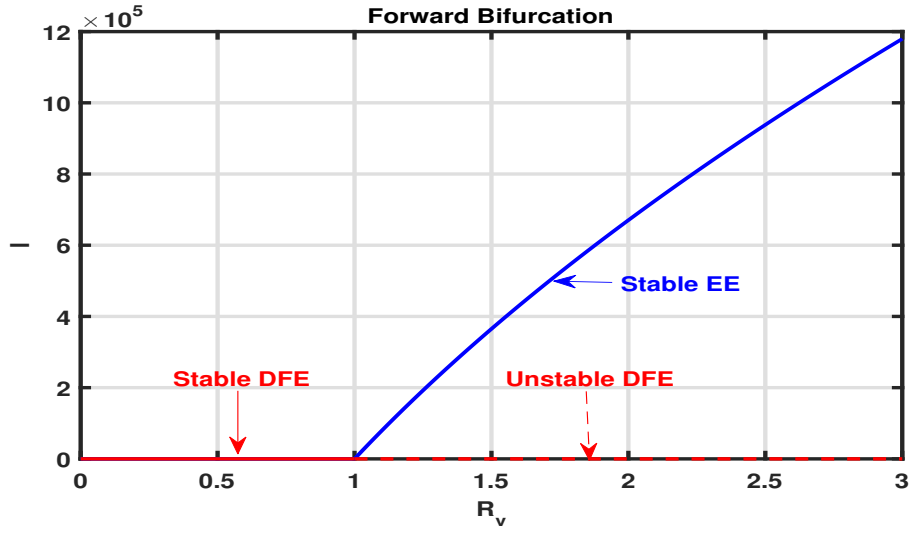


FIGURE 3.2: The forward bifurcation diagram for model (3.9).

### For the Case of a Non-zero Influx of Infective Restocked Small Ruminants

In this section, we explore the dynamics of the model (3.7) under the scenario of a non-zero influx of infected restocked small ruminants within the feasible region $\Gamma$. As $\left(\frac{dE}{dt} + \frac{dI}{dt}\right)_{E=I=0} > 0$, it follows that model (3.7) lacks a disease-free equilibrium of PPR. Consequently, the system may have a unique endemic equilibrium. We analyze the global dynamics of the disease based on the endemic equilibrium point using an approach similar to that employed in prior studies (Khan et al., 2021; Sigdel et al., 2014).

Let $\bar{\xi} = (\bar{S}, \bar{V}, \bar{E}, \bar{I}, \bar{B})$ represent the endemic equilibrium of system (3.7) and satisfy the following equilibrium equations

$$\begin{cases} (1-\rho)\Lambda = -\alpha_1 B + \beta SI + (\omega + \mu)S, \\ \rho\Lambda = -\omega S + \epsilon\beta VI + \mu V, \\ (\sigma + \mu)E = \beta I(\epsilon V + S) + \alpha_2 B, \\ (\delta + \gamma + \mu)I = \sigma E + \alpha_3 B, \\ \kappa = \bar{\alpha} B, \end{cases} \tag{3.21}$$

where $\bar{\alpha} = \alpha_1 + \alpha_2 + \alpha_3 + \mu$. The expression for the endemic equilibrium can be given by:

$$\begin{cases} \bar{S} = \dfrac{(1-\rho)\Lambda) + \alpha_1 \bar{B}}{\beta \bar{I} + \omega + \mu}, \\ \bar{V} = \dfrac{\omega \bar{S} + \rho\Lambda}{\epsilon\beta\bar{I} + \mu}, \\ \bar{E} = \dfrac{(\gamma + \delta + \mu)\bar{I} - \alpha_3 \bar{B}}{\sigma}, \\ \bar{B} = \dfrac{\kappa}{\bar{\alpha}}, \end{cases} \tag{3.22}$$

and from equations (3.22) and (3.21), $\bar{I}$ is the positive root of the cubic polynomial:

$$\mathcal{G}(\bar{I}, \alpha_1, \alpha) = \bar{a}\bar{I}^3 + \bar{b}\bar{I}^2 + \bar{c}\bar{I} + \bar{d} := \bar{I}\mathcal{F}(\bar{I}) - \frac{\alpha\bar{B}\beta(\mu + \epsilon(\omega + \mu))}{(\sigma + \mu)(\delta + \gamma + \mu)}\bar{I} + d = 0, \tag{3.23}$$

where

$$\mathcal{F}(I^*) = \bar{a}\bar{I}^2 + \bar{b}\bar{I} + \bar{c_0},$$

$$\begin{cases} \bar{a} = \epsilon\beta^2, \\ \bar{b} = \beta(\epsilon(\omega + \mu) + \mu) - \dfrac{\epsilon\beta^2(\alpha\bar{B} + \sigma(\Lambda + \alpha_1\bar{B}))}{(\delta + \gamma + \mu)(\sigma + \mu)}, \\ \bar{c} = \mu(\mu + \omega) - \dfrac{\sigma\beta(\epsilon\rho\Lambda(\omega + \mu) + (\epsilon\omega + \mu)(\Lambda(1-\rho) + \alpha_1\bar{B}))}{(\sigma + \mu)(\delta + \gamma + \mu)} - \dfrac{\alpha\bar{B}\beta(\mu + \epsilon(\omega + \mu))}{(\sigma + \mu)(\delta + \gamma + \mu)}, \\ \bar{c_0} = \mu(\mu + \omega) - \dfrac{\sigma\beta(\epsilon\rho\Lambda(\omega + \mu) + (\epsilon\omega + \mu)(\Lambda(1-\rho) + \alpha_1\bar{B}))}{(\sigma + \mu)(\delta + \gamma + \mu)}, \\ \bar{d} = -\dfrac{\alpha\bar{B}\mu(\mu + \omega)}{(\delta + \gamma + \mu)(\sigma + \mu)}, \\ \alpha = (\alpha_2\sigma + \alpha_3(\sigma + \mu)). \end{cases} \tag{3.24}$$

Notice that when $\alpha_2 = \alpha_3 = 0$, or $\alpha = 0$ in (3.23), the equation $\mathcal{G}(\bar{I}, \alpha_1, 0) = 0$ reduces to $\bar{I}\mathcal{F}(\bar{I}) = 0$. Consequently, we have $\bar{I} = 0$ for the disease-free equilibrium (DFE), and $\mathcal{F}(\bar{I}) = 0$, which is equivalent to equation (3.14). This equation has a unique positive root for the endemic equilibrium if $\bar{c_0} < 0$, which is equivalent to $\mathcal{R}_v > 1$. Furthermore, we observe that $\mathcal{G}(\bar{I}, \alpha_1, \alpha) < \bar{I}\mathcal{F}(\bar{I})$ for $\alpha > 0$ and $\bar{I} > 0$. To analyze the number of positive roots for $\mathcal{G}(\bar{I}, \alpha_1, \alpha) = 0$, we need to consider three cases based on the signs of $\bar{b}$ and $\bar{c_0}$ in (3.24). A similar approach has been employed in the study of the model (Shim, 2004; Alexander et al., 2004).

In the case where $\bar{c_0} < 0$, according to Descartes' Rule of Signs, the equation $\mathcal{G}(\bar{I}, \alpha_1, \alpha) = 0$ has at most one positive root, regardless of the sign of $\bar{b}$. This result holds because $\bar{a} > 0$, $\bar{c} < 0$, and $\bar{d} < 0$. On the other hand, equation $\mathcal{F}(\bar{I}) = 0$ has a unique positive root denoted as $\hat{I}$. Consequently, we can deduce that $\mathcal{G}(\hat{I}, \alpha_1, \alpha) < 0$, as $\mathcal{G}(\bar{I}, \alpha_1, \alpha) < \bar{I}\mathcal{F}(\bar{I})$ for $\alpha > 0$. Furthermore, it can be observed that $\mathcal{G}(\bar{I}, \alpha_1, \alpha) \to \infty$ as $\bar{I} \to \infty$, which confirms the existence of a positive root for $\mathcal{G}(\bar{I}, \alpha_1, \alpha)$.

In the case where $\bar{c_0} > 0$ and $\bar{b} > 0$, let $r_1$, $r_2$, and $r_3$ denote the roots of $\mathcal{G}(\bar{I}, \alpha_1, \alpha)$. In this scenario, given that $\bar{a} > 0$ and $\bar{b} > 0$, it follows that $r_1 + r_2 + r_3 = -\bar{b}/\bar{a} < 0$ and $r_1 r_2 r_3 > 0$. Consequently, it can be concluded that $\mathcal{G}(\bar{I}, \alpha_1, \alpha)$ has a unique positive root for any $\alpha > 0$.

For the final case where $\bar{c_0} > 0$ and $\bar{b} < 0$, if $\bar{b}^2 - 4\bar{a}\bar{c_0} > 0$, Descartes' Rule of Signs indicates

that $\mathcal{F}(\bar{I})$ possesses two positive roots. Thus, if $\bar{b}^2 - 4\bar{a}\bar{c_0} > 0$, $\mathcal{G}(\bar{I}, \alpha_1, 0)$ has two positive roots. Since $\mathcal{G}(\bar{I}, \alpha_1, \alpha)$ is a cubic function of $\bar{I}$ and a decreasing function of $\alpha$ for $\bar{I} > 0$, it can be observed that there exists a positive value $\hat{\alpha}$ such that $\mathcal{G}(\bar{I}, \alpha_1, \alpha)$ has three positive roots if $0 < \alpha < \hat{\alpha}$, two positive roots (one with multiplicity 2) if $\alpha = \hat{\alpha}$, and a unique positive root if $\alpha > \hat{\alpha}$. It should be noted that $\hat{\alpha} < \alpha_0$, where

$$\alpha_0 = \frac{\bar{c_0}(\sigma + \mu)(\delta + \gamma + \mu)}{\bar{B}\beta(\epsilon(\omega + \mu) + \mu)}.$$

To illustrate this, suppose $\alpha \geq \alpha_0$. If $\mathcal{G}(\bar{I}, \alpha_1, \alpha)$ has exactly one real root, then from $r_1 r_2 r_3 = -\frac{\bar{d}}{\bar{a}} > 0$, it can be deduced that this root must be positive. If the roots of $\mathcal{G}(\bar{I}, \alpha_1, \alpha)$ are all real, considering that $r_1 r_2 + r_1 r_3 + r_2 r_3 = \frac{\bar{c_0} - \frac{\alpha \bar{B}\beta(\epsilon(\omega+\mu)+\mu)}{(\sigma+\mu)(\delta+\gamma+\mu)}}{\bar{a}} \leq 0$ when $\alpha \geq \alpha_0$, it can be observed that $\mathcal{G}(\bar{I}, \alpha_1, \alpha)$ also possesses a unique positive root in this case. These findings are summarized below.

**Theorem 3.3.8.** *i. If $\omega < \omega_c$ or $\alpha > \alpha_0$, or $\bar{c_0} < 0$, then the model (3.7) has a unique positive endemic equilibrium.*

*ii. If $\omega > \omega_c$ or, $\bar{c_0} > 0$,$\bar{b} > 0$ then the model (3.7) has a unique positive endemic equilibrium for $\alpha > 0$.*

*iii. If $\omega > \omega_c$, $\bar{b} < 0$, and $\bar{b}^2 - 4\bar{a}\bar{c_0} > 0$, then there is a positive $\hat{\alpha} < \alpha_0$ such that $\mathcal{G}(\bar{I}, \alpha_1, \alpha)$ has a unique positive root if $\alpha > \hat{\alpha}$.*

In general, since $\mathcal{G}(\bar{I}, \alpha_1, \alpha)$ is a decreasing function of $\alpha$, $\lim_{\bar{I}\to 0^+} \mathcal{G}(\bar{I}, \alpha_1, 0) = 0$, and $\lim_{\bar{I}\to\infty} \mathcal{G}(\bar{I}, \alpha_1, \alpha) = \infty$, it follows that $\mathcal{G}(\bar{I}, \alpha_1, \alpha)$ has at least one positive root, and hence at least one endemic equilibrium always exists.

**Theorem 3.3.9.** *For system (3.7) the endemic equilibrium $(\bar{S}, \bar{V}, \bar{E}, \bar{I}, \bar{B})$ is globally asymptotically stable on the set $\Gamma$.*

**Proof** Let $\bar{\xi} = (\bar{S}, \bar{V}, \bar{E}, \bar{I}, \bar{B})$ denote the endemic equilibrium. Consider a Lyapunov function

$$L(x) = \bar{S}g(\frac{S}{\bar{S}}) + \bar{V}g(\frac{V}{\bar{V}}) + \bar{E}g(\frac{E}{\bar{E}}) + D\bar{I}g(\frac{I}{\bar{I}}) + \bar{B}g(\frac{B}{\bar{B}})$$

where $g(x) = x - 1 - \ln x$ and $D = \frac{\sigma+\mu}{\sigma}, \bar{\alpha} = \alpha_1 + \alpha_2 + \alpha_3 + \mu$.
Note that $L(x)$ is positive definite with respect to $\bar{\xi}$ because $\bar{x}g\left(\frac{x}{\bar{x}}\right)$ achieves a global minimum value of 0 at $x = \bar{x}$.

The derivative of $L$ along a solution $(S(t), V(t), E(t), I(t), B(t))$ of the system (3.7) is expressed as follows:

$$\frac{dL}{dt} = \left(1 - \frac{\bar{S}}{S}\right)\frac{dS}{dt} + \left(1 - \frac{\bar{V}}{V}\right)\frac{dV}{dt} + \left(1 - \frac{\bar{E}}{E}\right)\frac{dE}{dt} + D\left(1 - \frac{\bar{I}}{I}\right)\frac{dI}{dt} + \left(1 - \frac{\bar{B}}{B}\right)\frac{dB}{dt}. \tag{3.25}$$

To establish the characteristics of a Lyapunov function for which $\frac{dL}{dt} \leq 0$, we consider each terms in (3.25) independently then sum them up.

By the first equations in (3.7) and (3.21), it follows that

$$\begin{aligned}\left(1-\frac{\bar{S}}{S}\right)\frac{dS}{dt} &= \left(1-\frac{\bar{S}}{S}\right)(-\alpha_1\bar{B}+\beta\bar{S}\bar{I}+(\omega+\mu)\bar{S}-\beta SI-(\omega+\mu)S)\\ &= \left(1-\frac{\bar{S}}{S}\right)(\alpha_1(B-\bar{B})+\beta\bar{S}\bar{I}(1-\frac{SI}{\bar{S}\bar{I}})+(\omega+\mu)\bar{S}(1-\frac{S}{\bar{S}})), \text{Since} \quad B\le\frac{\kappa}{\bar{\alpha}}=\bar{B}\\ &\le \beta\bar{S}\bar{I}\left(1-\frac{SI}{\bar{S}\bar{I}}-\frac{\bar{S}}{S}+\frac{I}{\bar{I}}\right)-(\omega+\mu)\frac{(S-\bar{S})^2}{S}.\end{aligned} \tag{3.26}$$

By the second equations in (3.7) and (3.21), it follows that

$$\begin{aligned}\left(1-\frac{\bar{V}}{V}\right)\frac{dV}{dt} &= \left(1-\frac{\bar{V}}{V}\right)(-\omega\bar{S}+\epsilon\beta\bar{V}\bar{I}+\mu\bar{V}+\omega S-\epsilon\beta VI-\mu V)\\ &= -\omega\bar{S}\left(1-\frac{S}{\bar{S}}-\frac{\bar{V}}{V}+\frac{\bar{V}S}{V\bar{S}}\right)+\epsilon\beta\bar{V}\bar{I}\left(1-\frac{\bar{V}}{V}+\frac{I}{\bar{I}}-\frac{VI}{\bar{V}\bar{I}}\right)-\mu\frac{(V-\bar{V})^2}{V}.\end{aligned} \tag{3.27}$$

Similarly, by (3.7) and endemic equilibrium equations in (3.21), we have

$$\begin{aligned}\left(1-\frac{\bar{E}}{E}\right)\frac{dE}{dt} &= \left(1-\frac{\bar{E}}{E}\right)(\beta SI+\epsilon\beta VI+\alpha_2 B-(\sigma+\mu)E), \text{Since} \quad B\le\bar{B}\\ &\le \beta SI+\epsilon\beta VI+\alpha_2\bar{B}-(\sigma+\mu)E-\alpha_2\bar{B}\frac{\bar{E}}{E}-(\beta SI+\epsilon\beta VI)\frac{\bar{E}}{E}+(\sigma+\mu)\bar{E}\\ &= \beta\bar{S}\bar{I}\left(1+\frac{SI}{\bar{S}\bar{I}}-\frac{SI\bar{E}}{\bar{S}\bar{I}E}\right)+\epsilon\beta\bar{V}\bar{I}\left(1+\frac{VI}{\bar{V}\bar{I}}-\frac{VI\bar{E}}{\bar{V}\bar{I}E}\right)+\alpha_2\bar{B}(2-\frac{\bar{E}}{E})-(\sigma+\mu)\bar{E}\frac{\bar{E}}{E},\end{aligned} \tag{3.28}$$

$$\begin{aligned}D\left(1-\frac{\bar{I}}{I}\right)\frac{dI}{dt} &= D\left(1-\frac{\bar{I}}{I}\right)(\sigma E+\alpha_3 B-(\delta+\gamma+\mu)I), \text{Since} \quad B\le\bar{B}\\ &\le D(\sigma E+\alpha_3\bar{B}-(\delta+\gamma+\mu)I-\sigma E\frac{\bar{I}}{I}-\alpha_3\bar{B}\frac{\bar{I}}{I}+(\delta+\gamma+\mu)\bar{I})\\ &= D\sigma\bar{E}\frac{E}{\bar{E}}-D(\delta+\gamma+\mu)\bar{I}\frac{I}{\bar{I}}+D\alpha_3\bar{B}(2-\frac{\bar{I}}{I})+D\sigma\bar{E}\left(1-\frac{E\bar{I}}{\bar{E}I}\right)\\ &= (\alpha_2\bar{B}+\beta\bar{S}\bar{I}+\epsilon\beta\bar{V}\bar{I})\frac{E}{\bar{E}}-D(\delta+\gamma+\mu)\bar{I}\frac{I}{\bar{I}}+D\alpha_3\bar{B}(2-\frac{\bar{I}}{I})\\ &+(\alpha_2\bar{B}+\beta\bar{S}\bar{I}+\epsilon\beta\bar{V}\bar{I})\left(1-\frac{E\bar{I}}{\bar{E}I}\right).\end{aligned} \tag{3.29}$$

Since $D=\frac{\sigma+\mu}{\sigma}$, we have used relation $D\sigma\bar{E}=\alpha_2\bar{B}+\beta\bar{S}\bar{I}+\epsilon\beta\bar{V}\bar{I}$.

From the fifth equation in (3.7), we have

$$\begin{aligned}\left(1-\frac{\bar{B}}{B}\right)\frac{dB}{dt} &= \left(1-\frac{\bar{B}}{B}\right)(\bar{\alpha}\bar{B}-\bar{\alpha}B)\\ &= -\bar{\alpha}\frac{(B-\bar{B})^2}{B}.\end{aligned} \tag{3.30}$$

Substituting (3.26)- (3.30) into (3.25) and rearranging terms, we obtain

$$\begin{aligned}\frac{dL}{dt} \leq & -(\omega+\mu)\frac{(S-\bar{S})^2}{S} - \mu\frac{(V-\bar{V})^2}{V} - \bar{\alpha}\frac{(B-\bar{B})^2}{B} \\ & + \beta\bar{S}\bar{I}\left(3 - \frac{\bar{S}}{S} - \frac{E\bar{I}}{\bar{E}I} - \frac{S\bar{E}I}{\bar{S}E\bar{I}}\right) + \epsilon\beta\bar{V}\bar{I}\left(3 - \frac{\bar{V}}{V} - \frac{E\bar{I}}{\bar{E}I} - \frac{V\bar{E}I}{\bar{V}E\bar{I}}\right) \\ & - \omega\bar{S}\left(1 - \frac{S}{\bar{S}} - \frac{\bar{V}}{V} + \frac{\bar{V}S}{V\bar{S}}\right) + (\beta\bar{S}\bar{I} + \epsilon\beta\bar{V}\bar{I})\left(\frac{I}{\bar{I}} + \frac{E}{\bar{E}}\right) \\ & - (\sigma+\mu)\bar{E}\frac{E}{\bar{E}} + \alpha_2\bar{B}\left(3 - \frac{\bar{E}}{E} + \frac{E}{\bar{E}} - \frac{E\bar{I}}{\bar{E}I}\right) - D(\delta+\gamma+\mu)I \\ & + D\alpha_3\bar{B}\left(2 - \frac{\bar{I}}{I}\right).\end{aligned} \tag{3.31}$$

From (3.21), we have the relations:

$$\begin{cases}\beta\bar{S}\bar{I} + \epsilon\beta\bar{V}\bar{I} = (\sigma+\mu)\bar{E} - \alpha_2\bar{B}, \\ D\sigma\bar{E} = (\delta+\gamma+\mu)\bar{I} - \alpha_3\bar{B} \\ \qquad\quad = (\sigma+\mu)\bar{E}.\end{cases}$$

Thus, the inequality in (3.31) becomes:

$$\begin{aligned}\frac{dL}{dt} \leq & -(\omega+\mu)\frac{(S-\bar{S})^2}{S} - \mu\frac{(V-\bar{V})^2}{V} - \bar{\alpha}\frac{(B-\bar{B})^2}{B} \\ & + \beta\bar{S}\bar{I}\left(3 - \frac{\bar{S}}{S} - \frac{E\bar{I}}{\bar{E}I} - \frac{S\bar{E}I}{\bar{S}E\bar{I}}\right) + \epsilon\beta\bar{V}\bar{I}\left(3 - \frac{\bar{V}}{V} - \frac{E\bar{I}}{\bar{E}I} - \frac{V\bar{E}I}{\bar{V}E\bar{I}}\right) \\ & - \omega\bar{S}\left(1 - \frac{S}{\bar{S}} - \frac{\bar{V}}{V} + \frac{\bar{V}S}{V\bar{S}}\right) + \alpha_2\bar{B}\left(3 - \frac{\bar{E}}{E} - \frac{I}{\bar{I}} - \frac{E\bar{I}}{\bar{E}I}\right) \\ & + D\alpha_3\bar{B}\left(2 - \frac{I}{\bar{I}} - \frac{\bar{I}}{I}\right).\end{aligned}$$

By the inequality of arithmetic and geometric means:

$$x_1 + x_2 + ... + x_n \geq n(x_1x_2...x_n)^{\frac{1}{n}}, \quad \forall x_i \geq 0$$

and since $S \geq \bar{S}$ all the model parameters are non-negative, it follows that $L' \leq 0$. As a result, $L' = 0$ holds only at $\xi^{**}$, and $L'$ is negative definite with respect to $\bar{\xi}$. Standard Lyapunov stability theorem implies that $\bar{\xi}$ is locally asymptotically stable and globally attracting in $\Gamma$. The global stability of $\bar{\xi}$ also implies that $\bar{\xi}$ is unique in $\Gamma$.

## 3.4 Parameter Estimation

In this study, we estimate the parameters in the system (3.7) using monthly PPR disease incidence data that span from January 2019 to August 2022 in the Amhara regional state, Ethiopia. Data were acquired through a filtering process that specifically targeted the incidence of PPR within the Amhara region, using the Ethiopian National Animal Disease Surveillance System

(NADSS). In particular, the data were sourced from the monthly disease outbreak and vaccination activity reporting (DOVAR), which operates under the authorization of the Minister of Agriculture. Furthermore, we incorporated data on the death rate attributable to PPR from the World Organization for Animal Health (WOAH) dashboard (WOAH, 2023), which provided summarized data for reporting purposes. To estimate the recruitment rate through birth and the total population, we relied on data obtained from the Ethiopian Central Statistical Agency (CSA) for the year 2021/2022 ((CSA), 2021).

The primary objective of this study is to determine the optimal parameters that allow our model (3.7) to be best aligned with the available data. To achieve this, we employ the nonlinear least-squares approximation method, which aims to minimize the sum of squared errors.

$$SSE = \sum_{j=1} (I_j - I^*(t_j))^2 \tag{3.32}$$

where $I_j$ is the prevalence data and $I^*(t_j) = E(t) + I(t)$ is the simulation result (predicted) at time step j of prevalence of PPR. We used the initial value $(S_0, V_0, E_0, I_0, B_0, R_0) = (14063965, 3000000, 10, 684, 10000, 100)$, while all estimated parameter values are listed in Table (3.2) and the visualization of the result is shown in Figure (5.2A). The blue curve represents the simulation result of $I^*(t)$ from the model (3.7), while the red dot is monthly prevalence data of PPR disease from January 2019 to Aug. 2022. Figure (3.3B) illustrates the residuals between the predicted and observed data.

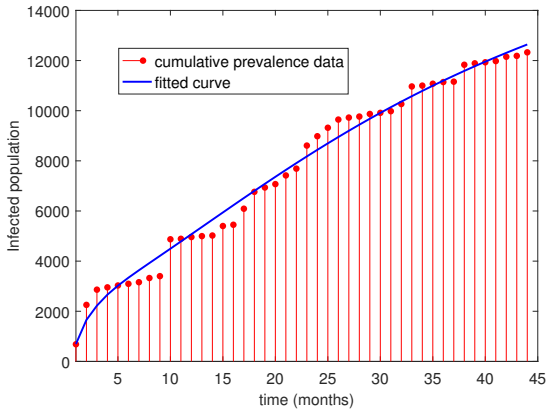


(A) The fitted curve (blue solid line) and observed data (red dots)

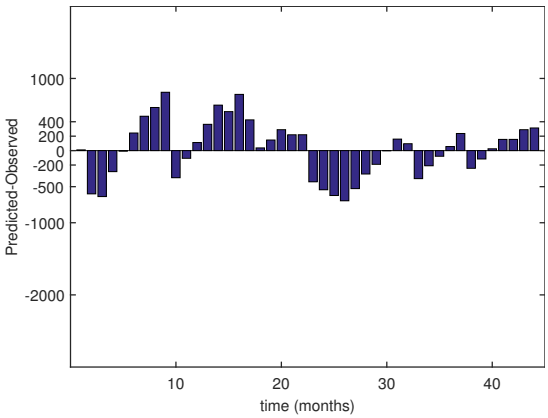


(B) Residual of predicted and observed data

FIGURE 3.3: Comparison between the monthly prevalence of PPR disease data and simulation $I^*(t)$ with their residual

TABLE 3.2: Parameter Values from Estimation, Literature Sources, and Assumptions for the Case of Zero Infective Restocked Animals

| Parameter | Value (unit of per month) with CI | Source |
|---|---|---|
| $\beta$ | 2.0914e-7 (CI:1.8985e-7 2.2843e-7) | Estimated |
| $\sigma$ | 0.6058 (CI:0.5747 1.7864) | Estimated |
| $\gamma$ | 0.4753 (CI:0.0615 1.5664) | Estimated |
| $\mu$ | 0.0527 | (CSA), 2021 |
| $\omega$ | 0.5694 (CI:0.3328 1.8072) | Estimated |
| $\delta$ | 0.3 | WOAH, 2023 |
| $\kappa$ | 224674 | (CSA), 2021 |
| $\alpha_1$ | 0.01 | Assumption |
| $\Lambda$ | 645990 | Estimated |
| $\rho$ | 0.1681 | Assumption |
| $\epsilon$ | 0.3 | Fournié et al., 2018 |

Using the parameters in Table (3.2), we estimated the control reproduction number ($\mathcal{R}_v$) for PPR in the Amhara region of Ethiopia, producing a value of 1.0518. Under the assumption of zero influx of infectious restocked small ruminants and a newborn vaccination rate of 16.8%, the analysis predicts that PPR will remain an endemic disease in the Amhara region in the absence of better management efforts.

## 3.5 Sensitivity Analysis

In order to assess the model's resistance to different parameter values, a sensitivity analysis was conducted. Understanding the relative roles played by various model parameters in the occurrence and spread of a given disease is vital. This understanding helps us identify where interventions should be focused to reduce disease-related mortality and morbidity. Several parameters contribute to ($\mathcal{R}_v$) in the case of small ruminants with zero restocked infectious ($\alpha_2 = \alpha_3 = 0$), as illustrated in equation (3.10). Consequently, a sensitivity analysis was performed in ($\mathcal{R}_v$) to identify key variables that can limit the spread of PPR. To measure the relative change in the model parameter $p$ relative to the relative change in ($\mathcal{R}_v$), a forward normalized sensitivity index denoted $\gamma_p^{\mathcal{R}_v}$ was used. This index is defined using partial derivatives if ($\mathcal{R}_v$) is a differentiable function of the model parameter $p$. The specific definition of this index can be found in (Sanchez et al., 1997). It can be expressed as:

$$\gamma_p^{\mathcal{R}_v} = \frac{\partial \mathcal{R}_v}{\partial p} \times \frac{p}{\mathcal{R}_v}, \tag{3.33}$$

where $\gamma_p^{\mathcal{R}_v}$ is the sensitivity index (SI) of ($\mathcal{R}_v$) with respect to parameter p, hence we evaluate the sensitivity indices of these parameters at the parameter values as given in Table (3.3). For

example, using the definition in (3.33), the sensitivity index of $\mathcal{R}_v$ with respect to $\beta$ is given by

$$\gamma_{\beta}^{\mathcal{R}_v} = \frac{\partial \mathcal{R}_v}{\partial \beta} \times \frac{\beta}{\mathcal{R}_v} = 1.$$

This can be interpreted as increasing (or decreasing) the transmission rate $\beta$ by 10%, increasing (or decreasing) $\mathcal{R}_v$ by 10%. In the same way, increasing (or decreasing) vaccination efficacy $(1-\epsilon)$, decreases (or increases) $\mathcal{R}_v$, by 7.9%. In general, the positive sign sensitivity indices in Table (3.3) imply that the value of $\mathcal{R}_v$ increases with increase, whereas the negative sign sensitivity indices show that the value of $\mathcal{R}_v$ decreases with increase.

TABLE 3.3: Sensitivity indices of $\mathcal{R}_v$ for the PPR model (3.7) with $(\alpha_2 = \alpha_3 = 0)$.

| Parameters: | $\beta$ | $\mu$ | $\sigma$ | $\gamma$ | $\alpha_1$ | $\rho$ | $\epsilon$ | $\delta$ | $\kappa$ | $\omega$ |
|---|---|---|---|---|---|---|---|---|---|---|
| Index sign: | + | - | + | - | + | - | + | - | + | - |
| SI values: | 1.000 | 1.0586 | 0.0800 | 0.5740 | 0.0454 | 0.0270 | 0.7964 | 0.3623 | 0.0539 | 0.1304 |

Based on the results of the sensitivity analysis presented in Table (3.3), it is evident that enhancing the efficacy of the vaccine, reducing the transmission rate, and mitigating susceptibility resulting from restocking are all effective measures in preventing the spread of PPR disease. Furthermore, this finding is supported and verified in the numerical simulation section.

## 3.6 Numerical Simulation

In this section, we examined the effects of parameter values on the dynamics of PPR and validated the analytical results using numerical methods. For numerical simulations, we used the parameter values specified in Table (3.2).

### 3.6.1 Effects of Vaccination ($\rho$ and $\omega$) on the Dynamics of PPR

Given that the efficacy of the vaccine at both the regional and national levels falls within the range of $60-80\%$ (Waret-Szkuta et al., 2008; Fournié et al., 2018), or equivalently, $\epsilon$ lies within the range of $0.2-0.4$. In particular $\epsilon = 0.35$, we can determine the critical value related to the vaccine from Remark (3.3.3)(i) as $\epsilon_c = 1/\mathcal{R}_0 = 0.3326$ (that is, $\epsilon > \epsilon_c$). Figure (3.4A) presents a 3D plot of $\mathcal{R}_v$ in the $\rho\omega$-$\mathcal{R}_v$ plane, consistently positioned above the plane $\mathcal{R}_v = 1$. This observation indicates that $\mathcal{R}_v$ never falls below 1. Consequently, despite the high levels of vaccination considered and the absence of infectious restocking of small ruminants, the PPR disease will persist in the small ruminant population.

Furthermore, for $\epsilon = 0.2 (< \epsilon_c)$, it is observed that the trajectory of $\mathcal{R}_v$ intersects the plane $\mathcal{R}_v = 1$. This can be seen in Figure (3.4B). The simulation illustrates that with a combination of high efficacy and coverage of vaccination, the disease will eventually decline within the population (i.e., $\mathcal{R}_v < 1$). Therefore, this numerical result provides empirical validation for the influence of $\epsilon$, as demonstrated by the sensitivity index.

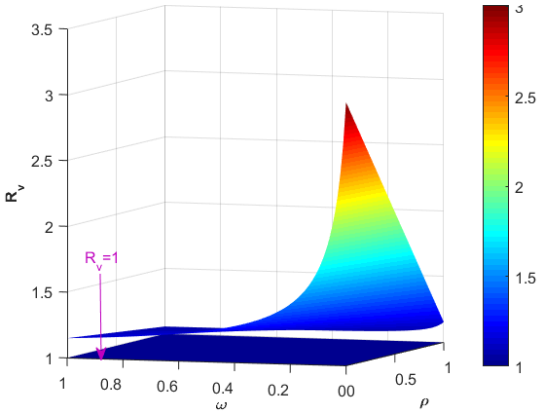


(A) Effects of newborn vaccination ($\rho$) and susceptible vaccination ($\omega$) on $R_v$ when $\epsilon = 0.35$

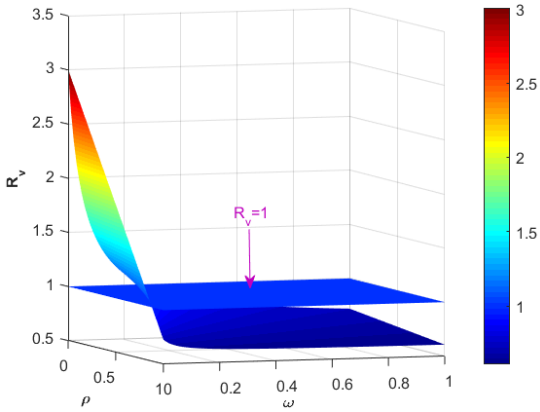


(B) Effects of newborn vaccination ($\rho$) and susceptible vaccination ($\omega$) on $R_v$ when $\epsilon = 0.2$

FIGURE 3.4: 3D-plots to show the effects of $\omega, \rho, \epsilon$ on $\mathcal{R}_v$

### 3.6.2 Effects of Transmission Rate ($\beta$) and Fraction of Restocked Susceptible Population ($\alpha_1$)

We present a discussion on the influence of $\beta$ and $\alpha_1$ on the dynamics of the infectious class $I$, as depicted in Figure (3.5A). Through an examination of various values for $\beta$ and $\alpha_1$, we demonstrate the impact on the reproduction number. The figure clearly illustrates that an increase in both $\alpha_1$ and $\beta$ corresponds to an increase in the reproduction number, with the trajectory of $\mathcal{R}_v$ intersecting the plane $\mathcal{R}_v = 1$. Notably, at $(\alpha_1 = 0.01, \beta = 2.0e-7)$, the trajectory coincides with $\mathcal{R}_v = 1$, indicating that the disease will cease to propagate when $\beta < 2.0e-7$, while it will persist if $\beta > 2.0e-7$. Additionally, we have substantiated this result through a time series plot of the infection class in Figure (3.5B). The analysis of forward bifurcation reveals that even a minor change or increment in the transmission rate can lead to significant alterations in the dynamics of the disease.

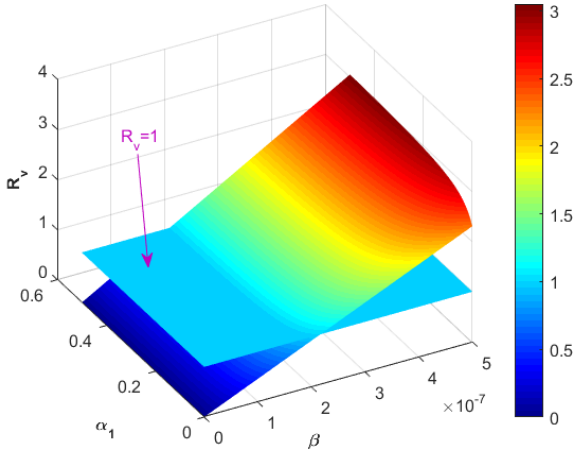


(A) Effects of $\alpha_1$ and $\beta$ on $R_v$.

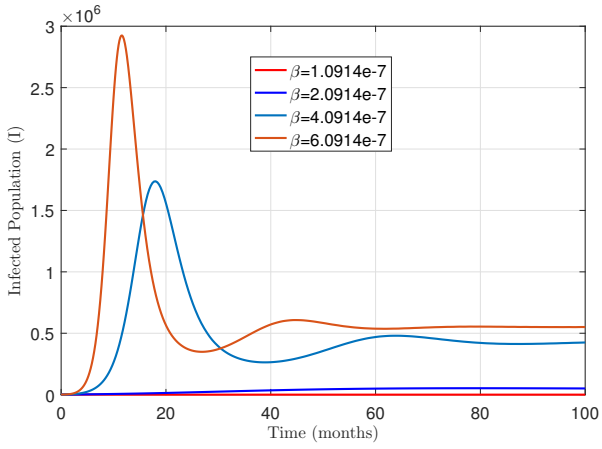


(B) Effects of different transmission rate on $I$.

FIGURE 3.5: Effects of fraction of susceptible restocked animal ($\alpha_1$) and transmission rate on the dynamics of PPR in the case of $\alpha_2 = \alpha_3 = 0$.

### 3.6.3 Interplay between Restocking and Vaccination in the PPR Dynamics

To support the analytic results, we consider the parameter values presented in Table 3.2. We investigated the effects of values of $\epsilon$ in the range; $\epsilon = (0.1, 0.4)$, while considering different initial conditions (IC) for the model. The IC values are as follows:

$$\begin{cases} \mathrm{IC}_1 = (13009000, 3000000, 200, 600, 100, 100), \\ \mathrm{IC}_2 = (12009000, 4000000, 100, 600, 150, 150), \\ \mathrm{IC}_3 = (10008000, 6000000, 400, 600, 800, 200), \\ \mathrm{IC}_4 = (14006000, 2000000, 500, 500, 2000, 1000), \\ \mathrm{IC}_5 = (11009000, 5000000, 300, 500, 150, 50). \end{cases} \tag{3.34}$$

In Figure 3.6A, we observe that the trajectory of the infectious variable $I$ in the time series plot converges to the endemic equilibrium $I^* = 1.338 \times 10^5$ with a vaccination efficacy of $1-\epsilon = 0.65$, assuming the absence of infection inflow from the restocked class. This result verifies the findings of Remark 3.3.3(i) and Theorem 3.3.6. Moreover, when there is less loss of immunity, that is, efficiency $1 - \epsilon = 0.8$ (80%), the dynamics of the disease change significantly and the trajectory of $I$ converges to the disease-free equilibrium (I=0), as shown in Figure 3.6B.

Furthermore, in Figure (3.6C), we notice the presence of infective inflow through restocking (i.e., $\alpha_1 = 0.01, \alpha_{2,3} = 0.01$) results in the existence of a globally stable endemic state $\bar{I} = 1634$, even when high efficacy vaccination ($\epsilon = 0.1$) and a vaccination coverage rate of $\omega = 56.9\%$ of the susceptible population are applied. This result indicates that the introduction of infective individuals through restocking facilitates the persistence of the PPR virus in the region. Therefore, additional control mechanisms must be implemented alongside vaccination. However, vaccination campaigns should be strengthened with high efficiency to reduce the burden of PPR in the region.

In Figure (3.6D), it can be observed that there is a high flow of small infectious ruminants. This is indicated by the fact that $\omega > \omega_c$ and $\bar{b} > 0$, as derived from the result presented in Theorem 3.3.8 (ii). As a consequence, all the state variables in the model (3.9) converge to the endemic equilibrium $\bar{\xi} = (8.562\times10^5, 8.616\times10^6, 4.320\times10^5, 3.990\times10^5, 3.605\times10^6, 3.442\times10^5)$. This outcome of the simulation is consistent with the findings stated in Theorem 3.3.8.

Figure (3.6E) illustrates the impact of restocking on the dynamics of PPR by considering different combinations of $\alpha_i$ values, where $i = 1, 2, 3$. It can be observed that as the total fraction of infective restocked population increases, the infection population also increases within the small ruminant population. This emphasizes the significance of restocking in influencing the spread of PPR.

In Figure (3.7), we present a $3 \times 3$ subplot layout to examine the interaction between vaccination efficacy and restocking dynamics during disease outbreaks. Each column focuses on the effects of restocking parameters $(\alpha_1, \alpha_2, \alpha_3)$, with each row representing increasing levels of vaccination efficacy. Each subfigures displays varying restocking levels. In the first column, the subfigures (3.7(a),3.7(b) and 3.7(c)) illustrate the effect of $\alpha_1$. Results indicate that higher values of $\alpha_1$ increase the infection peak, as more susceptible ruminants are available for the disease to spread, particularly when vaccination efficacy is low. However, with high vaccination

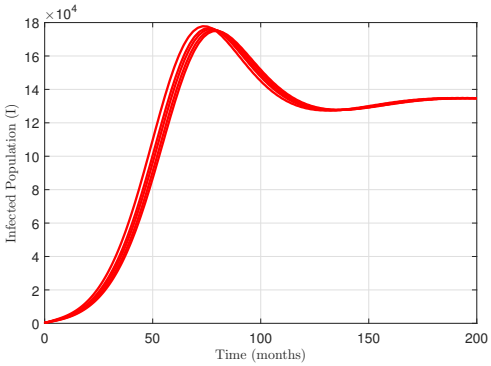


(A) Time series plot of I with $\epsilon = 0.35, \alpha_1 = 0.01, \alpha_2 = \alpha_3 = 0$

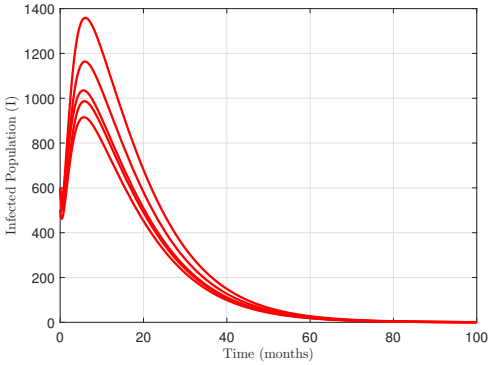


(B) Time series plot of I with $\epsilon = 0.2, \alpha_1 = 0.01, \alpha_2 = \alpha_3 = 0$

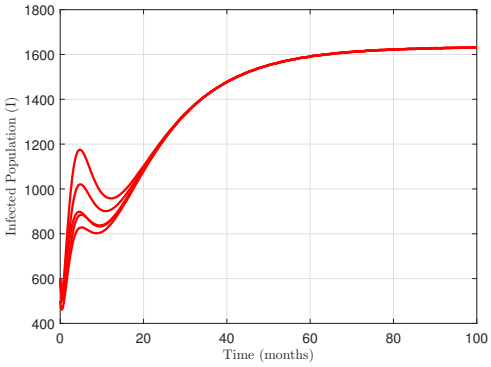


(C) Time series plot of I with $\epsilon = 0.1, \alpha_1 = 0.01, \alpha_2 = \alpha_3 = 0.0001$

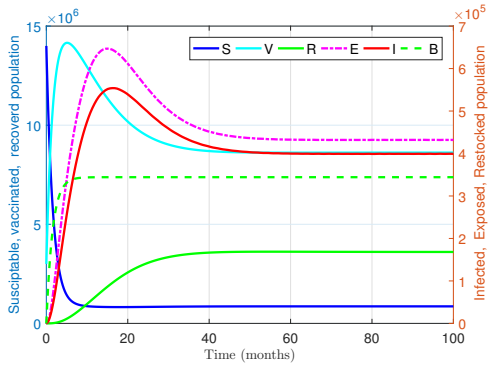


(D) Time series plot of all state variable with $\epsilon = 0.2, \alpha_1 = \alpha_2 = \alpha_3 = 0.2$

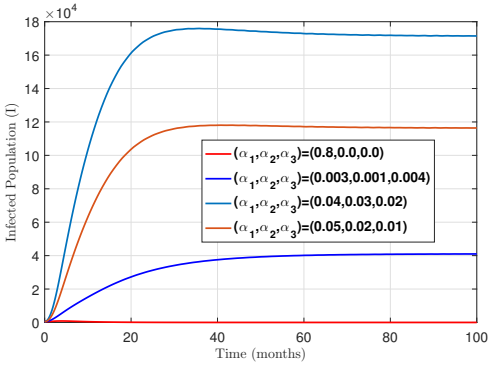


(E) Trajectories of I with different combinations of values of $\alpha_i, i = 1, 2, 3$

FIGURE 3.6: Simulation results to show effects of $\epsilon$ and $\alpha$ on I

efficacy, the impact of $\alpha_1$ is reduced. The effects of $\alpha_2$ and $\alpha_3$ are illustrated in the subfigures located in the second and third columns, respectively. The infection peaks are notably higher with increased values of $\alpha_2$ and $\alpha_3$, as demonstrated in Figures (3.7d-3.7i), thereby extending the duration of the outbreak. Although high vaccination efficacy reduces the number of infections, it cannot completely eliminate the disease. This underscores the need for additional interventions to control outbreaks due to the restocking of infected animals.

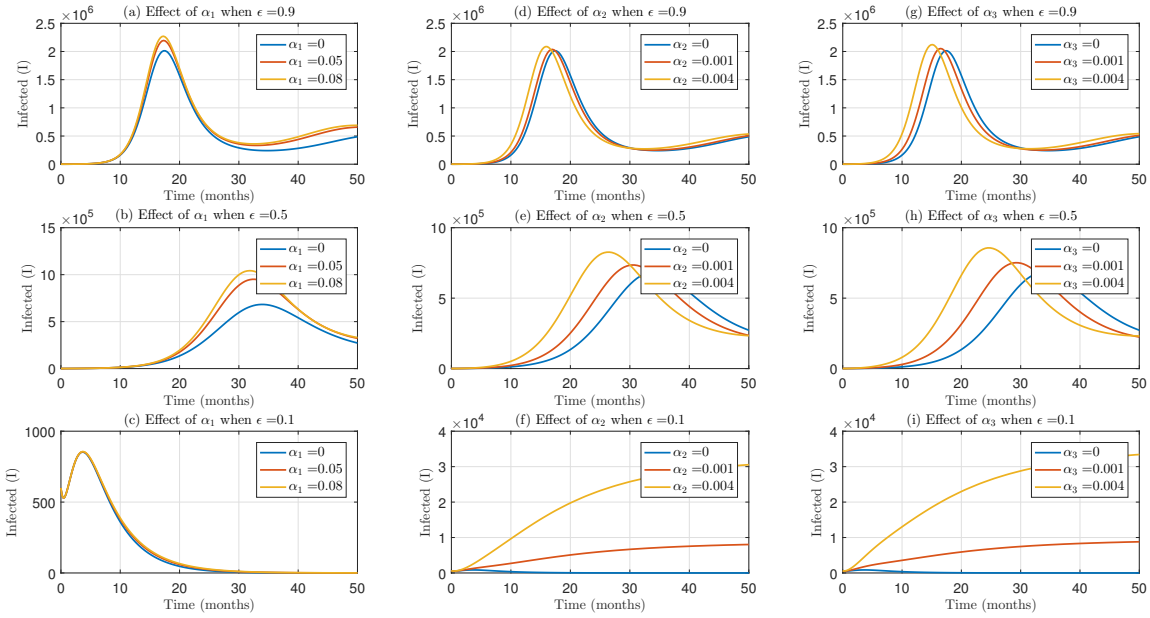


FIGURE 3.7: Interplay between restocking and vaccination in PPR disease

### 3.6.4 Numerical Verification of Global Stability of DFE and EEP

As indicated by the analytical results presented in Theorems (3.3.5 and 3.3.9), the global stability of both the disease-free equilibrium (DFE) and the endemic equilibrium points (EEP) offers valuable insights into the long-term behavior of PPR within the small ruminant population. It informs us whether the disease can be effectively controlled or is likely to persist and become endemic. A comprehensive understanding of the global stability of these equilibrium points plays a crucial role in interpreting the potential impact of interventions, evaluating the dynamics of disease transmission, and guiding strategies for disease prevention and control on a global scale. Considering various initial conditions specified in (3.34), numerical verification can be used to establish the global stability of disease-free equilibrium (DFE) and endemic equilibrium points (EEP) for the two models (3.7) and (3.9).

In Figure (3.8A), we present the dynamic trajectory of the model (3.9) with specific parameter values: $\epsilon = 0.3$, $\alpha_1 = 0.9$ and the remaining parameters listed in Table (3.2). The figure shows that the system (3.9) exhibits an endemic equilibrium $\xi^* = (S^*, V^*, E^*, I^*, B^*, R^*) = (1.106 \times 10^6, 1.066 \times 10^7, 3.623 \times 10^5, 2.651 \times 10^5, 2.358 \times 10^5, 2.393 \times 10^6)$, which is globally asymptotically stable. Similarly, Figure (3.8B) illustrates the behavior of model (3.9) with the

same parameter values, except for $\epsilon$ which is set to $\epsilon = 0.15$. In this case, the model exhibits a disease-free equilibrium $\xi_0 = (1.205 \times 10^6, 1.509 \times 10^7, 0, 0, 2.358 \times 10^5, 0)$, which is globally asymptotically stable for different initial values in (3.34). These results provide empirical support for the analytical findings presented in Theorem (3.3.5).

Furthermore, Figure (3.8C) indicates that the trajectories of the state variables in model (3.7) converge to a unique endemic equilibrium point $\bar{\xi} = (8.597 \times 10^5, 8.567 \times 10^6, 4.426 \times 10^5, 4.094 \times 10^5, 2.219 \times 10^5, 3.695 \times 10^6)$ where $\epsilon = 0.2$ and $\alpha_i = 0.32, i = 1, 2, 3$. Moreover, with the initial conditions specified in (3.34), this equilibrium point $\bar{\xi}$ is globally asymptotically stable. This numerical verification reinforces the result stated in Theorem (3.3.9).

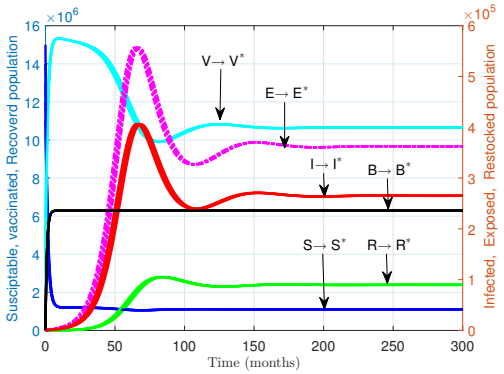


(A) Global stability of EEP $\xi^*$ with $\epsilon = 0.3, \alpha_1 = 0.9, \alpha_2 = \alpha_3 = 0$.

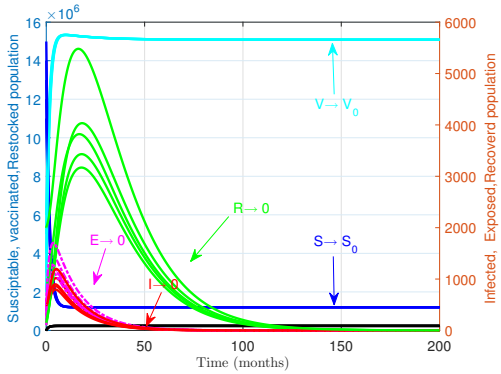


(B) Global stability of DFE $\xi_0$ with $\epsilon = 0.15, \alpha_1 = 0.9, \alpha_2 = \alpha_3 = 0$.

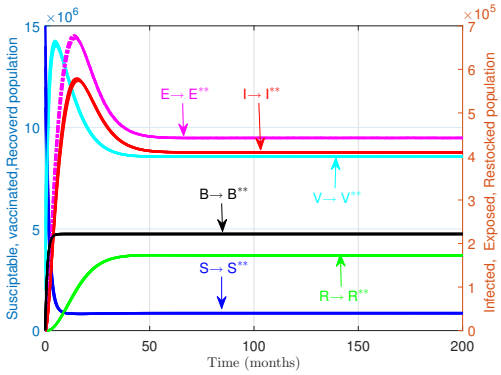


(C) Global stability of $\xi^{**} = \bar{\xi}$ with $\epsilon = 0.2, \alpha_1 = \alpha_2 = \alpha_3 = 0.32$.

FIGURE 3.8: Verification of Global stability using different initial conditions in (3.34).

## 3.7 Results and Discussion

Peste des petits ruminants (PPR) remains a significant endemic disease of small ruminants in Ethiopia, with outbreaks continuing despite the availability of effective vaccines. In this study, we developed a deterministic SEVIR epidemic model incorporating a restocked group to evaluate the impact of animal movement on disease persistence. Our analytical and numerical results reveal critical insights into the mechanisms sustaining PPR transmission in the Amhara region. In the absence of restocking, the basic reproduction number ($\mathcal{R}_v$) was estimated at 1.0518,

confirming the endemic status of PPR in the study area and indicating that achieving disease eradication would require maintaining vaccination coverage exceeding 89.6% a threshold highly sensitive to real-world constraints in vaccine supply, cold chain maintenance, and field efficacy. The disease-free equilibrium was globally asymptotically stable when $\mathcal{R}_v < 1$, while the endemic equilibrium was locally stable when $\mathcal{R}_v > 1$. However, the introduction of restocking fundamentally alters this disease landscape. When the influx of susceptible and infected animals from surrounding regions is considered, the system exhibits a unique endemic equilibrium that remains globally asymptotically stable, demonstrating that even with optimal vaccination coverage and efficacy, the continuous introduction of infected animals through restocking sustains disease transmission. This finding explains the observed paradox in PPR control: despite vaccination campaigns, outbreaks persist because traditional control strategies do not account for external sources of infection. Our results align with previous studies Fournié et al., 2018, which demonstrated that the Amhara region's highland sedentary systems interact with adjacent lowland pastoral areas that serve as viral reservoirs, with socioeconomic practices facilitating animal movement and further complicating control efforts. Evidence from seroprevalence studies (Fentie et al., 2018; Waret-Szkuta et al., 2008) supports our findings on disease epidemiology, though our mathematical modeling approach extends this understanding by predicting disease trends and simulating the intricate interaction between vaccination efforts and risk factors such as restocking. Several limitations warrant consideration, particularly the availability of relevant data that constrained parameter estimation, as well as the deterministic framework that does not capture stochastic fluctuations significant in smaller populations. Future studies should incorporate a broader spectrum of risk factors, investigate optimal control problems using different intervention strategies, and utilize stronger datasets for more extensive modeling. In conclusion, effective PPR control in the Amhara region requires integrated strategies that extend beyond vaccination to include rigorous pre-restocking evaluations and enhanced biosecurity measures. By implementing strong vaccination programs complemented by movement controls, we can considerably limit the impact of restocking on PPR dynamics and work toward the health of small ruminant populations in the region and at the national level.

# Chapter 4

# Infective Recruitment and Cost-Effective Optimal Control of PPR in Ethiopia

## 4.1 Introduction

The control and eventual eradication of Peste des Petits Ruminants (PPR) remain critical challenges in regions where small ruminant farming is a cornerstone of rural livelihoods and national economies. Despite the availability of safe and effective live attenuated vaccines, persistent outbreaks continue to undermine productivity and food security, particularly in Africa and Asia (Fathelrahman et al., 2021). In Ethiopia, recent surveillance data highlight the ongoing challenge, with new outbreaks reported annually despite national and international control initiatives.

Mathematical modeling has become an indispensable tool for understanding the transmission dynamics of animal diseases and for designing and evaluating control strategies. While early studies primarily addressed the epidemiological characteristics and seroprevalence of PPR (Ahaduzzaman, 2020; Waret-Szkuta et al., 2008; Balamurugan et al., 2014; Fentie et al., 2018), more recent work has emphasized the importance of incorporating risk factors such as animal movement, restocking practices, and spatial heterogeneity into disease models. For example, a two-patch deterministic model illuminated the impact of ruminant movement between ecological zones, underscoring the necessity of coordinated vaccination and movement control (Walle et al., 2025). Similarly, integrating vaccinated and restocked subpopulations into a SEIR framework demonstrated that vaccination alone may be insufficient for disease elimination without accompanying biosecurity and movement restrictions (Walle et al., 2024).

Metapopulation models have further highlighted the significance of vaccination coverage and spatial factors in endemic settings (Fournié et al., 2018), while cost-effectiveness analyses from other regions have reinforced the need for integrated approaches that combine vaccination with movement control for optimal outcomes (Fathelrahman et al., 2021). Despite these advances, there remains a notable gap concerning the development and analysis of optimal control strategies tailored specifically to PPR management, particularly in the context of restocking and imperfect vaccination.

Optimal control theory provides a rigorous mathematical framework for identifying intervention strategies that minimize both disease burden and associated costs. Its application to animal

diseases has yielded valuable insights, particularly in balancing resource allocation among competing interventions such as vaccination, treatment, and biosecurity measures (Makinde et al., 2011; Mushayabasa et al., 2011b; Nyerere et al., 2020b; Osman et al., 2020). However, the integration of restocking dynamics and the cost-effectiveness of combined interventions in the context of PPR have received limited attention.

In light of these gaps, this chapter develops and analyzes a deterministic optimal control model for PPR that explicitly incorporates infective recruits through restocking, along with time-dependent interventions: External and internal biosecurity measures, vaccination, and treatment. The model's structure allows for the evaluation of both the biological feasibility and stability of disease equilibria, the sensitivity of outcomes to key parameters, and the cost-effectiveness of alternative control strategies using empirical data from recent Ethiopian outbreaks. The optimal allocation of resources across interventions is studied via Pontryagin's maximum principle, with the goal of informing national strategies to meet the 2027 target for PPR eradication. Through this approach, the chapter aims to provide quantitative guidance for policymakers and practitioners, contributing to more effective and sustainable PPR control and eradication efforts in Ethiopia and similar settings.

## 4.2 Model Formulation

This section presents the formulation of a nonlinear epidemic model that incorporates a restocking effect. The homogeneous small ruminant population, denoted as $N(t)$, is categorized into different compartments: susceptible individuals $S(t)$, vaccinated individuals $V(t)$, exposed individuals $E(t)$, infectious individuals $I(t)$, and recovered individuals $R(t)$. As a result, the overall population can be expressed as follows:

$$N(t) = S(t) + V(t) + E(t) + I(t) + R(t).$$

We substitute $S, V, E, I, R$ for $S(t), V(t), E(t), I(t), and R(t)$, respectively, in order to simplify. The transmission diagram in Figure (4.1), which illustrates the population and explains the transmission and transition processes of our suggested model, is used to build the model.

Susceptible individuals are recruited at a rate $(1 - (\alpha_1 + \alpha_2))\Lambda$ where $\alpha_1$ and $\alpha_2$ are the fractions of infected (exposed) and infectious restocked small ruminants into the population respectively and $\Lambda$ is the recruitment rate through birth and restocking. The susceptible population acquires PPR infection due to effective contact with PPR-infected ruminants at a mass action incidence rate $\beta SI$, where $\beta$ is the disease transmission rate relative to infected ruminants in the I(t) class. This population is decreased by vaccination at the rate $\omega$ and natural death at the rate $\mu$.

We suppose that a fraction of susceptible small ruminants receive vaccinations at a rate of $\omega$ and become members of the vaccinated class to characterize the vaccination class. Inadequate vaccination delivery might cause small ruminants to lose their immunity in addition to being vaccinated. Nonetheless, there is a chance that this immunization will lessen the likelihood of an infection being successful by $\epsilon$. Small ruminants are perfectly protected from PPR by the vaccine if $\epsilon = 0$, and vice versa if $\epsilon = 1$. The natural death rate ($\mu$) lowers this population.

The population in the exposed compartment is generated following the infection of susceptible and vaccinated ruminants after getting an infection when interacting with PPRV-infected ruminants. The population is reduced by the transfer rate $\sigma$ (incubation period of $1/\sigma$) to the infected class and the natural death rate $\mu$. Furthermore, a fraction $\alpha_1$ of the recruitment rate $\Lambda$ restocked ruminants move into the exposed class.

The infected ruminants are decreased by the natural death rate $\mu$ and rate of death induced by the disease $\delta$ and increased by a constant flow from restocking with a fraction $\alpha_1$ of the recruitment rate $\Lambda$ in unit time. This class is further decreased by moving the individuals to the recovered class at the rate $\gamma$.

The recovered class is generated through transfer rates $\gamma$ and is subject to reduction by the natural death rate $\mu$. It is assumed that animals infected with the Peste des Petits Ruminants (PPR) acquire lifelong immunity upon recovery from the disease.

Based on the above assumptions of the model and Figure 4.1, the proposed model is given as follows:

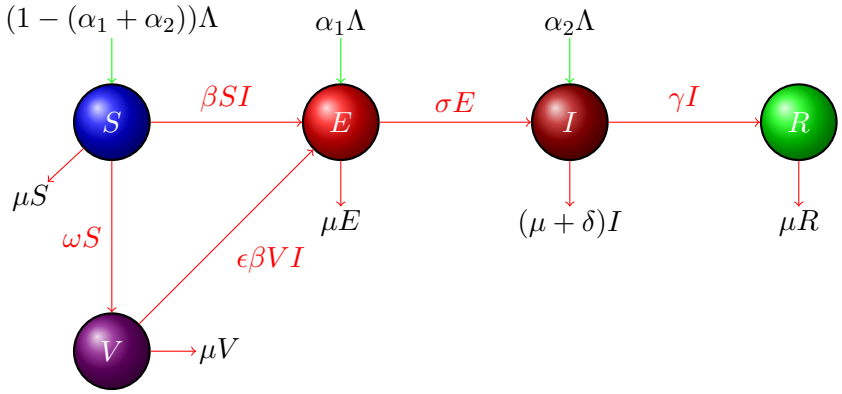


FIGURE 4.1: The Compartmental diagram for PPR disease transmission model (4.1)

$$\begin{cases} \dfrac{dS}{dt} = (1-(\alpha_1+\alpha_2))\Lambda - \beta SI - (\mu+\omega)S, \\ \dfrac{dV}{dt} = \omega S - \epsilon\beta VI - \mu V, \\ \dfrac{dE}{dt} = \alpha_1\Lambda + \beta I(\epsilon V + S) - (\sigma+\mu)E, \\ \dfrac{dI}{dt} = \alpha_2\Lambda + \sigma E - (\mu+\delta+\gamma)I, \\ \dfrac{dR}{dt} = \gamma I - \mu R \end{cases} \tag{4.1}$$

with the initial conditions $S(0) \geq 0, V(0) \geq 0, E(0) \geq 0, I(0) > 0, R(0) \geq 0$, and assumption $0 \leq \alpha_1, \alpha_2, \alpha_1+\alpha_2 < 1$.

To ensure that the overall host population remains confined, all parameters in Equation (4.1) are constrained to non-negative values. Table (4.1) outlines the biological significance of each parameter.

## 4.3 Model Analysis

### 4.3.1 Well-Posedness of the Model

In this section, it is crucial to demonstrate the existence of a non-negative solution, uniqueness, and boundedness of solution to the model (4.1) for mathematical and epidemiological interpretation.

**Lemma 4.3.1.** *For any initial condition*

$$(S_0, V_0, E_0, I_0, R_0) \in \mathbb{R}^5_+,$$

*system* (4.1) *admits a unique solution*

$$\big(S(t), V(t), E(t), I(t), R(t)\big)$$

*defined for all* $t \geq 0$ *that satisfies the initial conditions, remains nonnegative, and is bounded for all* $t \geq 0$. *Moreover, the feasible region*

$$\Gamma = \left\{(S, V, E, I, R) \in \mathbb{R}^5_+ : \ N(t) = S + V + E + I + R \leq \frac{\Lambda}{\mu}\right\}$$

*is positively invariant with respect to* (4.1).

**Proof** Let

$$x(t) = \begin{pmatrix} S(t) \\ V(t) \\ E(t) \\ I(t) \\ R(t) \end{pmatrix}, \qquad x_0 = \begin{pmatrix} S_0 \\ V_0 \\ E_0 \\ I_0 \\ R_0 \end{pmatrix} \in \mathbb{R}^5_+.$$

Write system (4.1) in the vector form

$$\frac{dx}{dt} = f(x), \qquad x(0) = x_0, \tag{4.2}$$

where $f : \mathbb{R}^5 \to \mathbb{R}^5$ is given by the right-hand sides of the compartmental equations. Each component of $f$ is a polynomial in the state variables; hence $f \in C^1(\mathbb{R}^5)$ and therefore $f$ is locally Lipschitz on $\mathbb{R}^5$. By the Picard–Lindelöf theorem there exists a unique solution $x(t)$ on a maximal interval $[0, t_{\max})$.

Next we show nonnegativity. Consider the closed set

$$D = \mathbb{R}^5_+ = \{(S, V, E, I, R) \in \mathbb{R}^5 : \ S \geq 0, \ V \geq 0, \ E \geq 0, \ I \geq 0, \ R \geq 0\}.$$

It suffices to check that for every boundary point $x \in \partial D$, the vector field $f$ points into $D$ or is tangent to $\partial D$; equivalently, whenever a coordinate $x_i = 0$ we have $f_i(x) \geq 0$.

Denote the components of $f$ by $f_1, f_2, f_3, f_4, f_5$ corresponding respectively to $S, V, E, I, R$. On the boundary where the indicated coordinate vanishes we have:

If $S = 0$, then

$$f_1(x) = \frac{dS}{dt} = (1 - (\alpha_1 + \alpha_2))\Lambda \geq 0,$$

because $0 \leq \alpha_1 + \alpha_2 \leq 1$.

If $V = 0$, then

$$f_2(x) = \frac{dV}{dt} = \omega S \geq 0,$$

since $S \geq 0$.

If $E = 0$, then

$$f_3(x) = \frac{dE}{dt} = \alpha_1\Lambda + \beta I(\varepsilon V + S) \geq 0,$$

because $\alpha_1 \geq 0$, $\beta \geq 0$, $\varepsilon \geq 0$ and $S, V, I \geq 0$.

If $I = 0$, then

$$f_4(x) = \frac{dI}{dt} = \alpha_2\Lambda + \sigma E \geq 0,$$

since $\alpha_2 \geq 0$, $\sigma \geq 0$, $E \geq 0$.

If $R = 0$, then

$$f_5(x) = \frac{dR}{dt} = \gamma I \geq 0,$$

because $\gamma \geq 0$ and $I \geq 0$.

Thus $f$ points inward or is tangent on $\partial D$. By the invariance theorem (see Thieme, 2018, Theorem A.4) the set $D = \mathbb{R}^5_+$ is positively invariant for (4.2). Hence if $x_0 \in \mathbb{R}^5_+$ then $x(t) \in \mathbb{R}^5_+$ for all $t \in [0, t_{\max})$.

Define the total population

$$N(t) = S(t) + V(t) + E(t) + I(t) + R(t).$$

Summing the equations of system (4.1) yields

$$\frac{dN}{dt} = \Lambda - \mu N - \delta I. \tag{4.3}$$

Since $I(t) \geq 0$ for all $t$, from (4.3) we obtain the differential inequality

$$\frac{dN}{dt} \leq \Lambda - \mu N. \tag{4.4}$$

This is a linear differential inequality. On the maximal interval $[0, t_{\max})$, we can apply the Gronwall inequality or comparison with the ordinary differential equation

$$\frac{dy}{dt} = \Lambda - \mu y, \qquad y(0) = N_0,$$

, to conclude that

$$N(t) \leq \max\left\{N_0, \frac{\Lambda}{\mu}\right\} \quad \text{for all } t \in [0, t_{\max}).$$

In particular,

$$\limsup_{t\to\infty} N(t) \leq \frac{\Lambda}{\mu},$$

and therefore each component satisfies

$$0 \leq S(t),\ V(t),\ E(t),\ I(t),\ R(t) \leq \frac{\Lambda}{\mu} \qquad \text{for all } t \in [0, t_{\max}).$$

Boundedness of the solution on the finite interval $[0, t_{\max})$ implies, by standard continuation theory for ordinary differential equations, that $t_{\max} = \infty$. Hence the solution exists globally and remains nonnegative and bounded for all $t \geq 0$.

If $N_0 \leq \Lambda/\mu$ then the above bound yields $N(t) \leq \Lambda/\mu$ for every $t \geq 0$. If $N_0 > \Lambda/\mu$ then $N(t)$ decreases and approaches $\Lambda/\mu$ exponentially as $t \to \infty$. Thus the feasible region

$$\Gamma = \left\{ (S, V, E, I, R) \in \mathbb{R}^5_+ :\ N \leq \frac{\Lambda}{\mu} \right\}$$

is positively invariant. This completes the proof.

### 4.3.2 Existence of Equilibria and Reproduction Number

In the absence of restocked infective ruminants, where $\alpha = \alpha_1 + \alpha_2 = 0$, the model (4.1) is analogous to that presented in (Gumel et al., 2006) and exhibits a disease-free equilibrium (DFE) denoted as $\xi^0$. The DFE represents the state of the system (4.1) where no infections are present in the population. Mathematically, the DFE occurs when the number of infected individuals is zero, and the population is entirely composed of susceptible and vaccinated animals. It is expressed as:

$$\xi^0 = \left( \frac{\Lambda}{\omega + \mu}, \frac{\omega\Lambda}{\mu(\omega + \mu)}, 0, 0, 0 \right).$$

In this study, we employ the next generation matrix operator approach proposed by Van den Driessche et al. (2002) to derive the control reproduction number $\mathcal{R}_v$. The control reproduction number $\mathcal{R}_v$ quantifies the average number of secondary infections produced by a single infected individual in a population under the influence of vaccination. A value of $\mathcal{R}_v < 1$ indicates that the disease will decline and eventually be eliminated, while $\mathcal{R}_v > 1$ suggests that the disease can persist and potentially lead to outbreaks. Understanding $\mathcal{R}_v$ is crucial for evaluating the effectiveness of intervention strategies aimed at controlling Peste des Petits Ruminants (PPR). The control reproduction number of the model (4.1) $\mathcal{R}_v$, is calculated using the next generation matrix and is given by:

$$\mathcal{R}_v = \frac{\Lambda\sigma\beta(\epsilon\omega + \mu)}{\mu(\omega + \mu)(\sigma + \mu)(\gamma + \delta + \mu)}. \tag{4.5}$$

and similar threshold quantity can be obtained by setting $\omega = 0$, namely basic reproduction number,

$$\mathcal{R}_0 = \frac{\Lambda\sigma\beta}{\mu(\sigma + \mu)(\gamma + \delta + \mu)}.$$

**Remark 4.3.2.** *(i.) Since $\omega \geq 0$ and $0 \leq \epsilon \leq 1$, then $\mathcal{R}_0 \geq \mathcal{R}_v \geq \epsilon\mathcal{R}_0$. Thus if $\epsilon\mathcal{R}_0 > 1 (i.e, \epsilon > \frac{1}{\mathcal{R}_0} = \epsilon_c)$ then $\mathcal{R}_v > 1$, and therefore no amount of vaccination can bring $\mathcal{R}_v < 1$. Hence, the $\epsilon_c$ defines the critical value for vaccine-related reduction rate of infection. Furthermore,*

*setting* $\mathcal{R}_v = 1$ *and solving for* $\omega$ *give the threshold vaccination rate,* $\omega_c$ *as :*

$$\omega_c = \frac{\Lambda\sigma\beta\mu - \mu^2(\sigma+\mu)(\delta+\gamma+\mu)}{\mu(\sigma+\mu)(\delta+\gamma+\mu) - \Lambda\sigma\beta\epsilon} = \frac{\mu(\mathcal{R}_0 - 1)}{1 - \epsilon\mathcal{R}_0}.$$

*(ii.) In the absence of infective animals through restocking* ($\alpha_i = 0, i = 1, 2$)*, the local and global dynamics of the model at the disease-free equilibrium (DFE) are similar to those presented in (Gumel et al., 2006), based on the threshold value of* $\mathcal{R}_v$ ($> 1$ *or* $< 1$)*. The local and global stability of the DFE in the context of Peste des Petits Ruminants (PPR) indicates that the population can effectively return to a disease-free state following minor disturbances, such as the introduction of a few infected animals. This resilience suggests that current intervention strategy, vaccination is sufficient to control the spread of PPR even if it is imperfect. Furthermore, the global stability of the DFE implies that regardless of the initial number of infected individuals, the population will ultimately converge to a disease-free state. In other word, to ensure that the PPR eradication is independent of the initial sizes of the sub-populations of the model. This finding reinforces the effectiveness of sustained vaccination efforts and highlights the potential for successful long-term management of PPR. These results underscore the importance of continued investment in disease prevention strategies to protect livestock health and ensure the stability of pastoral communities that rely on small ruminants.*

The endemic equilibrium of model (4.1) are obtained as:

$$\begin{cases} \Pi = S^*\beta I^* + (\omega+\mu)S^*, \text{where } \Pi = (1-(\alpha_1+\alpha_2))\Lambda \\ V^* = \dfrac{\omega\Pi}{(\epsilon\beta I^* + \mu)(\beta I^* + \omega + \mu)}, \\ (\sigma+\mu)E^* = \alpha_1\Lambda + \beta I^*(\epsilon V^* + S^*) \\ (\gamma+\delta+\mu)I^* = \alpha_2\Lambda + \sigma E^*, \\ R^* = \dfrac{\gamma}{\mu} I^* \end{cases} \tag{4.6}$$

and $I^*$ is the positive root of a cubic polynomial of the form:

$$\mathcal{G}(I^*, \alpha_1, \alpha_2) = AI^{*3} + BI^{*2} + CI^* + D := I^*\mathcal{H}(I^*) - \left(\frac{\alpha\sigma\beta\Lambda(\epsilon(\omega+\mu)+\mu)}{(\sigma+\mu)(\delta+\gamma+\mu)}\right) I^* + D = 0, \tag{4.7}$$

where

$$\mathcal{H}(I^*) = AI^{*2} + BI^* + C_0,$$

$$\begin{cases} A = \epsilon\beta^2, \\ B = \beta(\epsilon(\omega+\mu)+\mu) - \dfrac{\epsilon\beta^2\sigma\Lambda(\alpha+\frac{\Pi}{\Lambda})}{(\delta+\gamma+\mu)(\sigma+\mu)}, \\ C = \mu(\mu+\omega) - \dfrac{\Pi\beta\sigma(\epsilon\omega+\mu)}{(\sigma+\mu)(\delta+\gamma+\mu)} - \dfrac{\alpha\sigma\beta\Lambda}{(\sigma+\mu)(\delta+\gamma+\mu)}(\epsilon(\omega+\mu)+\mu), \\ C_0 = \mu(\mu+\omega) - \dfrac{\Pi\beta\sigma(\epsilon\omega+\mu)}{(\sigma+\mu)(\delta+\gamma+\mu)}, \\ D = -\dfrac{\alpha\sigma\Lambda\mu(\mu+\omega)}{(\delta+\gamma+\mu)(\sigma+\mu)}, \\ \alpha = (\alpha_1 + \alpha_2(\dfrac{\sigma+\mu}{\sigma})). \end{cases} \tag{4.8}$$

For simplicity, $\mathcal{G}(I^*, \alpha_1, \alpha_2)$ can be rewite as $\mathcal{G}(I^*, \alpha)$ and equation (4.7) becomes;

$$\mathcal{G}(I^*, \alpha) = AI^{*3} + BI^{*2} + \left[C_0 - \frac{\alpha\sigma\beta\Lambda}{(\sigma+\mu)(\delta+\gamma+\mu)}(\epsilon(\omega+\mu)+\mu))\right] I^* - \frac{\alpha\sigma\Lambda\mu(\mu+\omega)}{(\delta+\gamma+\mu)(\sigma+\mu)}.$$

Notice that when $\alpha_1 = \alpha_2 = 0$, or $\alpha = 0$, $\mathcal{G}(I^*, 0) = 0$ is reduced to $I^*\mathcal{H}(I^*) = 0$. It follows that $\mathcal{H}(I^*) = 0$, as $I^* > 0$, has a unique positive root $I^*$ if $C_0 < 0$, it is equivalent to $\mathcal{R}_v > 1$. Furthermore, $\mathcal{G}(I^*, \alpha) < I^*\mathcal{H}(I^*)$ for $\alpha > 0$ and $I^* > 0$. There are three cases to be considered (depending on the signs of $B$ and $C_0$) to study the number of positive roots of $\mathcal{G}(I^*, \alpha) = 0$. A similar approach is followed in the study of model (Shim, 2004; Alexander et al., 2004).

For the case $C_0 < 0$, by Descarte's Rule of Signs, $\mathcal{G}(I^*, \alpha) = 0$ has at most one positive root regardless of the sign of B, since $A > 0, C < 0$ and $D < 0$. $\mathcal{H}(I^*) = 0$ has a unique positive root, $\bar{I}$. It follows that $\mathcal{G}(\bar{I}, \alpha) < 0$, since $\mathcal{G}(I^*, \alpha) < I^*\mathcal{H}(I^*)$ for $\alpha > 0$. Furthermore, $\mathcal{G}(I^*, \alpha) \to \infty$ as $I^* \to \infty$ , which proves that $\mathcal{G}(I^*, \alpha)$ has a positive root.

For the case $C_0 > 0$ and $B > 0$ and let $r_1, r_2$, and $r_3$ represent the roots of $\mathcal{G}(\bar{I}, \alpha)$. In this case, since $A > 0$ and $B > 0$, it follows that $r_1 + r_2 + r_3 = -B/A < 0$ and $r_1r_2r_3 > 0$. This implies that $\mathcal{G}(\bar{I}, \alpha)$ has a unique positive root for any $\alpha > 0$.

For the last case $C_0 > 0$ and $B < 0$, if $B^2 - 4AC_0 > 0$, then from Descarte's Rule of Signs, it follows that $\mathcal{H}(I^*)$ has two positive roots. Thus, $\mathcal{G}(I^*, 0)$ has two positive roots if $B^2 - 4AC_0 > 0$. Since $\mathcal{G}(I^*, \alpha)$ is a cubic function of $I^*$ and is a decreasing function of $\alpha$ for $I^* > 0$, it can be seen that there is a positive $\bar{\alpha}$ such that $\mathcal{G}(I^*, \alpha)$ has three positive roots if $0 < \alpha < \bar{\alpha}$; two positive roots (one with multiplicity 2) if $\alpha = \bar{\alpha}$; and a unique positive root if $\alpha > \bar{\alpha}$. It should be noted that $\bar{\alpha} < \alpha_0$, where

$$\alpha_0 = \frac{C_0(\sigma+\mu)(\delta+\gamma+\mu)}{\sigma\Lambda\beta(\epsilon(\omega+\mu)+\mu)}.$$

To see this, suppose $\alpha \geq \alpha_0$. If $\mathcal{G}(\bar{I}, \alpha)$ has exactly one real root, then it follows from $r_1r_2r_3 = -\frac{D}{A} > 0$ that this root must be positive. If the roots of $\mathcal{G}(I^*, \alpha)$ are all real, since

$$r_1r_2 + r_1r_3 + r_2r_3 = \frac{C_0 - \frac{\alpha\sigma\beta\Lambda}{(\sigma+\mu)(\delta+\gamma+\mu)}(\epsilon(\omega+\mu)+\mu))}{A} \leq 0,$$

when $\alpha \geq \alpha_0$, it can be seen that $\mathcal{G}(I^*, \alpha)$ also has a unique positive root in this case. These results are summarized below.

**Theorem 4.3.3.** *i. If $\omega < \omega_c$ or $\alpha > \alpha_0$, or $C_0 < 0$, then the model (4.1) has a unique positive endemic equilibrium.*

*ii. If $\omega > \omega_c$ or $C_0 > 0$,$B > 0$ then the model (4.1) has a unique positive endemic equilibrium for $\alpha > 0$.*

*iii. If $\omega > \omega_c$, $B < 0$, and $B^2 - 4AC_0 > 0$, then there is a positive $\bar{\alpha} < \alpha_0$ such that $\mathcal{G}(I^*, \alpha)$ has a unique positive root if $\alpha > \bar{\alpha}$.*

In general, considering that $\mathcal{G}(I^*, \alpha)$ is a decreasing function of $\alpha$, it can be observed that as $I^* \to 0^+$, $\lim_{\alpha\to 0} \mathcal{G}(I^*, \alpha) = 0$. Additionally, as $I^* \to \infty$, $\lim_{\alpha\to\infty} \mathcal{G}(I^*, \alpha) = \infty$. Therefore, it can be concluded that $\mathcal{G}(I^*, \alpha)$ possesses at least one positive root, indicating the existence of at least one endemic equilibrium.

Next, we show the global dynamics of PPR in the presence of infectives recruited through restocking. Since the recovery class $R$ is not involved in the first four equations in (4.1), we reduce the system to four equations to demonstrate the global stability of the endemic equilibrium point.

**Theorem 4.3.4.** *For system (4.1) the endemic equilibrium $(S^*, V^*, E^*, I^*)$ is globally asymptotically stable on the set $\Gamma$.*

**Proof** Let $\xi^* = (S^*, V^*, E^*, I^*)$ denote the endemic equilibrium. Consider a Lyapunov function

$$L(x) = S^* g\left(\frac{S}{S^*}\right) + V^* g\left(\frac{V}{V^*}\right) + E^* g\left(\frac{E}{E^*}\right) + DI^* g\left(\frac{I}{I^*}\right)$$

where $g(x) = x - 1 - \ln(x)$ and $D = \frac{\sigma+\mu}{\sigma}$,
Note that $L(x)$ is positive definite with respect to $\xi^*$ because $x^* g\left(\frac{x}{x^*}\right)$ achieves a global minimum value of 0 at $x = x^*$.

The derivative of $L$ along a solution $(S(t), V(t), E(t), I(t))$ of the system (4.1) is expressed as follows:

$$\frac{dL}{dt} = \left(1 - \frac{S^*}{S}\right)\frac{dS}{dt} + \left(1 - \frac{V^*}{V}\right)\frac{dV}{dt} + \left(1 - \frac{E^*}{E}\right)\frac{dE}{dt} + D\left(1 - \frac{I^*}{I}\right)\frac{dI}{dt}. \tag{4.9}$$

By the first equations in (4.1) and (4.6), it follows that

$$\begin{aligned}\left(1 - \frac{S^*}{S}\right)\frac{dS}{dt} &= \left(1 - \frac{S^*}{S}\right)(\beta S^* I^* + (\omega+\mu)S^* - \beta SI - (\omega+\mu)S) \\ &= \left(1 - \frac{S^*}{S}\right)\left(\beta S^* I^*(1 - \frac{SI}{S^*I^*}) + (\omega+\mu)S^*(1 - \frac{S}{S^*})\right) \\ &= \beta S^* I^*\left(1 - \frac{SI}{S^*I^*} - \frac{S^*}{S} + \frac{I}{I^*}\right) - (\omega+\mu)\frac{(S-S^*)^2}{S}.\end{aligned} \tag{4.10}$$

By the second equations in (4.1) and (4.6), it follows that

$$\begin{aligned}\left(1 - \frac{V^*}{V}\right)\frac{dV}{dt} &= \left(1 - \frac{V^*}{V}\right)(-\omega S^* + \epsilon\beta V^* I^* + \mu V^* + \omega S - \epsilon\beta VI - \mu V) \\ &= -\omega S^*\left(1 - \frac{S}{S^*} - \frac{V^*}{V} + \frac{V^* S}{VS^*}\right) + \epsilon\beta V^* I^*\left(1 - \frac{V^*}{V} + \frac{I}{I^*} - \frac{VI}{V^*I^*}\right) - \mu\frac{(V-V^*)^2}{V}.\end{aligned} \tag{4.11}$$

Similarly, by (4.1) and endemic equilibrium equations in (4.6), we have

$$\begin{aligned}\left(1-\frac{E^*}{E}\right)\frac{dE}{dt} &= \left(1-\frac{E^*}{E}\right)(\beta SI+\epsilon\beta VI+\alpha_1\Lambda-(\sigma+\mu)E),\\ &= \beta SI+\epsilon\beta VI+\alpha_1\Lambda-(\sigma+\mu)E-\alpha_1\Lambda\frac{E^*}{E}-(\beta SI+\epsilon\beta VI)\frac{E^*}{E}+(\sigma+\mu)E^*\\ &= \beta S^*I^*\left(1+\frac{SI}{S^*I^*}-\frac{SIE^*}{S^*I^*E}\right)+\epsilon\beta V^*I^*\left(1+\frac{VI}{V^*I^*}-\frac{VIE^*}{V^*I^*E}\right)+\alpha_1\Lambda(2-\frac{E^*}{E})\\ &\quad-(\sigma+\mu)E^*\frac{E}{E^*},\end{aligned} \tag{4.12}$$

and

$$\begin{aligned}D\left(1-\frac{I^*}{I}\right)\frac{dI}{dt} &= D\left(1-\frac{I^*}{I}\right)(\sigma E+\alpha_2\Lambda-(\delta+\gamma+\mu)I),\\ &= D(\sigma E+\alpha_2\Lambda-(\delta+\gamma+\mu)I-\sigma E\frac{I^*}{I}-\alpha_2\Lambda\frac{I^*}{I}+(\delta+\gamma+\mu)I^*)\\ &= D\sigma E^*\frac{E}{E^*}-D(\delta+\gamma+\mu)I^*\frac{I}{I^*}+D\alpha_2\Lambda(2-\frac{I^*}{I})+D\sigma E^*\left(1-\frac{EI^*}{E^*I}\right)\\ &= (\alpha_1\Lambda+\beta S^*I^*+\epsilon\beta V^*I^*)\frac{E}{E^*}-D(\delta+\gamma+\mu)I^*\frac{I}{I^*}+D\alpha_2\Lambda(2-\frac{I^*}{I})\\ &\quad+(\alpha_1\Lambda+\beta S^*I^*+\epsilon\beta V^*I^*)\left(1-\frac{EI^*}{E^*I}\right).\end{aligned} \tag{4.13}$$

Since $D=\frac{\sigma+\mu}{\sigma}$, we have used relation $D\sigma E^*=\alpha_1\Lambda+\beta S^*I^*+\epsilon\beta V^*I^*$. Substituting (4.10) – (4.13) into (4.9) and rearranging terms, we obtain

$$\begin{aligned}\frac{dL}{dt} &= -\mu\frac{(S-S^*)^2}{S}-\mu\frac{(V-V^*)^2}{V}\\ &\quad+\beta S^*I^*\left(3-\frac{S^*}{S}-\frac{EI^*}{E^*I}-\frac{SE^*I}{S^*EI^*}\right)+\epsilon\beta V^*I^*\left(3-\frac{V^*}{V}-\frac{EI^*}{E^*I}-\frac{VE^*I}{V^*EI^*}\right)\\ &\quad-\omega S^*\left(1-\frac{S}{S^*}\right)\left(1-\frac{V^*}{V}\right)+(\beta S^*I^*+\epsilon\beta V^*I^*)\left(\frac{I}{I^*}+\frac{E}{E^*}\right)\\ &\quad-(\sigma+\mu)E^*\frac{E}{E^*}+\alpha_1\Lambda\left(3-\frac{E^*}{E}+\frac{E}{E^*}-\frac{EI^*}{E^*I}\right)-D(\delta+\gamma+\mu)I^*\frac{I}{I^*}\\ &\quad+D\alpha_2\Lambda\left(2-\frac{I^*}{I}\right).\end{aligned} \tag{4.14}$$

From (4.6), we have the relations:

$$\begin{cases}\beta S^*I^*+\epsilon\beta V^*I^*=(\sigma+\mu)E^*-\alpha_1\Lambda,\\ D\sigma E^*=D(\delta+\gamma+\mu)I^*-D\alpha_2\Lambda\\ \qquad\quad=(\sigma+\mu)E^*.\end{cases} \tag{4.15}$$

By taking each relation from (4.15) and substituting the corresponding terms in (4.14), we collect like terms that have the same coefficients, namely $D\alpha_2\Lambda$ and $\alpha_1\Lambda$. Thus,

$$\begin{aligned}\frac{dL}{dt} &= -\mu\frac{(S-S^*)^2}{S} - \mu\frac{(V-V^*)^2}{V} \\ &+ \beta S^* I^* \left(3 - \frac{S^*}{S} - \frac{EI^*}{E^*I} - \frac{SE^*I}{S^*EI^*}\right) + \epsilon\beta V^* I^* \left(3 - \frac{V^*}{V} - \frac{EI^*}{E^*I} - \frac{VE^*I}{V^*EI^*}\right) \\ &- \omega S^* \left(1 - \frac{S}{S^*}\right)\left(1 - \frac{V^*}{V}\right) + \alpha_1\Lambda\left(3 - \frac{E^*}{E} - \frac{I}{I^*} - \frac{EI^*}{E^*I}\right) \\ &+ D\alpha_2\Lambda\left(2 - \frac{I}{I^*} - \frac{I^*}{I}\right).\end{aligned}$$

Since $S \geq S^*$ and $V^* \geq V$, for all $t \geq 0$ and due to the inequality of arithmetic and geometric means:

$$x_1 + x_2 + ... + x_n \geq n(x_1x_2...x_n)^{\frac{1}{n}}, \quad \forall x_i \geq 0$$

and given that all the model parameters are non-negative, it follows that $L' \leq 0$. As a result, $L' = 0$ holds only at $\xi^*$, and $L'$ is negative definite with respect to $\xi^*$. Standard Lyapunov stability theorem (LaSalle, 2012) implies that $\xi^*$ is locally asymptotically stable and globally attracting in $\Gamma$. The global stability of $\xi^*$ also implies that $\xi^*$ is unique in $\Gamma$.

## 4.4 Parameter Estimation

In this study, we used a six-month report on PPR disease incidence data from January 2005 to December 2023 in Ethiopia to estimate parameters values in the system (4.1). The World Organization for Animal Health (WOAH) dashboard (WOAH, 2023) offered summarized data for reporting purposes, and this is where the data came from. We estimated the values for $\beta, \gamma, \sigma$, and $\omega$ using the provided data set, utilizing fixed parameter values for $\Lambda, \mu, \delta$ from the literature (Fournié et al., 2018; WOAH, 2023) and assuming all recruited small ruminants are susceptible (i.e $\alpha_1 = \alpha_2 = 0$). Finding the ideal parameters to enable our model (4.1) to be most closely aligned with the given data. To achieve this, we employ the non-linear least-squares approximation method and following the same approach of fitting models to data as stated in ((Martcheva, 2015), p.123) , which aims to minimize the sum of squared errors.

$$SSE = \sum_{j=1} (I_j - I^*(t_j))^2 \tag{4.16}$$

where $I^*(t_j)$ is the expected simulation result for the cumulative incidence of PPR at time step j and $I_j$ is the cumulative incidence data observed. The initial value that we utilized was $(S_0, V_0, E_0, I_0, R_0) = (43943625, 51300, 0, 5075, 0)$. The estimated parameter values are presented in Table (4.1), and Figure (4.2) shows the visualization of the results. The red dot shows the semester-wise prevalence statistics of PPR disease from January 2005 to December 2023, whereas the blue curve shows the simulation result of $I^*(t_j)$ from the model (4.1). Furthermore, in the absence of an infectiously recruited small ruminant through restocking, the control reproduction

number calculated in (4.5) is 1.020 using the estimated parameter values. This finding indicates that the disease is endemic in the country.

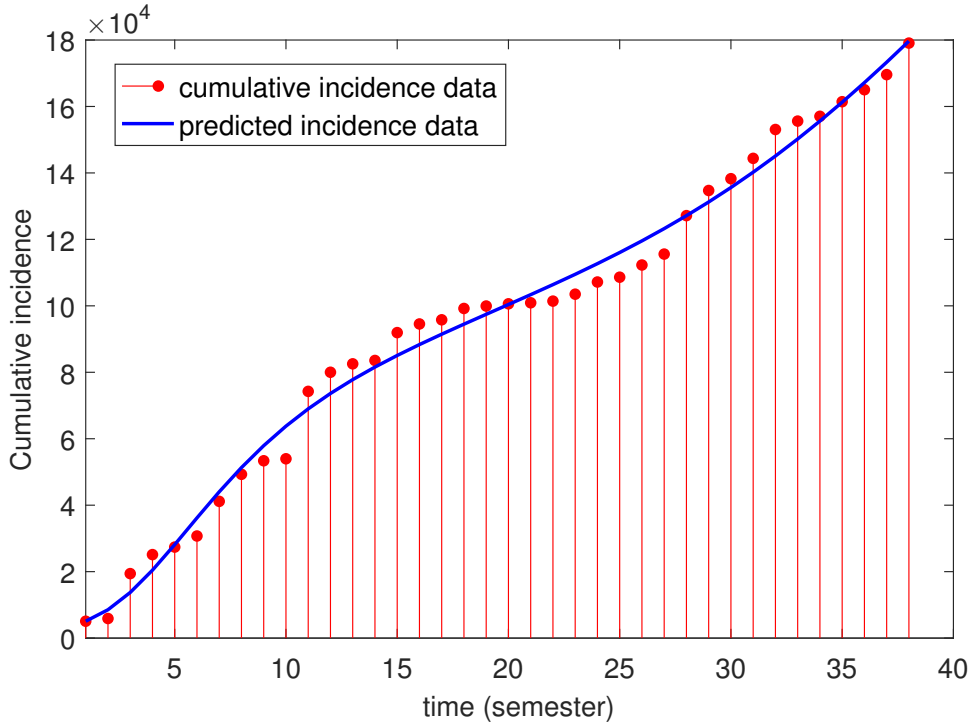


FIGURE 4.2: Fitting the model to observed incidence data, illustrating the alignment between the predicted and actual infection rates over time.

## 4.5 Sensitivity Analysis

To find out how resistant the model was to different parameter values, we performed a sensitivity analysis. Understanding the relative roles played by the various model parameters in the occurrence and spread of any given disease is crucial. This will help us identify where to focus interventions that will reduce disease-related mortality and morbidity. Various parameters are involved in $(\mathcal{R}_v)$ in the case of zero infective recruits through restocking ($\alpha_1 = \alpha_2 = 0$), as illustrated in the equation (4.5). Consequently, to identify the key variables that will restrict the spread of PPR, we performed a sensitivity analysis on $(\mathcal{R}_v)$. To measure the relative change in the model parameter $p$ with respect to the relative change in $(\mathcal{R}_v)$, we employ a forward normalized sensitivity index denoted as $\gamma_p^{\mathcal{R}_v}$. This index is defined using partial derivatives if $(\mathcal{R}_v)$ is a differentiable function of the model parameter $p$. The specific definition of this index can be found in (Sanchez et al., 1997). It can be given by:

$$\gamma_p^{\mathcal{R}_v} = \frac{\partial \mathcal{R}_v}{\partial p} \times \frac{p}{\mathcal{R}_v}, \tag{4.17}$$

where $\gamma_p^{\mathcal{R}_v}$ is the sensitivity index (SI) of $(\mathcal{R}_v)$ with respect to parameter p, hence we evaluate the sensitivity indices of these parameters at the parameter values as given in Table (4.2). For

TABLE 4.1: Parameter description and estimated values

| Parameter | Description | value (unit= per six months) | Source |
|---|---|---|---|
| $\Lambda$ | Recruitment rate | $7.8845 \times 10^6$ | Fournié et al., 2018 |
| $\mu$ | natural death rate | 0.125 | Fournié et al., 2018 |
| $\beta$ | Disease transmission rate | $6.32 \times 10^{-7}$ | Estimated |
| $\delta$ | Disease induced death rate | 0.3549 | WOAH, 2023 |
| $\gamma$ | Recovery rate of infective | 25.1479(1/7.257per day) | Estimated |
| $\sigma$ | Progression from exposed class to infectious | 15.0172 (1/12.15 per day) | Estimated |
| $\omega$ | vaccination rate to susceptible population | 0.1030 | Estimated |
| $1-\epsilon$ | Vaccine efficacy | 70%-90% | Fournié et al., 2018 |

example, the sensitivity index of $\mathcal{R}_v$ with respect to $\beta$ is given by

$$\gamma_{\beta}^{\mathcal{R}_v} = \frac{\partial \mathcal{R}_v}{\partial \beta} \times \frac{\beta}{\mathcal{R}_v} = 1.$$

This can be interpreted as increasing (or decreasing) the transmission rate $\beta$ by 10%, increasing (or decreasing) $\mathcal{R}_v$ by 10%. In the same way, increasing (or decreasing) vaccination efficacy $1-\epsilon$, decreases (or increases) $\mathcal{R}_v$, by 1.71%. In general, the positive sign sensitivity indices in Table (4.2) imply that the value of $\mathcal{R}_v$ rises with increase, whereas negative sign sensitivity indices show that the value of $\mathcal{R}_v$ falls with increase.

TABLE 4.2: Sensitivity indices of $\mathcal{R}_v$ for the PPR model (4.19) with $(\alpha_1 = \alpha_2 = 0)$.

| Parameters: | $\beta$ | $\mu$ | $\sigma$ | $\gamma$ | $\omega$ | $\epsilon$ | $\delta$ |
|---|---|---|---|---|---|---|---|
| Index sign: | + | - | + | - | - | + | - |
| SI values: | 1.000 | 0.7321 | 0.0082 | 0.9813 | 0.2810 | 0.1709 | 0.0137 |

According to Table (4.2)'s sensitivity analysis results, treating the infected population, increasing the efficacy of the vaccine, and lowering the transmission rate would all help prevent the spread of PPR disease.

The requirements for the best control of the influence of infectious recruits through restocking on PPR disease are ascertained in the following section by applying optimal control theory.

## 4.6 Optimal Control Problem

In this section, we formulate a corresponding control problem by considering strict biosecurity measures, vaccination, and treatment as control interventions. In the following, we discuss in detail about these control interventions:

i. **Biosecurity Measures:** Biosecurity is a set of management practices designed to prevent the introduction, establishment, and spread of infectious diseases, parasites, and pests into and within an animal population. We distinguish two complementary controls in our optimal control framework: external biosecurity $u_1(t)$ and internal biosecurity $u_2(t)$. External biosecurity (prevention of introduction) includes quarantine and testing of new or returning animals, closed-herd or certified sourcing, strict movement control for animals, vehicles, and equipment, controlled access (fencing, checkpoints, visitor logs), wildlife exclusion, and protection of water and feed; operationally, $u_1(t)$ reduces the external force of infection, for example $(1-\alpha_1+\alpha_2)\Lambda \mapsto \big(1-(\alpha_1+\alpha_2)\,u_1(t)\big)\Lambda$. Internal biosecurity (containment if infection is present) includes rapid isolation of suspect or clinical animals, cohorting and all-in/all-out with downtime, rigorous hygiene and disinfection (herd- and equipment-level sanitation), ventilation and stocking-density management, staff training and compliance auditing, and awareness-raising among livestock owners; operationally, $u_2(t)$ reduces within-farm transmission, for example $\beta S(t)I(t) \mapsto \big(1-u_2(t)\big)\beta S(t)I(t)$.

ii. **Vaccination to Susceptible Population:** The main strategy for controlling PPR (Peste des Petits Ruminants) is to vaccinate susceptible small ruminant populations in endemic locations or countries. The goal is to achieve an optimal immunity rate within a specific period to prevent transmission of the PPR virus. However, implementing mass immunization can be challenging and costly, especially in small-holder agricultural systems where animals are scattered and infrastructure is insufficient (Hammami et al., 2018). The control variable $u_3(t)$ is utilized to minimize vaccination costs and reduce the burden of PPR diseases.

iii. **Recovery via Treatment to Infective:** As mentioned in the introduction, there is currently no specific treatment available for animals infected with Peste des Petits Ruminants (PPR). Therefore, the primary approach revolves around offering supportive care to aid affected animals in their recovery and symptom management. Supportive care measures include isolation, symptomatic treatment, fluid therapy, nutritional support, management of secondary infections, and veterinary care. The treatment control variable $u_4(t)$ is considered to determine the intervention that is both highly effective and cost-effective.

Our objective in the optimal control problem is to minimize the number of infected animals, including those that are exposed and infectious, while keeping the intervention costs at a minimum. Therefore, we define our cost function as follows:

$$J(u_1,u_2,u_3,u_4)=\int_0^{T_f}\left(a_1E+a_2I+\frac{c_1}{2}u_1^2+\frac{c_2}{2}u_2^2+\frac{c_3}{2}u_3^2+\frac{c_4}{2}u_4^2\right)dt \tag{4.18}$$

with respect to the system

$$\begin{cases} \dfrac{dS}{dt} = (1-(\alpha_1+\alpha_2)(1-u_1(t)))\Lambda - (1-u_2(t))\beta S(t)I(t) - u_3(t)S(t) - \mu S(t), \\ \dfrac{dV}{dt} = u_3(t)S(t) - (1-u_2(t))\epsilon\beta V(t)I(t) - \mu V(t), \\ \dfrac{dE}{dt} = (1-u_1(t))\alpha_1\Lambda + (1-u_2(t))\beta I(t)(\epsilon V(t)+S(t)) - (\sigma+\mu)E(t), \\ \dfrac{dI}{dt} = (1-u_1(t))\alpha_2\Lambda + \sigma E(t) - (\gamma+\delta+\mu)I(t) - u_4(t)I(t), \\ \dfrac{dR}{dt} = (\gamma+u_4(t))I(t) - \mu R(t), \end{cases} \tag{4.19}$$

with

$$S(0) \geq 0, V(0) \geq 0, E(0) \geq 0, I(0) > 0, R(0) \geq 0.$$

The coefficients $\{a_1, a_2, c_1, c_2, c_3, c_4\}$ in the integrand represent positive weight parameters that ensure the balance of each component within the objective function. The initial two terms of the integrand in equation (4.18), namely $a_1E$ and $a_2I$ , account for the cost associated with PPR disease morbidity and mortality, encompassing significant economic losses such as decreased productivity, trade restrictions, and diminished market value for the affected animals (Jemberu et al., 2022; Fournié et al., 2018). The final four terms in equation. (4.18) represent the costs associated with biosecurity measures $(u_1, u_2)$, vaccination $(u_3)$, and treatment $(u_4)$, respectively. In this context, the nonlinearity of the second order is considered for the four control interventions to reflect their high level of effort, severity, and costliness (Makinde et al., 2011; Nyerere et al., 2020b).

The goal is to find an optimal control, $\mathbf{u} = (u_1^*(t), u_2^*(t), u_3^*(t), u_4^*(t))$, such that

$$J(u_1^*(t), u_2^*(t), u_3^*(t), u_4^*(t)) = \min_{\mathbf{U}} J(u_1(t), u_2(t), u_3(t), u_4(t)) \tag{4.20}$$

where $\mathbf{U}$ is the non-empty control set defned as

$$\mathbf{U} = \{(u_1(t), u_2(t), u_3(t), u_4(t)) | 0 \leq u_i \leq u_{imax} \leq 1, \quad \text{Lebesgue measurable}, i = 1,2,3,4 \quad t \in [0, T_f]\}. \tag{4.21}$$

The optimal control must satisfy the necessary conditions that are formulated by Pontryagin's Maximum Principle (Pontryagin, 1987; Shim, 2004). This principle changes the system of Equations in (4.19) into a problem of minimizing point-wise a Hamiltonian $(\mathcal{H})$, with respect to $u_1(t), u_2(t), u_3(t), u_4(t)$. For deriving the necessary conditions, we define the Hamiltonian $\mathcal{H}$ as

$$\begin{aligned} \mathcal{H} = {} & a_1E + a_2I + \frac{c_1}{2}u_1^2 + \frac{c_2}{2}u_2^2 + \frac{c_3}{2}u_3^2 + \frac{c_4}{2}u_4^2 \\ & + \lambda_s\left((1-(\alpha_1+\alpha_2)(1-u_1(t)))\Lambda - (1-u_2(t))\beta S(t)I(t) - u_3(t)S(t) - \mu S(t)\right) \\ & + \lambda_v\left(u_3(t)S(t) - (1-u_2(t))\epsilon\beta V(t)I(t) - \mu V(t)\right) \\ & + \lambda_e\left((1-u_1(t))\alpha_1\Lambda + (1-u_2(t))\beta I(t)(\epsilon V(t)+S(t)) - (\sigma+\mu)E(t)\right) \\ & + \lambda_i\left(((1-u_1(t))\alpha_2\Lambda + \sigma E(t) - (\gamma+\delta+\mu)I(t) - u_4(t)I(t)\right) \\ & + \lambda_r\left((\gamma+u_4(t))I(t) - \mu R(t)\right) \end{aligned} \tag{4.22}$$

where $\lambda_s, \lambda_v, \lambda_e, \lambda_i$, and $\lambda_r$ are the adjoint variables or co-state variables. By applying Pontryagin's Maximum Principle (Lenhart et al., 2007) and the existence result for the optimal control from Fleming et al. (2012), we acquire the following theorem.

**Theorem 4.6.1.** *There exists an optimal control quadruple* $\mathbf{u} = (u_1^*, u_2^*, u_3^*, u_4^*)$ *and the corresponding solution* $(S^*, V^*, E^*, I^*, R^*)$ *of the system (4.19), that minimizes* $J(u_1^*, u_2^*, u_3^*, u_4^*)$ *over* $\mathbf{U}$. *Furthermore, there exist adjoint functions,* $\lambda_s(t), \lambda_v(t), \lambda_e(t), \lambda_i(t)$ , *and* $\lambda_r(t)$, *such that*

$$\begin{cases} \dfrac{d\lambda_s}{dt} = (\lambda_s - \lambda_e)(1-u_2)\beta I + (\lambda_s - \lambda_v)u_3 + \mu\lambda_s, \\ \dfrac{d\lambda_v}{dt} = (\lambda_v - \lambda_e)(1-u_2)\epsilon\beta I + \mu\lambda_v, \\ \dfrac{d\lambda_e}{dt} = (\lambda_e - \lambda_i)\sigma + \mu\lambda_e - a_1, \\ \dfrac{d\lambda_i}{dt} = (\lambda_s - \lambda_e)(1-u_2)\beta S + (\lambda_v - \lambda_e)(1-u_2)\epsilon\beta V + (\lambda_i - \lambda_r)(\gamma + u_4) + \lambda_i(\delta + \mu) - a_2 \\ \dfrac{d\lambda_r}{dt} = \lambda_r\mu, \end{cases} \tag{4.23}$$

*with the transversality conditions:*

$$\lambda_s(T_f) = 0, \lambda_v(T_f) = 0, \lambda_e(T_f) = 0, \lambda_i(T_f) = 0, \lambda_r(T_f) = 0. \tag{4.24}$$

*Furthermore, the optimal controls are characterized by*

$$\begin{cases} u_1^* = \max\left\{0, \min\left\{\dfrac{(\lambda_e - \lambda_s)\alpha_1\Lambda + (\lambda_i - \lambda_s)\alpha_2\Lambda}{c_1}, 1\right\}\right\}, \\ u_2^* = \max\left\{0, \min\left\{\dfrac{(\lambda_e - \lambda_s)\beta SI + (\lambda_e - \lambda_v)\epsilon\beta VI}{c_2}, 1\right\}\right\}, \\ u_3^* = \max\left\{0, \min\left\{\dfrac{S(\lambda_s - \lambda_v)}{c_3}, 1\right\}\right\}, \\ u_4^* = \max\left\{0, \min\left\{\dfrac{I(\lambda_i - \lambda_r)}{c_4}, 1\right\}\right\}. \end{cases} \tag{4.25}$$

**Proof** Firstly, we verify the conditions in Corollary 4.1 of (Fleming et al., 2012) for the existence of an optimal control triple $(u_1^*, u_2^*, u_3^*, u_4^*)$.

i. The convexity of the admissible control set $\mathbf{U}$ and the integrand of J with respect to $\mathbf{U}$;

Let $v, w \in \mathbf{U} = [0,1] \times [0, 0.8] \times [0,1] \times [0,1]$, be any two arbitrary points. Using definition of a convex set, it follows that

$$\tau v + (1-\tau)w \in \mathbf{U}, \text{for all } \tau \in [0,1].$$

Hence, $\mathbf{U}$ is convex.

To show the convexity of the intgerand of $J$, it is denoted by $\mathcal{L}$ and defined as

$$\mathcal{L}(t, \mathbf{x}, \mathbf{u}) = a_1 E + a_2 I + \frac{c_1}{2}u_1^2 + \frac{c_2}{2}u_2^2 + \frac{c_3}{2}u_3^2 + \frac{c_4}{2}u_4^2, \tag{4.26}$$

where $\mathbf{x} = (S, V, E, I, R)$, $\mathbf{u} = (u_1, u_2, u_3, u_4)$,

we follow the definition of convex function,

$$(1-\tau)\mathcal{L}(t, \mathbf{x}, \mathbf{v}) + \tau\mathcal{L}(t, \mathbf{x}, \mathbf{w} \geq \mathcal{L}(t, \mathbf{x}, (1-\tau)\mathbf{v} + \tau\mathbf{w}),$$

for arbitrary $\mathbf{v} = (v_1, v_2, v_3, v_4), \mathbf{w} = (w_1, w_2, w_3, w_4) \in \mathbf{U}$ and $\tau \in [0, 1]$.

Equivalently, the above inequality written as

$$(1-\tau)\mathcal{L}(t, \mathbf{x}, \mathbf{v}) + \tau\mathcal{L}(t, \mathbf{x}, \mathbf{w} - \mathcal{L}(t, \mathbf{x}, (1-\tau)\mathbf{v} + \tau\mathbf{w}) \geq 0.$$

From Eq (4.26) and algebraic simplification, we have

$$\begin{aligned}(1-\tau)\mathcal{L}(t, \mathbf{x}, \mathbf{v}) + \tau\mathcal{L}(t, \mathbf{x}, \mathbf{w} - \mathcal{L}(t, \mathbf{x}, (1-\tau)\mathbf{v} + \tau\mathbf{w}) &= \frac{1}{2}(\tau(1-\tau)\sum_{j=1}^{4} c_j(v_j - w_j)^2) \\ &\geq 0, \text{since } \tau \in [0, 1].\end{aligned}$$

Thus, $\mathcal{L}$ is convex.

ii. a priori boundedness of the state solutions;

We note that the right-hand sides of differential equations in(4.19) are linear in each of the controls and can be written as

$$f(t, \mathbf{x}, \mathbf{u}) = \phi(t, \mathbf{x}) + \psi(t, \mathbf{x})\mathbf{u}$$

where

$$\phi(t, \mathbf{x}) = \begin{bmatrix} (1-(\alpha_1+\alpha_2))\Lambda - \beta SI - \mu S \\ -\epsilon\beta VI - \mu V \\ \alpha_1\Lambda + \beta I(\epsilon V + S) - (\sigma+\mu)E \\ \alpha_2\Lambda + \sigma E - (\gamma+\delta+\mu)I \\ \gamma I - \mu R \end{bmatrix}, \quad \psi(t, \mathbf{x}) = \begin{bmatrix} (\alpha_1+\alpha_2)\Lambda & \beta SI & -S & 0 \\ 0 & \epsilon\beta VI & S & 0 \\ -\alpha_1\Lambda & -\beta I(\epsilon V + S) & 0 & 0 \\ -\alpha_2\Lambda & 0 & 0 & -I \\ 0 & 0 & 0 & I \end{bmatrix},$$

$\mathbf{x} = (S, V, E, I, R)$, and $\mathbf{u} = (u_1, u_2, u_3, u_4)$.

The boundedness of the solutions implies $||\phi(t, \mathbf{x})|| \leq M_0$, $||\psi(t, \mathbf{x})|| \leq M_1$, where $M_0$ and $M_1$ are positive constants. It follows that

$$\begin{aligned}||f(t, \mathbf{x}, \mathbf{u})|| &\leq ||\phi(t, \mathbf{x})|| + ||\psi(t, \mathbf{x})||||\mathbf{u}|| \\ &\leq M_0 + M_1||\mathbf{u}|| \\ &\leq M(1 + ||\mathbf{u}||)\end{aligned}$$

where $M = \max\{M_0, M_1\}$.

ii. The integrand $\mathcal{L}$ is bounded below. i.e $\mathcal{L}(t, \mathbf{x}, \mathbf{u}) \geq g(t, \mathbf{x}, \mathbf{u})$, where

$$g(t, \mathbf{x}, \mathbf{u}) = \theta_0 ||\mathbf{u}||^{\theta_2} - \theta_1, \text{ for all } \theta_0, \theta_1 > 0 \text{ and } \theta_2 > 1.$$

This property can be verified as follows:

$$\begin{aligned}
\mathcal{L}(t, \mathbf{x}, \mathbf{u}) &= a_1 E + a_2 I + \frac{c_1}{2} u_1^2 + \frac{c_2}{2} u_2^2 + \frac{c_3}{2} u_3^2 + \frac{c_4}{2} u_4^2 \\
&\geq \frac{c_1}{2} u_1^2 + \frac{c_2}{2} u_2^2 + \frac{c_3}{2} u_3^2 + \frac{c_4}{2} u_4^2 \\
&\geq \theta_0 \left( |u_1|^2 + |u_2|^2 + |u_3|^2 + |u_4|^2 \right)^{\frac{2}{2}} - \theta_1 \\
&= \theta_0 ||\mathbf{u}||^2 - \theta_1 \\
&= g(t, \mathbf{x}, \mathbf{u})
\end{aligned}$$

where $\theta_0 = \frac{1}{2} \min\{c_1, c_2, c_3, c_4\}$, $\theta_1 > 0$, and $\theta_2 = 2$. Consequently, $\mathcal{L}(t, \mathbf{x}, \mathbf{u}) \geq g(t, x, u)$.

Thus, applying Pontryagin's Maximum Principle(Lenhart et al., 2007), we convert (4.18), (4.19) and (4.20) into a problem of minimizing a Hamiltonian, $\mathcal{H}$, pointwise with respect to the control variables $u_1, u_2, u_3$ and $u_4$:

$$\mathcal{H} = a_1 E + a_2 I + \frac{c_1}{2} u_1^2 + \frac{c_2}{2} u_2^2 + \frac{c_3}{2} u_3^2 + \frac{c_4}{2} u_4^2 + \lambda_s f_1 + \lambda_v f_2 + \lambda_e f_3 + \lambda_i f_4 + \lambda_r f_5$$

where $f_i, i = 1, ..., 5$ are the right-hand sides of the system (4.19) and we have the adjoint equations

$$\begin{cases}
\dfrac{d\lambda_s}{dt} = -\dfrac{\partial \mathcal{H}}{\partial S}, \lambda_s(T_f) = 0, \\
\dfrac{d\lambda_v}{dt} = -\dfrac{\partial \mathcal{H}}{\partial V}, \lambda_v(T_f) = 0, \\
\dfrac{d\lambda_e}{dt} = -\dfrac{\partial \mathcal{H}}{\partial E}, \lambda_e(T_f) = 0, \\
\dfrac{d\lambda_i}{dt} = -\dfrac{\partial \mathcal{H}}{\partial I}, \lambda_i(T_f) = 0, \\
\dfrac{d\lambda_r}{dt} = -\dfrac{\partial \mathcal{H}}{\partial R}, \lambda_r(T_f) = 0.
\end{cases} \tag{4.27}$$

From Equation (4.27) we obtain equations in (4.23) for adjoint variables $\lambda' s$. And computing

$$u_1^*(t) = \frac{\partial \mathcal{H}}{\partial u_1}, u_2^*(t) = \frac{\partial \mathcal{H}}{\partial u_2}, u_3^*(t) = \frac{\partial \mathcal{H}}{\partial u_3}, u_4^*(t) = \frac{\partial \mathcal{H}}{\partial u_4}$$

and using the property of control set $\mathbf{U}$, we have required optimal control functions as mentioned in equation (4.25).

## 4.7 Numerical Results and Discussion

Numerical simulations play a crucial role in dynamic modeling as they offer a visual representation of the proposed model, thereby complementing theoretical analyses. Hence, by employing the parameter values specified in Table 4.2, we examine the impact of these parameters, along with four control measures and their associated costs, on the dynamics of the PPR disease through

numerical simulations. The numerical scheme employed for the optimal control problem was obtained from (Lenhart et al., 2007), and we utilized MATLAB to conduct the simulations.

### 4.7.1 Effects of constant vaccination and treatment rates

In the first numerical simulation, we considered the estimated parameter values in Table (4.2) and the case of $\alpha_1 = 0 = \alpha_2$ (i.e., no influx of infective ruminants). From the parameter values and in eq(4.5), the control reproduction number becomes $\mathcal{R}_v = 1.020$. This threshold number indicates that PPR disease is endemic in a small ruminant population. Furthermore, the effects of $\beta, \epsilon$ and $u_2, u_3$ on the reproduction number $\mathcal{R}_v$ are shown in 3-D Figures 4.3 (a) and (b), respectively. From the two 3D figures plotted, we verify the variation in $\mathcal{R}_v$ which is a threshold for the existence of infection in the population. It is observed (see Fig. 4.4A and 4.4B) that the surface of $\mathcal{R}_v$ crosses the plane $\mathcal{R}_v = 1$ in $u_2, u_3$-plane and $\beta, \epsilon$-plane.

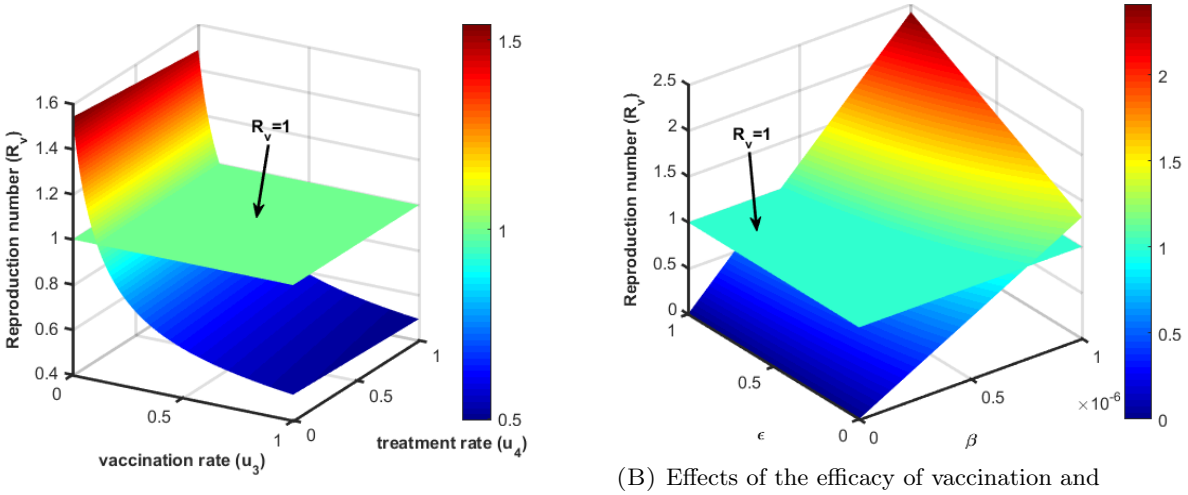


(A) Effects of vaccination and treatment rates on $\mathcal{R}_v$

(B) Effects of the efficacy of vaccination and transmission rate on $R_v$

FIGURE 4.3: Effects of parameters on the reproduction number

Figures 4.4A and 4.4B show the results obtained by setting the initial conditions as $S(0) = 40481014, V(0) = 3500000, E(0) = 9493, I(0) = 9493, R(0) = 0$ and considering a scenario without infective restocking. It is observed from Figure 4.4A that a high rate of treatment of the infected population effectively suppresses the spread of Peste des Petits Ruminants (PPR). Similarly, Figure 4.4B illustrates that the coverage of vaccination among the susceptible population above 15% positively contributes to the eradication of disease.

Figure 4.4C illustrates a numerical simulation that takes into account a non-zero infective inflow through restocking ($\alpha = \alpha_1 + \alpha_2 \neq 0$) and assumes a high vaccine efficacy of $\epsilon = 0.1$ (equivalent to 90% efficacy). The results demonstrate that the dynamics of the disease are influenced by the small proportion of infectious influx into the population, indicating the persistence of the disease within the population. These findings emphasize the necessity of implementing additional control measures, such as strict relocation protocols for small ruminants, improved animal identification upon arrival, and isolation practices, in order to achieve complete eradication of the disease. These measures are crucial components of comprehensive biosecurity measures.

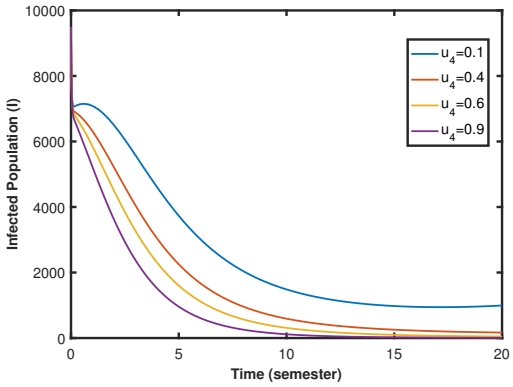


(A) Effects of different rates of treatment on I

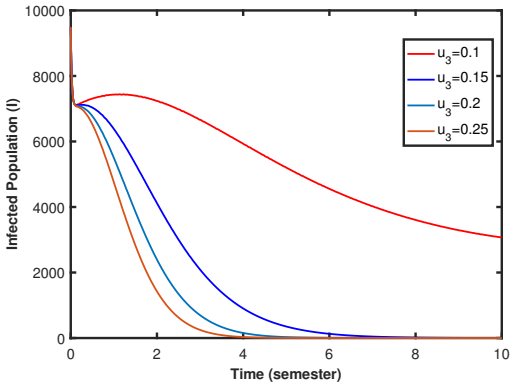


(B) Effects of different rates of vaccination on I

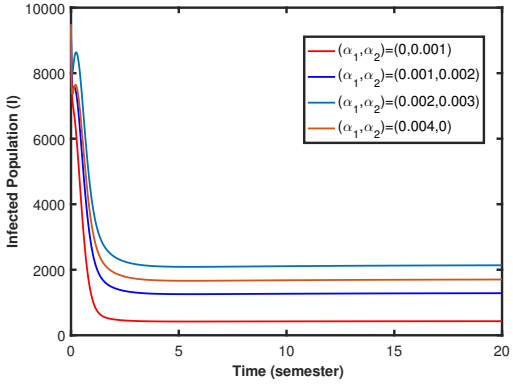


(C) Effect of infective restocked $(\alpha_1, \alpha_2)$ on I

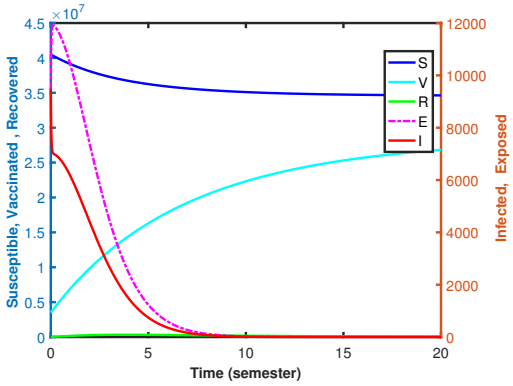


(D) The population profile for the case $(\alpha_1, \alpha_2) = (0, 0)$ and $\epsilon = 0.1, u_3 = 0.103, u_4 = 0$

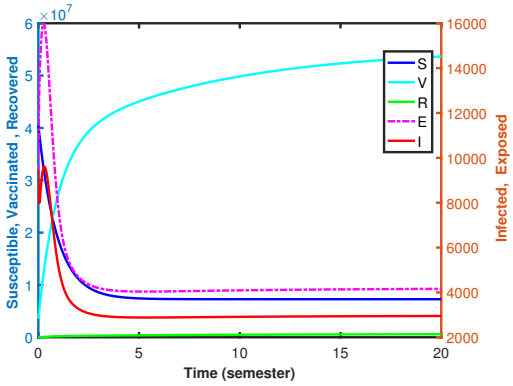


(E) The population profile for the case $(\alpha_1, \alpha_2) = (0.005, 0.002)$ and $\epsilon = 0.1, u_3 = 0.95, u_4 = 0.9$

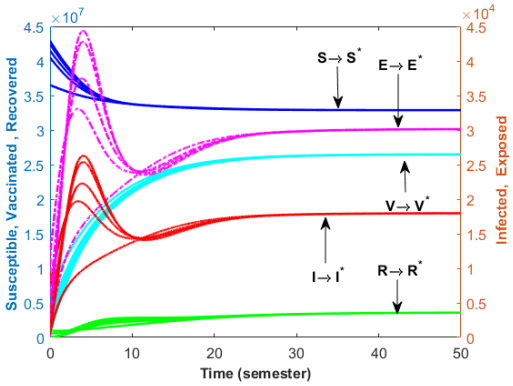


(F) The population profile with different initial conditions for the case $(\alpha_1, \alpha_2) = (0.001, 0.001)$ and $\epsilon = 0.25$

FIGURE 4.4: Numerical simulation results: effects of different constant rates of vaccination $u_3$ (b), treatment $u_4$ (a), and fraction of infective restocked $(\alpha_i)$ (c), with fixed $\epsilon = 0.3$. Figures (d) and (e) represent the population profile with varying values of $\epsilon, u_3, u_4$, while figure (f) illustrates the global stability of the endemic point.

In Figures 4.4D and 4.4E, we conducted a numerical simulation using the same initial conditions and parameter values as in the previous simulation. When the treatment rate $(u_3)$ was set to zero, we observed that the two plotted figures confirmed the analytical results presented in Section 4.3.2. Specifically, in Figure 4.4D, when $\epsilon = 0.1$ as stated in Remark (4.3.2) (i), which implies that $\epsilon_c > \epsilon$, the trajectories in system (4.1) converge to the disease-free equilibrium (i.e.,

$\mathcal{R}_v < 1$).

In Figure 4.4E, we demonstrate the impact of a nonzero influx of infective animals, where $(\alpha_1, \alpha_2) = (0.005, 0.002)$. The results indicate that the trajectories converge to a unique endemic equilibrium, even with a high vaccination coverage rate ($u_3 = 0.95$), maximum vaccination efficacy ($\epsilon = 0.1$ or 90%), and a high treatment rate for infected animals ($u_4 = 0.9$). Figure 4.4F illustrates the global stability of the endemic equilibrium point, indicating the persistence of the disease for the specific case where $(\alpha_1, \alpha_2) = (0.001, 0.001)$ under various initial conditions. This result is consistent with the findings presented in Theorem (4.3.4).

### 4.7.2 Numerical simulation for optimal control

We solve the optimal control problem for model (4.19) using the parameter values in Table 4.1, the initial state $(S_0, V_0, E_0, I_0, R_0) = (40{,}481{,}014,\ 3{,}500{,}000,\ 9{,}493,\ 9{,}493,\ 0)$, and infective recruitment fractions $(\alpha_1, \alpha_2) = (0.002,\ 0.001)$. The forward–backward sweep method (Lenhart et al., 2007) is employed: the state system (4.19) is integrated forward in time and the adjoint system (4.23) backward, both with classical fourth-order Runge–Kutta (RK4) schemes. Standard numerical stability and convergence diagnostics were satisfactory.

To assess accuracy, we estimate the observed order of convergence via

$$p \approx \log_2\left(\frac{\|e(h)\|}{\|e(h/2)\|}\right), \quad e(h) = \|x_{h/2} - x_h\|, \quad x_h = \{S_h, V_h, E_h, I_h, R_h\},$$

where norms are root-mean-square (RMS) over time and $x_h$ denotes the RK4 solution with step size $h$. We obtained $p \approx 3.5$ for $V$, $E$, and $R$, close to the RK4 theoretical order, while $S$ and $I$ exhibited lower rates ($p \approx 2.9$ and $p \approx 2.45$, respectively). These reductions are consistent with pre-asymptotic effects, strong nonlinear coupling through the $\beta SI$ term, and mild transient stiffness. Practically, halving the step size reduces the RMS error by approximately $2^{3.5} \approx 11$ for $V/E/R$ and by $2^{2.45} \approx 5.5$–$6$ for $I$.

Control bounds and cost weights are specified in Table (4.3). We selected weights via a two-stage procedure: (i) baseline values $\{5, 20, 10, 30, 50, 10\}$ informed by expert opinion and the study (Jemberu et al., 2022), followed by (ii) a PRCC-based local sensitivity analysis using 25 Latin hypercube samples per coefficient. The analysis identified $a_1$ and $a_2$ as the most influential. Among candidate combinations, we retained the configuration in Table (4.3) that minimized total cost while maximizing infections averted.

Over a time horizon of $T_f = 4$ semesters, we evaluate only combined interventions, grouped as: (i) two-control, (ii) three-control, and (iii) four-control strategies, with comparative cost-effectiveness. Single-control strategies are not considered. The specific combinations are described below.

TABLE 4.3: Weight balances and maximum bounds of control variables.

| Parameters: | $a_1$ | $a_2$ | $c_1$ | $c_2$ | $c_3$ | $c_4$ | $u_{1\,\max}$ | $u_{2\,\max}$ | $u_{3\,\max}$ | $u_{4\,\max}$ |
|---|---|---|---|---|---|---|---|---|---|---|
| value: | 2.5 | 10 | 7.5 | 30 | 80 | 5 | 1 | 0.8 | 1 | 1 |

## Scenario $\mathcal{A}$

In this secenario, we cosidered all strategies contains two controls.

### Strategy $S_{A1}$

This strategy utilizes a combination of controls $u_1$ and $u_2$ to optimize the objective function $J$. As illustrated in Figure 4.5, the number of infections is significantly lower in the controlled scenario compared to the uncontrolled case. The simulation results, with parameters $\alpha_1 = 0.005$ and $\alpha_2 = 0.002$, reflect small fractions of infectious recruits. The data clearly demonstrate that applying both control measures simultaneously leads to a notable reduction in the number of infected and exposed animals, converging to $(E, I) \approx (1.370, 0.812)$ by the end of the simulation. Throughout the simulation, external biosecurity measure $u_1$ is maintained at maximum levels, while internal measure $u_2$ is maximized for the first 3.5 semesters before tapering off as infections decline. Overall, the interventions result in a reduction of approximately $4.824 \times 10^4$ new infections over four semesters, with a total intervention cost of $4.611 \times 10^4$. This underscores the effectiveness of sustained external measures and strategic internal interventions in controlling disease transmission.

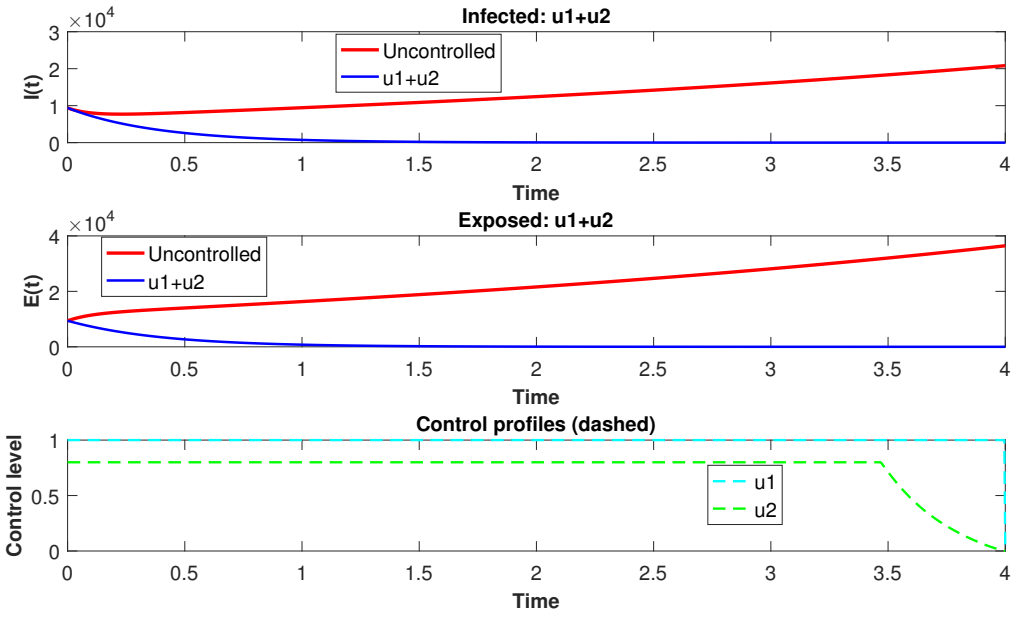


FIGURE 4.5: Strategy $A_1$: Comparison of controlled I & E with uncontrolled and the control profile.

### Strategy $S_{A2}$

This strategy employs a combination of external biosecurity measures ($u_1$) and vaccination ($u_3$) to optimize disease control. As illustrated in Figure 4.6, the implementation of these control measures, particularly in scenarios where $\alpha_i \neq 0$, results in a substantial decrease in both exposed and infectious populations. The trajectories for the exposed ($E$) and infectious ($I$) classes

indicate that the simultaneous application of both control measures culminates in a final state of approximately $(E, I) \approx (1090, 755)$ by the end of the simulation. Throughout this period, the external biosecurity measure $u_1$ is consistently maintained at its maximum efficacy, while vaccination $u_3$ is applied at peak levels during the first 3.7 semesters, subsequently tapering off in response to declining infection rates. Overall, the integration of these two interventions over four semesters is projected to avert approximately $3.5876825 \times 10^4$ new infections, incurring a total intervention cost of $2.231 \times 10^5$. This highlights the effectiveness of combining external biosecurity measures with vaccination strategies in controlling disease transmission and emphasizes the importance of sustained intervention efforts.

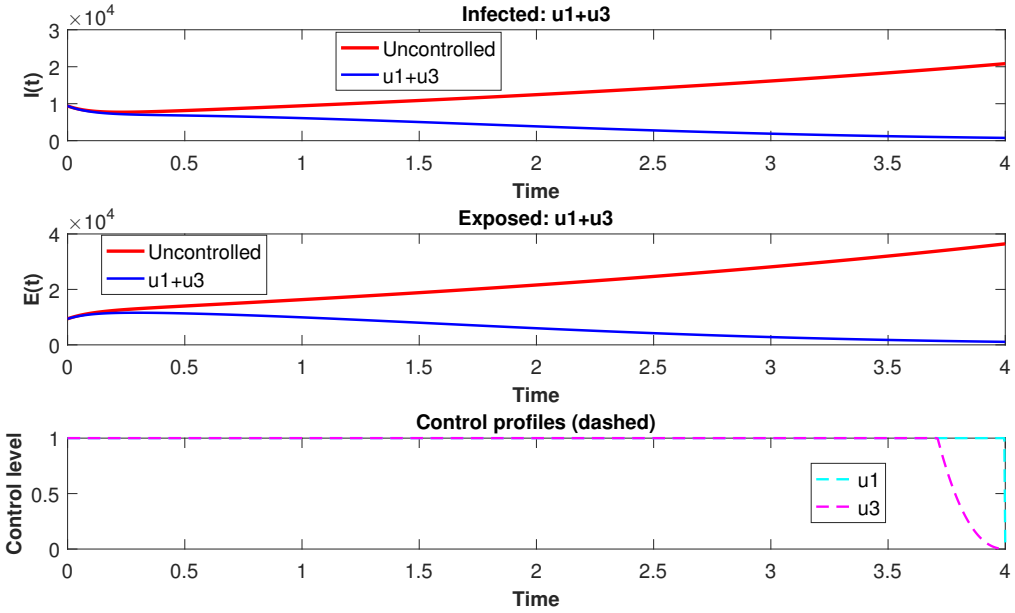


FIGURE 4.6: Strategy $A_2$: Comparison of controlled I & E with uncontrolled and the control profile.

### Strategy $S_{A3}$

In this strategy, we optimize $J$ using the two controls-external biosecurity measures ($u_1$) and treatment control ($u_4$). Despite maintaining maximum levels of control efforts throughout the entire simulation period, the reduction in the number of infectious animals is less significant compared to previous strategies, as illustrated in Figure 4.7. The trajectories for the exposed and infectious classes, $(E, I)$, converge to the endemic equilibrium point of $(1.228 \times 10^4, 6860)$. Additionally, the combination of these two interventions over four semesters is projected to reduce new infections by approximately $2.551 \times 10^4$, with a total intervention cost of $3.792 \times 10^5$.

### Strategy $S_{A4}$

The internal biosecurity control $u_2$ and vaccination control $u_3$ are employed to optimize the objective function $J$. As illustrated in Figure 4.8, the number of exposed individuals and infections in the controlled case is reduced compared to the uncontrolled case. Furthermore, the

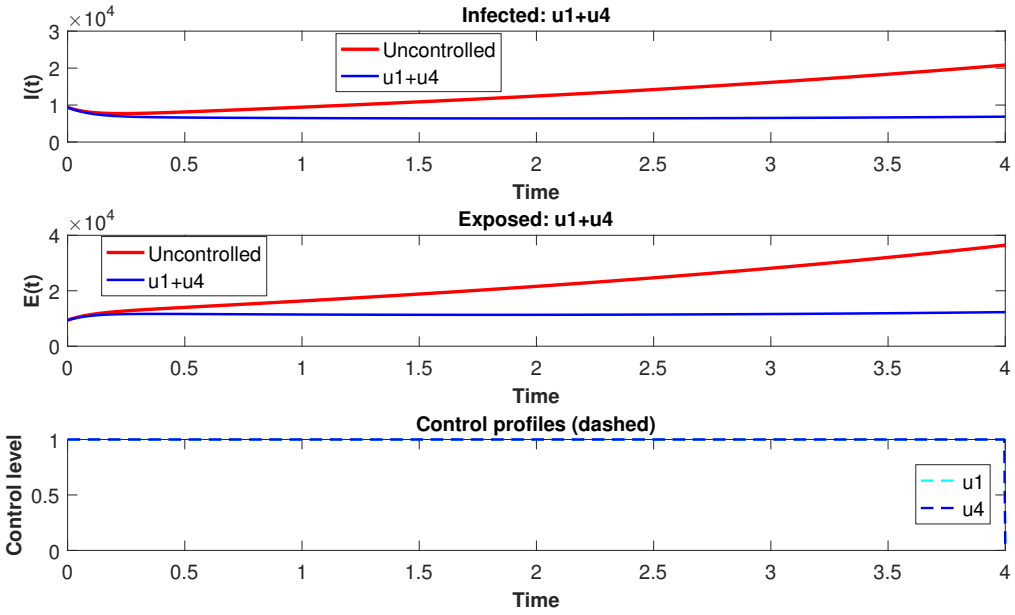


FIGURE 4.7: Strategy $A_3$: Comparison of controlled I & E with uncontrolled and the control profile.

trajectories of $E$ and $I$ demonstrate the persistence of the disease and converge to the point $(1274, 1055)$. Regarding the control profiles, Figure 4.8 suggests that the internal biosecurity control $u_2$ should be maintained at its upper bound throughout the intervention period, while the vaccination control $u_3$ should gradually decrease from the upper bound to zero after the time $t = 3.4$. Additionally, it is noted that the two interventions over the simulation period can reduce new infections by $4.439 \times 10^4$ at an intervention cost of $9.648 \times 10^4$.

### Strategy $S_{A5}$

Figure 4.9 illustrates the impact of implementing the controls $u_2$ and $u_4$ on the dynamics of the exposed and infectious classes, as well as on the cost function $J$. The results indicate that, despite maximizing the efforts of these controls throughout the entire simulation period, the trajectories converge to the endemic equilibrium point $(E, I) \mapsto (1455, 1112)$. This suggests that while Strategy $S_{A5}$ does not suffice to eradicate the disease from the population, it does contribute positively by alleviating the overall burden posed by the disease. Moreover, it is noteworthy that the two interventions implemented during the simulation period can reduce new infections by $4.446 \times 10^4$, incurring an intervention cost of $9.668 \times 10^4$. This finding highlights the effectiveness of these control measures in managing the disease, even if they do not lead to complete eradication.

### Strategy $S_{A6}$

In this strategy, we employed the controls $u_3$ and $u_4$ to optimize the cost function $J$ with maximum effort throughout the entire simulation period. The simulation results, as illustrated in Figure 4.10, indicate a reduction in the number of infections relative to the uncontrolled case,

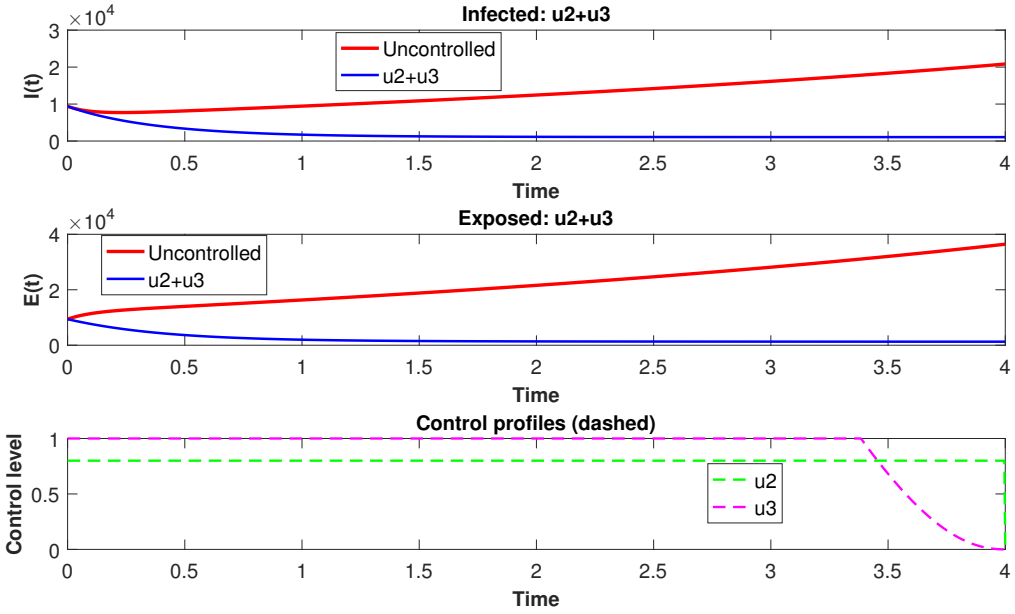


FIGURE 4.8: Strategy $A_4$: Comparison of controlled I & E with uncontrolled and the control profile.

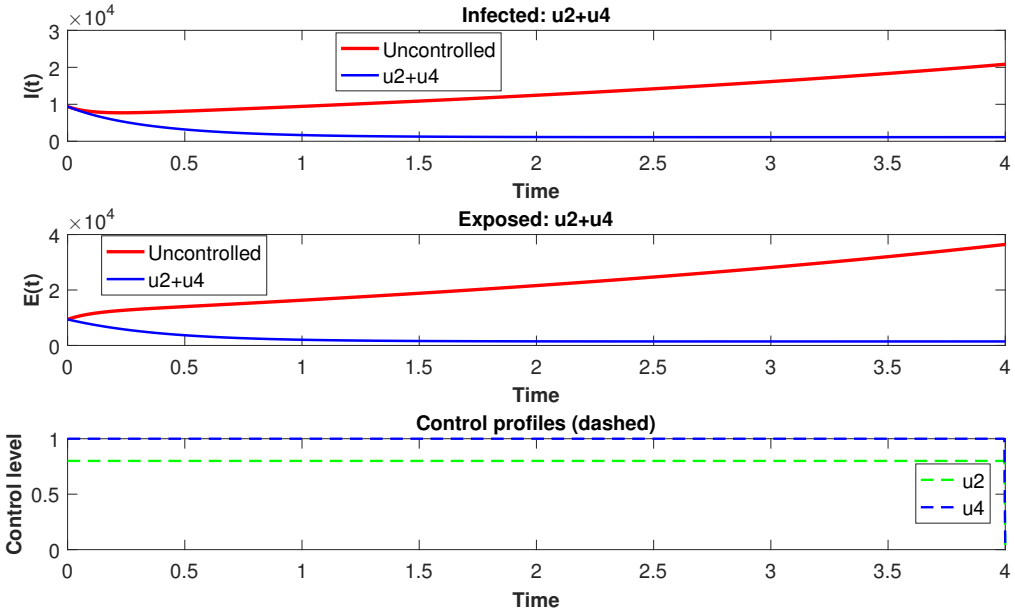


FIGURE 4.9: Strategy $A_5$: Comparison of controlled I & E with uncontrolled and the control profile.

with the trajectories for the exposed and infectious classes $E$ and $I$ converging to the endemic equilibrium point $(E, I) \mapsto (4547, 2995)$. While this strategy is insufficient for the complete eradication of the disease, it is important to note that the two interventions implemented during the simulation period can reduce new infections by $2.901 \times 10^4$ at an intervention cost of $3.21 \times 10^5$.

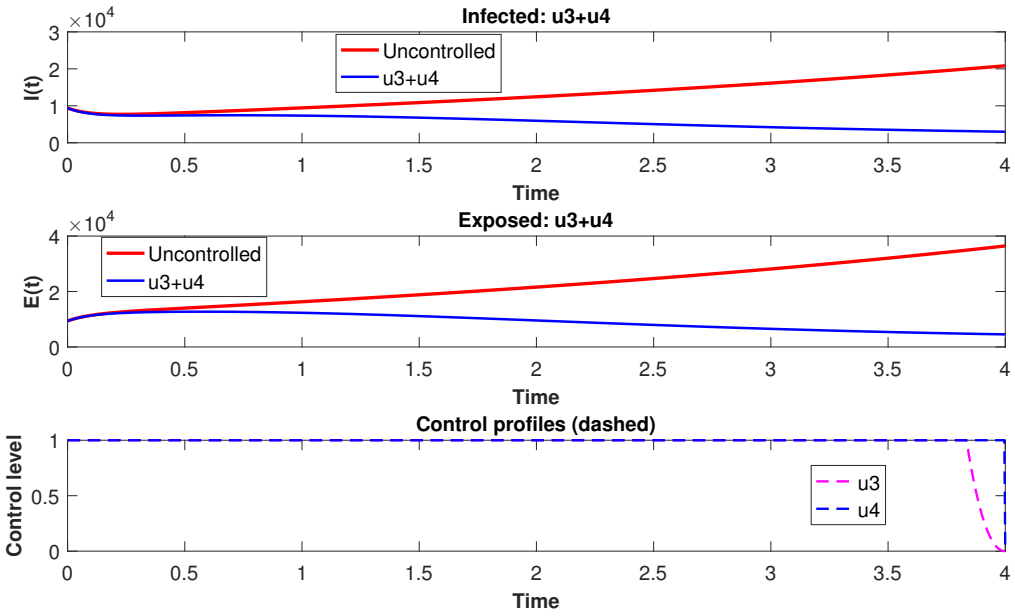


FIGURE 4.10: Strategy $A_6$: Comparison of controlled I & E with uncontrolled and the control profile.

## Scenario $\mathcal{B}$

In this secinario, we considered strategies of three controls.

### Strategy $S_{B1}$

We optimize the cost function $J$ using external biosecurity $(u_1)$, internal biosecurity $(u_2)$, and vaccination $(u_3)$. Relative to the uncontrolled baseline, the controlled trajectories shown in Figure 4.11 demonstrate significant declines in both classes, converging to the point $(E, I) \mapsto (0.852, 0.5403)$ by the end of the simulation horizon. The control profile for $u_3$ is front-loaded, operating at its maximum level for the first 1.2 semesters before gradually decreasing to zero as prevalence declines. In contrast, $u_1$ and $u_2$ are maintained at high levels, with $u_2$ tapering slightly later in the period. Over the course of four semesters, the three interventions collectively avert approximately $4.829 \times 10^4$ new infections at a total cost of $4.534 \times 10^4$. This outcome indicates an efficient reduction of transmission through an early intensive application of $u_3$ combined with sustained biosecurity measures via $u_1$ and $u_2$.

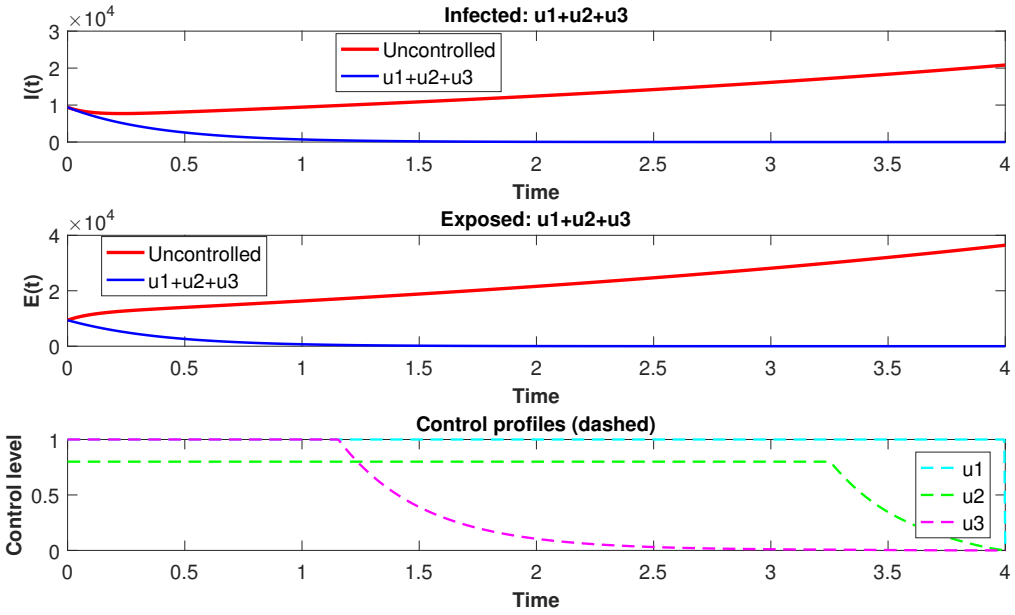


FIGURE 4.11: Strategy $B_1$: Comparison of controlled I & E with uncontrolled and the control profile.

### Strategy $S_{B2}$

The simulation results for the optimal control problem using controls $u_1, u_2$, and $u_4$, as depicted in Figure 4.12, reveal significant insights into the dynamics of the exposed and infected classes over the intervention period. The trajectories for $(E, I)$ converge to the equilibrium point $(1.241, 0.732)$, indicating a disease almost dieout under the implemented control measures. Importantly, the three interventions employed during the simulation period effectively reduce new infections by approximately $4.841 \times 10^4$ at a total intervention cost of $4.425 \times 10^4$. Regarding the control profiles, $u_4$ is applied at maximum effort until 2.7 semesters, after which it gradually declines to zero. This front-loaded approach allows for an initial intensive intervention, effectively reducing the number of infections early in the simulation. Similarly, $u_2$ is applied at its maximum level until 3.4 semesters, demonstrating a sustained effort to control the disease.

### Strategy $S_{B3}$

The simulation results for the optimal control problem, as shown in Figure 4.13, indicate that the trajectories for $(E, I)$ converge to the equilibrium point $(777, 522)$. This convergence highlights the stabilization of disease prevalence under the applied control measures. The three interventions $(u_1, u_2, u_4)$ effectively reduce new infections by approximately $3.791 \times 10^4$ at a total cost of $1.963 \times 10^5$, demonstrating their cost-effectiveness in mitigating disease spread. In terms of control profiles, $u_3$ is applied at maximum effort until 3.7 semesters, after which it gradually declines to zero. In contrast, $u_1$ and $u_2$ are sustained at maximum levels throughout the simulation, ensuring continuous control over disease transmission.

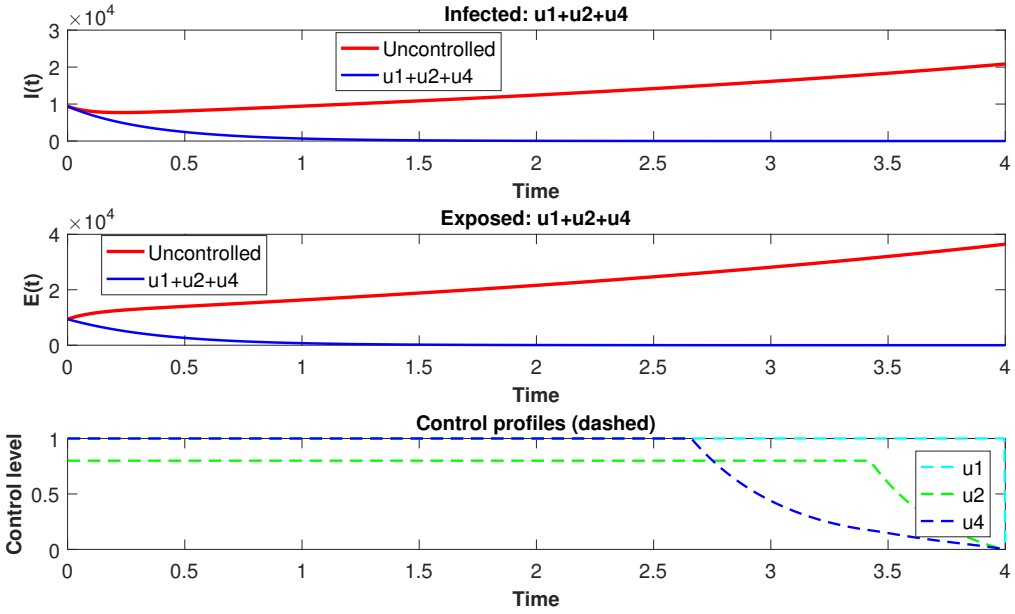


FIGURE 4.12: Strategy $B_2$: Comparison of controlled I & E with uncontrolled and the control profile.

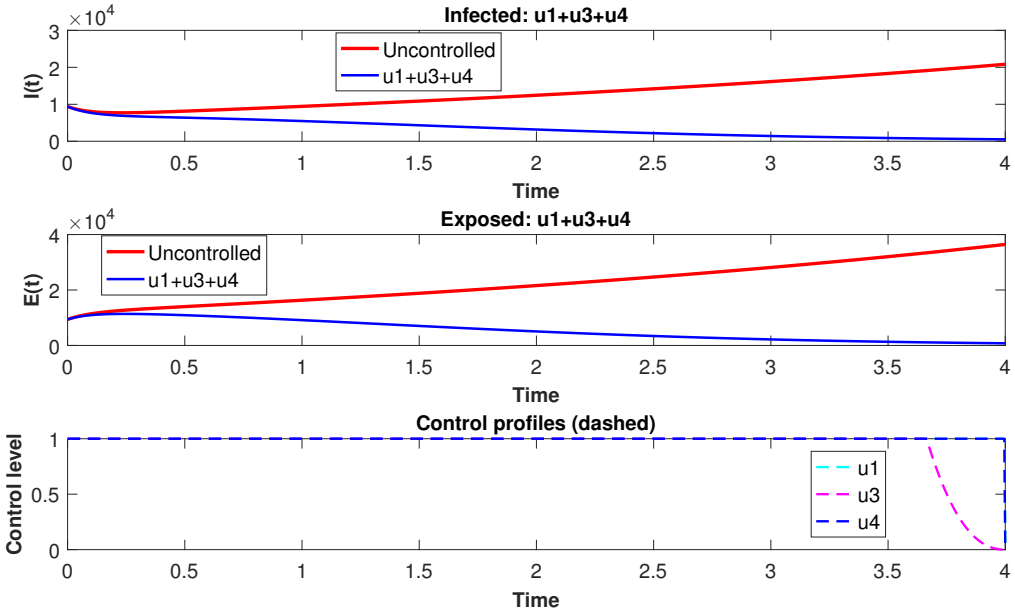


FIGURE 4.13: Strategy $B_3$: Comparison of controlled I & E with uncontrolled and the control profile.

**Strategy** $S_{B4}$

The simulation results for the optimal control problem, depicted in Figure 4.14, reveal that the trajectories for the exposed and infected classes converge to the equilibrium point $(1264, 1010)$. This convergence indicates a stabilization of disease prevalence under the implemented control measures. The three interventions $(u_2, u_3, u_4)$ significantly reduce new infections by approximately $4.472 \times 10^4$ at a total intervention cost of $9.03 \times 10^4$, demonstrating their effectiveness in controlling disease spread. In terms of control profiles, $u_3$ is applied at maximum effort until 3.4 semesters, after which it gradually declines to zero. In contrast, $u_2$ and $u_4$ are maintained at maximum levels throughout the simulation, ensuring continuous control over the infection dynamics. However, the presence of uncontrolled external infections through restocking contributes to the persistence of the disease in the population.

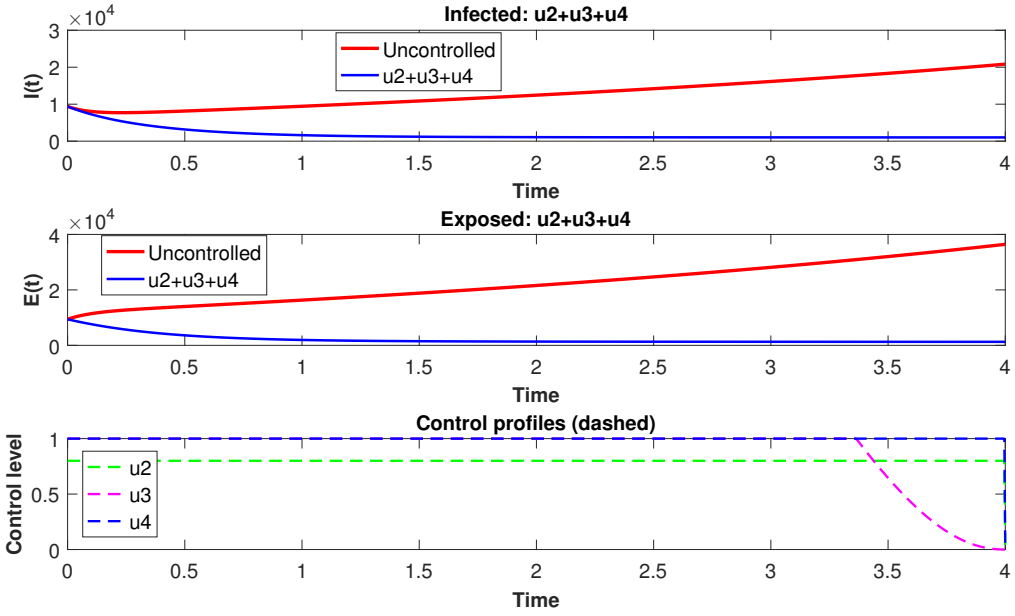


FIGURE 4.14: Strategy $B_4$: Comparison of controlled I & E with uncontrolled and the control profile.

## Scenario $\mathcal{C}$

In this secinario, we considered strategy of four controls. **Strategy** $S_C$**:** The final simulation results for the optimal control problem, as depicted in Figure 4.15, show that the trajectories for the exposed and infected populations converge to the equilibrium point $(0.80, 0.5)$. This convergence indicates a successful control of disease prevalence through the implemented control measures. The combination of four interventions $(u_1, u_2, u_3, u_4)$ effectively reduces new infections by approximately $4.846 \times 10^4$ at a total intervention cost of $4.357 \times 10^4$. This demonstrates the cost-effectiveness and efficiency of the adopted strategy in managing disease transmission. Examining the control profiles, $u_2$ is applied at maximum effort until 3.2 semesters, after which it gradually declines to zero. Similarly, $u_3$ is maximized until 1.1 semesters, and $u_4$ until 2.5

semesters, both tapering off thereafter. In contrast, $u_1$ is sustained at maximum effort throughout the entire simulation period, providing continuous control over the infection dynamics. The strategic deployment of these interventions highlights their effectiveness in curbing infection rates. The initial intensive interventions, coupled with the sustained effort of $u_1$, play a crucial role in achieving significant reductions in new infections.

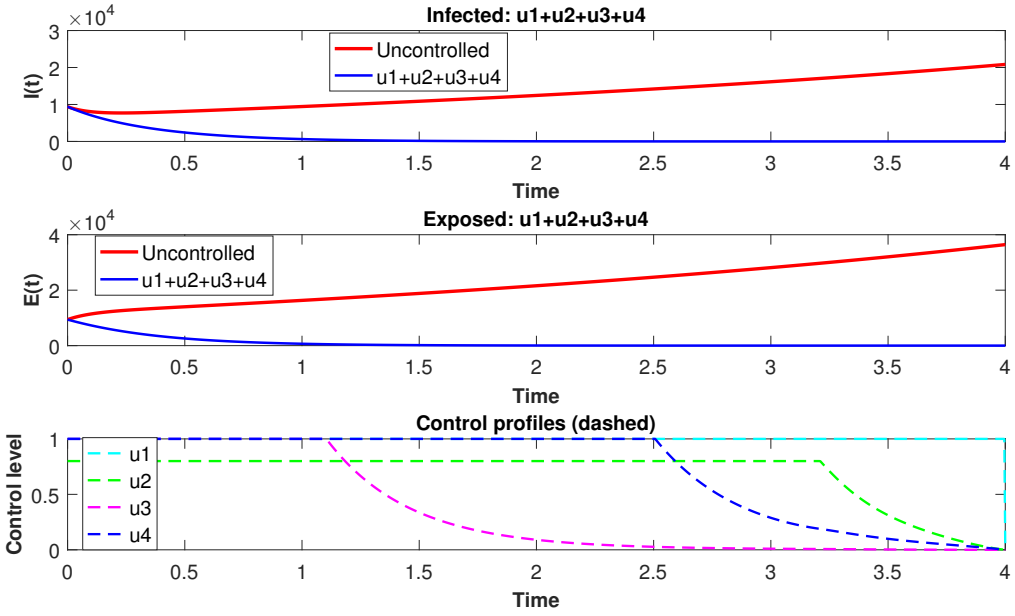


FIGURE 4.15: Strategy $C$: Comparison of controlled I & E with uncontrolled and the control profile.

In summary, the simulation results underscore the importance of a well-coordinated intervention strategy that combines both initial intensive efforts and ongoing support to effectively manage and reduce disease prevalence over time. Moreover, the next section provides a summarized result on the effectiveness of the control regarding infections averted and associated control costs in Table 4.4 and the bar graph in Figure 4.16.

### 4.7.3 Cost-Effectiveness Analysis

In this section, we evaluate the cost-effectiveness of various control strategies across different scenarios using the Incremental Cost-Effectiveness Ratio (ICER).

The Incremental Cost-Effectiveness Ratio (ICER) quantifies the change in costs relative to the change in health benefits (e.g., cases averted) between two competing intervention strategies. Considering strategies $S_1$ and $S_2$ as two competing control interventions, the ICER is calculated as follows:

$$\text{ICER} = \frac{\text{Change in total costs between strategies } S_1 \text{ and } S_2}{\text{Change in health benefits between strategies } S_1 \text{ and } S_2}.$$

A lower ICER indicates a more cost-effective strategy.

The total number of averted infections is computed using the following equation:

$$\text{Total Averted} = \int_0^{T_f} [I^{\text{wout}} - I^{\text{w}}]\, dt$$

where $I^{\text{wout}}$ represents infections without control, and $I^{\text{w}}$ represents infections with control. The total cost is calculated based on the objective functional defined in Equation (4.18).

Using the total number of averted cases and the associated costs provided in Table (4.4), we first calculate the ICER for each scenario independently. Subsequently, we compare the cost-effectiveness of the strategies across the three scenarios.

**Cost-Effectiveness Analysis for Scenario $\mathcal{A}$**

Based on the increasing order of cases averted (as shown in Table (4.4)), we compute the ICER for each strategy as follows:

1. **Comparison between Strategies $S_{A3}$ and $S_{A6}$:**

$$\text{ICER}(S_{A3}) = \frac{379,200}{25,510} = 14.8647,$$

$$\text{ICER}(S_{A6}) = \frac{321,000 - 379,200}{29,010 - 25,510} = -16.6286.$$

   The results indicate that Strategy $S_{A3}$ is strongly dominated, as it incurs higher costs compared to Strategy $S_{A6}$. Therefore, Strategy $S_{A3}$ is excluded from further consideration. The next comparison is conducted between Strategies $S_{A6}$ and $S_{A2}$.

2. **Comparison between Strategies $S_{A6}$ and $S_{A2}$:**

$$\text{ICER}(S_{A6}) = \frac{321,000}{29,010} = 11.0651,$$

$$\text{ICER}(S_{A2}) = \frac{223,100 - 321,000}{35,870 - 29,010} = -14.2711.$$

   Here, Strategy $S_{A6}$ is dominated by Strategy $S_{A2}$, as it has a higher ICER. Thus, Strategy $S_{A6}$ is excluded, and the next comparison is conducted between Strategies $S_{A2}$ and $S_{A4}$.

3. **Comparison between Strategies $S_{A2}$ and $S_{A4}$:**

$$\text{ICER}(S_{A2}) = \frac{223,100}{35,870} = 6.2197.$$

$$\text{ICER}(S_{A4}) = \frac{96,480 - 223,100}{44,390 - 35,870} = -14.8615.$$

   Since $\text{ICER}(S_{A4}) < \text{ICER}(S_{A2})$, Strategy $S_{A4}$ is more cost-effective, and Strategy $S_{A2}$ is excluded. The next comparison is conducted between Strategies $S_{A4}$ and $S_{A5}$.

4. **Comparison between Strategies $S_{A4}$ and $S_{A5}$:**

$$\text{ICER}(S_{A4}) = \frac{96,480}{44,390} = 2.1739,$$

$$\text{ICER}(S_{A5}) = \frac{96,680 - 96,480}{44,460 - 44,390} = 2.8571.$$

Since $\text{ICER}(S_{A4}) < \text{ICER}(S_{A5})$, Strategy $S_{A5}$ is excluded. The final comparison is conducted between Strategies $S_{A4}$ and $S_{A1}$.

5. **Comparison between Strategies $S_{A4}$ and $S_{A1}$:**

$$\text{ICER}(S_{A1}) = \frac{46,110 - 96,480}{48,240 - 44,390} = -13.0831.$$

The analysis shows that Strategy $S_{A1}$ is the most cost-effective strategy in Scenario $\mathcal{A}$ for reducing PPR disease at the minimum cost.

**Cost-Effectiveness Analysis for Scenario $\mathcal{B}$**

1. **Comparison between Strategies $S_{B3}$ and $S_{B4}$:**

$$\text{ICER}(S_{B3}) = \frac{196,300}{37,910} = 5.1781,$$

$$\text{ICER}(S_{B4}) = \frac{93,000 - 196,300}{44,720 - 37,910} = -15.1689.$$

Strategy $S_{B4}$ is more cost-effective than Strategy $S_{B3}$, so Strategy $S_{B3}$ is excluded. The next comparison is between Strategies $S_{B4}$ and $S_{B1}$.

2. **Comparison between Strategies $S_{B4}$ and $S_{B1}$:**

$$\text{ICER}(S_{B4}) = \frac{93,000}{44,720} = 2.0796,$$

$$\text{ICER}(S_{B1}) = \frac{45,340 - 93,000}{48,290 - 44,720} = -13.0831.$$

Strategy $S_{B1}$ is more cost-effective than Strategy $S_{B4}$, so Strategy $S_{B4}$ is excluded. The final comparison is between Strategies $S_{B1}$ and $S_{B2}$.

3. **Comparison between Strategies $S_{B1}$ and $S_{B2}$:**

$$\text{ICER}(S_{B1}) = \frac{45,340}{48,290} = 0.9389,$$

$$\text{ICER}(S_{B2}) = \frac{44,250 - 45,340}{48,410 - 48,290} = -9.0837.$$

Since $\text{ICER}(S_{B2}) < \text{ICER}(S_{B1})$, Strategy $S_{B2}$ is the most cost-effective strategy in Scenario $\mathcal{B}$.

**Cost-Effectiveness Analysis for Scenario $\mathcal{C}$**

In Scenario $\mathcal{C}$, there is only one strategy with four controls $(u_1, u_2, u_3, u_4)$. The ICER is computed as follows:

$$\text{ICER}(S_C) = \frac{43,570}{48,460} = 0.8990.$$

**Final Comparison Across Scenarios**

Comparing the most cost-effective strategies from each scenario, the strategy in Scenario $\mathcal{C}$ emerges as the most effective, followed by Strategy $S_{B2}$ from Scenario $\mathcal{B}$, and Strategy $S_{A1}$ from Scenario $\mathcal{A}$.

TABLE 4.4: Total cost and averted infection of each strategies

| Optimal control Scenarios | Strategies ($\mathbf{S}$) | Total averted infection | Total cost | cost-effective strategy | most cost-effective strategy |
|---|---|---|---|---|---|
| Scenario $\mathcal{A}$ | $\mathbf{S}_{A1}$ $(u_1+u_2)$ | $4.824\times10^4$ | $4.611\times10^4$ | $\mathbf{S}_{A1}$ | $\mathbf{S}_C$ |
| | $\mathbf{S}_{A2}$ $(u_1+u_3)$ | $3.587\times10^4$ | $2.231\times10^5$ | | |
| | $\mathbf{S}_{A3}$ $(u_1+u_4)$ | $2.551\times10^4$ | $3.792\times10^5$ | | |
| | $\mathbf{S}_{A4}$ $(u_2+u_3)$ | $4.439\times10^4$ | $9.648\times10^4$ | | |
| | $\mathbf{S}_{A5}$ $(u_2+u_4)$ | $4.446\times10^4$ | $9.668\times10^4$ | | |
| | $\mathbf{S}_{A6}$ $(u_3+u_4)$ | $2.901\times10^4$ | $3.21\times10^5$ | | |
| Scenario $\mathcal{B}$ | $\mathbf{S}_{B1}$ $(u_1+u_2+u_3)$ | $4.829\times10^4$ | $4.534\times10^4$ | $\mathbf{S}_{B2}$ | |
| | $\mathbf{S}_{B2}$ $(u_1+u_2+u_4)$ | $4.841\times10^4$ | $4.425\times10^4$ | | |
| | $\mathbf{S}_{B3}$ $(u_1+u_3+u_4)$ | $3.791\times10^4$ | $1.963\times10^5$ | | |
| | $\mathbf{S}_{B4}$ $(u_2+u_3+u_4)$ | $4.472\times10^4$ | $9.30\times10^4$ | | |
| Scenario $\mathcal{C}$ | $\mathbf{S}_C$ $(u_1+u_2+u_3+u_4)$ | $4.846\times10^4$ | $4.357\times10^4$ | $\mathbf{S}_C$ | |

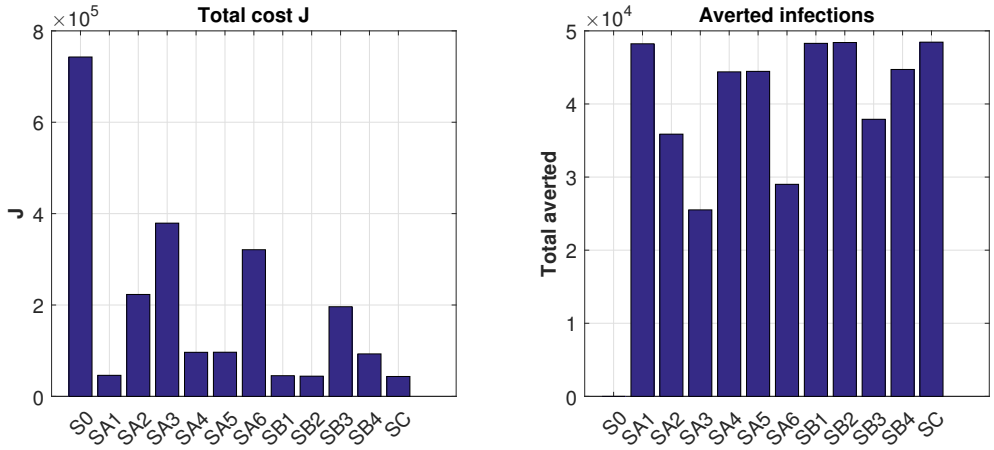


FIGURE 4.16: Bar graphs: Comparison of each strategy with repect to infection averted and total cost.

## 4.8 Results and Discussion

Peste des petits ruminants (PPR) is a highly contagious viral disease affecting small ruminants, with substantial implications for animal health and socioeconomics. In this study, we developed

a deterministic compartmental model to describe PPR transmission and formulated an optimal control problem to evaluate intervention strategies, particularly focusing on the effect of restocking on disease dynamics. Our analytical results establish the existence and global stability of an endemic equilibrium for relevant parameter regimes, and sensitivity analysis identifies the parameters most significantly affecting transmission and control outcomes. Numerical simulations using a fourth-order Runge–Kutta scheme reveal that the introduction of infected restocked animals substantially undermines vaccination programs, with continuous inflow of infectious animals sustaining transmission even when vaccination is in place. Conversely, stringent biosecurity measures—both external measures that reduce the inflow of infectious animals and internal measures enabling identification, segregation, and treatment—markedly reduce the risks associated with restocking and improve overall control effectiveness. Parameter estimates calibrated to World Organisation for Animal Health (OIE) incidence data for Ethiopia yield a control reproduction number $\mathcal{R}_v \approx 1.02$ in the absence of restocking, consistent with observed endemicity in the region. However, incorporating restocking into the model clarifies why vaccination-alone strategies fail in practice: infective inflow maintains $\mathcal{R}_v$ at or above one unless complemented by biosecurity and treatment measures. Cost-effectiveness analysis shows that a combined strategy incorporating external biosecurity, internal biosecurity, vaccination, and treatment ($S_C$) produces the largest reduction in infections per unit cost, followed by strategy $S_{B2}$ and then $S_{A1}$, underscoring that multi-pronged interventions are generally more efficient than single-measure approaches. These findings align with previous recommendations on movement restrictions and vaccination Fathelrahman et al., 2021 but diverge from analyses that ignored restocking effects Waret-Szkuta et al., 2008, highlighting the critical importance of incorporating connectivity into epidemiological models. Consistent with serological and molecular studies Fentie et al., 2018; Fournié et al., 2018; Alemu et al., 2019, our results support the persistent endemicity of PPR at the national scale while uniquely quantifying the additional role of restocking in maintaining transmission. The study's limitations include incomplete or imprecise incidence and parameter data from OIE and literature sources, which reduce confidence in estimates like $\mathcal{R}_v$, as well as the omission of time delays, stochasticity in restocking events, and socioeconomic factors affecting biosecurity compliance. Future research should incorporate stochastic and delay formulations, develop hybrid statistical-mechanistic frameworks using advanced parameter-estimation techniques and machine learning, and model the probability of introducing infectious animals via restocking. Motivated by recent studies (Saber et al., 2025; Althubyani et al., 2025; Adam et al., 2025), extending the integer-order model to a fractional-order formulation could better capture memory and hereditary effects in PPR dynamics. In conclusion, achieving PPR eradication targets such as the 2027 goal requires integrated strategies that combine vaccination, treatment, and robust biosecurity to prevent the importation and onward transmission of infection. The modeling framework and optimal-control analyses presented here provide quantitative guidance for policymakers to design cost-effective, evidence-based PPR control programs.

# Chapter 5

# The Impact of Movement and Vaccination on PPR Disease Spread between Two Different Agroecological Zones

## 5.1 Introduction

Effective control of Peste des Petits Ruminants (PPR) remains a priority for Ethiopia, where the disease is endemic and small ruminant production is a major component of the agricultural economy. Despite ongoing vaccination campaigns, persistent outbreaks are reported across the country, with heterogeneous seroprevalence and transmission patterns linked to varying agroecological zones and livestock management systems (Waret-Szkuta et al., 2008; Fournié et al., 2018; Dubie et al., 2022; Fentie et al., 2018).

In Ethiopia, highland (sedentary) and lowland (pastoral) zones differ markedly in animal husbandry practices and patterns of small ruminant movement. Seasonal migration and trade-driven movements between these zones play a significant role in facilitating PPRV circulation and challenge the effectiveness of vaccination programs (Fournié et al., 2018). Recent studies have demonstrated that the spatial structure and movement of animals substantially influence the persistence and spread of PPR, underscoring the need for spatially explicit models that incorporate these factors (Fournié et al., 2018; Martcheva, 2015; Burton et al., 2012).

National seroprevalence surveys and retrospective analyses have revealed that PPR incidence and immunity levels vary by region, and that outbreaks are frequently associated with animal movements between agroecological zones (Waret-Szkuta et al., 2008; Fentie et al., 2018; Dubie et al., 2022). Discrete and continuous metapopulation models have been employed to capture the dynamics of PPR transmission at the national scale, providing valuable insights into the effectiveness of vaccination and the critical thresholds required for disease elimination in the presence of population mobility (Fournié et al., 2018; Martcheva, 2015).

Building on these findings, this chapter develops a coupled two-patch SEIR model to investigate the impact of small ruminant movement and vaccination strategies on the spatial spread and persistence of PPR between Ethiopia's highland and lowland zones. The model enables

estimation of transmission parameters and vaccination coverage based on empirical data, and facilitates evaluation of coordinated vaccination and movement control measures. Through numerical simulations, we explore how different combinations of population movement and vaccination strategies influence disease persistence and the likelihood of eradication. The results reinforce the importance of integrating vaccination programs across zones with effective movement controls to optimize PPR management and support national eradication efforts.

## 5.2 Model Formulation

In the formulation of the model, two coupled subpopulations (districts) are used as metapopulation patches to investigate the impact of animal movement between districts on the dynamics of PPR disease. These subpopulations consist of highland and lowland groups of small ruminants. The disease dynamics of each population is described using the SEIR model.

Let $(S_l, S_h)$, $(E_l, E_h)$, $(I_l, I_h)$, and $(R_l, R_h)$ represent the susceptible, exposed, infectious, and recovered disease classes of the two groups, respectively. It is assumed that the rates of movement between the two groups (districts) differ. The rate at which susceptible, exposed, infectious, and recovered small ruminants move from the lowland district to the highland district is denoted by $a_{hl}$, $b_{hl}$, $c_{hl}$, and $d_{hl}$, respectively. Similarly, the rates of movement in the opposite direction, from the highland district to the lowland district, are denoted by $a_{lh}$, $b_{lh}$, $c_{lh}$, and $d_{lh}$.

In the lowland group, the total population of small ruminants is $N_l$, where $N_l = S_l + E_l + I_l + R_l$. In the highland group, the total population of small ruminants is $N_h$, where $N_h = S_h + E_h + I_h + R_h$.

For each sub-population i (i = l, h), the recruitment rate of the sub-population per unit of time is denoted as $\Lambda_i$. The progression rates of incubation, recovery, disease-related death, and natural death rates are represented by $\sigma_i$, $\gamma_i$, $\delta_i$, and $\mu_i$, respectively. The vaccination rate of the susceptible population is denoted as $\omega_i$. In this model formulation, we consider the following assumptions:

- The population structure of the two sub-populations mixing is homogeneous. Since the disease transmission occurs through direct contact between infectious and susceptible individuals, we assume a mass action incidence rate, $\beta_i S_i I_i$, where $\beta_i$ is the disease transmission rate per individual per unit time.
- The mobility matrices are not necessarily symmetric, but they are irreducible.
- Without loss of generality, we assume that $a_{ii} = b_{ii} = c_{ii} = d_{ii} = 0$.
- The model assumes that vaccination is perfect, resulting in lifelong immunity for vaccinated small ruminants. Vaccination is administered after the outbreak of PPR.
- We assume that individuals do not change their disease state during migration (movement).
- All parameters are positive constants, except for $a_{ij}$, $b_{ij}$, $c_{ij}$, $d_{ij}$, and $\delta_i$, which are non-negative.

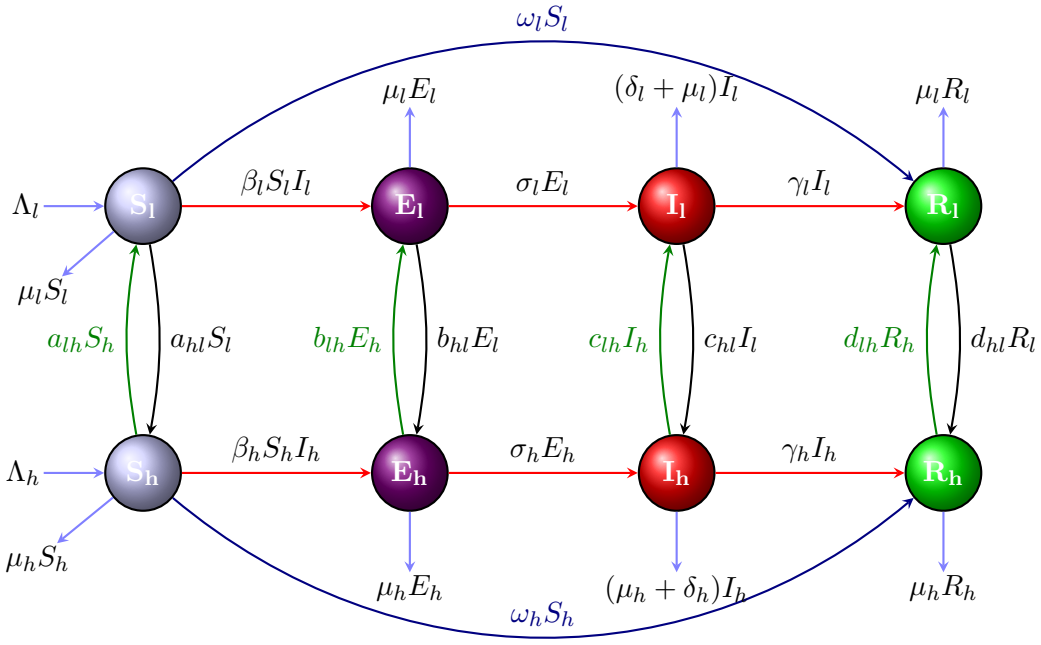


FIGURE 5.1: A schematic diagram for the transmission of PPR in small ruminant population with the effect of movement.

The aforementioned assumptions, description, and the model flow diagram (Figure 5.1) result in the model system (5.1).

$$\begin{cases} \frac{dS_l}{dt} = \Lambda_l - \beta_l S_l(t) I_l(t) + a_{lh} S_h(t) - (a_{hl} + \omega_l + \mu_l) S_l(t), \\ \frac{dE_l}{dt} = \beta_l S_l(t) I_l(t) + b_{lh} E_h(t) - (b_{hl} + \sigma_l + \mu_l) E_l(t), \\ \frac{dI_l}{dt} = \sigma_l E_l(t) + c_{lh} I_h(t) - (c_{hl} + \delta_l + \gamma_l + \mu_l) I_l(t), \\ \frac{dR_l}{dt} = \gamma_l I_l(t) + \omega_l S_l(t) + d_{lh} R_h(t) - (d_{hl} + \mu_l) R_l(t), \\ \frac{dS_h}{dt} = \Lambda_h - \beta_h S_h(t) I_h(t) + a_{hl} S_l(t) - (a_{lh} + \omega_h + \mu_h) S_h(t), \\ \frac{dE_h}{dt} = \beta_h S_h(t) I_h(t) + b_{hl} E_l(t) - (b_{lh} + \sigma_h + \mu_h) E_h(t), \\ \frac{dI_h}{dt} = \sigma_h E_h(t) + c_{hl} I_l(t) - (c_{lh} + \delta_h + \gamma_h + \mu_h) I_h(t), \\ \frac{dR_h}{dt} = \gamma_h I_h(t) + \omega_h S_h(t) + d_{hl} R_l(t) - (d_{lh} + \mu_h) R_h(t). \end{cases} \tag{5.1}$$

## 5.3 Model Analysis

### 5.3.1 Positively Invariant Region and Boundedness of Solution

In this subsection, we examine the fundamental outcomes regarding the solutions of the system (5.1), which carry significant importance in both mathematical and epidemiological interpretations.

**Lemma 5.3.1.** *Every non-negative solution of system (5.1) is bounded in $L^1$-norm by $max\{N(0), \frac{\bar{\Lambda}}{\mu}\}$.*

**Proof** The total population in two subpopulations at any time $t$ is $N(t) = N_l(t) + N_h(t)$, can be determined by adding all equations in (5.1). Let $\mu = min\{\mu_l, \mu_h\}$ and $\bar{\Lambda} = \Lambda_l + \Lambda_h$. i.e

$$\frac{dN}{dt} = \bar{\Lambda} - \mu N - (\delta_l I_l + \delta_h I_h) \leq \bar{\Lambda} - \mu N. \tag{5.2}$$

Solving the differential inequality (5.2) with non-negative initial condition $N(0) = N_0$ using 'Groonwall's Inequality' gives;

$$N(t) \leq N_0 e^{-\mu t} + \frac{\bar{\Lambda}}{\mu}(1 - e^{-\mu t}),$$

a standard comparison argument shows that $\lim_{t\to\infty} \sup N(t) \leq \frac{\bar{\Lambda}}{\mu}$.

The norm $L^1$ for each non-negative solution is N and satisfies the inequality $N' \leq \bar{\Lambda} - \mu N$. The solutions of equation $M' = \bar{\Lambda} - \mu M$ are increasing and bounded by $\frac{\Lambda}{\mu}$ if $M(0) < \bar{\Lambda}/\mu$. They are monotonically decreasing and bounded above if $M(0) \geq \bar{\Lambda}/\mu$. Since $N' \leq M'$, the claim follows.

Furthermore, it is crucial to demonstrate the existence of a unique solution to the model (5.1).

**Lemma 5.3.2.** *For any non-negative initial condition*

$$\mathbf{x}_0 = (S_{l0}, E_{l0}, I_{l0}, R_{l0}, S_{h0}, E_{h0}, I_{h0}, R_{h0}) \in \mathbf{R}^8_+,$$

*system (5.1) admits a unique solution*

$$\mathbf{x}(t) = (S_l(t), E_l(t), I_l(t), R_l(t), S_h(t), E_h(t), I_h(t), R_h(t))$$

*defined on $[0, \infty)$ that satisfies the initial conditions and remains non-negative and bounded for all $t \geq 0$.*

**Proof** The proof follows two main steps, with the boundedness property following directly from Lemma 5.3.1.

**Step 1: Local existence and uniqueness.** Let

$$\mathbf{x}(t) = (S_l(t), E_l(t), I_l(t), R_l(t), S_h(t), E_h(t), I_h(t), R_h(t))^T$$

and write system (5.1) as

$$\frac{d\mathbf{x}}{dt} = f(\mathbf{x}), \quad \mathbf{x}(0) = \mathbf{x}_0 \in \mathbf{R}^8_+,$$

where $f : \mathbf{R}^8 \to \mathbf{R}^8$ consists of the right-hand sides of the equations. Each component of $f$ is a polynomial in the state variables; therefore $f$ is continuously differentiable ($C^1$) on $\mathbf{R}^8$. A $C^1$ function is locally Lipschitz continuous. By the Picard–Lindelöf theorem, for each $\mathbf{x}_0$ there exists a unique solution defined on a maximal interval $[0, t_{\max})$.

**Step 2: Non-negativity of solutions.** We apply the invariance theorem of (Theorem A.4 in Thieme, 2018) to the closed set $D = \mathbf{R}^8_+$. For $\mathbf{x} \in \partial D$, a coordinate $\mathbf{x}_i = 0$ must satisfy $f_i(\mathbf{x}) \geq 0$ to prevent the flow from leaving $D$. We verify this condition for a few state variables; the remaining cases follow analogously.

Consider the lowland susceptible population $S_l$. When $S_l = 0$,

$$f_1(\mathbf{x}) = \frac{dS_l}{dt} = \Lambda_l + a_{lh}S_h \geq 0,$$

since $\Lambda_l > 0$ and $S_h \geq 0$.

Similarly, when the lowland exposed population $E_l = 0$,

$$f_2(\mathbf{x}) = \frac{dE_l}{dt} = \beta_l S_l I_l + b_{lh}E_h \geq 0,$$

because all quantities on the right are non-negative.

Proceeding in the same manner, one can verify that for every variable $x_i$ (including $I_l, R_l, S_h, E_h, I_h, R_h$), the condition $x_i = 0$ implies $f_i(\mathbf{x}) \geq 0$. Consequently, the vector field $f$ points inward (or is tangent) on $\partial D$. By Thieme's theorem, $\mathbf{R}^8_+$ is positively invariant: if $\mathbf{x}_0 \in \mathbf{R}^8_+$, then $\mathbf{x}(t) \in \mathbf{R}^8_+$ for all $t \in [0, t_{\max})$.

**Step 3: Global existence and boundedness.** From Lemma 5.3.1, every non-negative solution of system (5.1) is bounded in $L^1$-norm by $\max\left\{N(0), \frac{\bar{\Lambda}}{\mu}\right\}$, where $\bar{\Lambda} = \Lambda_l + \Lambda_h$ and $\mu = \min\{\mu_l, \mu_h\}$. This implies that all state variables remain bounded on $[0, t_{\max})$.

Since the solution remains bounded on the finite interval $[0, t_{\max})$, standard continuation theory for ODEs guarantees that $t_{\max} = \infty$. Hence the solution exists globally on $[0, \infty)$ and is bounded for all $t \geq 0$. This completes the proof.

**Remark 5.3.3.** *Lemma 5.3.2 establishes the well-posedness of system (5.1), while Lemma 5.3.1 provides the explicit bound* $\max\left\{N(0), \frac{\bar{\Lambda}}{\mu}\right\}$ *for the* $L^1$*-norm of solutions. Together, they ensure that the biologically feasible region*

$$\Gamma = \left\{(S_l, E_l, I_l, R_l, S_h, E_h, I_h, R_h) \in \mathbf{R}^8_+ : N \leq \frac{\bar{\Lambda}}{\mu}\right\}$$

*is positively invariant and that all solutions starting in* $\mathbf{R}^8_+$ *remain in* $\Gamma$ *for all* $t \geq 0$.

### 5.3.2 The Control Reproduction Number and Stability Analysis of Equilibria

The first step involves demonstrating the existence of a unique equilibrium point in the model system, which represents a state free from disease. Subsequently, the next generation matrix method Van den Driessche et al., 2002 is employed to calculate the basic reproduction number, $\mathcal{R}_v$, which is then used to assess the stability of the system.

To determine the disease-free equilibrium (DFE) of the system (5.1), the variables $E_i$ and $I_i$ are set to zero for $i = l, h$ in (5.1) at a steady state, where $\frac{dS}{dt} = 0 = \frac{dR}{dt}$. This process yields separate systems of equations for $S_i^0$ and $R_i^0$.

$$\begin{cases} CS = \Lambda \\ DR = \omega S, \end{cases} \tag{5.3}$$

where

$$C = \begin{bmatrix} a_{hl} + \omega_l + \mu & -a_{lh} \\ -a_{hl} & a_{lh} + \omega_h + \mu \end{bmatrix}, D = \begin{bmatrix} d_{hl} + \mu & -d_{lh} \\ -d_{hl} & d_{lh} + \mu \end{bmatrix}, \Lambda = [\Lambda_l, \Lambda_h]^T, \ , S = [S_l, S_h]^T,$$

$\omega = [\omega_l, \omega_h]$, and $R = [R_l, R_h]^T$.

Since all off-diagonal entries of matrices $C$ and $D$ are non-positive and the sum of the entries in each column of $C$ and $D$ is positive, $C$ and $D$ are non-singular M-matrices and $C^{-1} \geq 0$ and $D^{-1} \geq 0$ (Berman et al., 1994, p. 137). Therefore, linear systems in (5.3) have unique positive solutions $S^0 = (S_l^0, S_h^0)^T = C^{-1}\Lambda > 0$ and $R^0 = (R_l^0, R_h^0) = D^{-1}\omega S^0 > 0$. As a consequence, the system (5.1) has a unique disease-free equilibrium $\xi^0 = (S_l^0, 0, 0, R_l^0, S_l^0, 0, 0, R_l^0)$, where

$$\begin{cases} S_l^0 = \dfrac{(a_{lh} + \omega_h + \mu)\Lambda_l + a_{lh\Lambda_h}}{(\mu + \omega_l)(a_{lh} + \omega_h + \mu) + a_{hl}(\omega_h + \mu)}, \\ S_h^0 = \dfrac{(a_{hl} + \omega_l + \mu)\Lambda_h + a_{hl\Lambda_l}}{(\mu + \omega_l)(a_{lh} + \omega_h + \mu) + a_{hl}(\omega_h + \mu)}, \\ R_l^0 = \dfrac{(d_{lh} + \mu)\omega_l S_l^0 + d_{lh}\omega_h S_h^0}{\mu(\mu + d_{hl} + d_{lh})}, \\ R_l^0 = \dfrac{(d_{hl} + \mu)\omega_h S_h^0 + d_{hl}\omega_l S_l^0}{\mu(\mu + d_{hl} + d_{lh})}. \end{cases} \tag{5.4}$$

Thus, we have the following result.

**Proposition 5.3.4.** *The model system (5.1) always has a unique disease-free equilibrium $\xi^0$.*

The local stability of $\xi^0$ can be determined by calculating the control reproduction number, denoted $\mathcal{R}_v$, using the next-generation operator method developed by Van den Driessche and Walmough Van den Driessche et al., 2002. The control reproduction number, $\mathcal{R}_v$, serves as a threshold parameter that predicts the spread of the disease within the population. It quantifies the expected number of new cases of PPR generated by a single infected small ruminant in a completely susceptible population that resides in a region with a vaccination program. If $\mathcal{R}_v < 1$, the infection will eventually die out. In contrast, if $\mathcal{R}_v > 1$, the disease will persist within the population.

**Theorem 5.3.5.** *The model system (5.1) with non-negative initial conditions, the disease-free equilibrium of PPR $\xi^0$ is locally asymptotically stable if $\mathcal{R}_v < 1$ and unstable if $\mathcal{R}_v > 1$.*

**Proof** Let $u = (E_l, E_h, I_l, I_h)^T$ is the vector of infected state variables. The Jacobian matrix of system (5.1) at the PPR-disease free equilibrium state $\xi^0$ is given by

$$J(\xi^0) = \begin{bmatrix} F - V & 0 \\ J_{21} & J_{22} \end{bmatrix}$$

where $F = \left(\frac{\partial \mathcal{F}}{\partial u}\right)_{\xi^0}$, $\mathcal{F}$ is the rates of new infection and $V = \left(\frac{\partial \mathcal{V}}{\partial u}\right)_{\xi^0}$, $\mathcal{V}$ is the rate of transfer from in and out of the infected compartments in the system (5.1). From the right side equations in the system (5.1), we consider the exposed and infectious as infected classes, then

$$\mathcal{F} = \begin{bmatrix} \beta_l S_l I_l \\ \beta_h S_h I_h \\ 0 \\ 0 \end{bmatrix} \quad \text{and} \quad \mathcal{V} = \begin{bmatrix} -b_{lh}E_h + (b_{hl} + \sigma_l + \mu)E_l \\ -b_{hl}E_l + (b_{lh} + \sigma_h + \mu)E_h \\ -\sigma_l E_l - c_{lh}I_h + (c_{hl} + \delta_l + \gamma_l + \mu)I_l \\ -\sigma_h E_h - c_{hl}I_l + (c_{lh} + \delta_h + \gamma_h + \mu)I_h \end{bmatrix}.$$

Here we write the matrices $F$ and $V$ as block matrices

$$F = \begin{bmatrix} 0 & F_{12} \\ 0 & 0 \end{bmatrix}, \text{where} \quad F_{12} = \begin{bmatrix} \beta_l S_l^{(0)} & 0 \\ 0 & \beta_h S_h^{(0)} \end{bmatrix}$$

$$V = \begin{bmatrix} V_{11} & 0 \\ V_{21} & V_{22} \end{bmatrix}, \text{where} \quad V_{11} = \begin{bmatrix} b_{hl} + \sigma_l + \mu & -b_{lh} \\ -b_{hl} & b_{lh} + \sigma_h + \mu \end{bmatrix}, V_{21} = \begin{bmatrix} -\sigma_l & 0 \\ 0 & -\sigma_h \end{bmatrix},$$

$$V_{22} = \begin{bmatrix} c_{hl} + \alpha_1 & -c_{lh} \\ -c_{hl} & c_{lh} + \alpha_2 \end{bmatrix}$$

where $\alpha_1 = \delta_l + \gamma_l + \mu$ and $\alpha_2 = \delta_h + \gamma_h + \mu$. And

$$J_{22} = \begin{bmatrix} -(a_{hl} + \omega_l + \mu) & a_{lh} & 0 & 0 \\ a_{hl} & -(a_{lh} + \omega_h + \mu) & 0 & 0 \\ \omega_l & 0 & -(d_{hl} + \mu) & d_{lh} \\ 0 & \omega_h & d_{hl} & -(d_{lh} + \mu) \end{bmatrix}$$

The disease-free equilibrium $\xi^0$ is said to be locally asymptotically stable if all eigenvalues of the Jacobian matrix $J(\xi^0)$ of the system (5.1) evaluated at $\xi^0$ have negative real parts. Conversely, the disease-free equilibrium $\xi^0$ is unstable if the Jacobian matrix $J(\xi^0)$ has at least one eigenvalue with a positive real part. Furthermore, the negativity of the eigenvalues of the Jacobian matrix $J$ is determined by the matrices $F - V$ and $J_{22}$, where $F$ and $V$ are the matrices appearing in the next generation operator formulation of the system, and $J_{22}$ is the submatrix of $J$ corresponding to the infected compartments.

The eigenvalues of the matrix $J_{22}$ are given by:

$$\begin{cases} \lambda_1 = -\mu, \\ \lambda_2 = -(d_{hl} + d_{lh} + \mu), \\ \lambda_{3,4} = \dfrac{-1}{2}\left(a_{lh} + a_{hl} + \omega_h + \omega_l + 2\mu \pm \sqrt{\mathcal{H}}\right) \end{cases}$$

where $\mathcal{H} = (a_{hl} + a_{lh} + \omega_h - \omega_l)^2 - 4a_{hl}(\omega_h - \omega_l)$.

It can be shown that $\lambda_3$ and $\lambda_4$ are always negative using the same approach as Burton et al., 2012. Let $\mathcal{G} = a_{lh} + a_{hl} + \omega_h + \omega_l + 2\mu$, and consider $\mathcal{H}$ as a quadratic expression in $\omega_h$. The

absolute minimum of $\mathcal{H}$ occurs when $\frac{d\mathcal{H}}{d\omega_h} = 0$, which gives $\omega_h = a_{hl} - a_{lh} + \omega_l$. Substituting this expression into $\mathcal{H}$ yields $4a_{hl}a_{lh} > 0$, implying that $\mathcal{H} > 0$ for all $\omega_h$. Therefore, $\lambda_3$ and $\lambda_4$ are real-valued. Next, we check that $\mathcal{G} \pm \sqrt{\mathcal{H}} > 0$. Since $\mathcal{G} + \sqrt{\mathcal{H}} > 0$, we have $\lambda_3 < 0$. For $\lambda_4 < 0$, we require $\mathcal{G} > \sqrt{\mathcal{H}}$, which is equivalent to $\omega_h > -\frac{\mu^2+\mu a_{hl}+a_{lh}\mu+\mu\omega_l+a_{lh}\omega_l}{\mu+\omega_l+a_{hl}}$. Since we assume $\omega_h > 0$, this condition is always satisfied. Therefore, $\mathcal{G} - \sqrt{\mathcal{H}} > 0$, which implies $\lambda_4 < 0$. Consequently, the local stability of the PPR disease-free equilibrium depends only on the eigenvalues of the matrix $F - V$. According to the ((Van den Driessche et al., 2002), proof of Thoerem 2), all eigenvalues of $F - V$ have negative real parts if and only if $s(F - V) < 0$, which is equivalent to $\rho\{FV^{-1}\} < 1$. Since $V$ is an irreducible non-singular M-matrix, it has a positive inverse ((Berman et al., 1994), p. 141), and $FV^{-1}$ is a non-negative matrix and given by

$$FV^{-1} = \left[\begin{array}{c|c} 0 & F_{12} \\ \hline 0 & 0 \end{array}\right] \left[\begin{array}{c|c} V_{11}^{-1} & 0 \\ \hline B & V_{22}^{-1} \end{array}\right] = \left[\begin{array}{c|c} F_{12}B & F_{12}V^{-1} \\ \hline 0 & 0 \end{array}\right]$$

where $B = V_{22}^{-1}\text{diag}(\sigma_l, \sigma_h)V_{11}^{-1}$.

The control reproduction number ($\mathcal{R}_v$), which is the spectral radius of matrix (Van den Driessche et al., 2002), $\rho(FV^{-1})$, is given as

$$\mathcal{R}_v = \rho\Big\{\text{diag}(b_1, b_2)V_{22}^{-1}\text{diag}(\sigma_l, \sigma_h)V_{11}^{-1}\Big\} = \rho\left\{\begin{pmatrix} K_{11} & K_{12} \\ K_{21} & K_{22} \end{pmatrix}\right\}$$

where

$$\begin{cases} K_{11} = \dfrac{b_1((c_{lh}+\alpha_2)\sigma_l(b_{lh}+\sigma_h+\mu) + c_{lh}\sigma_h b_{hl})}{((b_{lh}+\sigma_h+\mu)\sigma_l + \mu^2 + (b_{hl}+b_{lh}+\sigma_h)\mu + b_{hl}\sigma_h)(\alpha_1 c_{lh} + \alpha_2(c_{hl}+\alpha_1))}, \\ K_{12} = \dfrac{b_1((c_{lh}+\alpha_2)\sigma_l b_{lh} + c_{lh}\sigma_h(b_{hl}+\sigma_l+\mu))}{((b_{hl}+\sigma_l+\mu)\sigma_h + (\mu+b_{lh})\sigma_l + \mu(\mu+b_{hl}+b_{lh}))(\alpha_1 c_{lh} + \alpha_2(c_{hl}+\alpha_1))}, \\ K_{21} = \dfrac{b_2((c_{hl}\sigma_l + b_{hl}(c_{hl}+\alpha_1))\sigma_h + c_{hl}\sigma_l(\mu+b_{lh}))}{((b_{hl}+\sigma_l+\mu)\sigma_h + (\mu+b_{lh})\sigma_l + \mu(\mu+b_{hl}+b_{lh}))((c_{lh}+\alpha_2)\alpha_1 + \alpha_2 c_{hl})}, \\ K_{22} = \dfrac{b_2(c_{hl}\sigma_l b_{lh} + (c_{hl}+\alpha_1)\sigma_h(b_{hl}+\sigma_l+\mu))}{((b_{hl}+\sigma_l+\mu)\sigma_h + \mu^2 + (\sigma_l+b_{hl}+b_{lh})\mu + \sigma_l b_{lh})((c_{lh}+\alpha_2)\alpha_1 + \alpha_2 c_{hl})}. \end{cases}$$

Thus

$$\mathcal{R}_v = \frac{1}{2}\left(K_{11} + K_{22} + \sqrt{(K_{11}-K_{22})^2 + 4K_{12}K_{21}}\right)$$

where $b_1 = \beta_l S_l^{(0)}$ and $b_2 = \beta_h S_h^{(0)}$.

By Theorem B.8 in (Salmani et al., 2006), if the reproduction number $\mathcal{R}_v < 1$, then the spectral bound $s(F - V) < 0$. Consequently, all the eigenvalues of the system lie in the left half of the complex plane. According to Definition B.9 in (Salmani et al., 2006), the system (5.1) is then locally asymptotically stable.

Conversely, if the reproduction number $\mathcal{R}_v > 1$, then the spectral bound $s(F - V) > 0$. This implies that at least one eigenvalue of the system lies in the right half of the complex plane. In this case, according to Definition B.9 in (Salmani et al., 2006), the system (5.1) is unstable.

**Remark 5.3.6.** *The control reproduction numbers ($\mathcal{R}_v^i$) of each subpopulation (district) in the absence of small ruminant movement (migration) between the Highland and Lowland districts*

*(groups) (i.e., when the two districts are isolated) can be determined using the following expressions:*

$$\mathcal{R}_v^l = \frac{\beta_l \sigma_l \Lambda_l}{\alpha_1(\mu+\omega_l)(\sigma_l+\mu)} \quad and \quad \mathcal{R}_v^h = \frac{\beta_h \sigma_h \Lambda_h}{\alpha_2(\omega_h+\mu)(\sigma_h+\mu)}$$

*for the Lowland and Highland PPR dynamics, respectively.*

**Remark 5.3.7.** *In the special case in which there is only movement of small ruminants from the lowland district to the highland district (i.e $a_{lh} = b_{lh} = c_{lh} = d_{lh} = 0$), the basic control reproduction number becomes*

$$\mathcal{R}_v = max\Big\{\frac{b_1\sigma_l}{(c_{hl}+\alpha_1)(b_{hl}+\sigma_l+\mu)}, \frac{b_2\sigma_h}{\alpha_2(\sigma_h+\mu)}\Big\}$$

*where* $b_1 = \beta_l S_l^{(0)}, b_2 = \beta_h S_h^{(0)}$, *with* $S_h^{(0)} = \frac{\Lambda_h(\omega_l+\mu)+(\Lambda_h+\Lambda_l)a_{hl}}{(\omega_h+\mu)(\mu+\omega_l+a_{hl})}, S_l^{(0)} = \frac{\Lambda_l}{\mu+\omega_l+a_{hl}}$.

*Furthermore, a similar threshold quantity known as the basic reproduction number $\mathcal{R}_0$, is obtained by setting $\omega_l = 0 = \omega_h$ in $\mathcal{R}_v$*

$$\mathcal{R}_0 = max\Big\{\frac{\beta_l\sigma_l\Lambda_l}{(c_{hl}+\alpha_1)(b_{hl}+\sigma_l+\mu)(\mu+a_{hl})}, \frac{\beta_h\sigma_h(\mu\Lambda_h+(\Lambda_l+\Lambda_h)a_{hl})}{\mu\alpha_2(\sigma_h+\mu)(\mu+a_{hl})}\Big\}.$$

**Theorem 5.3.8.** *The PPR disease-free equilibrium $\xi_0$ of model system (5.1) is globally asymptotically stable provided $\mathcal{R}_v < 1$, and unstable if $\mathcal{R}_v > 1$.*

**Proof** To investigate the global asymptotically stable of the model (5.1), we follow the method in (Castillo-Chavez et al., 2004). First, we write system (5.1) in the form

$$\begin{cases} \dfrac{dX}{dt} = F(X,Y), \\ \dfrac{dY}{dt} = G(X,Y), G(X,0) = 0. \end{cases} \tag{5.5}$$

Where $X = (S_l, S_h, R_l, R_h)$ denote the number of uninfected small ruminants, and the components of $Y = (E_l, E_h, I_l, I_h)$ denote the number of infected small ruminants. Let $X^*$ be the disease-free equilibrium of the system $\frac{dX}{dt} = F(X,0)$ where $X^* = (S_l^{(0)}, S_h^{(0)}, R_l^{(0)}, R_h^{(0)})$. The DFE $\xi_0$ is guaranteed to be GAS if $\mathcal{R}_v < 1$ (which is locally asymptotically stable), and the following two conditions $H_1$ and$H_2$ hold.

$H_1$. For $\frac{dX}{dt} = F(X,0)$, $X^*$ is globally asymptotically stable.

$H_2$. $G(X,Y) = AY - \bar{G}(X,Y)$, $\bar{G}(X,Y) \geq 0$ for all $(X,Y) \in \Omega$ where $A = \frac{\partial G(X^*)}{\partial Y}$ is an M-matrix.

Now consider the system

$$F(X,0) = \begin{bmatrix} \Lambda_l + a_{lh}S_h(t) - (a_{hl}+\omega_l+\mu)S_l(t) \\ \Lambda_h + a_{hl}S_l(t) - (a_{lh}+\omega_h+\mu)S_h(t) \\ \omega_l S_l(t) + d_{lh}R_h(t) - (d_{hl}+\mu)R_l(t) \\ \omega_h S_h(t) + d_{hl}R_l(t) - (d_{lh}+\mu)R_h(t) \end{bmatrix} \tag{5.6}$$

From the first and second equation in (5.6), we have non-homogeneous system

$$\frac{dS}{dt} = AS + C \tag{5.7}$$

where $A = \begin{bmatrix} -(a_{hl} + \omega_l + \mu) & a_{lh} \\ a_{hl} & -(a_{lh} + \omega_h + \mu) \end{bmatrix}$, $S = [S_l, S_h]^T$, and $C = [\Lambda_l, \Lambda_h]^T$.
The solution of (5.7) is the sum of the homogeneous solution and particular solution. Since $A$ is the negative of a non-singular M-matrix, by Theorem B.5 in (Salmani et al., 2006), all eigenvalues lie in the left half plane. Thus $\lim_{t\to\infty} S_H(t) = 0$ with $S_H(t)$ denoting the homogeneous solution of (5.7) ($\frac{dS}{dt} = AS$). And matrix $-A$ is an irreducible non-singular M-matrix and therefore by Theorem B.4 in (Salmani et al., 2006), has a positive inverse. Therefore $S_p = -A^{-1}C$ is a particular solution for (5.7), and $S(t) = S_H(t) + S_p$ is the general solution for (5.7). Thus $\lim_{t\to\infty} S = S_p = S^{(0)} = (S_l^{(0)}, S_h^{(0)})$. Similarly, from the third and fourth equation of recovery classes in F, we have $\lim_{t\to\infty} R = R_p = R^{(0)} = (R_l^{(0)}, R_h^{(0)})$. Thus, all points with respect to this condition converges to $X^*$. Hence $X^*$ is globally asymptotically stable.

Next, we have

$$G(X,Y) = \begin{bmatrix} \beta_l S_l(t) I_l(t) + b_{lh} E_h(t) - (b_{hl} + \sigma_l + \mu_l) E_l(t) \\ \beta_h S_h(t) I_h(t) + b_{hl} E_l(t) - (b_{lh} + \sigma_h + \mu_h) E_h(t) \\ \sigma_l E_l(t) + c_{lh} I_h(t) - (c_{hl} + \delta_l + \gamma_l + \mu_l) I_l(t) \\ \sigma_h E_h(t) + c_{hl} I_l(t) - (c_{lh} + \delta_h + \gamma_h + \mu_h) I_h(t) \end{bmatrix},$$

then obtain

$$\begin{aligned} A = \frac{\partial G(X^*, 0)}{\partial Y} &= \begin{bmatrix} -(b_{hl} + \sigma_l + \mu) & b_{lh} & \beta_l S_l^{(0)} & 0 \\ b_{hl} & -(b_{lh} + \sigma_h + \mu) & 0 & \beta_h S_h^{(0)} \\ \sigma_l & 0 & -(c_{hl} + \delta_l + \gamma_l + \mu) & c_{lh} \\ 0 & \sigma_h & c_{hl} & -(c_{lh} + \delta_h + \gamma_h + \mu) \end{bmatrix} \\ &= F - V \end{aligned}$$

which is clearly M-matrix. And

$$\bar{G}(X,Y) = AY - G(X,Y) = \begin{bmatrix} \beta_l I_l (S_l^{(0)} - S_l) \\ \beta_h I_h (S_h^{(0)} - S_h) \\ 0 \\ 0 \end{bmatrix}.$$

Since all parameters are non-negative, thus $0 \le S_l \le S_l^{(0)}$and $0 \le S_h \le S_h^{(0)}$. Hence, $\bar{G}(X,Y) \ge 0$ for all $(X,Y) \in \Omega$. Therefore, the disease-free equilibrium of PPR $\xi_0$ of the model (5.1) is globally asymptotically stable.

**Remark 5.3.9.** *For assessing the critical role of vaccination as a control strategy, the stability properties of the disease-free equilibrium (DFE) are crucial. Our analytical analysis in Theorems*

*(5.3.5) and (5.3.8) shows that a threshold value of the reproduction number $\mathcal{R}_v < 1$ ensures the local and global asymptotic stability of the DFE. This indicates that, under these conditions, any small outbreak will diminish over time, leading to the eventual eradication of the disease.*

*In this context, vaccination can directly influence the reproduction number. By increasing the vaccination rate, we can effectively reduce $\mathcal{R}_v$. To illustrate this critical vaccination rate, we considered the scenarios in Remarks (5.3.6) and (5.3.7).*

- *For the case of an isolated group of the population, the necessary vaccination rates to achieve and maintain $\mathcal{R}_v < 1$ can be expressed as:*

$$\omega_i > \frac{\beta_i\sigma_i\Lambda_i - \mu(\gamma_i+\delta_i+\mu)(\sigma_i+\mu)}{(\gamma_i+\delta_i+\mu)(\sigma_i+\mu)} = \omega_c, \quad \forall i = l, h.$$

- *For the coupled system, specifically in the scenario where the influx of population occurs from the Lowland to the Highland zone only, the critical vaccination rate can be determined using the computed formula for $\mathcal{R}_v$ from Remark (5.3.7). Suppose that $\mathcal{R}_v = \frac{b_2\sigma_h}{(\gamma_h+\delta_h+\mu)(\sigma_h+\mu)}$; thus, the expected vaccination rate becomes:*

$$\omega_l > \frac{\beta_h\sigma_h(\Lambda_h(\mu+a_{hl}) + \Lambda_l a_{hl}) - (\omega_h+\mu)(\mu+a_{hl})(\gamma_h+\delta_h+\mu)(\sigma_h+\mu)}{\beta_h\sigma_h\Lambda_h - (\omega_h+\mu)(\gamma_h+\delta_h+\mu)(\sigma_h+\mu)}.$$

*Alternatively, if $\mathcal{R}_v = \frac{b_1\sigma_l}{(c_{hl}+\gamma_l+\delta_l+\mu)(b_{hl}+\sigma_l+\mu)}$, then the expected vaccination rate to control the disease becomes:*

$$\omega_l > \frac{\beta_l\Lambda_l\sigma_l - (\mu+a_{hl})(c_{hl}+\gamma_l+\delta_l+\mu)(b_{hl}+\sigma_l+\mu)}{(c_{hl}+\gamma_l+\delta_l+\mu)(b_{hl}+\sigma_l+\mu)}.$$

*Furthermore, the global stability of the DFE suggests that even in scenarios where the disease spreads beyond initial expectations, a robust vaccination strategy can return the system to the DFE. This highlights the importance of designing vaccination programs that are adaptable and responsive to the dynamics of the outbreak, thus ensuring long-term control of the disease. These analytical results can be illustrated in the numerical simulation section.*

*Overall, this stability analysis provides a strong framework for policy makers to develop effective vaccination strategies that align with the dynamics of disease spread.*

**Remark 5.3.10.** *For the existence of unique endemic equilibrium:*

*i. The case in which the system is uncoupled (the two population are isolated), If $\mathcal{R}_v^i > 1, i = l, h$, the system (5.1) has a unique endemic equilibrium $\xi^* = (S_i^*, E_i^*, I_i^*, R_i^*)$, where*

$$S_i^* = \frac{(\gamma_i+\delta_i+\mu)(\mu+\sigma_i)}{\beta_i\sigma_i}, E_i^* = \frac{(\gamma_i+\delta_i+\mu)(\mu+\omega_i)}{\beta_i\sigma_i}\left(\mathcal{R}_v^i - 1\right), I_i^* = \frac{(\mu+\omega_i)}{\beta_i}\left(\mathcal{R}_v^i - 1\right),$$

*and*

$$R_i^* = \frac{\sigma_i\gamma_i(\mu+\omega_i)(\mathcal{R}_v^i - 1) + \omega_i(\gamma_i+\delta_i+\mu)(\mu+\sigma_i)}{\mu\beta_i\sigma_i}.$$

*Furthermore, in the specific case where $\omega_i = 0$, the model becomes the classical SEIR model. Thus, the local and global stability of the endemic equilibrium is proved in (Martcheva, 2015, p. 151-157).*

ii. *For the scenario in which the system (5.1) is coupled, implying that the mobility matrices $B = (b_{ij})$ and $C = (c_{ij})$ are irreducible or satisfy the conditions $(b_{ij} > 0, c_{ij} > 0, i = l, h)$, and if $\mathcal{R}_v > 1$, with evidence of instability of disease-free equilibrium, $\xi^0$ as stated in Theorem (5.3.8), we can establish the same conclusion as study (Liu et al., 2023) for the uniform persistence of the system (5.1). This conclusion can be drawn since the model corresponds to a specific case presented in (Liu et al., 2023), utilizing a uniform persistence result derived from (Freedman et al., 1994), along with a similar argument as presented in the proof of Theorem 4.3 in (Liu et al., 2023). Furthermore, it can be deduced from a similar argument as demonstrated in the proof of (Li et al., 2009) that the system (5.1) has an endemic equilibrium.*

## 5.4 Parameter Estimation

In this study, our main focus is on the estimation of parameters in the model (5.1) for two distinct populations of small ruminants: the Highland and Lowland populations. We assumed that there is no movement between the two patches or groups, resulting in a decoupled system. Consequently, we considered the dynamics of each group independently for the purpose of parameter estimation. We used monthly PPR-disease incidence data from January 2019 to August 2022, spanning four years. These data were collected from the National Animal Disease Surveillance System (NADSS), specifically the Monthly Disease Occurrence and Vaccination Activity Reporting System (DOVAR), which operates with the authorization of the Minister of Agriculture. Furthermore, we incorporated data on the death rate due to PPR from the WOAH (World Organization for Animal Health) dashboard (WOAH, 2023), which provided summarized data for reporting purposes. To estimate the birth rate and total population, we relied on data from the Central Statistical Agency (CSA) of Ethiopia for the year 2021/2022 ((CSA), 2021). In particular, to fit the model to the data, we transformed the incidence data into prevalence by utilizing cumulative sums (cumsum) in MATLAB. This approach facilitated the determination of the optimal parameters that would best align our model (5.1) with the available data. To accomplish this, we employ the nonlinear least-squares approximation method, which seeks to minimize the sum of squared errors.

The sum of squared errors (SSE) is defined as follows:

$$SSE = \sum_{j=1} (I_j - I^*(t_j))^2. \tag{5.8}$$

Here, $I_j$ represents the prevalence data and $I^*(t_j) = I(t_j) + E(t_j)$ represents the simulation result for the prevalence of the disease at time step j. We used initial conditions for the two groups: for the Lowland group, $(S_{l0}, E_{l0}, I_{l0}, R_{l0}) = (38307832, 200, 8340, 0)$, and for the Highland group, $(S_{h0}, E_{h0}, I_{h0}, R_{h0}) = (45412074, 100, 817, 0)$. The estimated parameter values are listed in Table (5.1), and the visualization of the results is shown in Figure (5.2). In figures (5.2A)

and (5.2C), the blue curves represent the simulation results of $I_i^*(t), i = l, h$ from the model (5.1), while the red dots indicate the monthly PPR disease data from January 2019 to August 2022 for the cases of Lowland and Highlands. Furthermore, Figures (5.2B) and (5.2D) depict the residuals of the observed and predicted cases.

Our analysis yielded estimated parameters for both the Highland and Lowland populations. By comparing these parameter values between the two groups, we were able to identify possible variations in the dynamics of the disease. These findings provide valuable information on the differences in disease transmission patterns between the two populations. Furthermore, despite variations in parameter estimation methods, observed data and analysis methods (model formulation), both the results obtained from parameter estimation in (Fournié et al., 2018) and our model indicate a high tendency or potential for the spread of PPR disease in the Lowland districts compared to the Highland districts. In the numerical simulation section, we elaborate on the implications of these estimated parameters and thoroughly examine their significance.

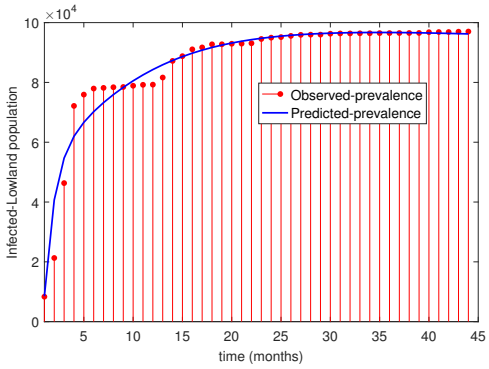


(A) In Lowland population;Fitted curve(blue line) and observed data (red stem dot) from parameter estimation

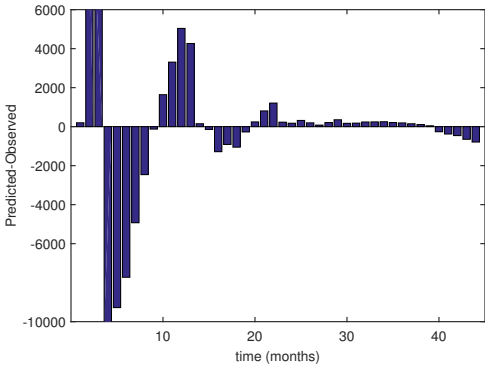


(B) Residual Bar Graph depicting the Differences between Fitted Curve and Observed Data for Lowland population

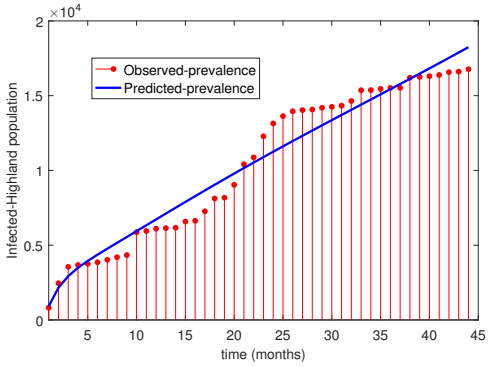


(C) In Highland population;Fitted curve(blue line) and observed data (red stem dot) from parameter estimation

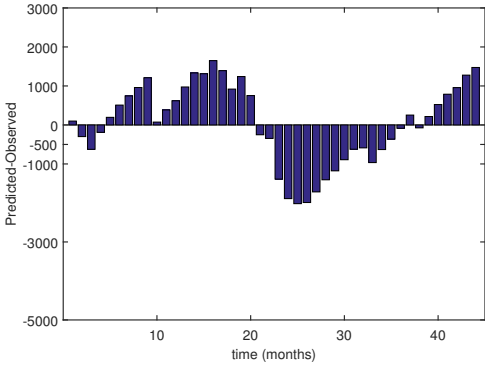


(D) Residual Bar Graph depicting the Differences between Fitted Curve and Observed Data for Highland population

FIGURE 5.2: Comparison of Fitted Curve and Observed Data from Parameter Estimation.

TABLE 5.1: Description and values of Parameters

| Parameter | Description | Values | | Reference |
|---|---|---|---|---|
| | | Lowland District | Highland District | |
| $\Lambda$ | Recruitment rate | 1194826 | 1427805 | (CSA), 2021 |
| $\beta$ | transmission rate | 1.7485e-7 | 5.5019e-8 | Estimated |
| $\gamma$ | recovery rate | 0.6006 | 0.3517 | Estimated |
| $\delta$ | Death rate due to PPR | 0.2 | 0.15 | WOAH, 2023 |
| $\sigma$ | rate of progression from E to I | 0.0143 | 0.0442 | Estimated |
| $\omega$ | vaccination rate | 0.0628 | 0.0778 | Estimated |
| $\mu$ | natural death rate | 0.0116 | 0.0116 | (CSA), 2021 |

## 5.5 Numerical Simulation and Discussion

The simulations were performed using the fourth-order Runge-Kutta method, which was implemented within MATLAB's `ode45` function. This approach is suitable for solving ordinary differential equations (ODEs). The parameter values were obtained from Table (5.1). Using several situations, we show how mobility and immunization affect disease dynamics. To show global stability, we applied the following initial conditions:

$$\begin{aligned}
&\text{IC1:} \quad [38307832, 200, 8340, 0, 45412074, 100, 817, 0]\\
&\text{IC2:} \quad [38309372, 2000, 5000, 0, 45412541, 150, 300, 0]\\
&\text{IC3:} \quad [38313372, 500, 2500, 0, 45411241, 700, 1050, 0]\\
&\text{IC4:} \quad [38315672, 200, 500, 0, 45408791, 200, 4000, 0]\\
&\text{IC5:} \quad [38308872, 200, 7300, 0, 45404431, 530, 8030, 0].
\end{aligned}$$

We specified a simulation time period of 0 to 300 months to observe the model's long-term behavior.

### 5.5.1 Impact of Movement of Small Ruminants between Lowland and Highland on PPR Disease Dynamics

In this discussion, we examined various scenarios, as described in Table (5.2), to investigate the impact of small ruminant movement with different disease states between the two groups on PPR dynamics. In the first scenario, it was assumed that there was no movement of small ruminants between the two groups, thus isolating the two groups. The vaccination rates per month, as provided in Table (5.1), were $\omega_l = 0.0628$ and $\omega_h = 0.0778$ for the Lowland and Highland groups, respectively. The results presented in Table (5.2) indicate that the control reproduction numbers $\mathcal{R}_v^l = 1.9081$ and $\mathcal{R}_v^h = 1.3560$ for the disease in the Lowland and Highland groups, respectively. These findings demonstrate the current endemicity status of PPR in the two groups of the small ruminant population. Furthermore, Figure (5.3A) serves as an illustration of this scenario, showing that after fifty months of simulation, the infected trajectories in both groups

TABLE 5.2: Different scenarios on the movements of small ruminants from Highland and Lowland districts and corresponding reproduction numbers

| No. | Scenario | Values(rates of influx) | | | | | | | | $R_v$ |
|---|---|---|---|---|---|---|---|---|---|---|
| | | $a_{lh}$ | $b_{lh}$ | $c_{lh}$ | $d_{lh}$ | $a_{hl}$ | $b_{hl}$ | $c_{hl}$ | $d_{hl}$ | |
| 1 | No movement from both groups | - | - | - | - | - | - | - | - | $\mathcal{R}_v^l = 1.9081$, $\mathcal{R}_v^h = 1.3560$ |
| 2 | Only movement from Lowland to Highland | - | - | - | - | 0.04 | 0.02 | 0.02 | 0.04 | $\mathcal{R}_v = 1.7527$ |
| 3 | Only movement from Highland to Lowland | 0.03 | 0.02 | 0.02 | 0.03 | - | - | - | - | $\mathcal{R}_v = 2.4810$ |
| 4 | Movement both districts (patches ) | 0.03 | 0.01 | 0.01 | 0.03 | 0.03 | 0.01 | 0.01 | 0.03 | $\mathcal{R}_v = 1.6280$ |
| 5 | Movement from both groups with formal screening of infected individuals | 0.02 | - | - | 0.02 | 0.04 | - | - | 0.04 | $\mathcal{R}_v = 1.6153$ |
| 6 | Enable movement by control infected animals' mobility from Highland | 0.04 | - | - | 0.04 | 0.04 | 0.04 | 0.04 | 0.04 | $\mathcal{R}_v = 1.3577$ |

increase and approach the endemic points after 700 months (approximately 58 years). This suggests that the disease will persist within the two populations if there is no improvement in controlling strategies. To make our findings more realistic, it is important to incorporate the effects of movements between the two groups. Consequently, these results prompt us to explore other movement scenarios that contribute to the endemicity of the disease at the district and national levels.

Based on the information provided in Table (5.1), the second case involves allowing movement only from the Lowland to the Highland group, with corresponding rates of influx for all disease statuses. The findings of this scenario reveal that the control reproduction number for the coupled system (5.1) is $\mathcal{R}_v = 1.7527$. This value is relatively higher than that in the first scenario. Additionally, as depicted in Figure (5.3B), the trajectory of infected individuals from the Highland converges to the endemic point, indicating that the disease will become endemic in the Highland population, while the trajectory of the Lowland converges to the disease-free equilibrium point, indicating that the disease becomes extinct in the Lowland population after 200 months (approximately 16 years). Here, we observe that the effect of movement from the Lowland increases the burden of PPR in the Highland population, but such movement reduces or even eradicates the disease in the Lowland with the help of the referenced vaccination rate.

In the scenario where movement is only permitted from the Highland to the Lowland group, a lower rate of influx is observed compared to the second case. This disparity can be attributed to the limited availability of grazing land and water points in the Lowland (pastoral) district as compared to the Highland (Fournié et al., 2018). Consequently, there is a reduced rate of inflow from the Highland to the Lowland population. The findings, as illustrated in Table (5.2) and Figure (5.3C), present a situation that is analogous to the second scenario, indicating that the

disease subsides in the Highland but persists in the Lowland population with an $\mathcal{R}_v$ value of 2.4810. This signifies a relatively high burden in the Lowland population.

In the context of permitting movement from both groups as described in Table (5.2), it has been observed that the coexistence of movement from both groups, combined with the specified influx rate, contributes to the sustained presence of the disease in both populations. The reproductive number under control measures in this particular scenario is calculated to be $\mathcal{R}_v = 1.6280$. Figure (5.3D) depicts the trajectories of the infected populations in both groups, demonstrating their convergence to an endemic state. This movement, in turn, facilitates the recirculation of the disease within both districts.

In the case of allowing movement from both groups, while screening the infected animals and considering the influx rate of susceptible and immunized or recovered populations as provided in Table (5.2), the control reproduction number $\mathcal{R}_v$ is calculated to be 1.6153. However, implementing screening in both populations is not highly feasible. Nonetheless, the results demonstrate a significant reduction in the number of infected individuals compared to the fourth scenario. Furthermore, an interesting observation is made: the movement of the susceptible population contributes to the sustainability of the disease. This can be seen in Figure (5.3E), where the disease is endemic in both groups.

In the final scenario, it is assumed that animals that are exposed and infectious in the Highland district are unable to move to the Lowland district. However, animals from the Lowland population can move to the Highland district, as indicated in Table (5.2). In other words, this scenario considers the implementation of screening or strict movement control measures. The results show a similar outcome to scenario two, but with a relatively lower disease burden in the Highland population. Figure (5.3F) illustrates that the trajectory of infected individuals in the Lowland district converges to the disease-free equilibrium (DFE), while the trajectory of infected individuals in the Highland district converges to an endemic point.

In summary, the key findings from the analysis highlight the significant impact of animal movements on the persistence and extinction of the PPR disease in the two districts. The analysis shows that with the specified vaccination rate of susceptible individuals, the control reproduction numbers are greater than unity, indicating that the disease will continue to spread. Based on the second scenario, it is particularly important to ban the movement of both infected and susceptible animals from the Highland group, which has a lower disease transmission rate, to the Lowland group, which has a higher disease transmission rate. This measure would help reduce the overall disease burden in the Lowland group. The analysis also reveals that the movement of small ruminants from both districts strongly contributes to the endemic nature of the disease, not only at the local level, but also at the national level. This observation is particularly noteworthy, as the merged scenario represents the dynamics of the disease at the national scale. Overall, the analysis underscores the critical role that animal movements play in the persistence and spread of the PPR disease, and provides important insights for informing disease control and prevention strategies at both the local and national levels.

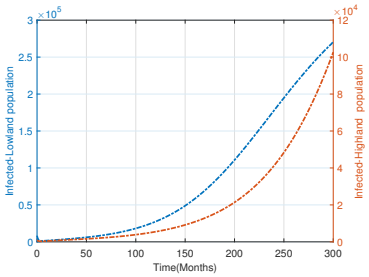


(A) Time Series Plots of Infected population in Highland (red) and Lowland(blue) Populations for Scenario 1.

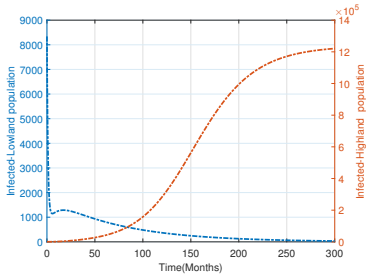


(B) Time Series Plots of Infected population in Highland (red) and Lowland(blue) Populations for Scenario 2.

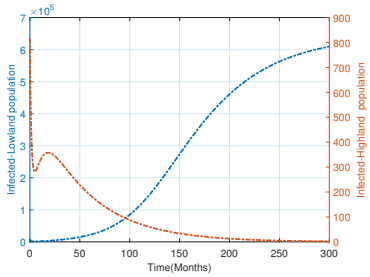


(C) Time Series Plots of Infected population in Highland (red) and Lowland(blue) Populations for Scenario 3.

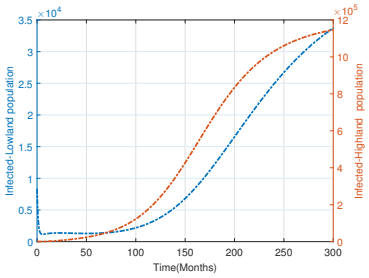


(D) Time Series Plots of Infected population in Highland (red) and Lowland(blue) Populations for Scenario 4.

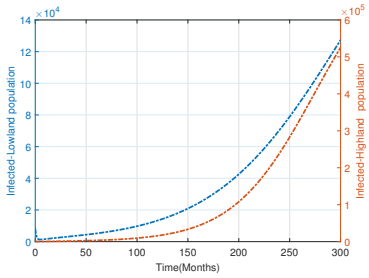


(E) Time Series Plots of Infected population in Highland (red) and Lowland(blue) Populations for Scenario 5.

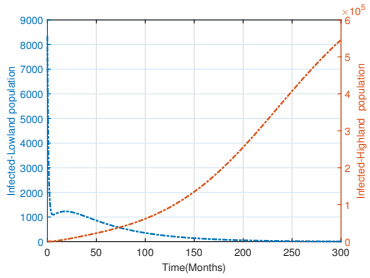


(F) Time Series Plots of Infected population in Highland (red) and Lowland(blue) Populations for Scenario 6.

FIGURE 5.3: Impact of Small Ruminant Migration(movement of small ruminant population) on PPR Dynamics in Two Subpopulations - Scenario Analysis

### 5.5.2 Impact of Vaccination and Movement of Animals (Immigration) on PPR Disease Dynamics

In this section, we have investigated the impact of vaccination on the dynamics of PPR by considering scenarios related to the movement of small ruminants in section (5.5.1) and determining the specific region in $\omega_l\omega_h - \mathcal{R}_v$ contour plot where $\mathcal{R}_v < 1$. For our analysis, we have used as initial conditions:

$$(S_l(0), E_l(0), I_l(0), R_l(0), S_h(0), E_h(0), I_h(0), R_h(0)) = (38307832; 200; 8340; 0; 45412074; 100; 817; 0)$$

.

In Figure (5.4), when there is no movement between the two districts, the system is uncoupled. Consequently, we can independently analyze the dynamics of the two groups. The vaccination rate required to eliminate the disease from the Lowland district or $\mathcal{R}_v^l < 1$, is found to be $\omega_l > 0.1333$ (above 13.33%) as depicted in Figure (5.4A). Similarly, the vaccination rate required to eradicate the disease ($\mathcal{R}_v^h < 1$) in the Highland district is $\omega_h > 0.1121$ (above 11. 21%) per month, as shown in Figure (5.4B). In particular, when considering values $(\omega_l, \omega_h) = (0.3, 0.2)$ within the given range, the disease dies in both districts after 150 months, as illustrated in Figure (5.4C).

In the contour plot depicted in Figure (5.5A), it illustrates the region in the $\omega_l - \omega_h$ plane where $\mathcal{R}_v < 1$. Specifically, for the case of small ruminant influx from the Highlands to the

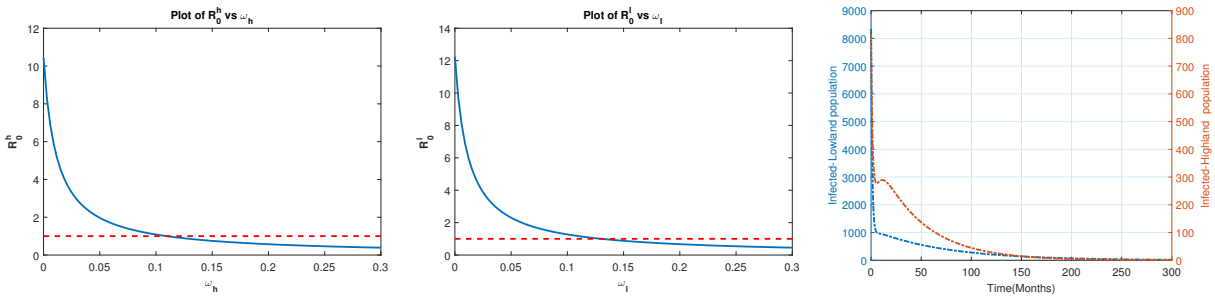


(A) Effect of $\omega_h$ on $\mathcal{R}_v^h$ (B) Effect of $\omega_l$ on $\mathcal{R}_v^l$ (C) Trajectories of $I_l$ and $I_h$

FIGURE 5.4: Impact of vaccination on $\mathcal{R}_v$ for the case of Uncoupled system(3.7) or the first scenario.

Lowlands, with the influx rate specified in Table (5.2) of the third case, the region is characterized by $0.1459 < \omega_l \leq 1$ and $0.04560 < \omega_h \leq 1$. Furthermore, in Figure (5.5D), the trajectories of the infected individuals in both groups converge to zero for the particular vaccination rates $(\omega_l = 0.2874, \omega_h = 0.2091)$ in the given range of vaccination. However, it should be noted that the disease in the Highlands subsides earlier than in the Lowlands.

Figures 5.5B and 5.5C represent the contour plots used to determine the regions where $\mathcal{R}_v < 1$ for the second and fourth cases of movement described in Table 5.2. The results indicate that for the second case, the region is defined by $0.02727 < \omega_l \leq 1$ and $0.1232 < \omega_h \leq 1$, while for the fourth case, the region is defined by $0.0848 < \omega_l \leq 1$ and $0.0788 < \omega_h \leq 1$. Furthermore, Figures 5.5E and 5.5F show that the trajectories of the infected population converge to zero for the particular vaccination rates $(\omega_l, \omega_h) = (0.1606, 0.2273)$ and $(\omega_l, \omega_h) = (0.290, 0.2879)$, respectively.

In the discussion presented above, the key summarized points are as follows: If there is movement between districts when implementing the vaccination program, the time required to eradicate the disease may differ between the two groups, as shown in Figure 5.5. To control the disease in both groups within the same time period, it may be necessary to implement strict control of movement and achieve high coverage of vaccination. In general, the discussion provides information on the potential impact of population movement on the effectiveness of a vaccination program.

Finally, to illustrate the global stability of the Disease-Free Equilibrium (DFE) for the cases mentioned in Remark 5.3.9, we considered different initial conditions with a specific vaccination rate. As shown in Figure 5.6, with the particular vaccination rates $(\omega_l, \omega_h) = (0.25, 0.20)$, all trajectories of the exposed and infected classes converge to zero in the case of an uncoupled system (where the two population groups are isolated). In Figure 5.7, the results indicate that all the trajectories of the exposed and infected classes, with varying initial conditions $(IC_i : i = 1, \ldots, 5)$, also converge to zero at the specified vaccination rates $(\omega_l, \omega_h) = (0.1606, 0.2273)$ for the second scenario. This scenario implies that an increase in the flow from lowland areas increases the burden on the highland population, necessitating additional vaccination efforts.

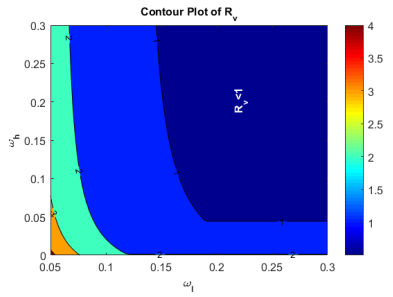


(A) Contour Plot of $\mathcal{R}_v$ with the third Case of Influx of Small Ruminants and vaccination ($\omega_{l,h}$).

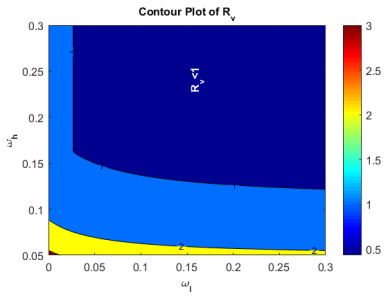


(B) Contour Plot of $\mathcal{R}_v$ with the second Case of Influx of Small Ruminants and vaccination ($\omega_{l,h}$).

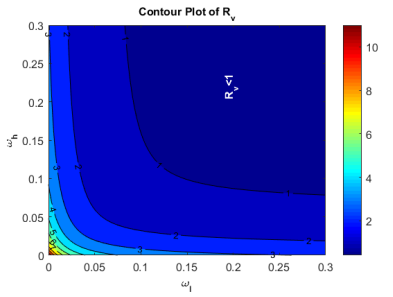


(C) Contour Plot of $\mathcal{R}_v$ with the fourth Case of Influx of Small Ruminants and vaccination ($\omega_{l,h}$).

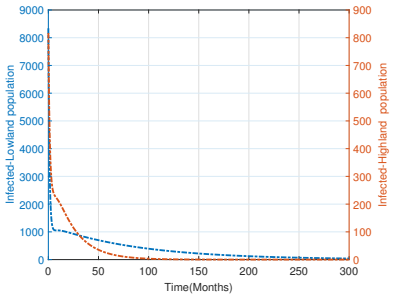


(D) Trajectories of $I_i, i = l, h$ for which $(\omega_l = 0.2874, \omega_h = 0.2091)$ in Figure (5.5A)

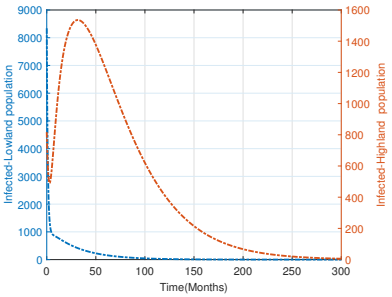


(E) Trajectories of $I_i, i = l, h$ for which $(\omega_l, \omega_h) = (0.1606, 0.2273)$ in Figure (5.5B)

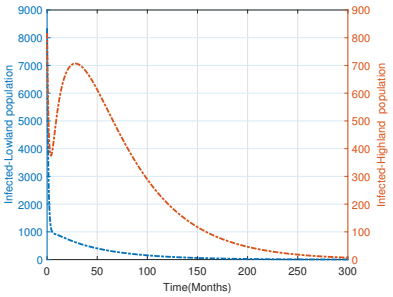


(F) Trajectories of $I_i, i = l, h$ for which $(\omega_l, \omega_h) = (0.290, 0.2879)$ in Figure (5.5C)

FIGURE 5.5: Contour Plot and Time Series Plot Illustrating the Interplay between Vaccination and Migration in the Dynamics of PPR. Trajectories of $I_i, i = l, h$ for Specific Cases of Vaccination and Influx, where $\mathcal{R}_v < 1$.

## 5.6 Results and Discussion

Peste des petits ruminants (PPR) is a highly contagious viral disease affecting small ruminants, with substantial implications for animal health and socioeconomics. In this study, we developed a deterministic compartmental model to describe PPR transmission and formulated an optimal control problem to evaluate intervention strategies, particularly focusing on the effect of restocking on disease dynamics. Our analytical results establish the existence and global stability of an endemic equilibrium for relevant parameter regimes, and sensitivity analysis identifies the parameters most significantly affecting transmission and control outcomes. Numerical simulations using a fourth-order Runge–Kutta scheme reveal that the introduction of infected restocked animals substantially undermines vaccination programs, with continuous inflow of infectious animals sustaining transmission even when vaccination is in place. Conversely, stringent biosecurity measures—both external measures that reduce the inflow of infectious animals and internal measures enabling identification, segregation, and treatment—markedly reduce the risks associated with restocking and improve overall control effectiveness. Parameter estimates calibrated to World Organisation for Animal Health (OIE) incidence data for Ethiopia yield a control reproduction number $\mathcal{R}_v \approx 1.02$ in the absence of restocking, consistent with observed endemicity in the region. However, incorporating restocking into the model clarifies why vaccination-alone strategies fail in practice: infective inflow maintains $\mathcal{R}_v$ at or above one unless complemented by biosecurity and treatment measures. Cost-effectiveness analysis shows that a combined strategy incorporating

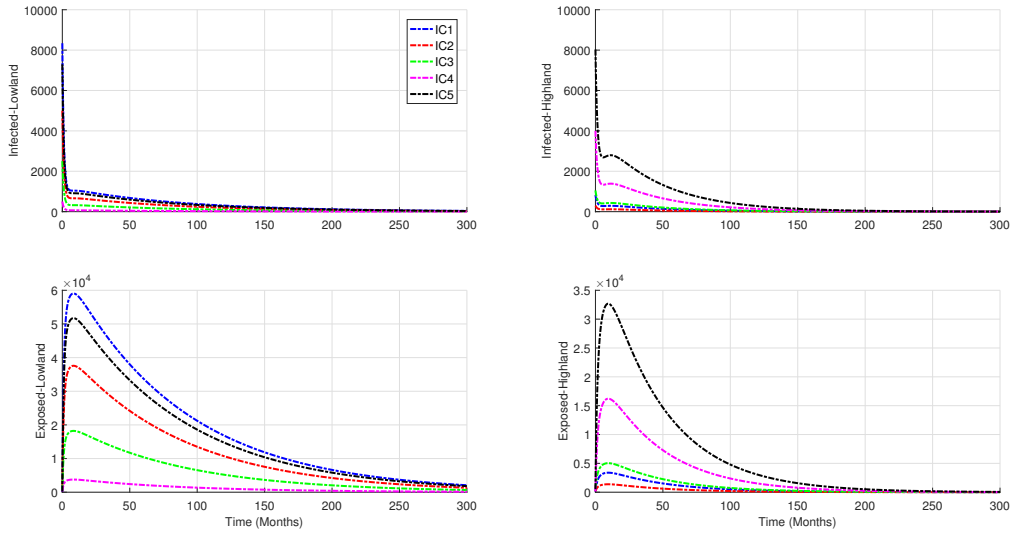


FIGURE 5.6: Trajectories of the exposed and infected classes for Scenario 1 with varying initial conditions. All trajectories converge to zero under the vaccination rates $(\omega_l, \omega_h) = (0.25, 0.20)$, indicating the stability of the Disease-Free Equilibrium.

external biosecurity, internal biosecurity, vaccination, and treatment ($S_C$) produces the largest reduction in infections per unit cost, followed by strategy $S_{B2}$ and then $S_{A1}$, underscoring that multi-pronged interventions are generally more efficient than single-measure approaches. These findings align with previous recommendations on movement restrictions and vaccination Fathelrahman et al., 2021 but diverge from analyses that ignored restocking effects Waret-Szkuta et al., 2008, highlighting the critical importance of incorporating connectivity into epidemiological models. Consistent with serological and molecular studies Fentie et al., 2018; Fournié et al., 2018; Alemu et al., 2019, our results support the persistent endemicity of PPR at the national scale while uniquely quantifying the additional role of restocking in maintaining transmission. The study's limitations include incomplete or imprecise incidence and parameter data from OIE and literature sources, which reduce confidence in estimates like $\mathcal{R}_v$, as well as the omission of time delays, stochasticity in restocking events, and socioeconomic factors affecting biosecurity compliance. Future research should incorporate stochastic and delay formulations, develop hybrid statistical-mechanistic frameworks using advanced parameter-estimation techniques and machine learning, and model the probability of introducing infectious animals via restocking. Motivated by recent studies (Saber et al., 2025; Althubyani et al., 2025; Adam et al., 2025), extending the integer-order model to a fractional-order formulation could better capture memory and hereditary effects in PPR dynamics. In conclusion, achieving PPR eradication targets such as the 2027 goal requires integrated strategies that combine vaccination, treatment, and robust biosecurity to prevent the importation and onward transmission of infection. The modeling framework and optimal-control analyses presented here provide quantitative guidance for policymakers to design cost-effective, evidence-based PPR control programs.

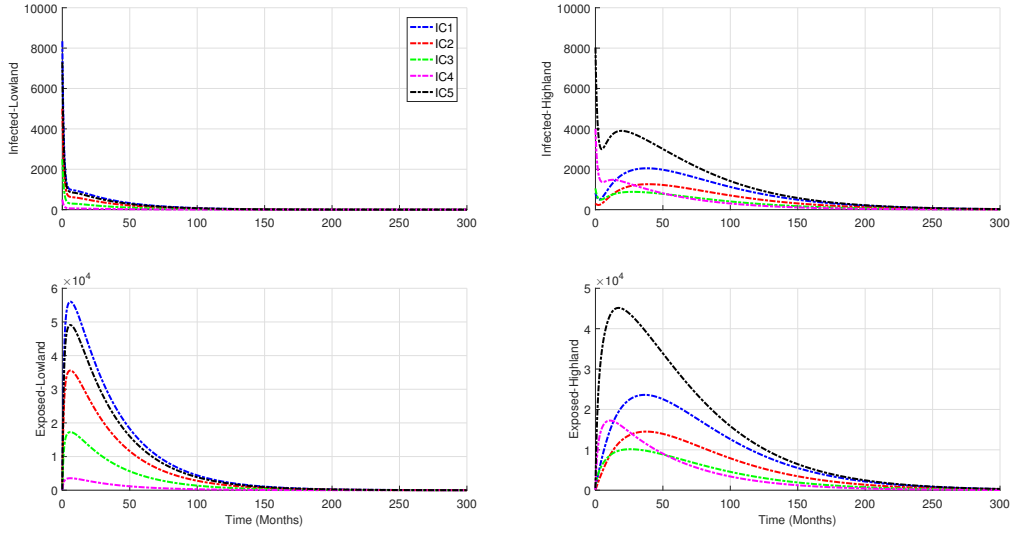


FIGURE 5.7: Trajectories of the exposed and infected classes for Scenario 2 with varying initial conditions. All trajectories converge to zero under the vaccination rates $(\omega_l, \omega_h) = (0.1606, 0.2273)$, indicating the stability of the Disease-Free Equilibrium.

## 5.7 Result and Conclusion

In this chapter, we consider an SEIR metapopulation model with vaccination to study the dynamics of PPR disease in a patchy environment consisting of highland sedentary (mixed livestock-crop farms) and lowland pastoral (livestock production) systems. We investigate the impacts of small ruminant migration and vaccination on disease dynamics. By fitting the national prevalence data from January 2019 to December 2022, we estimate the potential transmission of the disease in these two agroecological zones. Our results reveal that PPR disease continues to circulate in both zones. Through the analysis of the control reproduction number ($\mathcal{R}_v$), we demonstrate that the disease-free equilibrium ($\xi^0$) is locally and globally asymptotically stable when $\mathcal{R}_v < 1$. However, when $\mathcal{R}_v > 1$, we show that the system exhibits uniform persistence, indicating the presence of an endemic equilibrium. Furthermore, using numerical simulations, we investigate the impact of movement between the two districts by considering different scenarios and the interplay between vaccination and migration in the coupled system. We determine the vaccination levels at which $\mathcal{R}_v < 1$ for various scenarios. Our findings suggest that vaccination can effectively control the spread of disease in small populations with the presence of movement.

To place our findings in the perspective of the current literature on PPR in Ethiopia, we observe that most previous studies (Dubie et al., 2022; Fentie et al., 2018; Waret-Szkuta et al., 2008)have mainly focused on statistical techniques and epidemiological analyzes. These studies examine the spread of the disease based on seroprevalence and identify common risk factors such as sex, age, and species. Although these studies are useful for understanding the epidemiological characteristics of the disease, they do not predict disease transmission dynamics, evaluate immunization efficacy, or analyze the impact of small ruminant movement between spatially different geographic areas. Despite these drawbacks, research to date has consistently

shown that vaccination is the most effective primary control measure and that seroprevalence rates vary across agro-ecological zones. Furthermore, as noted in the literature review, we cite a significant study (Fournié et al., 2018) that, although using different methodologies, supports our conclusions on two important points: first, lowland populations have a higher potential disease transmission rate than highland populations; and second, the frequent movement of small ruminants from lowland to highland areas requires higher coverage of vaccination in lowland districts to effectively eradicate PPR and reduce its burden.

We anticipate that the findings of our study have significant implications for veterinary health policies and intervention strategies aimed at preventing the spread of PPR disease in Ethiopia. Our findings shed light on the potential transmission rates of PPR across different agro-ecological zones, highlight how animal movements contribute to the virus's national circulation, and demonstrate the impact of small ruminant movement on vaccination effectiveness in achieving eradication in a short period of time. Policymakers can use these findings to develop comprehensive intervention strategies that go beyond vaccination, such as implementing additional biosecurity measures such as testing or screening infected animals during movement, and increasing surveillance in high-risk areas.

Despite the fact that the study provides vital information for policymakers about the control of PPR Disease, there are significant limitations. Specifically, there is insufficient data on disease cases in the two agro-ecological zones to derive the best-fitted parameter values, and the lack of data on animal movement patterns between these zones forces us to utilize assumed values for movement parameters. These limitations bring uncertainty into our parameter estimates, potentially affecting the model's predictive capabilities. Although the general conclusions of our study remain valid, access to more comprehensive data would enhance the reliability of our findings and enable more informed public health.

In future research, we recommend several directions based on the findings of our study. Future work should incorporate short-term mixing due to movement patterns, particularly the interactions between infected and susceptible small ruminants from different zones at trade centers, grazing pastures, or water points. This can be achieved by adding terms related to the force of infection or incidence rate to the model that reflect these dynamics. Furthermore, improving parameter estimation through a more comprehensive data set improves the precision of PPR disease dynamics. Investigating optimal control strategies that include proposed interventions and assess related risk factors is crucial, especially given the limited resources for intervention costs. Formulating an optimal control problem helps to identify the most effective strategies for managing PPR while ensuring efficient allocation of resources. Such studies are vital for developing effective strategies to eradicate PPR within the timelines of the national eradication program, ultimately improving animal health and productivity.

Overall, this study contributes to our understanding of the dynamics of PPR disease in different agroecological zones and highlights the importance of spatial variation and movement in disease transmission. It also motivates further study in the field. The findings underscore the need for targeted vaccination strategies to control PPR, particularly in areas where the disease persists.

# Chapter 6

# Modeling and Control of the Co-infection of PPR with Sheep and Goat Pox

## 6.1 Introduction

Peste des petits ruminants (PPR) and Sheep and Goat Pox (SGP) are two of the most significant viral diseases affecting small ruminants worldwide, causing substantial economic and social burdens, particularly in Africa and Asia (Ahaduzzaman, 2020; Zewdie et al., 2021). While each disease individually poses considerable challenges, their considerable overlap in geographical distribution and susceptible host populations has raised increasing concern about the implications of co-infection for disease dynamics, animal health, and control efforts (Kgotlele et al., 2019; Ozmen et al., 2009).

SGP, caused by the Capripox virus, is an acute, febrile, and highly contagious disease characterized by systemic papules, nodules, and severe skin and pulmonary lesions, with morbidity rates reaching up to 100% in naive populations and case fatality as high as 85% (Zewdie et al., 2021; Fentie et al., 2017; Wondimu et al., 2021). Like PPR, SGP is notifiable to the World Organization for Animal Health (WOAH), and both diseases are endemic across Ethiopia and neighboring regions, where small ruminants play a vital economic and subsistence role (Tadesse et al., 2022). From 2005 to 2023, Ethiopia recorded over 3,400 outbreaks of SGP and 1,600 outbreaks of PPR, resulting in nearly 600,000 cases and over 134,000 deaths combined—figures that highlight the urgent need for effective control strategies.

Recent studies have documented the occurrence of co-infection with PPR virus (PPRV) and SGP virus (SGPV), as well as with other poxviruses, in both Asia and Africa (Zhang et al., 2021; Adedeji et al., 2019; Malik et al., 2011; Birindwa et al., 2017; Kgotlele et al., 2019; Ozmen et al., 2009). Co-infection can exacerbate clinical severity, increase morbidity and mortality, and complicate diagnosis and control. In vitro and in vivo evidence demonstrates that these pathogens can interact at the cellular level, potentially influencing host susceptibility and disease outcomes (Zhang et al., 2021; Derouin et al., 1998). However, the mechanisms of interaction and the impact of co-infection on epidemiological patterns remain insufficiently understood, necessitating quantitative approaches to better inform intervention strategies.

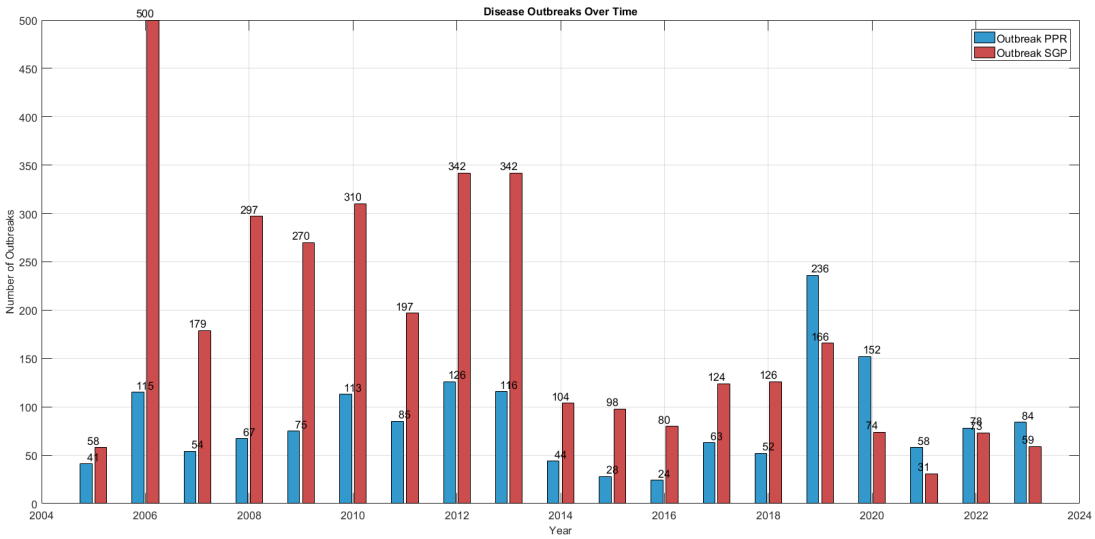


FIGURE 6.1: Number of outbreaks of PPR and SGP reported in Ethiopia (2005–2023). (Source: WOAH (2023))

Vaccination remains the cornerstone of control for both PPR and SGP, with effective live attenuated vaccines available (Fentie et al., 2018; Waret-Szkuta et al., 2008; World Organisation for Animal Health (WOAH), 2023; Jemberu et al., 2022). Given the logistical and financial challenges of separate mass vaccination campaigns, the development and deployment of combined PPR/SGP vaccines have emerged as a promising and cost-effective solution for endemic settings (Fakri et al., 2015). Additional measures, such as culling, movement restrictions, and environmental disinfection, are also employed to reduce transmission.

Despite these interventions, the persistent high burden of both diseases and the additional complexity posed by co-infections underscore the need for integrated approaches. Mathematical modeling-especially via deterministic models and optimal control theory-offers a powerful framework for evaluating the dynamics of co-infection, estimating key epidemiological thresholds, and designing robust, resource-efficient control strategies (Kouidere et al., 2021; Nyerere et al., 2020a; Hugo et al., 2017; Sseguya et al., 2022).

This chapter presents a deterministic mathematical model of PPR and SGP co-infection in small ruminants, with a focus on Ethiopia as a case study. The model is structured into sub-models for each disease and incorporates co-infection dynamics, transmission parameters, and environmental persistence. By deriving fundamental epidemiological metrics (such as reproduction numbers and equilibria), we characterize the persistence and control of co-infection. Importantly, we extend the model to an optimal control setting, evaluating the impact of a combined vaccination strategy alongside treatment and disinfection. Numerical simulations based on recent outbreak data provide evidence for the superior effectiveness and cost-efficiency of integrated vaccination (including newborns and susceptibles) compared to separate interventions.

By offering the first detailed modeling analysis of PPR and SGP co-infection with optimal control, this chapter aims to guide policymakers and veterinary health professionals in designing evidence-based strategies to mitigate the impact of these diseases on animal health and rural livelihoods.

## 6.2 Model Description and Formulation

In this section, we formulat a non-linear determinstic SVIR-B model for the co-infection of PPR and SGP disease transmission, as depicted in Fig. 6.2. To uderstand the proposed model, some descriptions or assumptions are concisely listed here.

- Small ruminant population is described by SVIR model, that is, the total small ruminant population $N$ is divided into six mutually compartments subclasses: susceptible S, vaccinated V, PPR infected $I_p$, SGP infected, $I_c$, co-infected $I_{pc}$, and the recovered population from both diseases R. Then, a class of viral concentration is be considered and denoted by B.

- New recruitment (including birth, migration, etc.) is assumed to enter the population at a constant rate $\Lambda$, with a fraction $\rho$ regarded as being under vaccination control, which directly enters the vaccinated class. In addition, the natural death rate of all animals, denoted as $\mu$, along with the death rates due to PPR, SGP, and co-infection, represented by $\delta_p$, $\delta_c$, and $\delta_{pc}$, respectively, are also considered.

- The susceptible population acquires PPR infection through effective contact with PPR-infected only or coinfected animal at a standard incidence rate of $\beta_p S(I_{pc} + I_p)/N$, where $\beta_p$ represents the disease transmission rate relative to infected ruminants in the $I_p(t)$ class. In a similar way a susceptible population acquires SGP infection through direct contact with SGP-infected only or coinfected animal or indirect contact with contaminated environmental sources of virus at a standard incidence rate of $\beta_c S(I_c + I_{pc} + \alpha B)/N$, where $\beta_c$ and $\alpha$ denote the disease transmission rate relative to infected ruminants in the $I_c(t)$ class and modification factor concerning transmission from compartment B, respectively.

- A combination of PPR and SGP vaccines is considerd and assuming that it is perfect, animals onced received vaccines will develop long immunity for the two diseases. In addition, it is assume that susceptible animal enter the vaccinated compartment at a constant rate $\omega$.

- Assume that the growth rate of viral concentration is proportional to the infected animal $I_c + \epsilon I_{pc}$, i.e., each infected individual from $I_c$ and $I_{pc}$ promoted the increase in viral concentration at the rate of $\xi$ and where $\epsilon$ is modification parameter. Further, viral concentration is assumed to decay at a rate constant $\theta$.

- The PPR infected animal recovers from the disease at a rate of $\gamma_p$, while the remaining population either acquires SGP infection and moves to a co-infectious compartment or dies due to the disease, causing a death rate of $\gamma_p$.

- SGP-infected animal recovers from the disease at a rate of $\gamma_c$, while the remaining portion is either affected by PPR infection and moves to a co-infectious compartment or dies due to the disease-causing death rate of $\delta_c$.

- A co-infected population can recover from one infection at a rate of $\gamma_{pc}$ and move to an infected compartment belonging to another disease with a probability of $p$ or $q$ or recovering from both disease with a probability of $(1-(p+q))$.

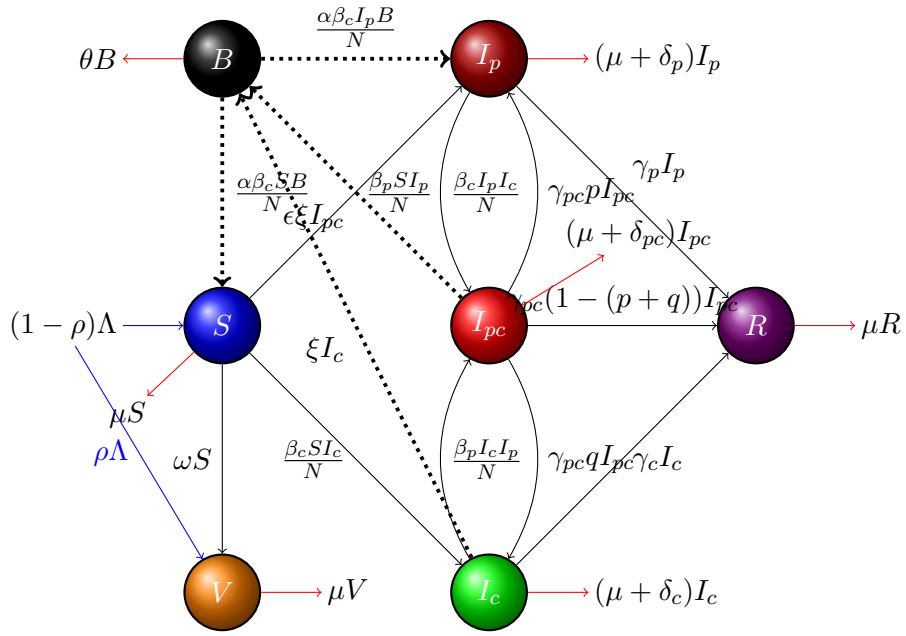


FIGURE 6.2: Flow diagram for PPR-SGP co-infection model. Dashed lines represent indirect infection of SGP.

As mentioned above, the co-infection model can be described as follows:

$$\begin{cases} \frac{dS}{dt} = (1-\rho)\Lambda - (\chi_p+\chi_c)S - (\mu+\omega)S, \\ \frac{dV}{dt} = \rho\Lambda + \omega S - \mu V, \\ \frac{dI_p}{dt} = \chi_p S + \gamma_{pc} pI_{pc} - \chi_c I_p - (\gamma_p+\delta_p+\mu)I_p, \\ \frac{dI_c}{dt} = \chi_c S + \gamma_{pc} qI_{pc} - \chi_p I_c - (\gamma_c+\delta_c+\mu)I_c, \\ \frac{dI_{pc}}{dt} = \chi_p I_c + \chi_c I_p - (\gamma_{pc}+\delta_{pc}+\mu)I_{pc}, \\ \frac{dR}{dt} = \gamma_p I_p + \gamma_c I_c + \gamma_{pc}(1-(p+q))I_{pc} - \mu R, \\ \frac{dB}{dt} = \xi(I_c+\epsilon I_{pc}) - \theta B, \end{cases} \tag{6.1}$$

where

$$\chi_p = \frac{\beta_p(I_p+I_{pc})}{N} \quad \text{and} \quad \chi_c = \frac{\beta_c(I_c+I_{pc}+\alpha B)}{N}$$

with the initial condition $S(0) = S_0 \geq 0, V(0) = V_0 \geq 0, I_p(0) = I_{p,0} > 0, I_c(0) = I_{c,0} > 0, I_{pc}(0) = I_{pc,0} \geq 0, R(0) = R_0 \geq 0, B(0) = B_0 \geq 0$. where, we assume that $0 \leq \alpha, \epsilon, p+q, < 1$.

TABLE 6.1: Parameter description of model (6.1).

| Parameter | Description |
|---|---|
| $\Lambda$ | Recruitment rate |
| $\beta_p$ | PPR transmission rate |
| $\beta_c$ | SGP transmission rate |
| $\mu$ | Natural mortality rate |
| $\omega$ | The rate at which susceptible individuals are vaccinated |
| $\alpha$ | Modification factor concerning transmission from compartment B |
| $\delta_p$ | PPR induced mortality rate |
| $\epsilon$ | Modification parameters |
| $\theta$ | decay rate of concentration of SGP virus |
| $\xi$ | Contribution rate of SPG infected animals to viral load in the enviorn-ment |
| $\delta_c$ | SGP induced mortality rate |
| $\delta_{pc}$ | PPR and SGP induced mortality rate |
| $\gamma_p$ | Rate of natural recovery from $I_p$ class |
| $\gamma_c$ | Rates of natural recovery from $I_c$ class |
| $\gamma_{pc}$ | Rates of natural recovery from $I_{pc}$ class |
| $\rho$ | Fraction of recruited small ruminants that are vaccinated |
| $p$ | Fraction of coinfected at which recoverd from PPR-only |
| $q$ | Fraction of coinfected at which recoverd from SGP-only |

## 6.3 Model Analysis

### 6.3.1 Well-Posedness of the Model

In this section, it is crucial to provide evidence for the existence of a non-negative solution, as well as to establish the boundedness of the solution, as these aspects are essential for the mathematical and epidemiological interpretation of the model (6.1).

**Lemma 6.3.1.** *For any non-negative initial condition* $X_0 = (S_0, V_0, I_{p0}, I_{c0}, I_{pc0}, R_0, B_0) \in \mathbf{R}+^7$, *system* (6.1) *admits a unique solution* $X(t) = (S(t), V(t), I_p(t), I_c(t), Ipc(t), R(t), B(t))$ *defined on* $[0, \infty)$ *that remains non-negative for all* $t \geq 0$. *Moreover, all solutions are uniformly bounded and eventually enter the compact feasible region*

$$\Omega = \left\{ (S, V, I_p, I_c, I_{pc}, R, B) \in \mathbf{R}_+^7 : N = S + V + I_p + I_c + I_{pc} + R \leq \frac{\Lambda}{\mu},\ B \leq \frac{\xi(1+\epsilon)\Lambda}{\theta\mu} \right\}.$$

**Proof** We prove the lemma in three steps.

**Step 1: Local existence and uniqueness.** Let $x(t) = (S(t), V(t), I_p(t), I_c(t), I_{pc}(t), R(t), B(t))^T$ and write system (6.1) as

$$\frac{dx}{dt} = f(x), \quad x(0) = x_0 \in \mathbf{R}_+^7,$$

where $f : \mathbf{R}^7 \to \mathbf{R}^7$ is given by the right-hand sides. Each component of $f$ is a rational function of the state variables (through $\chi_p$ and $\chi_c$) that is $C^1$ on any domain where $N > 0$. Since we consider only non-negative states and $N = 0$ only when all compartments are zero (a trivial

equilibrium), $f$ is locally Lipschitz on $\mathbf{R}^7_+$. By the Picard–Lindelöf theorem, for each $x_0$ there exists a unique solution defined on a maximal interval $[0, t_{\max})$.

**Step 2: Non-negativity of solutions.** We apply the invariance theorem of (Theorem A.4 in Thieme, 2018) to the closed set $D = \mathbf{R}^7_+$. For $x \in \partial D$, a coordinate $x_i = 0$ must satisfy $f_i(x) \geq 0$ to prevent the flow from leaving $D$. Verifying this condition for each variable yields:

When $S = 0$:

$$f_1(x) = \frac{dS}{dt} = (1-\rho)\Lambda \geq 0.$$

When $V = 0$:

$$f_2(x) = \frac{dV}{dt} = \rho\Lambda + \omega S \geq 0.$$

When $I_p = 0$:

$$f_3(x) = \frac{dI_p}{dt} = \chi_p S + \gamma_{pc} p I_{pc} \geq 0.$$

When $I_c = 0$:

$$f_4(x) = \frac{dI_c}{dt} = \chi_c S + \gamma_{pc} q I_{pc} \geq 0.$$

When $I_{pc} = 0$:

$$f_5(x) = \frac{dI_{pc}}{dt} = \chi_p I_c + \chi_c I_p \geq 0.$$

When $R = 0$:

$$f_6(x) = \frac{dR}{dt} = \gamma_p I_p + \gamma_c I_c + \gamma_{pc}(1-(p+q)) I_{pc} \geq 0.$$

When $B = 0$:

$$f_7(x) = \frac{dB}{dt} = \xi(I_c + \epsilon I_{pc}) \geq 0.$$

All inequalities hold because the remaining variables are non-negative on $D$. Hence the vector field $f$ points inward (or is tangent) on $\partial D$. By Thieme's theorem, $\mathbf{R}^7_+$ is positively invariant: if $x_0 \in \mathbf{R}^7_+$, then $x(t) \in \mathbf{R}^7_+$ for all $t \in [0, t_{\max})$.

**Step 3: Boundedness and global existence.** Define the total host population $N(t) = S(t) + V(t) + I_p(t) + I_c(t) + I_{pc}(t) + R(t)$. Adding the host equations of (6.1) gives

$$\frac{dN}{dt} = \Lambda - \mu N - (\delta_p I_p + \delta_c I_c + \delta_{pc} I_{pc}) \leq \Lambda - \mu N.$$

Solving this differential inequality using the Gronwall inequality on maximal interval $[0, t_{\max})$ yields

$$N(t) \leq N_0 e^{-\mu t} + \frac{\Lambda}{\mu}\left(1 - e^{-\mu t}\right).$$

Consequently, $N(t) \leq \max\left(N_0, \frac{\Lambda}{\mu}\right)$ for all $t \in [0, t_{\max})$.

For the environmental pathogen $B(t)$, using the bound $I_c + I_{pc} \leq N \leq \frac{\Lambda}{\mu}$ (for $t$ large enough) we have

$$\frac{dB}{dt} = \xi(I_c + \epsilon I_{pc}) \leq \xi(1+\epsilon)\frac{\Lambda}{\mu} - \theta B.$$

Hence

$$B(t) \leq B_0 e^{-\theta t} + \frac{\xi(1+\epsilon)\Lambda}{\theta\mu}\left(1 - e^{-\theta t}\right).$$

Thus $B(t) \leq \max\left(B_0, \frac{\xi(1+\epsilon)\Lambda}{\theta\mu}\right)$ for all $t \in [0, t_{\max})$.

Since all components remain bounded on the finite interval $[0, t_{\max})$, the continuation theorem implies $t_{\max} = \infty$, so solutions exist globally on $[0, \infty)$. Moreover, for any initial condition, $N(t)$ and $B(t)$ eventually enter and remain in the intervals $[0, \frac{\Lambda}{\mu}]$ and $[0, \frac{\xi(1+\epsilon)\Lambda}{\theta\mu}]$, respectively. Therefore the region $\Omega$ is positively invariant and attracts all solutions, completing the proof.

Before analyzing the dynamics of the co-infection model, analyze the sub-models first, i.e.,PPR-only model and SGP-only model.

### 6.3.2 PPR-Only Model

The model is derived by setting $I_c = I_{pc} = B = 0$ in equation (6.1). Additionally, the PPR vaccination is administered solely to newborn and susceptible animals. Consequently, we have:

$$\begin{cases} \frac{dS}{dt} = (1-\rho_p)\Lambda - \frac{\beta_p S I_p}{N} - \omega_p S - \mu S, \\ \frac{dV_p}{dt} = \rho_p \Lambda + \omega_p S - \mu V_p, \\ \frac{dI_p}{dt} = \frac{\beta_p S I_p}{N} - (\delta_p + \gamma_p + \mu) I_p, \\ \frac{dR_p}{dt} = \gamma_p I_p - \mu R_p, \end{cases} \tag{6.2}$$

with initial condition $S(0) = S_0 \geq 0, V_p(0) = V_{p0} \geq 0, I_p(0) = I_{p0} > 0, R_p(0) = R_{p0}0 \geq 0$ where,

$$N(t) = S(t) + V_p(t) + I_p(t) + R_P(t).$$

In the region

$$\Omega_p = \left\{ (S, V_p, I_p, R_p) \in \mathbb{R}^4_+ : N \leq \frac{\Lambda}{\mu} \right\},$$

all solutions of the model (6.2) that start in $\Omega_p$ remain within $\Omega_p$ for all $t \geq 0$. In other words, $\Omega_p$ is positively invariant with respect to the model (6.2). Therefore, we will examine the dynamics of the model (6.2) within the region $\Omega_p$.

#### Existence and Stability Analysis of Equilibria

In the absence of PPR in the population of small ruminants, model (6.2) admits an equilibrium point known as disease-free , and it is given by

$$\xi_0^p = \left( \frac{(1-\rho_p)\Lambda}{(\omega_p + \mu)}, \frac{\Lambda(\rho_p \mu + \omega_p)}{\mu(\omega_p + \mu)}, 0, 0 \right).$$

Following the next-generation method (Van den Driessche et al., 2002), the control reproduction number of model (6.2) is

$$\mathcal{R}_v^p = \frac{\beta_p \mu (1-\rho_p)}{(\gamma_p + \delta_p + \mu)(\omega_p + \mu)}.$$

**Theorem 6.3.2.** *The disease-free equilibrium $\xi_0^p$ of the PPR-only model (6.2) is locally asymptotically stable if $\mathcal{R}_v^p < 1$, and unstable if $\mathcal{R}_v^p > 1$.*

**Proof** Using linearization method, the Jacobian matrix of system (6.2) at the $\xi_0^p$ is

$$J_{\xi_0^p} = \begin{bmatrix} -\mu - \omega_p & 0 & -\frac{\beta_p \mu(1-\rho_p)}{\omega_p+\mu} & 0 \\ \omega_p & -\mu & 0 & 0 \\ 0 & 0 & \frac{\beta_p \mu(1-\rho_p)}{\omega_p+\mu} - \gamma_p - \delta_p - \mu & 0 \\ 0 & 0 & \gamma_p & -\mu \end{bmatrix}$$

Here, the eigenvalues for $J_{\xi_0^p}$ are

$$\begin{cases} \lambda_1 = -(\omega_p + \mu) \\ \lambda_2 = -\mu, \\ \lambda_3 = (\gamma_p + \delta_p + \mu)\left(\mathcal{R}_v^p - 1\right), \\ \lambda_4 = -\mu. \end{cases} \tag{6.3}$$

Therefore, the DFE ($\xi_0^p$) is locally asymptomatically stable if $\mathcal{R}_v^p < 1$ and otherwise unstable.

**Theorem 6.3.3.** *The disease-free equilibrium of the system (6.2) is globally asymptotically stable if $\mathcal{R}_v^p < 1$ and unstable if $\mathcal{R}_v^p > 1$.*

**Proof** Suppose that $\mathcal{R}_v^p < 1$ and consider the Lyapunove function as:

$$\mathcal{L} = \left(\frac{1}{\gamma_p + \delta_p + \mu}\right) I_p.$$

Its time derivative along the solutions of system (6.2), becomes

$$\begin{aligned} \frac{d\mathcal{L}}{dt} &= \left(\frac{1}{\gamma_p + \delta_p + \mu}\right) I_p' \\ &= \frac{1}{\gamma_p + \delta_p + \mu}\left(\frac{\beta_p S}{N} - (\gamma_p + \delta_p + \mu)\right) I_p. \end{aligned} \tag{6.4}$$

From evidence that as $\lim_{t\to\infty} N(t) = \lim_{t\to\infty}(S(t) + V_p(t) + I_p(t) + R_p(t)) \leq S_0 + V_{p0}$ and since $S \leq S_0$, and $V \leq V_{p0}$, it follows that $\frac{S}{N} \leq \frac{S_0}{S_0+V_{p0}}$.

Thus

$$\begin{aligned} \frac{d\mathcal{L}}{dt} &\leq \frac{1}{\gamma_p + \delta_p + \mu}\left(\frac{\beta_p S_0}{S_0 + V_{p0}} - (\gamma_p + \delta_p + \mu)\right) I_p \\ &= (\mathcal{R}_v^p - 1) I_p. \end{aligned}$$

It can be verified that $\mathcal{L}' \leq 0^{\cdot}$ for $\mathcal{R}_v^p < 1$. Further more, to verify LaSalle's Invariance Principle, let $E = \{(S, V_p, I_p, R_p) \in \Omega_p : \dot{\mathcal{L}} = 0\}$. Since $\mathcal{R}_v^p < 1$, $\dot{\mathcal{L}} = 0$ occurs only when $I_p = 0$. Thus $E = \{(S, V_p, 0, R_p) \in \Omega_p\}$.

The largest invariant set $M \subset E$ satisfies $I_p(t) \equiv 0$. Substituting $I_p = 0$ into (6.2):

$$\begin{aligned} S' &= (1-\rho_p)\Lambda - (\omega_p + \mu)S \to S^0, \\ V_p' &= \rho_p \Lambda + \omega_p S - \mu V_p \to V_p^0, \\ R_p' &= -\mu R_p \to 0. \end{aligned}$$

Hence $M = \{\xi_0^p\}$.

By LaSalle's Invariance Principle, all trajectories in $\Omega_p$ approach $M = \{\xi_0^p\}$. Therefore $\xi_0^p$ is globally asymptotically stable in $\Omega_p$ when $\mathcal{R}_v^p < 1$.

For $\mathcal{R}_v^p > 1$, linearization shows $\xi_0^p$ is unstable.

To compute the endemic equilibrium point, we assume that $I_p \neq 0$ and solve $\frac{dS}{dt} = \frac{dV_p}{dt} = \frac{dI_p}{dt} = \frac{dR_p}{dt} = 0$ for the endemic equilibrium $\xi_*^p = (S_*, V_{p*}, I_{p*}, R_{p*})$, we have

$$\begin{cases} S_* = \dfrac{\Lambda\ (\delta_p\, \rho_p + \gamma_p + \mu)}{\mu\, \beta_p - \delta_p(\,\mu + \,\omega_p)} \\ V_{p*} = \dfrac{\Lambda \rho_p + \omega_p S_*}{\mu}, \\ I_{p*} = \dfrac{\Lambda\ (\omega_p + \mu)\,(\mathcal{R}_v^p - 1)}{\mu\, \beta_p - \delta_p\ (\mu + \omega_p)}, \\ R_{p*} = \gamma_p I_{p*}. \end{cases} \tag{6.5}$$

Here we observe that the postivity of this equilibrium dependes on $\mathcal{R}_v^p$: its lessthan or greater than unity. Hence, the following result:

**Lemma 6.3.4.** *Unique endemic equilbrium point $\xi_*^p = (S_*, V_{p*}, I_{p*}, R_{p*})$ exists for the model (6.2) if $\mathcal{R}_v^p > 1$.*

### Sensitivity Analysis for the PPR-only Sub Model

In order to assess the model's resistance to different parameter values, a sensitivity analysis was conducted. Understanding the relative roles played by various model parameters in the occurrence and spread of a given disease is vital. This understanding helps us identify where interventions should be focused to reduce disease-related mortality and morbidity.

To measure the relative change in the model parameter $p$ with respect to the relative change in $(\mathcal{R}_v^p)$, a forward normalized sensitivity index denoted as $\Upsilon_p^{\mathcal{R}_v^p}$ was employed. This index is defined using partial derivatives if $(\mathcal{R}_v^p)$ is a differentiable function of the model parameter $p$. The specific definition of this index can be found in reference (Sanchez et al., 1997). It can be expressed as:

$$\Upsilon_p^{\mathcal{R}_v^p} = \frac{\partial \mathcal{R}_v^p}{\partial p} \times \frac{p}{\mathcal{R}_v^p}, \tag{6.6}$$

where $\Upsilon_p^{\mathcal{R}_v^p}$ is the sensitivity index (SI) of $(\mathcal{R}_v^p)$ with respect to parameter p. The sensitivity analysis for $\mathcal{R}_v^p$ of parameters in model (6.2) is given by:

$$\begin{aligned}
\Upsilon_{\beta_p}^{\mathcal{R}_v^p} &= \frac{\partial \mathcal{R}_v^p}{\partial \beta_p}\frac{\beta_p}{\mathcal{R}_v^p} = 1 > 0,\\
\Upsilon_{\rho_p}^{\mathcal{R}_v^p} &= \frac{\partial \mathcal{R}_v^p}{\partial \rho_p}\frac{\rho_p}{\mathcal{R}_v^p} = -\frac{\rho_p}{1-\rho_p} < 0,\\
\Upsilon_{\gamma_p}^{\mathcal{R}_v^p} &= \frac{\partial \mathcal{R}_v^p}{\partial \gamma_p}\frac{\gamma_p}{\mathcal{R}_v^p} = -\frac{\gamma_p}{\gamma_p+\delta_p+\mu} < 0,\\
\Upsilon_{\delta_p}^{\mathcal{R}_v^p} &= \frac{\partial \mathcal{R}_v^p}{\partial \delta_p}\frac{\delta_p}{\mathcal{R}_v^p} = -\frac{\delta_p}{\gamma_p+\delta_p+\mu} < 0,\\
\Upsilon_{\omega_p}^{\mathcal{R}_v^p} &= \frac{\partial \mathcal{R}_v^p}{\partial \omega_p}\frac{\omega_p}{\mathcal{R}_v^p} = -\frac{\omega_p}{\omega_p+\mu} < 0,\\
\Upsilon_{\mu}^{\mathcal{R}_v^p} &= \frac{\partial \mathcal{R}_v^p}{\partial \mu}\frac{\mu}{\mathcal{R}_v^p} = \frac{(\gamma_p+\delta_p)\,\omega_p-\mu^2}{(\omega_p+\mu)\,(\gamma_p+\delta_p+\mu)}.
\end{aligned}$$

In particular, the sensitivity index of $\mathcal{R}_v$ with respect to $\beta$ can be interpreted as follows: an increase (or decrease) of the transmission rate $\beta$ by 10% results in an increase (or decrease) of $\mathcal{R}_v$ by 10%. This indicates that the disease transmission rate $\beta_p$ has a significant impact on the spread of the disease.

Furthermore, the parameters with negative sensitivity indices, namely $\gamma_p$, $\delta_p$, $\omega_p$, and $\rho_p$, contribute to minimizing the burden of the disease in the population as their values increase. The sign of the sensitivity index of $\mathcal{R}_v^p$ with respect to $\mu$ depends on the values of $\mu$ and $(\gamma_p+\delta_p)\,\omega_p$.

### 6.3.3 Sheep and Goat Pox (SGP)-Only Model

The model is derived by setting $I_p = I_{pc} = 0$ in equation (6.1). Additionally, the SGP vaccination is administered solely to newborn and susceptible animals. Consequently, we have:

$$\begin{cases}
\dfrac{dS}{dt} = (1-\rho_c)\Lambda - \dfrac{\beta_c S(I_c+\alpha B)}{N} - \omega_c S - \mu S,\\
\dfrac{dV_c}{dt} = \rho_c\Lambda + \omega_c S - \mu V_c,\\
\dfrac{dI_c}{dt} = \dfrac{\beta_c S(I_c+\alpha B)}{N} - (\delta_c+\gamma_c+\mu)I_c,\\
\dfrac{dR_c}{dt} = \gamma_c I_c - \mu R_c,\\
\dfrac{dB}{dt} = \xi I_c - \theta B
\end{cases} \tag{6.7}$$

where,

$$N(t) = S(t) + V_c(t) + I_c(t) + R_c(t).$$

In the region

$$\Omega_c = \left\{(S, V_c, I_c, R_c, B) \in \mathbb{R}_+^4 \times \mathbb{R}_+ : N \le \frac{\Lambda}{\mu}, B \le \frac{\xi\Lambda}{\mu\theta}\right\},$$

all solutions of the model (6.7) that start in $\Omega_c$ remain within $\Omega_c$ for all $t \geq 0$. In other words, $\Omega_c$ is positively invariant with respect to the model (6.7). Therefore, we will examine the dynamics of the model (6.7) within the region $\Omega_c$.

**Existence and Stability Analysis of Equilibria**

In the absence of SGP ( $I_c = B = 0$) in the population of small ruminants, model (6.7) admits an equilibrium point known as SGP disease-free , and it is given by

$$\xi_0^c = \left( \frac{(1-\rho_c)\Lambda}{(\omega_c+\mu)}, \frac{\Lambda(\rho_c\mu+\omega_c)}{\mu(\omega_c+\mu)}, 0, 0, 0 \right).$$

Following the next-generation method Van den Driessche et al., 2002, the control reproduction number of model (6.7) is

$$\mathcal{R}_v^c = \frac{\beta_c(1-\rho_c)\mu(\alpha\xi+\theta)}{\theta(\mu+\omega_c)(\delta_c+\gamma_c+\mu)} = \widetilde{\mathcal{R}_v^c}\left(\frac{\alpha\xi+\theta}{\theta}\right),$$

where $\widetilde{\mathcal{R}_v^c} = \frac{\beta_c\mu(1-\rho_c)}{(\gamma_c+\delta_c+\mu)(\omega_c+\mu)}$, it represents the control reproduction number of the model (6.7) without infection through contact between the susceptible animal with the shedding virus in the environment.

**Theorem 6.3.5.** *The disease-free equilibrium $\xi_0^c$ of the SGP-only model (6.2) is locally asymptotically stable if $\mathcal{R}_v^c < 1$, and unstable if $\mathcal{R}_v^c > 1$.*

**Proof** Using linearization method, the Jacobian matrix of system (6.2) at the $\xi_0^c$ is

$$J_{\xi_0^c} = \begin{bmatrix} -\mu-\omega_c & 0 & -\frac{\beta_c(1-\rho_c)\mu}{\omega_c+\mu} & 0 & -\frac{\beta_c(1-\rho_c)\mu\alpha}{\omega_c+\mu} \\ \omega_c & -\mu & 0 & 0 & 0 \\ 0 & 0 & \frac{\beta_c(1-\rho_c)\mu}{\omega_c+\mu} - \gamma_c - \delta_c - \mu & 0 & \frac{\beta_c(1-\rho_c)\mu\alpha}{\omega_c+\mu} \\ 0 & 0 & \gamma_c & -\mu & 0 \\ 0 & 0 & \xi & 0 & -\theta \end{bmatrix}$$

Here, the charactersistic equation for $J_{\xi_0^c}$ is

$$(\lambda+\mu)^2(\lambda+\mu+\omega_c)\left(\lambda^2 + \left(\theta + (1-\widetilde{\mathcal{R}_v^c})(\delta_c+\gamma_c+\mu)\right)\lambda + \theta(\delta_c+\gamma_c+\mu)(1-\mathcal{R}_v^c)\right) = 0. \tag{6.8}$$

It is clearly demonstrated in equation (6.8) that, based on the Routh-Hurwitz criterion, a second-degree polynomial has two negative roots if $\mathcal{R}_v^c < 1$. Therefore, the Disease-Free Equilibrium (DFE) ($\xi_0^c$) is locally asymptotically stable if $\mathcal{R}_v^c < 1$; otherwise, it is unstable.

**Theorem 6.3.6.** *The SGP disease-free equilibrium $\xi_0^c$ of model system (6.7) is globally asymptotically stable provided $\mathcal{R}_v^c < 1$, and unstable if $\mathcal{R}_v^c > 1$.*

**Proof** To investigate the global asymptotically stable of the model (6.7), we follow the method in Castillo-Chavez et al. (2004). First, we write system (6.7) in the form

$$\begin{cases} \dfrac{dX}{dt} = F(X,Z), \\ \dfrac{dY}{dt} = G(X,Z), G(X,0) = 0. \end{cases} \tag{6.9}$$

Where $X = (S, V_c, R_c)$ denote the number of uninfected small ruminants, and the components of $Z = (I_c, B)$ denote infected classes. Let $X^*$ be the disease-free equilibrium of the system $\frac{dX}{dt} = F(X,0)$ where $X^* = \left(\frac{(1-\rho_c)\Lambda}{(\omega_c+\mu)}, \frac{\Lambda(\rho_c\mu+\omega_c)}{\mu(\omega_c+\mu)}, 0\right)$. The DFE $\xi_0^c$ is guaranteed to be GAS if $\mathcal{R}_v < 1$ (which is locally asymptotically stable), and the following two conditions $\mathcal{H}_1$ and $\mathcal{H}_2$ hold.

$\mathcal{H}_1$. For $\frac{dX}{dt} = F(X,0)$, $X^*$ is globally asymptotically stable.

$\mathcal{H}_2$. $G(X,Z) = AZ - \bar{G}(X,Z)$, $\bar{G}(X,Z) \geq 0$ for all $(X,Z) \in \Omega_c$ where $A = \frac{\partial G(X^*)}{\partial Z}$ is an M-matrix.

Now consider the system

$$F(X,0) = \begin{bmatrix} \frac{dS}{dt} \\ \frac{dV_c}{dt} \\ \frac{dR_c}{dt} \end{bmatrix} = \begin{bmatrix} (1-\rho_c)\Lambda - \omega_c S - \mu S \\ \rho_c\Lambda + \omega_c S - \mu V_c \\ -\mu R_c \end{bmatrix} \tag{6.10}$$

From equation in (6.10), As $t \to \infty$,$S \to \frac{(1-\rho_c)\Lambda}{(\omega_c+\mu)}, V_c \to \frac{\Lambda(\rho_c\mu+\omega_c)}{\mu(\omega_c+\mu)}$ and $R_c \to 0$. Therefore $X^*$ is globally asymptotically stable.

Next, we have

$$G(X,Y) = AZ - \bar{G}(X,Z) = \begin{bmatrix} \frac{\beta_c S(I_c+\alpha B)}{N} - (\delta_c + \gamma_c + \mu)I_c \\ \xi I_c - \theta B \end{bmatrix},$$

where,

$$A = \frac{\partial G(X^*,0)}{\partial Z} = \begin{bmatrix} \frac{\beta_c S_0 I_c}{S_0+V_{c0}} - (\delta_c + \gamma_c + \mu) & \frac{\alpha\beta_c S_0 I_c}{S_0+V_{c0}} \\ \xi & -\theta \end{bmatrix}$$

which is clearly M-matrix. And

$$\bar{G}(X,Z) = AZ - G(X,Z) = \begin{bmatrix} \beta_c(I_c + \alpha B)\left(\frac{S_0}{S_0+V_{c0}} - \frac{S}{N}\right) \\ 0 \end{bmatrix}.$$

From model (6.7), as $t \to \infty$,

$$\begin{aligned} N \to N_\infty &= S_\infty + V_{c\infty} + I_\infty + R_\infty \\ &\geq S_\infty + V_{c\infty} \\ &= S_0 + V_{c0}. \end{aligned}$$

Since $S \leq S_0$ and $V_c \leq V_{c0}$, it follows that $\frac{S}{N} \leq \frac{S_0}{S_0+V_{c0}}$ and all parameters are non-negative. Hence, the condition $\mathcal{H}_2$ holds true, which means that $\bar{G}(X,Y) \geq 0$ for all $(X,Z) \in \Omega_c$. Therefore, the disease-free equilibrium of the PPR, $\xi_0^c$, of the model (6.7) is globally asymptotically stable.

To compute the endemic equilibrium point, we assume that $I_c \neq 0, B \neq 0$ and solve $\frac{dS}{dt} = \frac{dV_c}{dt} = \frac{dI_c}{dt} = \frac{dR_c}{dt} = \frac{dB}{dt} = 0$ for the endemic equilibrium $\xi_c^* = (S^*, V_c^*, I_c^*, R_c^*, B^*)$, we have

$$\begin{cases} S^* = \dfrac{\Lambda\,\theta\,(\delta_c\,\rho_c + \gamma_c + \mu)}{\mu\,\beta_c(\theta + \alpha\xi) - \delta_c\,(\mu + \omega_c)} \\ V_c^* = \dfrac{\Lambda\rho_c + \omega_c S^*}{\mu}, \\ I_c^* = \dfrac{\theta\Lambda\,(\omega_p + \mu)\,(\mathcal{R}_v^c - 1)}{\mu\,\beta_c(\theta + \alpha\xi) - \delta_c\,(\mu + \omega_c)}, \\ R_c^* = \gamma_c I_c^*, \\ B^* = \dfrac{\xi I_c^*}{\theta}. \end{cases} \tag{6.11}$$

Here we observe that the postivity of this equilibrium dependes on $\mathcal{R}_v^c$: its lessthan or greater than unity. Hence, the following result:

**Lemma 6.3.7.** *Unique endemic equilbrium point $\xi_c^* = (S^*, V_c^*, I_c^*, R_c^*, B^*)$ exists for the model (6.2) if $\mathcal{R}_v^c > 1$.*

### Sensitivity Analysis

Similarly, we employed the normalized forward sensitivity analysis method, as described in Equation 6.6, to analyze the sensitivity of the reproduction number $\mathcal{R}_v^c$ of the SGP sub-model (6.7) with respect to the parameters. Therefore, the sensitivity index of $\mathcal{R}_v^c$ is given by:

$$
\begin{aligned}
\Upsilon_{\beta_c}^{\mathcal{R}_v^p} &= \frac{\partial \mathcal{R}_v^c}{\partial \beta_p c}\frac{\beta_c}{\mathcal{R}_v^c} = 1 > 0,\\
\Upsilon_{\rho_c}^{\mathcal{R}_v^c} &= \frac{\partial \mathcal{R}_v^c}{\partial \rho_c}\frac{\rho_c}{\mathcal{R}_v^c} = -\frac{\rho_c}{1-\rho_c} < 0,\\
\Upsilon_{\gamma_c}^{\mathcal{R}_v^c} &= \frac{\partial \mathcal{R}_v^c}{\partial \gamma_c}\frac{\gamma_c}{\mathcal{R}_v^c} = -\frac{\gamma_c}{\gamma_c+\delta_c+\mu} < 0,\\
\Upsilon_{\delta_c}^{\mathcal{R}_v^c} &= \frac{\partial \mathcal{R}_v^c}{\partial \delta_c}\frac{\delta_c}{\mathcal{R}_v^c} = -\frac{\delta_c}{\gamma_c+\delta_c+\mu} < 0,\\
\Upsilon_{\omega_c}^{\mathcal{R}_v^c} &= \frac{\partial \mathcal{R}_v^c}{\partial \omega_c}\frac{\omega_c}{\mathcal{R}_v^c} = -\frac{\omega_c}{\omega_c+\mu} < 0,\\
\Upsilon_{\mu}^{\mathcal{R}_v^c} &= \frac{\partial \mathcal{R}_v^c}{\partial \mu}\frac{\mu}{\mathcal{R}_v^c} = \frac{(\gamma_c+\delta_c)\,\omega_c-\mu^2}{(\omega_c+\mu)\,(\gamma_c+\delta_c+\mu)}\\
\Upsilon_{\gamma_c}^{\mathcal{R}_v^c} &= \frac{\partial \mathcal{R}_v^c}{\partial \gamma_c}\frac{\gamma_c}{\mathcal{R}_v^c} = -\frac{\gamma_c}{\gamma_c+\delta_c+\mu} < 0,\\
\Upsilon_{\xi}^{\mathcal{R}_v^c} &= \frac{\partial \mathcal{R}_v^c}{\partial \xi}\frac{\xi}{\mathcal{R}_v^c} = \frac{\alpha\,\xi}{\alpha\,\xi+\theta} > 0,\\
\Upsilon_{\theta}^{\mathcal{R}_v^c} &= \frac{\partial \mathcal{R}_v^c}{\partial \theta}\frac{\theta}{\mathcal{R}_v^c} = -\frac{\alpha\,\xi}{\alpha\,\xi+\theta} < 0,\\
\Upsilon_{\alpha}^{\mathcal{R}_v^c} &= \frac{\partial \mathcal{R}_v^c}{\partial \alpha}\frac{\alpha}{\mathcal{R}_v^c} = \frac{\alpha\,\xi}{\alpha\,\xi+\theta} > 0,
\end{aligned}
$$

The interpretation of these sensitivity index results depends on their sign. As shown in the results, the parameters $\beta_c$, $\xi$, and $\alpha$ have positive sensitivity indices, which means that increasing the values of these parameters, especially $\beta_c$, while keeping the other parameters constant, contributes to the incremental value of the control reproduction number relative to their values. This has a significant impact on the spread of the disease. Conversely, since the remaining parameters have negative sensitivity indices, they effectively minimize the burden of the disease in the small ruminant population as their values increase.

### 6.3.4 Co-infection Model

In this subsection, we illusrate the existence of DFE and Reproduction number of model (6.1), and based on the reproduction number we prove the local stability of DFE.

#### Existence and Staility of Equilibrium and Reproduction Number

It is clrealy that the DFE point can be obtained by setting $I_p = I_c = I_{pc} = B = 0$ and solve the right sides of equations in (6.1) by equating with zero,then we have the DFE as

$$
\xi_0^{pc} = \left(\frac{(1-\rho)\Lambda}{\mu+\omega}, \frac{\Lambda(\omega+\rho\mu)}{\mu(\mu+\omega)}, 0, 0, 0, 0, 0\right).
$$

The control Reproduction can be obtain by using next generation matrix method (Van den Driessche et al., 2002). According to the principle of the method, the control reprodution number is calculated as follows: consider column vectors $\mathcal{F}$ and $\mathcal{V}$ as representation of new infection cases and the amount of displacement of animals into and out of infection classes, respectively.

$$\mathcal{F} = \begin{pmatrix} \frac{\beta_p S(I_p+I_{pc})}{N} \\ \frac{\beta_c S(I_c+I_{pc}+\alpha B)}{N} \\ \frac{\beta_p I_c(I_p+I_{pc})}{N} + \frac{\beta_c I_p(I_c+I_{pc}+\alpha B)}{N} \\ 0 \end{pmatrix}, \mathcal{V} = \begin{pmatrix} \frac{\beta_c I_p(I_c+I_{pc}+\alpha B)}{N} + (\gamma_p+\delta_p+\mu)I_p - \gamma_{pc} p I_{pc} \\ \frac{\beta_p I_c(I_p+I_{pc})}{N} + (\gamma_c+\delta_c+\mu)I_c - \gamma_{pc} q I_{pc} \\ (\gamma_{pc}+\delta_{pc}+\mu)I_{pc} \\ \theta B - \xi(I_c+\epsilon I_{pc}) \end{pmatrix}$$

Thus

$$F = \begin{pmatrix} \frac{\beta_p S_0}{S_0+V_0} & 0 & \frac{\beta_p S_0}{S_0+V_0} & 0 \\ 0 & \frac{\beta_c S_0}{S_0+V_0} & \frac{\beta_c S_0}{S_0+V_0} & \frac{\alpha\beta_c S_0}{S_0+V_0} \\ 0 & 0 & 0 & 0 \\ 0 & 0 & 0 & 0 \end{pmatrix}, V = \begin{pmatrix} \gamma_p+\delta_p+\mu & 0 & -p\,\gamma_{pc} & 0 \\ 0 & \gamma_c+\delta_c+\mu & -q\,\gamma_{pc} & 0 \\ 0 & 0 & \gamma_{pc}+\delta_{pc}+\mu & 0 \\ 0 & -\xi & -\epsilon\xi & \theta \end{pmatrix}$$

The control reproduction number $\mathcal{R}_v^{pc}$ of the model (6.1) is the sepctral radius of the matrix $FV^{-1}$, then $\mathcal{R}_v^{pc}$ is given by

$$\mathcal{R}_v^{pc} = \max\left\{ \frac{\beta_c(1-\rho)\mu(\alpha\xi+\theta)}{\theta(\omega+\mu)(\gamma_c+\delta_c+\mu)}, \frac{\beta_p(1-\rho)\mu}{(\omega+\mu)(\gamma_p+\delta_p+\mu)} \right\} = \max\left\{\mathcal{R}_v^c, \mathcal{R}_v^p\right\}.$$

**Theorem 6.3.8.** *The disease-free equilibrium $\xi_0^{pc}$ of the model (6.1) is locally asymptotically stable if $\mathcal{R}_v^{pc} < 1$, and unstable if $\mathcal{R}_v^{pc} > 1$.*

**Proof** Using linearization method, the Jacobian matrix of system (6.1) at the $\xi_0^{pc}$ is

$$J_{\xi_0^{pc}} = \begin{bmatrix} -\omega-\mu & 0 & -\frac{\beta_p(1-\rho)\mu}{\omega+\mu} & -\frac{\beta_c(1-\rho)\mu}{\omega+\mu} & -\frac{\beta_p(1-\rho)\mu}{\omega+\mu} - \frac{\beta_c(1-\rho)\mu}{\omega+\mu} & 0 & -\frac{\alpha\beta_c(1-\rho)\mu}{\omega+\mu} \\ \omega & -\mu & 0 & 0 & 0 & 0 & 0 \\ 0 & 0 & r_1 & 0 & \frac{\beta_p(1-\rho)\mu}{\omega+\mu} + \gamma_{pc} p & 0 & 0 \\ 0 & 0 & 0 & r_2 & \frac{\beta_c(1-\rho)\mu}{\omega+\mu} + \gamma_{pc} q & 0 & \frac{\alpha\beta_c(1-\rho)\mu}{\omega+\mu} \\ 0 & 0 & 0 & 0 & -\gamma_{pc}-\delta_{pc}-\mu & 0 & 0 \\ 0 & 0 & \gamma_p & \gamma_c & \gamma_{pc}(1-p-q) & -\mu & 0 \\ 0 & 0 & 0 & \xi & \xi\,\epsilon & 0 & -\theta \end{bmatrix}$$

where $r_1 = \frac{\beta_p(1-\rho)\mu}{\omega+\mu} - \gamma_p - \delta_p - \mu$ and $r_2 = \frac{\beta_c(1-\rho)\mu}{\omega+\mu} - \gamma_c - \delta_c - \mu$
Here, the charactersistic equation for $J_{\xi_0^{pc}}$ is

$$(\lambda + (\gamma_p+\delta_p+\mu)(1-\mathcal{R}_v^p))(\lambda+\mu)^2(\lambda+\mu+\omega)(\lambda+\gamma_{pc}+\delta_{pc}+\mu)\left(\lambda^2+a_1\lambda+a_0\right) = 0. \tag{6.12}$$

where,

$$\begin{cases} a_0 = \theta(\delta_c+\gamma_c+\mu)(1-\mathcal{R}_v^c), \\ a_1 = (\gamma_c+\delta_c+\mu)\left(1-\frac{\theta\mathcal{R}_v^c}{\alpha\xi+\theta}\right)+\theta. \end{cases}$$

Equation (6.12) clearly illustrates that, according to the Routh-Hurwitz criterion, a second-degree polynomial will have two negative roots if $a_1 > 0$ and $a_0 > 0$. This implies that $\mathcal{R}_v^c < 1$, and the first factor in (6.12) indicates that the eigenvalue is negative when $\mathcal{R}_v^p < 1$. Thus, the Disease-Free Equilibrium (DFE) $\xi_0^{pc}$ is considered locally asymptotically stable if both $\mathcal{R}_v^p < 1$ and $\mathcal{R}_v^c < 1$; otherwise, it is deemed unstable.

## 6.4 Parameter Estimation

In this study, we estimated the basic parameters in the two sub-models (6.2, 6.7) using semester-wise reported incidence data for the two diseases, spanning from January 2005 to August 2023 in Ethiopia. The data were sourced from the World Organization for Animal Health (WOAH) dashboard (WOAH, 2023), which provided summarized information for investigating the dynamics of the diseases. The death rates $(\delta_p, \delta_s)$ due to Peste des Petits Ruminants (PPR) and Sheep and Goat Plague (SGP) were computed by taking the ratio of the reported number of cases to the deaths for both diseases.

For the parameter estimation process, we first employed the Interquartile Range (IQR) method to identify outlier data and applied a capping technique to preserve the dataset's integral structure while minimizing the influence of anomalous observations. This method effectively mitigated the risk of skewed parameter estimates that could arise from extreme values.

The primary objective of this study is to determine the optimal parameters that allow our models (6.2) and (6.7) to align best with the available data. To achieve this, we employ the nonlinear least-squares approximation method. The algorithm used in this method is the built-in `lsqcurvefit` function in MATLAB from the Optimization Toolbox, which aims to minimize the sum of squared errors.

$$SSE = \sum_{j=1}^{n} (I_j - I^*(t_j))^2 \tag{6.13}$$

where $I_j$ is the prevalence data and $I^*(t_j)$ is the simulation result (predicted) at time step $j$ for the prevalence of the disease. We used the cases in 2005 as initial values for the two sub-models:

$$IC_{\text{PPR}} = (S_0, V_{p0}, I_{p0}, R_{p0}) = (264225, 226300, 5075, 4400),$$

$$IC_{\text{SGP}} = (S_0, V_{c0}, I_{c0}, R_{c0}, B_0) = (359560, 340000, 4300, 1140, 100).$$

All estimated parameter values are listed in Table (6.2), and the visualization of the results is shown in Figures (6.3A) and (6.3B). The blue curves represent the simulation results for the cumulative incidences of $I_p^*(t)$ and $I_c^*(t)$ from the models (6.2) and (6.7) respectively, while the red dots indicate the prevalence data. Furthermore, the computed reproduction numbers for the two diseases, using these estimated parameter values, are given as $\mathcal{R}_v^p = 1.0710$ and $\mathcal{R}_v^c = 1.0892$. Since both reproduction numbers are greater than one, this indicates that the two diseases persist in the small ruminant population.

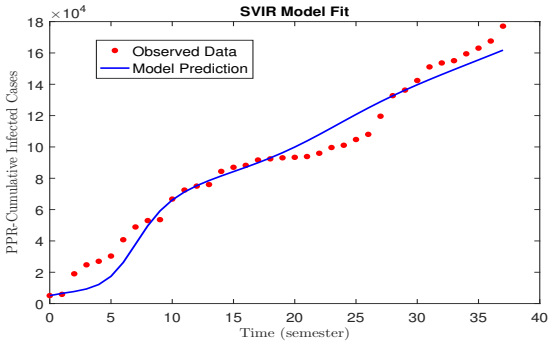


(A) Model fit for the case of PPR.

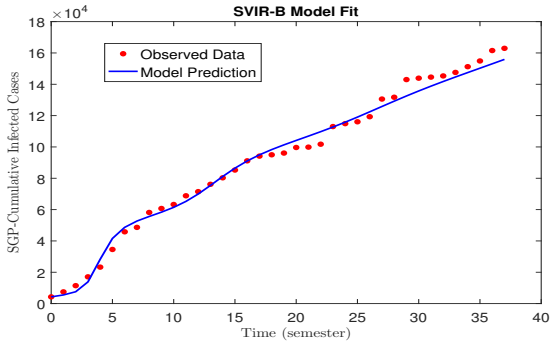


(B) Model fit for the case of SGP.

FIGURE 6.3: Model fit to historical PPR and SGP incidence data for Ethiopia (2005–2023).

TABLE 6.2: Parameter Values from Estimation

| For the case of PPR | | | For the case of SGP | | |
|---|---|---|---|---|---|
| parameter | Value(per semester) | Source | parameter | Value(per semester) | Source |
| $\Lambda$ | 312000 | Computed | $\Lambda$ | 440000 | Calculated |
| $\mu$ | 0.125 | Fournié et al., 2018 | $\mu$ | 0.125 | Chamchod, 2018 |
| $\beta_p$ | 10.0023 | Estimated | $\beta_c$ | 3.1476 | Estimated |
| $\delta_p$ | 0.3229 | Computed | $\delta_c$ | 0.0978 | Computed |
| $\gamma_p$ | 6.9695 | Estimated | $\gamma_c$ | 12.3202 | Estimated |
| $\rho_p$ | 0.01 | Assumed | $\rho_c$ | 0.015 | Assumed |
| $\omega_p$ | 0.03087 | Estimated | $\omega_c$ | 0.0452 | Estimated |
| | | | $\alpha$ | 0.05 | Assumed |
| | | | $\xi$ | $10^4$ copies/mL | Assumed |
| | | | $\theta$ | $10^2$ | Assumed |

## 6.5 Numerical Sensitivity Indices of the Reproduction Numbers

Following parameter estimation, the computed sensitivity indices of the reproduction numbers ($\mathcal{R}_v^p$ and $\mathcal{R}_v^c$) are presented in Table (6.3).

TABLE 6.3: Sensitivity Indices of $\mathcal{R}_v^p$ and $\mathcal{R}_v^c$

| Sensitivity Index of $\mathcal{R}_v^p$ | | Sensitivity Index of $\mathcal{R}_v^c$ | |
|---|---|---|---|
| Parameter | SI Value | Parameter | SI Value |
| $\mu$ | 0.1811 | $\mu$ | 0.2556 |
| $\beta_p$ | 1.0000 | $\beta_c$ | 1.0000 |
| $\delta_p$ | −0.0435 | $\delta_c$ | −0.0078 |
| $\gamma_p$ | −0.9396 | $\gamma_c$ | −0.9822 |
| $\rho_p$ | −0.0100 | $\rho_c$ | −0.0152 |
| $\omega_p$ | −0.1980 | $\omega_c$ | −0.2656 |
| | | $\alpha$ | 0.8333 |
| | | $\xi$ | 0.8333 |
| | | $\theta$ | −0.8333 |

As shown in Table (6.3), the results of the sensitivity analysis reveal that the transmission parameter $\beta_p$ and the recovery rate $\gamma_p$ are the most sensitive parameters in the PPR disease dynamics, followed by the vaccination rate, $\omega_p$. Similarly, for the SGP disease model (6.7), the transmission parameter $\beta_c$ and the recovery rate $\gamma_c$ exhibit the highest sensitivity, followed by the parameters $\alpha$, $\xi$, $\theta$, and $\omega_c$.

These results emphasize the critical roles of the transmission and recovery rates in the respective disease dynamics, as they have the most significant influence on the reproduction numbers. This finding is further corroborated by the numerical simulations presented in the subsequent sections, providing additional support for the sensitivity analysis conclusions.

## 6.6 Optimal Control Problem

In this section, we analyze an optimal control model for the co-infection dynamics of Peste des Petits Ruminants (PPR) and Sheep/Goat Pox (SGP) in small ruminants. The model incorporates four time-dependent control variables: vaccination of susceptible individuals, vaccination of newly recruited individuals (newborns and immigrants), sanitation or disinfection measures, and treatment of co-infected animals. We establish the existence of an optimal control solution and derive the necessary conditions for optimality using Pontryagin's Maximum Principle (PMP) (Pontryagin, 1987). Numerical simulations illustrate the impact of these controls on disease prevalence. Notation for each control variable, as well as the set of admissible controls, is defined below.

i. **Disinfection/Sanitation Protocol:** This practice is part of biosecurity measures and should be implemented to minimize the risk of SGP disease transmission. It includes maintaining proper hygiene, disinfecting contaminated areas (herds or flocks), implementing rigorous cleaning protocols, and raising awareness among livestock owners about the importance of disease prevention and control. These practices help prevent contact between concentrations of pathogens in the environment and susceptible animals, thereby reducing the likelihood of disease transmission. To investigate the optimal cost associated

with disinfection control, we denote $u_4(t)$ as the level of sanitation efforts, scaled such that $0 \leq u_4(t) \leq u_{4,\max} \leq 1$.

ii. **Vaccination of Susceptible and Recruited Populations:** The primary strategy for controlling PPR and SGP is to vaccinate both susceptible and newly recruited individuals, including newborns and immigrant small ruminants in endemic regions. The objective is to achieve an optimal immunity rate within a specified timeframe to prevent the transmission of both the PPR and SGP viruses. To date, independent monovalent live vaccines are used for these diseases; however, low vaccination coverage due to the extensive spatial distribution of animal populations and inadequate infrastructure contributes to the persistence and spread of the infections (Fakri et al., 2015). Implementing mass immunization can be challenging and costly Hammami et al., 2018. A combined vaccine could serve as an effective tool in endemic countries with limited infrastructure and extensive breeding management of small ruminant populations. Furthermore, utilizing a combined vaccine could reduce vaccination costs, making it more appealing to farmers in developing countries. Therefore, we employ such a combined vaccine for both diseases in our model. The control variables $u_1(t)$ and $u_2(t)$ represent vaccination control for newly recruited and susceptible populations, respectively, and are utilized to minimize vaccination costs while alleviating the burden of PPR diseases. The controls $u_1$ and $u_2$ are constrained within the range $0 \leq u_i \leq u_{i,\max}$, for $i = 1, 2$.

iii. **Treatment:** As PPR and SGP are viral diseases, there is currently no specific treatment available for animals infected with either disease. In our model, we assume that supportive care such as isolation, fluid therapy, nutritional support, management of secondary infections, and veterinary care is provided for animals severely infected with both diseases (co-infected). This approach helps reduce morbidity and mortality among infected animals and decreases the transmission rate. The treatment control variable $u_3(t)$ is introduced to determine the optimal intervention and is scaled such that $0 \leq u_3(t) \leq u_{3,\max} \leq 1$.

The goal of our optimal control problem is to minimize the disease burden while accounting for the costs of implementing the control strategies. The objective functional is given by:

$$J(u_1, u_2, u_3, u_4) = \int_0^{T_f} \left[ w_1 I_p + w_2 I_c + w_3 I_{pc} + \frac{1}{2} C_1 u_1^2 + \frac{1}{2} C_2 u_2^2 + \frac{1}{2} C_3 u_3^2 + \frac{1}{2} C_4 u_4^2 \right] dt, \quad (6.14)$$

with respect to the system

$$\begin{cases} \frac{dS}{dt} = (1-u_1)\Lambda - (\chi_p + \chi_c)S - (\mu + u_2)S, \\ \frac{dV}{dt} = u_1\Lambda + u_2 S - \mu V, \\ \frac{dI_p}{dt} = \chi_p S + (1-u_3)p\gamma_{pc}I_{pc} - \chi_c I_p - (\gamma_p + \delta_p + \mu)I_p, \\ \frac{dI_c}{dt} = \chi_c S + (1-u_3)q\gamma_{pc}I_{pc} - \chi_p I_c - (\gamma_c + \delta_c + \mu)I_c, \\ \frac{dI_{pc}}{dt} = \chi_p I_c + \chi_c I_p - ((1-u_3)(\gamma_{pc} + \delta_{pc}) + \mu + u_3)I_{pc}, \\ \frac{dR}{dt} = \gamma_p I_p + \gamma_c I_c + ((1-u_3)(1-(p+q))\gamma_{pc} + u_3)I_{pc} - \mu R, \\ \frac{dB}{dt} = \xi(I_c + \epsilon I_{pc}) - (\theta + u_4)B, \end{cases} \tag{6.15}$$

where the force of infections $\chi_p$ and $\chi_c$ are defined as:

$$\chi_p = \frac{\beta_p(I_p + I_{pc})}{N}, \quad \chi_c = \frac{\beta_c(I_c + I_{pc} + (1-u_4)\alpha B)}{N},$$

with $N = S + V + I_p + I_c + I_{pc} + R$ representing the total population size.

The initial conditions for the system are: $S(0) = S_0 \geq 0$, $V(0) = V_0 \geq 0$, $I_p(0) = I_{p,0} \geq 0$, $I_c(0) = I_{c,0} \geq 0$, $I_{pc}(0) = I_{pc,0} \geq 0$, $R(0) = R_0 \geq 0$, $B(0) = B_0 \geq 0$.

The coefficients $w_1, w_2$, and $w_3$ in the integrand represent positive weight parameters that ensure the balance of each component within the objective function (6.15). The first three terms of the integrand in equation (6.15), specifically $w_1 I_p, w_2 I_c$, and $w_3 I_{pc}$, account for the costs associated with morbidity and mortality due to PPR and SGP diseases. These costs encompass significant economic losses, including decreased productivity, trade restrictions, and diminished market value for the affected animals (Jemberu et al., 2022; Fournié et al., 2018). The final four terms in equation (6.15) represent the costs associated with control measures. In this context, the second-order nonlinearity is considered for the three control interventions to reflect their substantial effort, severity, and associated costs (Makinde et al., 2011; Nyerere et al., 2020b).

The goal is to find an optimal control quadruple, $\mathbf{u} = (u_1^*(t), u_2^*(t), u_3^*(t), u_4^*(t))$, such that

$$J(u_1^*(t), u_2^*(t), u_3^*(t), u_4^*(t)) = \min_{\mathbf{U}} J(u_1(t), u_2(t), u_3(t), u_4(t)) \tag{6.16}$$

where $\mathbf{U}$ is the non-empty control set defned as

$$\mathbf{U} = \{(u_1(t), u_2(t), u_3(t), u_4(t)) | 0 \leq u_i \leq u_{imax} \leq 1, \text{Lebesgue measurable}, i = 1,2,3,4 \quad t \in [0, T_f]\}. \tag{6.17}$$

### 6.6.1 Existence and Optimality System

The optimal control must satisfy the necessary conditions that are formulated by Pontryagin's Maximum Principle Shim, 2004. This principle changes the system of Equations in (6.15) into a problem of minimizing point-wise a Hamiltonian (H), with respect to $u_1(t), u_2(t), u_3(t), u_4(t)$.

For deriving the necessary conditions, we define the Hamiltonian ($\mathcal{H}$) as

$$\begin{aligned}\mathcal{H} &= w_1 I_p + w_2 I_c + w_3 I_{pc} + \frac{1}{2}C_1 u_1^2 + \frac{1}{2}C_2 u_2^2 + \frac{1}{2}C_3 u_3^2 + \frac{1}{2}C_4 u_4^2 \\ &+ \lambda_1 \left((1-u_1)\Lambda - (\chi_p + \chi_c)S - (\mu + u_2)S\right) \\ &+ \lambda_2 \left(u_1\Lambda + u_2 S - \mu V\right) \\ &+ \lambda_3 \left(\chi_p S + (1-u_3)p\gamma_{pc} I_{pc} - \chi_c I_p - (\gamma_p + \delta_p + \mu)I_p\right) \\ &+ \lambda_4 \left(\chi_c S + (1-u_3)q\gamma_{pc} I_{pc} - \chi_p I_c - (\gamma_c + \delta_c + \mu)I_c\right) \\ &+ \lambda_5 \left(\chi_p I_c + \chi_c I_p - ((1-u_3)(\gamma_{pc} + \delta_{pc}) + \mu + u_3)I_{pc}\right) \\ &+ \lambda_6 \left(\gamma_p I_p + \gamma_c I_c + ((1-u_3)\gamma_{pc}(1-(p+q)) + u_3)I_{pc} - \mu R\right) \\ &+ \lambda_7 \left(\xi(I_c + \epsilon I_{pc}) - (\theta + u_4)B\right)\end{aligned} \tag{6.18}$$

where $\lambda_i, i = 1, 2, ..., 7$ are the adjoint variables or co-state variables. By applying Pontryagin's Maximum Principle (Lenhart et al., 2007) and the existence result for the optimal control from (Fleming et al., 2012), we acquire the following theorem.

**Theorem 6.6.1.** *There exists an optimal control solution* $\mathbf{u}^* = (u_1^*, u_2^*, u_3^*, u_4^*) \in \mathbf{U}$ *and the corresponding solution* $(S^*, V^*, I_p^*, I_c^*, I_{pc}^*, R^*, B^*)$ *of the system (6.15), that minimizes* $J(\mathbf{u}^*)$ *over* $\mathbf{U}$. *Furthermore, there exist adjoint functions,* $\lambda_i(t), i = 1, 2, ..., 7$ *such that*

$$\begin{cases}
\frac{d\lambda_1}{dt} = (\lambda_1 - \lambda_3)\chi_p\left(1 - \frac{S}{N}\right) + (\lambda_1 - \lambda_4)\chi_c\left(1 - \frac{S}{N}\right) + (\lambda_1 - \lambda_2)u_2 + (\lambda_5 - \lambda_4)\frac{\chi_p I_c}{N} \\
\qquad + (\lambda_5 - \lambda_3)\frac{\chi_c I_p}{N} + \lambda_1\mu, \\
\frac{d\lambda_2}{dt} = (\lambda_3 - \lambda_1)\frac{\chi_p S}{N} + (\lambda_4 - \lambda_1)\frac{\chi_c S}{N} + (\lambda_5 - \lambda_3)\frac{\chi_c I_p}{N} + (\lambda_5 - \lambda_4)\frac{\chi_p I_c}{N} + \lambda_2\mu, \\
\frac{d\lambda_3}{dt} = (\lambda_1 - \lambda_3)\frac{S}{N}(\beta_p - \chi_p) + (\lambda_4 - \lambda_1)\frac{\chi_c S}{N} + (\lambda_4 - \lambda_5)\frac{I_c}{N}(\beta_p - \chi_p) + (\lambda_3 - \lambda_5)(1 - \frac{I_p}{N})\chi_c \\
\qquad + \lambda_3(\gamma_p + \delta_p + \mu) - \lambda_6\gamma_p - w_1, \\
\frac{d\lambda_4}{dt} = (\lambda_1 - \lambda_4)\frac{S}{N}(\beta_c - \chi_c) + (\lambda_3 - \lambda_5)\frac{I_p}{N}(\beta_c - \chi_c) + (\lambda_4 - \lambda_5)(1 - \frac{I_c}{N})\chi_p + (\lambda_3 - \lambda_1)\frac{S\chi_p}{N} \\
\qquad + \lambda_4(\gamma_c + \delta_c + \mu) - \lambda_6\gamma_c - \lambda_7\xi - w_2, \\
\frac{d\lambda_5}{dt} = -w_3 + (\lambda_1 - \lambda_3)\frac{S}{N}(\beta_p - \chi_p) + (\lambda_1 - \lambda_4)\frac{S}{N}(\beta_c - \chi_c) + (\lambda_3 - \lambda_5)\frac{I_p}{N}(\beta_c - \chi_c) \\
\qquad + (\lambda_4 - \lambda_5)\frac{I_p}{N}(\beta_p - \chi_p) - (\lambda_3 p + \lambda_4 q)(1 - u_3)\gamma_{pc} + \lambda_5((1-u_3)(\gamma_{pc} + \delta_{pc}) + \mu + u_3) \\
\qquad - \lambda_6((1-u_3)(1-(p+q))\gamma_{pc} + u_3) - \lambda_7\xi\epsilon, \\
\frac{d\lambda_6}{dt} = (\lambda_3 - \lambda_1)\frac{\chi_p S}{N} + (\lambda_4 - \lambda_1)\frac{\chi_c S}{N} + (\lambda_5 - \lambda_3)\frac{\chi_c I_p}{N} + (\lambda_5 - \lambda_4)\frac{\chi_p I_c}{N} + \lambda_6\mu, \\
\frac{d\lambda_7}{dt} = (\lambda_1 - \lambda_4)\frac{S\beta_c\alpha(1-u_4)}{N} + (\lambda_3 - \lambda_5)\frac{I_p\beta_c\alpha(1-u_4)}{N} + \lambda_7(\theta + u_4)
\end{cases} \tag{6.19}$$

*with the transversality conditions*

$$\lambda_i(T_f) = 0, \quad i = 1, 2, ..., 7. \tag{6.20}$$

*Furthermore, the optimal controls are characterized by*

$$\begin{cases} u_1^* = \max\left\{0, \min\left\{\dfrac{\Lambda(\lambda_1-\lambda_2)}{C_1}, 1\right\}\right\}, \\ u_2^* = \max\left\{0, \min\left\{\dfrac{S(\lambda_1-\lambda_2)}{C_2}, 1\right\}\right\}, \\ u_3^* = \max\left\{0, \min\left\{\dfrac{(\lambda_3 p+\lambda_4 q)\gamma_{pc} I_{pc} - \lambda_5 I_{pc}(\gamma_{pc}+\delta_{pc}-1) + \lambda_6(\gamma_{pc}(1-(p+q))-1)I_{pc}}{C_3}, 1\right\}\right\}, \\ u_4^* = \max\left\{0, \min\left\{\dfrac{(\lambda_4-\lambda_1)\left(\frac{\beta_c \alpha B S}{N}\right) + (\lambda_5-\lambda_3)\left(\frac{\beta_c \alpha B I_p}{N}\right) + \lambda_7 B}{C_4}, 1\right\}\right\}. \end{cases} \tag{6.21}$$

**Proof** To establish the existence of an optimal control, we verify the necessary conditions based on standard results in optimal control theory as presented in Fleming et al. (2012). These conditions are further validated in Chapter 4, Theorem (4.6.1). The conditions to be verified include:

❶ The convexity of the admissible control set $\mathbf{U}$.

❷ The a priori boundedness of the state solutions.

❸ The convexity and boundedness of the integrand in (6.14).

We note that the control set $\mathbf{U}$ is a compact subset of $\mathcal{R}^4$, as each control $u_i$ is bounded within $[0, u_{i,max}]$. This implies that the control set $\mathbf{U}$ is convex.

The right-hand side of the differential equations in (6.15) is linear with respect to each control and can be expressed as:

$$f(t, \mathbf{x}, \mathbf{u}) = \phi(t, \mathbf{x}) + \psi(t, \mathbf{x})\mathbf{u},$$

where $\mathbf{x} = (S, V, I_p, I_c, I_{pc}, R, B)$. From similar results on the boundedness of the system in (6.1), as demonstrated in Lemma 6.3.1, the system (6.15) is also bounded. Specifically, the boundedness of the solutions ensures that: $||\phi(t, \mathbf{x})|| \leq M_0$, $||\psi(t, \mathbf{x})|| \leq K_1$, where $K_0$ and $K_1$ are positive constants and

$$f(t, \mathbf{x}, \mathbf{u}) \leq K(1 + ||\mathbf{u}||), \quad \text{for } 0 \leq t \leq T_f. \quad \text{where} \quad K = \max\{K_0, K_1\}.$$

Furthermore, since the integrand in (6.14) is quadratic in $u_1, u_2, u_3$, and $u_4$, this guarantees its convexity. The final condition to be verified pertains to the integrand of the objective functional $\mathcal{L}$, which is given by:

$$\mathcal{L} = w_1 I_p + w_2 I_c + w_3 I_{pc} + \frac{1}{2}C_1 u_1^2 + \frac{1}{2}C_2 u_2^2 + \frac{1}{2}C_3 u_3^2 + \frac{1}{2}C_4 u_4^2.$$

To ensure the integrand $\mathcal{L}$ is bounded below, we demonstrate that:

$$\mathcal{L}(t, \mathbf{x}, \mathbf{u}) \geq g(t, \mathbf{x}, \mathbf{u}),$$

where:

$$g(t, \mathbf{x}, \mathbf{u}) = \theta_0 ||\mathbf{u}||^{\theta_2} - \theta_1, \quad \text{for all } \theta_0, \theta_1 > 0 \text{ and } \theta_2 > 1.$$

This condition holds for $\theta_0 = \frac{1}{2}\min\{C_1, C_2, C_3, C_4\}$, $\theta_1 > 0$, and $\theta_2 = 2$. Consequently, we have:

$$\mathcal{L}(t, \mathbf{x}, \mathbf{u}) \geq g(t, \mathbf{x}, \mathbf{u}).$$

Thus, applying Pontryagin's Maximum Principle (Lenhart et al., 2007), the system in (6.14), (6.15), and (6.16) is transformed into a problem of minimizing the Hamiltonian $H$ pointwise with respect to the control variables $u_1, u_2, u_3$ and $u_4$. The Hamiltonian is defined as:

$$\mathcal{H} = w_1 I_p + w_2 I_c + w_3 I_{pc} + \frac{1}{2}C_1 u_1^2 + \frac{1}{2}C_2 u_2^2 + \frac{1}{2}C_3 u_3^2 + \frac{1}{2}C_4 u_4^2 + \sum_{i=1}^{7} \lambda_i f_i,$$

where $f_i$ $(i = 1, \ldots, 7)$ are the right-hand sides of the system in (6.15). The adjoint equations are derived accordingly.

$$\begin{cases} \frac{d\lambda_1}{dt} = -\frac{\partial \mathcal{H}}{\partial S}, \lambda_1(T_f) = 0, \\ \frac{d\lambda_2}{dt} = -\frac{\partial \mathcal{H}}{\partial V}, \lambda_2(T_f) = 0, \\ \frac{d\lambda_3}{dt} = -\frac{\partial \mathcal{H}}{\partial I_p}, \lambda_3(T_f) = 0, \\ \frac{d\lambda_4}{dt} = -\frac{\partial \mathcal{H}}{\partial I_c}, \lambda_4(T_f) = 0, \\ \frac{d\lambda_5}{dt} = -\frac{\partial \mathcal{H}}{\partial I_{pc}}, \lambda_5(T_f) = 0, \\ \frac{d\lambda_6}{dt} = -\frac{\partial \mathcal{H}}{\partial R}, \lambda_6(T_f) = 0, \\ \frac{d\lambda_7}{dt} = -\frac{\partial \mathcal{H}}{\partial B}, \lambda_7(T_f) = 0. \end{cases} \tag{6.22}$$

From Equation (6.22) we obtain equations in (6.19) for adjoint variables $\lambda' s$. And computing

$$u_1^*(t) = \frac{\partial \mathcal{H}}{\partial u_1}, \quad u_2^*(t) = \frac{\partial \mathcal{H}}{\partial u_2}, \quad u_3^*(t) = \frac{\partial \mathcal{H}}{\partial u_3}, \quad u_4^*(t) = \frac{\partial \mathcal{H}}{\partial u_4}$$

and using the property of control set $\mathbf{U}$, we have required optimal control functions as mentioned in equation (6.21).

We also note that $\frac{\partial^2 \mathcal{H}}{\partial u_1^2}|_{u_1}^* = 2C_1 > 0$, $\frac{\partial^2 \mathcal{H}}{\partial u_1^2}|_{u_2}^* = 2C_2 > 0$, $\frac{\partial^2 \mathcal{H}}{\partial u_1^2}|_{u_3}^* = 2C_3 > 0$, and $\frac{\partial^2 \mathcal{H}}{\partial u_4^2}|_{u_4}^* = 2C_4 > 0$ indicating that the optimal controls minimize the Hamiltonian.

In this section, we verify and discuss the findings from the previous analytical analysis using numerical simulations applied to the sub-models (6.2 & 6.7) and the co-infected model (6.1). The simulations are conducted using the fourth-order Runge–Kutta method (Ode45) in MATLAB.

We examine the effects of various parameters and identify optimal control strategies to mitigate the spread of the diseases. The parameter values used in the simulations are provided in Table (6.2). In cases where reference values are unavailable, assumptions are made based on real-world scenarios and practical considerations.

### 6.6.2 Effects of Parameters

In this subsection, we analyze the effects of key parameters in the sub-models and the co-infected model. Figure (6.4A) illustrates the impact of varying $\alpha$ on the dynamics of SGP, with the initial conditions

$$(S_0, V_{c0}, I_{c0}, R_{c0}) = (276239, 21756, 1845, 160).$$

The results clearly show that $\alpha$ significantly influences the behavior of the system. Specifically, when $\alpha = 0.02$, the threshold quantity $\mathcal{R}_v^c < 1$, indicating disease eradication. This finding aligns with the conclusion in Theorem (6.3.5).

However, for larger values of $\alpha$, the system exhibits the existence of an endemic equilibrium ($\mathcal{R}_v^c > 1$), meaning that SGP persists in the population.

Similarly, Figure (6.4B) demonstrates the effects of increasing the vaccination rate $\omega$ on the PPR sub-model, using the initial conditions

$$(S_0, V_{p0}, I_{p0}, R_{p0}) = (1987709, 965059, 7460, 1920).$$

The simulation results indicate that for vaccination rates above 5% ($\omega \geq 0.05$), continuous vaccination efforts are effective in controlling the spread of PPR in small ruminant populations.

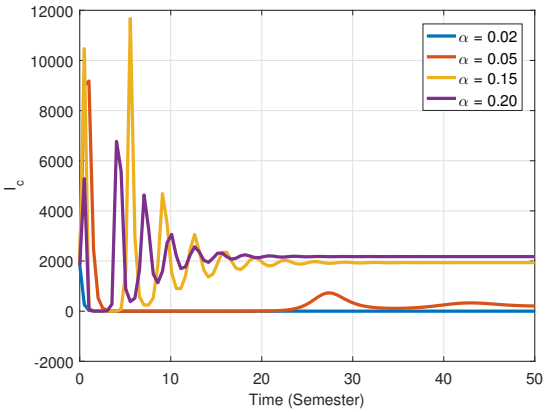


(A) Effects of $\alpha$ on $I_c$ in the SGP sub model (6.7)

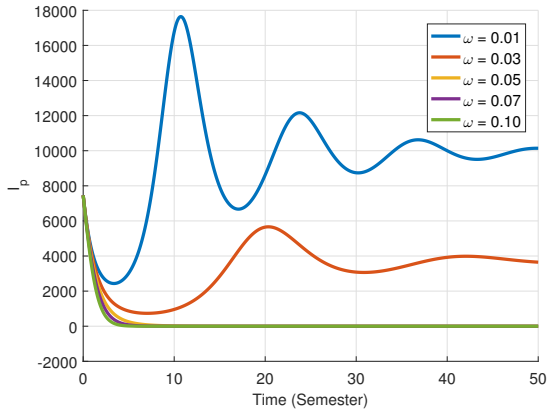


(B) Effects of $\omega$ on $I_p$ in the PPR sub model (6.2)

FIGURE 6.4: Effects of Parameters on sub models

The contour plots in Figure (6.6) illustrate the effects of parameters in model (6.1) on $\mathcal{R}_v^{pc}$. Figures 6.9A and 6.5B show that as the infection rates $\beta_p$ and $\beta_c$ increase, the value of $\mathcal{R}_v^{pc}$ also increases. Conversely, an increase in the vaccination rate $\omega$ leads to a decrease in $\mathcal{R}_v^{pc}$.

In Figure 6.5C, it is evident that the parameters $\theta$ and $\xi$ primarily influence the dynamics of SGP ($I_c$) and the co-infected population ($I_{pc}$). However, these two parameters exhibit opposing effects on $\mathcal{R}_v^{pc}$. Specifically, an increase in $\xi$ results in a rise in $\mathcal{R}_v^{pc}$, whereas an increase in $\theta$ (or a reduction in the concentration of SGPV in the flock) leads to a decrease in $\mathcal{R}_v^{pc}$.

As shown in Figure 6.5D, as expected, an increase in the vaccination rates for both newborns ($\rho$) and susceptibles ($\omega$) leads to a decrease in the control reproduction number $\mathcal{R}_v^{pc}$.

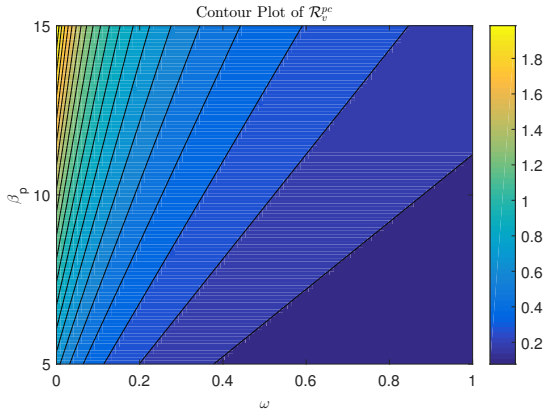


(A) Effects of $\beta_p$ and $\omega$ on $\mathcal{R}_v^{pc}$

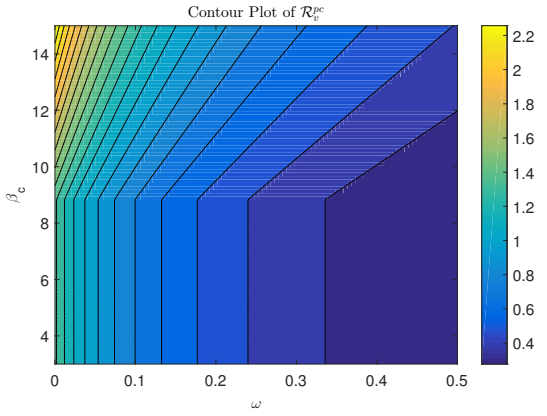


(B) Effects of $\beta_c$ and $\omega$ on $\mathcal{R}_v^{pc}$

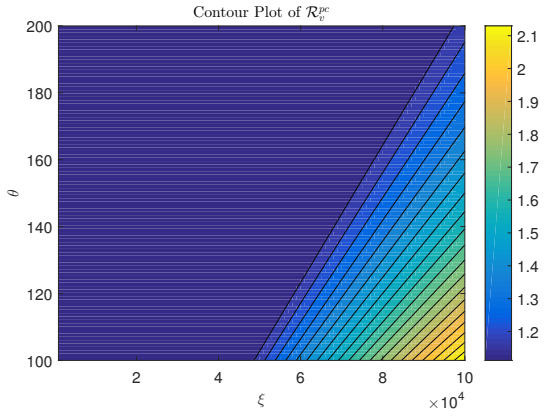


(C) Effects of *theta* and $\xi$ on $\mathcal{R}_v^{pc}$

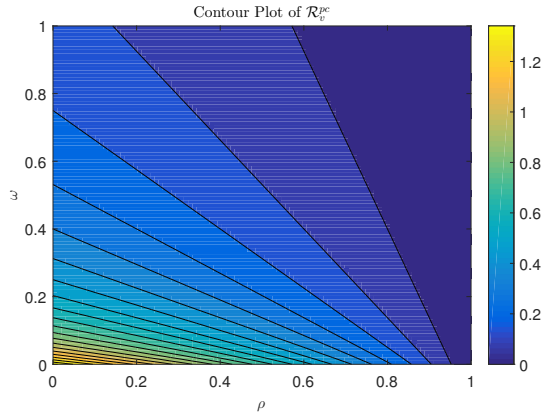


(D) Effects of $\omega_p$ and $\rho$ on $\mathcal{R}_v^{pc}$

FIGURE 6.5: Effects of Parameters on $\mathcal{R}_v^{pc}$

### 6.6.3 Effects of $\omega$ in the dynamics of model

In Figures 6.6A, 6.6B, and 6.6C, we illustrate the effects of the vaccination rate ($\omega$) on the infection classes ($I_p$, $I_c$, and $I_{pc}$) in model (6.1). These figures demonstrate that as the vaccination rate increases, the prevalence of PPR, SGP, and co-infection cases decreases. Specifically, when $\omega = 0.10$ and other parameters are as provided in Table (6.2), with the initial conditions

$$(S_0, V_0, I_{p0}, I_{c0}, I_{pc0}, R_0, B_0) = (3290595, 0, 7460, 1845, 100, 0, 100),$$

all trajectories of $I_p$, $I_c$, and $I_{pc}$ converge to zero.

In other words, for this particular case, the basic reproduction number is calculated as

$$\mathcal{R}_v^{pc} = \max\{\mathcal{R}_v^p, \mathcal{R}_v^c\} = 0.8239 < 1.$$

Consequently, as stated in Theorem (6.3.8), the disease-free equilibrium (DFE) is stable, and the disease can be eradicated with continuous implementation of an effective vaccination strategy at this rate for over ten years.

Furthermore, increasing the vaccination coverage rate and implementing additional preventive measures could significantly reduce the time required to control these diseases.

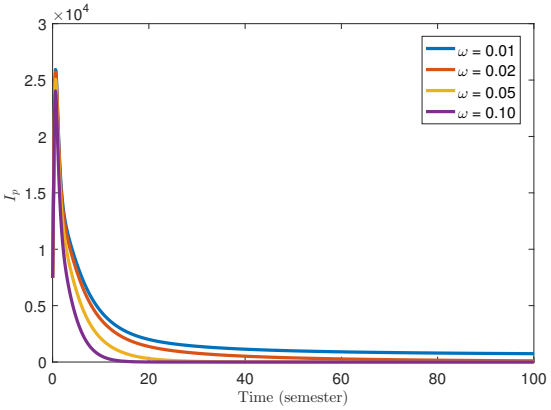


(A) Effects of $\omega$ on $I_p$

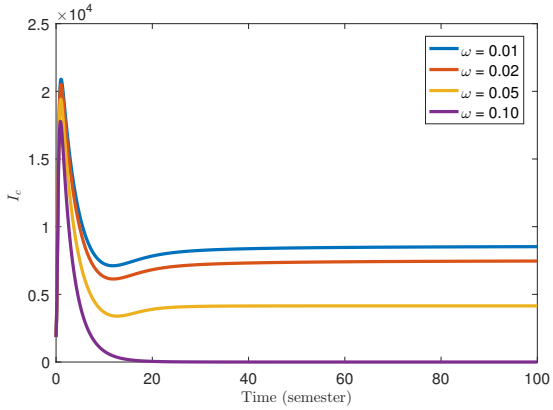


(B) Effects of $\omega$ on $I_c$

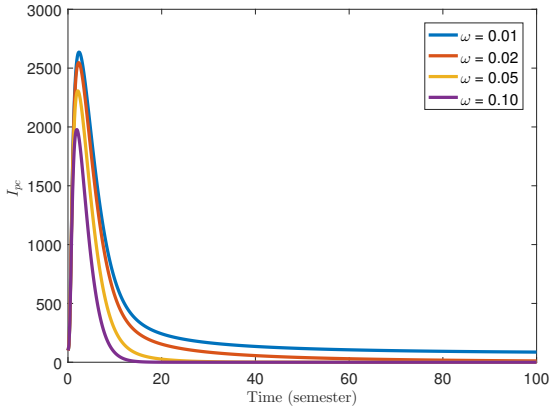


(C) Effects of $\omega$ on $I_{pc}$

FIGURE 6.6: Effects of Parameters on $\mathcal{R}_v^{pc}$

### 6.6.4 Numerical Simulation for optimal control

In this section, we numerically illustrate the solution of the optimal control problem proposed in model (6.15), using the parameter values provided in Table 6.2 and the following initial conditions:

$$(S_0, V_0, I_{p0}, I_{c0}, I_{pc0}, R_0, B_0) = (2000000, 0, 7460, 1845, 300, 0, 100).$$

To solve this problem, we employ the forward-backward sweep method as described in (Lenhart et al., 2007).

The cost coefficients associated with the control variables have been estimated as follows: $C_1 = 1.5$, $C_2 = 3.0$, $C_3 = 1.0$, and $C_4 = 1.0$. These estimated coefficients are based on expert opinion and practical considerations. Furthermore, the weights reflecting the relative efforts required to mitigate the classes contributing to the spread of diseases are established as $w_1 = 16$, $w_2 = 5$, and $w_3 = 20$. Furthermore, modeling and empirical evidence support the superior effectiveness and cost-efficiency of combined strategies (see, e.g., Anderson et al. (1991) and Hethcote (2000)). Therefore, we conduct numerical simulations of combined controls under the following three scenarios.

**Scenario $\mathcal{A}$**

In this scenario, we examined the application of two control measures in six potential combinations, referred to as strategies:

❶ **Strategy 1** ($S_1$): uses the combination of $u_1$ and $u_2$.

❷ **Strategy 2** ($S_2$): uses the combination of $u_1$ and $u_3$.

❸ **Strategy 3** ($S_3$): uses the combination of $u_1$ and $u_4$.

❹ **Strategy 4** ($S_4$): uses the combination of $u_2$ and $u_3$.

❺ **Strategy 5** ($S_5$): uses the combination of $u_2$ and $u_4$.

❻ **Strategy 6** ($S_6$): uses the combination of $u_3$ and $u_4$.

The numerical simulations presented in Figures (6.7A), (6.7B), and (6.7C) illustrate the infection dynamics for three compartments: $I_p$ (PPR infections), $I_c$ (SGP infections), and $I_{pc}$ (coinfections). The simulations compare the effectiveness of six strategies ($S_1$ to $S_6$) and the "without control" scenario. Additionally, Figures (6.7D) through (6.7I) depict the corresponding control profiles for each strategy.

Across all infection compartments ($I_p$, $I_c$, and $I_{pc}$), Strategy $S_1$ demonstrates the most significant reduction in infection levels. It achieves the fastest decay and lowest peak values, highlighting its superior effectiveness in mitigating infections. Strategy $S_2$ also performs well, achieving substantial reductions in infection levels but slightly less effectively than $S_1$. Strategy $S_4$ exhibits moderate performance, achieving reductions in infection levels but trailing behind $S_1$ and $S_2$. In contrast, Strategy $S_6$ consistently shows the least effectiveness, exhibiting the highest infection peaks among the six strategies across all compartments. Although $S_6$ achieves some reductions compared to the "without control" scenario, its limited effectiveness makes it the weakest strategy in this scenario.

The control profiles shown in Figures (6.7D) through (6.7I) provide insights into the timing and intensity of control measures for each strategy. Strategies $S_2$, $S_3$, $S_4$, and $S_5$, depicted in Figures (6.7E), (6.7F), (6.7G), and (6.7H), respectively, exhibit similar patterns. The control measures in these strategies are implemented at optimal levels up to approximately 8 semesters, after which they gradually decline. In these strategies, either $u_1$ or $u_2$ is utilized intensively throughout the simulation period, alternating as the dominant control variable.

Strategy $S_1$, shown in Figure (6.7D), employs $u_1$ at an optimal level throughout the entire simulation period, with gradual reduction near the end. This early and sustained intervention explains its consistent effectiveness across all infection compartments.

In contrast, Strategy $S_6$, depicted in Figure (6.7I), applies less intensive control measures. The control variable $u_3$ is used throughout the simulation period, while $u_4$ remains inactive until the final two semesters, when it is applied at an optimal level. The limited role of $u_4$ in this strategy reduces its overall effectiveness. Notably, $u_4$ plays a critical role in reducing pathogen concentration, thereby indirectly controlling the spread of SGP disease. The minimal application

of $u_4$ in $S_6$ contributes to its lower performance in mitigating infections compared to the other strategies.

These results highlight the importance of selecting and effectively utilizing control measures to achieve optimal outcomes in reducing infection levels.

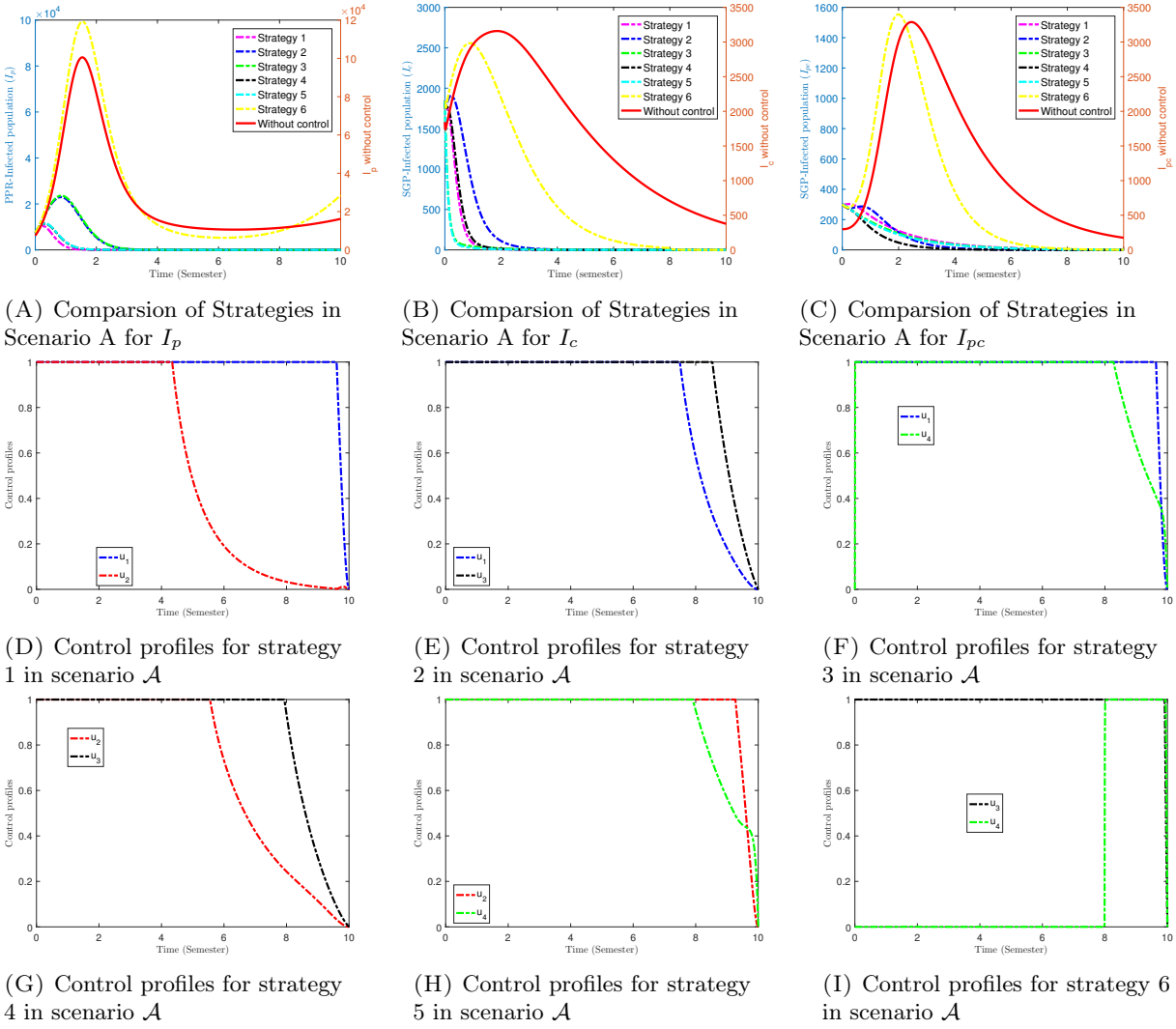


(A) Comparsion of Strategies in Scenario A for $I_p$

(B) Comparsion of Strategies in Scenario A for $I_c$

(C) Comparsion of Strategies in Scenario A for $I_{pc}$

(D) Control profiles for strategy 1 in scenario $\mathcal{A}$

(E) Control profiles for strategy 2 in scenario $\mathcal{A}$

(F) Control profiles for strategy 3 in scenario $\mathcal{A}$

(G) Control profiles for strategy 4 in scenario $\mathcal{A}$

(H) Control profiles for strategy 5 in scenario $\mathcal{A}$

(I) Control profiles for strategy 6 in scenario $\mathcal{A}$

FIGURE 6.7: Numerical Simulation results of scenario $\mathcal{A}$, comparing strategies with and without control measures and control profiles.

### Scenario $\mathcal{B}$

In this scenario, we examined the application of three control measures in four different combinations, defined as strategies:

- **Strategy A** ($S_A$): a combination of $u_1$, $u_2$, and $u_3$.
- **Strategy B** ($S_B$): a combination of $u_1$, $u_2$, and $u_4$.
- **Strategy C** ($S_C$): a combination of $u_1$, $u_3$, and $u_4$.
- **Strategy D** ($S_D$): a combination of $u_2$, $u_3$, and $u_4$.

The impacts of these strategies are depicted in Figures (6.8A), (6.8B), and (6.8C). The implementation of these intervention strategies results in a significant reduction in the number of infected individuals in the classes $I_p$, $I_c$, and $I_{pc}$, compared to the scenario without control measures.

Subplot (6.8A) shows the progression of the PPR-infected population $I_p$. Strategies A and D achieve the steepest decline, closely followed by Strategy C, while Strategy B exhibits a higher peak in $I_p$ before declining. Subplot (6.8B) examines the SGP-infected population $I_c$, where Strategies C and D consistently reduce the infection most effectively, followed by Strategy B and then Strategy A. Similarly, subplot (6.8C) analyzes the coinfected population $I_{pc}$. Here, Strategy C minimizes the coinfection most effectively, while Strategies A and B also perform well. Strategy D demonstrates relatively lower effectiveness, taking a longer time to bring the infection to zero.

The control profiles for each strategy are illustrated in subplots (6.8D)–(6.8G): For Strategy A (subplot 6.8D), the control variables $u_1$, $u_2$, and $u_3$ peak initially and then decay over time. Specifically, $u_1$ is implemented at its optimal level for the first 3.5 semesters, $u_2$ for the first 6 semesters, and $u_3$ for the first 8 semesters, after which they gradually decline toward the end of the simulation. This reflects a high initial effort to curb infections. - For Strategy B (subplot 6.8E), the controls $u_2$ and $u_4$ are applied aggressively during the first 5 semesters, followed by a gradual decline. Meanwhile, $u_1$ is maintained at a high level throughout almost the entire simulation period. For Strategy C (subplot 6.8F), the control $u_4$ starts with minimal effort during the first fraction of a semester, then immediately rises to its optimal level between 0.5 and 5 semesters, after which it gradually declines. Both $u_1$ and $u_3$ are applied at their maximum levels from the beginning until the 8th semester, after which they slowly taper off. Finally, for Strategy D (subplot 6.8G), the control patterns are similar to those of Strategy A, with the roles of $u_1$ and $u_2$ interchanged. The controls are initially implemented aggressively and then gradually reduced as the infection levels decrease.

These results demonstrate the importance of appropriately timed and optimized control measures in mitigating disease spread and coinfection, with each strategy offering distinct dynamics based on the combination of controls utilized.

**Scenario $\mathcal{C}$**

Figure 6.9 illustrates the numerical simulation results of scenario $\mathcal{C}$, focusing on the dynamics of PPR infection ($I_p$), SGP disease ($I_c$), and their coinfection ($I_{pc}$), with and without the application of four control measures. Subplot (6.9A) displays the progression of $I_p$. Without control (red curve), the infected population peaks sharply before gradually declining, reaching substantial levels throughout the time horizon. In contrast, the application of controls (blue curve) significantly suppresses the peak of $I_p$ and accelerates its decline. Subplot (6.9B) examines the dynamics of $I_c$, where the uncontrolled scenario (red curve) leads to a prominent peak in the SGP-infected population. With the introduction of controls (blue curve), the peak is notably reduced, and the infection levels diminish more rapidly over time. Subplot (6.9C) presents the dynamics of coinfection ($I_{pc}$), highlighting the compounding effects of PPR and SGP. Without

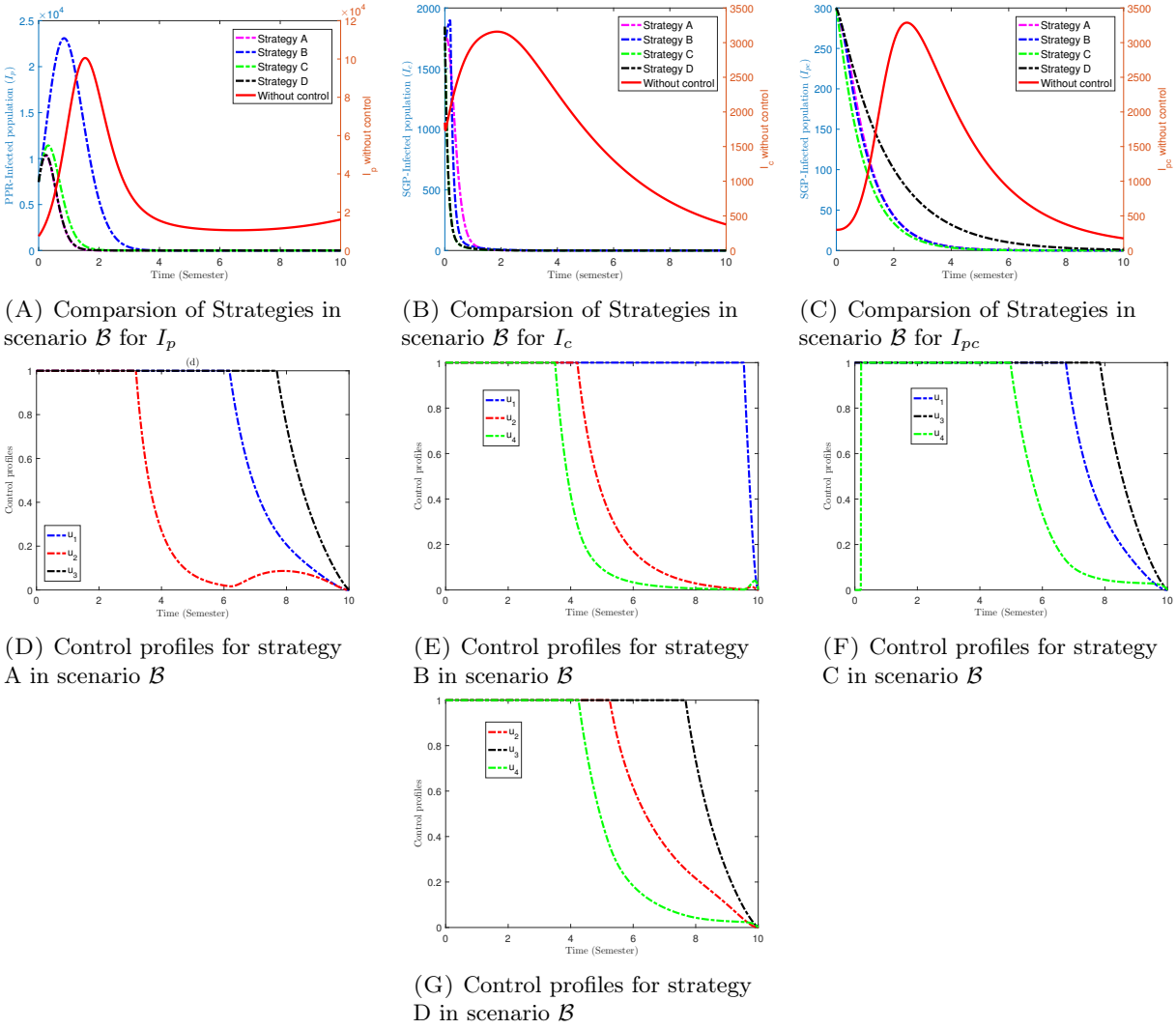


(A) Comparsion of Strategies in scenario $\mathcal{B}$ for $I_p$

(B) Comparsion of Strategies in scenario $\mathcal{B}$ for $I_c$

(C) Comparsion of Strategies in scenario $\mathcal{B}$ for $I_{pc}$

(D) Control profiles for strategy A in scenario $\mathcal{B}$

(E) Control profiles for strategy B in scenario $\mathcal{B}$

(F) Control profiles for strategy C in scenario $\mathcal{B}$

(G) Control profiles for strategy D in scenario $\mathcal{B}$

FIGURE 6.8: Numerical Simulation results of scenario $\mathcal{B}$, comparing strategies with and without control measures and control profiles.

control (red curve), $I_{pc}$ reaches a significant peak, whereas the implementation of controls (blue curve) effectively mitigates the peak and accelerates the reduction of coinfection prevalence.

Subplot (6.9D) provides insights into the control profiles for scenario $\mathcal{C}$, illustrating the temporal behavior of the four control variables ($u_1$, $u_2$, $u_3$, and $u_4$). All control variables exhibit an initial surge, reflecting an aggressive intervention at the onset of the epidemic. Over time, the controls gradually decline, indicating a reduced need for intervention as the infection levels diminish. Among the controls, $u_1$ and $u_3$ display higher initial values, emphasizing their critical role in managing PPR infection and coinfection. The results demonstrate the effectiveness of optimal control measures in reducing the prevalence of both single and coinfections, highlighting the importance of early and aggressive intervention to minimize disease impact.

In summarizing the results of all numerical simulations, it is evident that all strategies significantly contribute to disease control. Specifically, the strategies that incorporate controls $u_1$, $u_2$, or both have a predominantly positive impact on controlling PPR and SGP diseases in small ruminant populations. This finding aligns with other studies, which suggest that combined

vaccination is preferable for effectively controlling both PPR and SGP at optimal costs.

Furthermore, the effectiveness of each strategy is analyzed using a cost-effectiveness method, as detailed in the next subsection. The total investment costs for each strategy and the averted infections due to the implementation of these strategies are presented in Table 6.4.

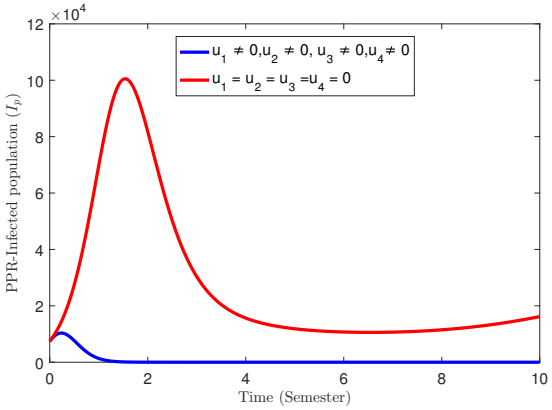


(A) Comparative plot of $I_p$ with and without control in Scenario $\mathcal{C}$

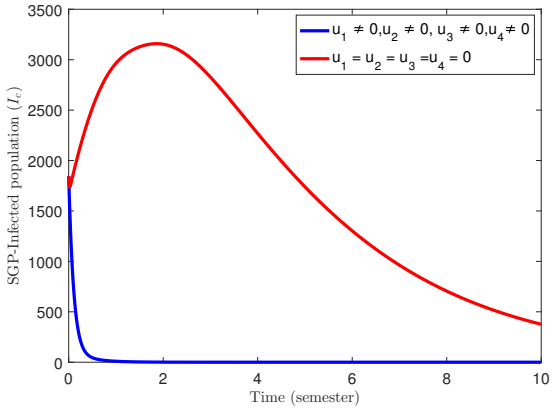


(B) Comparative plot of $I_c$ with and without control in Scenario $\mathcal{C}$

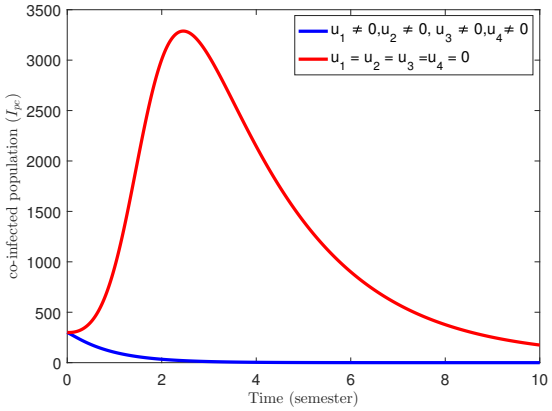


(C) Comparative plot of $I_{pc}$ with and without control in Scenario $\mathcal{C}$

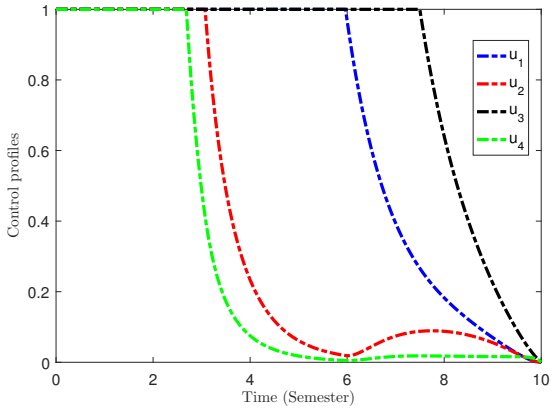


(D) Control profiles in Scenario $\mathcal{C}$

FIGURE 6.9: Numerical Simulation results of scenario $\mathcal{C}$, comparing strategies with and without control measures and control profiles.

### 6.6.5 Cost-Effectiveness Analysis

In this section, we evaluate the cost-effectiveness of various control strategies across different scenarios using the Incremental Cost-Effectiveness Ratio (ICER).

The Incremental Cost-Effectiveness Ratio (ICER) quantifies the change in costs relative to the change in health benefits (e.g., cases averted) between two competing intervention strategies. Considering strategies $S_1$ and $S_2$ as two competing control interventions, the ICER is calculated as follows:

$$\text{ICER} = \frac{\text{Change in total costs between strategies } S_1 \text{ and } S_2}{\text{Change in health benefits between strategies } S_1 \text{ and } S_2}.$$

A lower ICER indicates a more cost-effective strategy.

The total number of averted infections is computed using the following equation:

TABLE 6.4: Total cost and averted infection of each strategies

| Optimal control Scenarios | Strategies (**S**) | Total averted infection | Total cost | cost-effective strategy |
|---|---|---|---|---|
| Scenario $\mathcal{A}$ | $\mathbf{S}_1$ $(u_1, u_2)$ | 291637.43 | 131289.14 | $\mathbf{S}_1$ |
| | $\mathbf{S}_2$ $(u_1, u_3)$ | 263944.53 | 565788.17 | |
| | $\mathbf{S}_3$ $(u_1, u_4)$ | 264413 | 576269.34 | |
| | $\mathbf{S}_4$ $(u_2, u_3)$ | 289349.67 | 165559.73 | |
| | $\mathbf{S}_5$ $(u_2, u_4)$ | 289644.52 | 169389.25 | |
| | $\mathbf{S}_6$ $(u_3, u_4)$ | 43769.44 | 4070886 | |
| Scenario $\mathcal{B}$ | $\mathbf{S}_A$ $(u_1, u_2, u_3)$ | 292118.88 | 122745.43 | $\mathbf{S}_A$ |
| | $\mathbf{S}_B$ $(u_1, u_2, u_4)$ | 292355.34 | 125868.24 | |
| | $\mathbf{S}_C$ $(u_1, u_3, u_4)$ | 265363.04 | 556573.90 | |
| | $\mathbf{S}_D$ $(u_2, u_3, u_4)$ | 290166.25 | 160185.99 | |
| Scenario $\mathcal{C}$ | **S** $(u_1, u_2, u_3, u_4)$ | 292733.12 | 118872.05 | **S** |

$$\text{Total Averted} = \int_0^{T_f} [I_p^{\text{wout}} - I_p^{\text{w}}]\, dt + \int_0^{T_f} [I_c^{\text{wout}} - I_c^{\text{w}}]\, dt + \int_0^{T_f} [I_{pc}^{\text{wout}} - I_{pc}^{\text{w}}]\, dt,$$

where $I^{\text{wout}}$ represents infections without control, and $I^{\text{w}}$ represents infections with control. The total cost is calculated based on the objective functional defined in Equation (6.14).

Using the total number of averted cases and the associated costs provided in Table (6.4), we first calculate the ICER for each scenario independently. Subsequently, we compare the cost-effectiveness of the strategies across the three scenarios.

❍ **Cost-Effectiveness Analysis for Scenario $\mathcal{A}$**

Based on the increasing order of cases averted (as shown in Table (6.4)), we compute the ICER for each strategy as follows:

1. **Comparison between Strategies $S_6$ and $S_2$:**

$$\text{ICER}(S_6) = \frac{4,070,886}{43,769} = 930,084,$$

$$\text{ICER}(S_2) = \frac{565,788 - 4,070,886}{263,944 - 43,769} = -15.92.$$

The results indicate that Strategy $S_6$ is strongly dominated, as it incurs higher costs compared to Strategy $S_2$. Therefore, Strategy $S_6$ is excluded from further consideration. The next comparison is conducted between Strategies $S_2$ and $S_3$.

2. **Comparison between Strategies $S_2$ and $S_3$:**

$$\text{ICER}(S_2) = \frac{565,788}{263,944} = 2.14,$$

$$\text{ICER}(S_3) = \frac{576,269 - 565,788}{264,413 - 263,944} = 22.35.$$

Here, Strategy $S_3$ is dominated by Strategy $S_2$, as it has a higher ICER. Thus, Strategy $S_3$ is excluded, and the next comparison is conducted between Strategies $S_2$ and $S_4$.

3. **Comparison between Strategies $S_2$ and $S_4$:**

$$\text{ICER}(S_4) = \frac{165,559 - 565,788}{289,349 - 263,944} = -15.75.$$

Since $\text{ICER}(S_4) < \text{ICER}(S_2)$, Strategy $S_4$ is more cost-effective, and Strategy $S_2$ is excluded. The next comparison is conducted between Strategies $S_4$ and $S_5$.

4. **Comparison between Strategies $S_4$ and $S_5$:**

$$\text{ICER}(S_4) = \frac{165,559}{289,349} = 0.57,$$

$$\text{ICER}(S_5) = \frac{169,389 - 165,559}{289,644 - 289,349} = 12.98.$$

Since $\text{ICER}(S_4) < \text{ICER}(S_5)$, Strategy $S_5$ is excluded. The final comparison is conducted between Strategies $S_4$ and $S_1$.

5. **Comparison between Strategies $S_4$ and $S_1$:**

$$\text{ICER}(S_1) = \frac{131,289 - 165,559}{291,637 - 289,349} = -14.98.$$

The analysis shows that Strategy $S_1$ is the most cost-effective strategy in Scenario $\mathcal{A}$ for reducing PPR disease at the minimum cost.

❍ **Cost-Effectiveness Analysis for Scenario $\mathcal{B}$**

1. **Comparison between Strategies $S_C$ and $S_D$:**

$$\text{ICER}(S_C) = \frac{556,573}{265,363} = 2.10,$$

$$\text{ICER}(S_D) = \frac{160,185 - 556,573}{290,166 - 265,363} = -15.98.$$

Strategy $S_D$ is more cost-effective than Strategy $S_C$, so Strategy $S_C$ is excluded. The next comparison is between Strategies $S_D$ and $S_A$.

2. **Comparison between Strategies $S_D$ and $S_A$:**

$$\text{ICER}(S_D) = \frac{160,185}{290,166} = 0.55,$$

$$\text{ICER}(S_A) = \frac{122,745 - 160,185}{292,118 - 290,166} = -19.18.$$

Strategy $S_A$ is more cost-effective than Strategy $S_D$, so Strategy $S_D$ is excluded. The final comparison is between Strategies $S_A$ and $S_B$.

3. **Comparison between Strategies $S_A$ and $S_B$:**

$$\text{ICER}(S_A) = \frac{122,745}{292,118} = 0.42,$$

$$\text{ICER}(S_B) = \frac{125,868 - 122,745}{292,355 - 292,118} = 13.18.$$

Since $\text{ICER}(S_A) < \text{ICER}(S_B)$, Strategy $S_A$ is the most cost-effective strategy in Scenario $\mathcal{B}$.

- **Cost-Effectiveness Analysis for Scenario $\mathcal{C}$**

  In Scenario $\mathcal{C}$, there is only one strategy with four controls $(u_1, u_2, u_3, u_4)$. The ICER is computed as follows:

$$\text{ICER}(\mathbf{S}) = \frac{118,872}{292,733} = 0.41.$$

- **Final Comparison Across Scenarios**

  Comparing the most cost-effective strategies from each scenario, the strategy in Scenario $\mathcal{C}$ emerges as the most effective, followed by Strategy $S_A$ from Scenario $\mathcal{B}$, and Strategy $S_1$ from Scenario $\mathcal{A}$.

## 6.7 Results and Discussion

Peste des petits ruminants (PPR) and sheep and goat pox (SGP) are devastating and economically significant non-zoonotic viral diseases affecting small ruminants, particularly in Africa and Asia, where they pose substantial challenges for control efforts. Their overlapping geographical distributions, high seroprevalence, and co-occurrence in endemic regions create complex disease dynamics that exacerbate mortality rates and economic losses. In this study, we developed and analyzed a deterministic mathematical model to investigate the co-infection dynamics of PPR and SGP—an approach that appears to be the first in the literature. The model was structured into two sub-models (PPR and SGP) that were subsequently integrated into a full co-infection framework, with the well-posedness of the model established in both mathematical and epidemiological contexts. Analysis reveals that the control reproduction number of the co-infection model equals the maximum of the reproduction numbers of the two sub-models, and both the sub-models and the full co-infection model possess locally asymptotically stable disease-free equilibria when their respective control reproduction numbers are less than one, while stable endemic equilibria emerge when these exceed one—confirming the endemicity of both diseases in Ethiopia based on parameter estimations derived from WOAH-reported data. Sensitivity analysis identifies vaccination rates ($\omega$) as critical parameters influencing co-infection dynamics, highlighting the importance of vaccine coverage in controlling both diseases simultaneously and motivating the development of an optimal control problem incorporating four control variables: vaccination of newborns ($u_1$), vaccination of susceptibles ($u_2$), treatment of co-infected individuals ($u_3$), and disinfection to reduce SGPV concentration in the herd ($u_4$). Numerical simulations examining

various control combinations reveal that applying all four controls simultaneously is the most effective strategy for mitigating the spread of PPR and SGP. However, cost-effectiveness analysis suggests that strategies involving both vaccination controls ($u_1$ and $u_2$) individually or in combination are preferable for controlling and potentially eradicating these diseases in the region given resource constraints. While this study provides valuable insights into the transmission dynamics of PPR and SGP co-infection, it also opens avenues for future research. The deterministic SVIR co-infection model could be extended to incorporate stochastic effects and seasonal variations for more comprehensive analyses, and advanced parameter estimation methods using extended datasets could further enhance model validation. Future studies can also explore the impact of risk factors, incorporate exposed classes, or stratify populations by age to provide more targeted strategies for disease control. In conclusion, this study represents the first systematic investigation of PPR and SGP co-infection dynamics using mathematical modeling, demonstrating that vaccination plays a central role in controlling both diseases simultaneously while optimal control requires integrated strategies that account for the distinct transmission characteristics of each pathogen.

# Chapter 7

# Conclusion and Future Work

## 7.1 Introduction

This dissertation set out to advance understanding of Peste des petits ruminants (PPR) transmission dynamics in Ethiopia and to develop quantitative frameworks for designing effective control strategies. Through four interconnected studies, we progressively expanded the analytical lens from local transmission dynamics to spatially structured metapopulations and, finally, to co-inf dynamics with Sheep and Goat Pox (SGP). Each article addressed a specific objective while collectively contributing to a comprehensive understanding of disease persistence and control in complex production systems.

This final chapter synthesizes the cumulative findings from all four studies, integrates them into a coherent framework, and articulates the theoretical, empirical, and practical contributions of this dissertation. Rather than merely summarizing each article, I weave together the key insights to demonstrate how the whole constitutes more than the sum of its parts. I also reflect on methodological limitations, propose directions for future research, and conclude with the overarching implications for PPR control and eradication efforts.

## 7.2 Summary of Key Findings

The four articles comprising this dissertation address progressively more complex aspects of PPR transmission and control.

Chapter 3 (**Article 1**) established the foundational dynamics by developing a deterministic SEVIR model incorporating restocking as a source of external infection. The key finding was that restocking fundamentally alters disease persistence: even with optimal vaccination coverage (exceeding 89.6%), the continuous influx of infected animals maintains endemic transmission. This article demonstrated that vaccination alone cannot achieve eradication when animal movement introduces external infection, providing the initial motivation for considering connectivity in control strategies.

Chapter 4 (**Article 2**) extended this framework by formulating an optimal control problem that evaluated combinations of vaccination, treatment, and biosecurity measures. The cost-effectiveness analysis revealed that combined strategies are superior to single interventions, with the most comprehensive approach (external biosecurity + internal biosecurity + vaccination + treatment) producing the largest reduction in infections per unit cost. This article provided quantitative guidance for resource allocation in control programs.

Chapter 5 (**Article 3**) expanded the spatial scope by developing a metapopulation model capturing transmission across two distinct agroecological zones highland sedentary and lowland pastoral systems. The analysis revealed that lowland areas serve as viral reservoirs, and movement from these zones to highland areas necessitates higher vaccination coverage in source populations. This article highlighted the importance of coordinated control across connected systems.

Chapter 6 (**Article 4**) further broadened the scope by developing a co-infection model for PPR and SGP the first such framework in the literature. Analysis revealed that the control reproduction number for co-infection equals the maximum of the individual disease reproduction numbers, and vaccination remains critical for controlling both diseases simultaneously. Cost-effectiveness analysis identified vaccination-focused strategies as preferable for resource-constrained settings.

## 7.3 Synthesis and Integration

While each article contributes independently to understanding PPR dynamics, their integration yields insights that transcend individual findings. I propose a unified framework that synthesizes the cumulative evidence and identifies four interconnected principles governing PPR transmission and control in Ethiopia.

### 7.3.1 The Connectivity Principle

Across all four articles, connectivity emerges as a fundamental determinant of disease persistence. Article 1 demonstrated that restocking introduces external infection that undermines local control. Article 3 revealed that movement between agroecological zones creates transmission pathways that maintain national circulation. Article 2 showed that biosecurity measures addressing connectivity are cost-effective components of control strategies. Article 4, while focused on co-infection, implied that the connectivity between pathogens within hosts and between production systems creates complex dynamics requiring integrated approaches.

This principle suggests that PPR cannot be effectively controlled at the local level alone. Control programs must account for connectivity at multiple scales: between herds through restocking, between regions through animal movement, and between pathogens through co-infection.

### 7.3.2 The Vaccination-Limitation Principle

A consistent finding across all studies is that while vaccination is essential, it is insufficient when acting alone. Article 1 established that vaccination coverage exceeding 89.6% is theoretically required for eradication without restocking a threshold rarely achievable in practice. Article 2 demonstrated that even optimal vaccination fails in the presence of restocking unless complemented by biosecurity. Article 3 showed that vaccination effectiveness depends on movement patterns, requiring higher coverage in source populations. Article 4 revealed that vaccination remains critical for co-infection control but must be combined with other measures for optimal cost-effectiveness.

This principle reframes the role of vaccination from a standalone solution to a necessary but insufficient component of integrated control strategies.

### 7.3.3 The Spatial-Heterogeneity Principle

Article 3 most directly addressed spatial heterogeneity, revealing that transmission rates differ substantially between agroecological zones and that movement patterns create asymmetries in control requirements. However, this principle also manifests in other articles: Article 1's focus on restocking implicitly addresses spatial heterogeneity between regions, and Article 4's co-infection framework addresses pathogen heterogeneity. Collectively, these findings indicate that uniform control strategies applied without regard to spatial and pathogen heterogeneity are likely to be suboptimal.

### 7.3.4 The Cost-Effectiveness Principle

Articles 2 and 4 explicitly addressed cost-effectiveness, revealing that combined strategies are generally superior to single interventions but that resource constraints necessitate careful prioritization. The finding that vaccination-focused strategies are often most cost-effective (Article 4) might appear to contradict the vaccination-limitation principle, but this apparent tension resolves when considering context: vaccination is cost-effective when implemented as part of integrated strategies that include biosecurity and movement controls, but not when implemented alone.

### 7.3.5 An Integrated Framework for PPR Control

Based on these four principles, I propose an integrated framework for PPR control in Ethiopia (Figure 7.1). The framework conceptualizes control as operating across three dimensions: *scale* (local to national), *intervention type* (vaccination, biosecurity, movement control, treatment), and *target population* (highland sedentary, lowland pastoral, and interface zones). Effective control requires coordinated action across all dimensions, with resource allocation guided by cost-effectiveness analysis tailored to specific contexts.

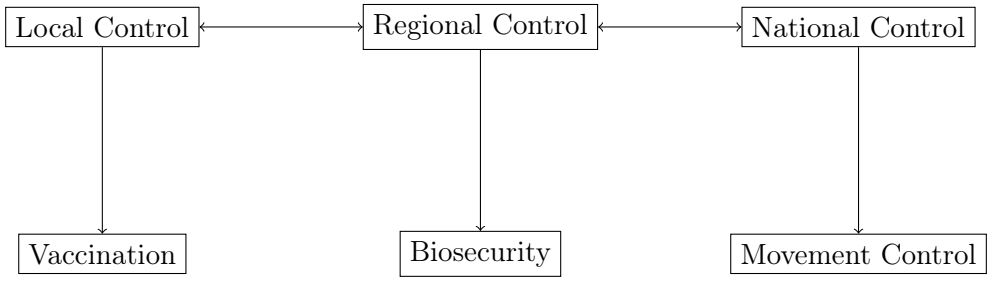


FIGURE 7.1: Integrated framework for PPR control showing the three dimensions of intervention: scale (local, regional, national) and intervention type (vaccination, biosecurity, movement control). Effective control requires coordinated action across all dimensions.

## 7.4 Contribution to Knowledge

This dissertation makes several distinct contributions to knowledge in veterinary epidemiology and disease modeling.

### 7.4.1 Theoretical Contributions

First, this work advances theoretical understanding of PPR transmission by explicitly incorporating restocking and movement dynamics into compartmental models. While previous models often treated populations as closed systems, our framework demonstrates that connectivity fundamentally alters disease persistence conditions. The finding that the control reproduction number in a metapopulation depends on both local transmission and movement rates extends theoretical understanding of disease persistence in connected systems.

Second, the co-infection model developed in Article 4 represents the first theoretical framework for understanding simultaneous PPR and SGP transmission. The result that the overall reproduction number equals the maximum of the individual disease reproduction numbers provides a theoretically grounded basis for prioritizing control efforts based on the more transmissible pathogen.

Third, the integration of optimal control with cost-effectiveness analysis provides a theoretical bridge between epidemiological modeling and policy decision-making. By explicitly linking intervention effectiveness with resource constraints, this framework enables theoretically grounded prioritization of control strategies.

### 7.4.2 Empirical Contributions

Empirically, this dissertation provides the first quantitative estimates of key transmission parameters for PPR in Ethiopia using a combination of literature data, OIE reports, and national prevalence data. The estimated basic reproduction number ($\mathcal{R}_v \approx 1.02 - 1.05$) provides a benchmark for assessing control requirements and aligns with observed endemicity patterns.

The parameter estimates for transmission rates across agroecological zones represent the first such quantification for Ethiopia. The finding that lowland areas exhibit higher transmission rates than highland areas provides empirical support for targeted control strategies.

The cost-effectiveness rankings of intervention combinations provide empirically grounded guidance for resource allocation that was previously unavailable to policymakers.

### 7.4.3 Methodological Contributions

Methodologically, this dissertation demonstrates the value of progressive model complexity—beginning with simple compartmental models and progressively adding restocking, spatial structure, and co-infection dynamics. This approach enables systematic investigation of how additional complexity changes model predictions and control implications.

The integration of optimal control with cost-effectiveness analysis provides a template for future modeling studies that aim to inform policy decisions. The framework developed here can be adapted to other livestock diseases and production systems.

## 7.5 Implications for Policy and Practice

The findings of this dissertation have several implications for PPR control programs in Ethiopia and similar settings.

### 7.5.1 Vaccination Programs

While vaccination remains the cornerstone of PPR control, our findings suggest that vaccination programs must be designed with attention to connectivity. In areas with high restocking rates or proximity to lowland pastoral systems, vaccination coverage targets should be set higher than the theoretical threshold derived from closed-population models. Furthermore, vaccination campaigns should be coordinated across connected areas rather than implemented independently.

### 7.5.2 Biosecurity and Movement Control

Our results strongly support the inclusion of biosecurity measures in PPR control programs. Pre-restocking evaluations, testing of animals before movement, and enhanced biosecurity at markets and grazing areas represent cost-effective complements to vaccination. The cost-effectiveness analysis suggests that investments in biosecurity yield significant returns in terms of infections averted.

### 7.5.3 Spatially Targeted Strategies

The finding that lowland areas serve as viral reservoirs suggests that control resources should be disproportionately allocated to these high-transmission zones. Vaccinating animals in lowland areas before they move to highland areas may be more effective than focusing vaccination efforts solely in highland areas. This aligns with the principle of controlling disease at its source.

### 7.5.4 Co-Infection Considerations

The co-infection model highlights that PPR control programs must consider the presence of other diseases such as SGP. Vaccination against PPR may have spillover benefits for SGP control by reducing overall susceptibility and transmission, but integrated programs that address both diseases simultaneously are likely to be more effective and cost-efficient.

## 7.6 Limitations and Future Research Directions

### 7.6.1 Data Limitations

Across all four studies, data limitations constrain the precision and generalizability of our findings. Incidence data from OIE reports may suffer from underreporting and inconsistent case definitions. Movement data between agroecological zones are largely unavailable, necessitating assumed parameter values. Parameter estimates for transmission rates, vaccine efficacy, and disease progression derive from disparate studies with varying methodologies.

Future research should prioritize enhanced data collection on animal movements, vaccination coverage, outbreak timing, and socioeconomic factors affecting control implementation. Standardized case definitions and reporting systems would improve data quality and comparability across regions.

### 7.6.2 Model Limitations

Several model limitations suggest avenues for methodological refinement. The deterministic framework used throughout this dissertation does not capture stochastic fluctuations that may be significant in smaller populations or during outbreak fade-outs. Time delays in detection, reporting, and vaccination response are not explicitly modeled. Homogeneous mixing assumptions may oversimplify contact structures in real production systems.

Future research should extend these models to incorporate stochastic effects, time delays, and heterogeneous mixing patterns. Fractional-order formulations, as suggested by recent studies Saber et al., 2025; Althubyani et al., 2025; Adam et al., 2025, could capture memory and hereditary effects in disease transmission.

### 7.6.3 Scope Limitations

This dissertation focused on PPR dynamics within Ethiopia, with limited consideration of cross-border movements from neighboring countries where the disease is also endemic. The co-infection model, while novel, did not incorporate potential interactions between pathogens beyond simple co-circulation.

Future research should extend the spatial framework to include cross-border movements and examine the implications for regional eradication efforts. Mechanistic models of within-host interactions between PPR and SGP could inform more realistic co-infection models.

### 7.6.4 Future Research Agenda

Building on the findings and limitations of this dissertation, I propose a future research agenda organized around three themes:

**Theme 1: Enhanced Data and Parameter Estimation.** High-resolution data collection on animal movements, vaccination coverage, outbreak timing, and socioeconomic factors, combined with advanced parameter estimation techniques including machine learning and Bayesian methods, would improve model calibration and predictive accuracy.

**Theme 2: Methodological Extensions.** Incorporating stochasticity, time delays, and heterogeneous mixing would capture important aspects of real-world dynamics. Fractional-order formulations and network models could represent more complex transmission pathways.

**Theme 3: Policy-Oriented Applications.** Developing user-friendly decision-support tools based on the models developed here would enable policymakers to evaluate intervention strategies under local conditions. Participatory modeling approaches engaging stakeholders in model development and scenario analysis would enhance policy relevance and uptake.

## 7.7 Concluding Remarks

This dissertation began with a simple question: why does PPR persist in Ethiopia despite the availability of effective vaccines? The answer, revealed through four progressively sophisticated modeling studies, lies in the interplay between vaccination, animal movement, spatial heterogeneity, and co-infection dynamics.

The central message of this work is that PPR cannot be controlled in isolation. It cannot be controlled at the local level without considering regional connectivity. It cannot be controlled by vaccination alone without addressing movement and biosecurity. And it cannot be controlled without considering the broader disease landscape, including co-circulating pathogens like SGP.

The integrated framework emerging from this dissertation suggests that achieving the 2027 PPR eradication goal requires a paradigm shift from single-intervention, closed-population thinking to multi-intervention, connected-systems approaches. This shift has implications not only for PPR but for livestock disease control more broadly, particularly in settings where smallholder production systems are characterized by complex movement patterns and multiple circulating pathogens.

As Ethiopia and other affected countries work toward PPR eradication, the models and insights developed here provide quantitative guidance for designing effective, cost-efficient control programs. More broadly, this work demonstrates the value of mathematical modeling as a tool for understanding complex disease systems and informing evidence-based policy decisions. The journey from simple compartmental models to integrated frameworks mirrors the intellectual trajectory of this dissertation progressive expansion of scope and complexity, always grounded in the fundamental question of how to translate scientific understanding into improved animal health and human livelihoods.

The eradication of PPR is not merely a technical challenge but a testament to what can be achieved when scientific understanding, policy commitment, and on-the-ground implementation align. This dissertation contributes to the scientific foundation upon which such success can be built.

# Appendix A

# Important Definitions, Theories and Theorems

In this appendix, we provide the fundamental mathematical and epidemiological definitions, theories, and methodologies necessary for analyzing and understanding the results presented in this thesis.

## A.1 Mathematical Preliminaries

**Definition A.1.1 (Dynamical System).** *Consider a nonlinear dynamical system described by the ordinary differential equation:*

$$\frac{d\mathbf{x}}{dt} = \mathbf{f}(t, \mathbf{x}), \quad \mathbf{x}(t_0) = \mathbf{x}_0, \tag{A.1}$$

*where* $\mathbf{f} : U \to \mathbb{R}^n$ *with* $\mathbf{x} \in U \subset \mathbb{R}^n$, $t \in \mathbb{R}_+$, *and* $n \in \mathbb{N}$, *with* $U$ *open in* $\mathbb{R}^n$ *and* $\mathbf{x} = [x_1, x_2, \ldots, x_n]^T$ *is the state vector and* $\mathbf{f}(\mathbf{x}) = [f_1(\mathbf{x}), f_2(\mathbf{x}), \ldots, f_n(\mathbf{x})]^T$ *is a vector of nonlinear functions. Differential equations in (A.1) that explicitly depend on time are called* ***non-autonomous****, while those that are independent of time are termed* ***autonomous****. In our work, we restrict our analysis to autonomous equations. Thus, for* $\mathbf{x} \in U \subset \mathbb{R}^n$, *we have*

$$\frac{d\mathbf{x}}{dt} = \mathbf{f}(\mathbf{x}), \quad \mathbf{x}(0) = \mathbf{x}_0, \tag{A.2}$$

**Theorem A.1.2 (Existence of Unique Solution (Smith et al., 2025)).** *From equation (A.2), suppose* $\mathbf{f}$ *and* $\frac{\partial \mathbf{f}}{\partial x_i}, i = 1, ..., n$ *are continuous functions of* $(x_1, x_2, ..., x_n)$ *on* $\mathbb{R}^n$, *then the intial value problem in (A.2) has a unique solution for any initial value* $\mathbf{x}_0 \in \mathbb{R}^n$.

*Although a unique solution exists, the maximal interval of existence* $[t_0, T)$ *may be finite,* $T < \infty$, *unless the solution is bounded.*

Alternatively, there are conditions that give the guarantie of existence solution of system (A.2)

**Definition A.1.3.** *Let* $U$ *be an open subset of* $\mathbb{R}^n$. *A function* $\mathbf{f} : U \to \mathbb{R}^n$ *is* ***Lipschitz*** *if for all* $\mathbf{x}, \mathbf{y} \in U$, *there is a* $L$ *called Lipschitz constant such that*

$$||\mathbf{f}(\mathbf{x}) - \mathbf{f}(\mathbf{y})|| \leq L||\mathbf{x} - \mathbf{y}||.$$

*where* $||.||$ *stands for the Euclidean norm in* $\mathbb{R}^n$. *If* $\mathbf{f}$ *is Lipschitz on every bounded subset of* $\mathbb{R}^n$, *then* $\mathbf{f}$ *is said to be* ***globally Lipschitz*** *(Meiss, 2007).*

**Theorem A.1.4.** *Let* $\mathbf{f} : \mathbb{R}^n \to \mathbb{R}^n$ *be* ***globally Lipschitz*** *on* $\mathbb{R}^n$. *Then there exist a unique solution* $\mathbf{x}(t)$ *to (A.2) for all* $t \in \mathbb{R}_+$. *Therefore system (A.2) defines a dynamical system in* $\mathbb{R}^n$ *(Stuart et al., 1998)*

**Definition A.1.5 (Equilibrium Solution).** *An equilibrium solution (steady-state solution, fixed point, or critical point) of the differential system (A.2) is a constant solution* $\mathbf{x}^*$ *satisfying* $\mathbf{f}(\mathbf{x}^*) = 0$.

**Definition A.1.6 (Invariant Set).** *A set of states* $M \subset \mathbb{R}^n$ *of (A.2) is called an invariant set of (A.2) if for all* $\mathbf{x}_0 \in M$ *and for all* $t \geq 0, \mathbf{x}(t) \in M$ *(Strogatz, 2001).*

If $t \geq 0$ in the above definition, then $M$ is said to be a positively invariant set. In other words, solutions in a positively invariant set remain there for all positive time.

**Definition A.1.7 (Stability of Equilibrium Points (Stuart et al., 1998)).**

*i. An equilibrium* $\mathbf{x}^*$ *of (A.2) is called* ***locally stable*** *if and only if the following holds: For any* $\epsilon > 0$ *there exists some* $\delta > 0$ *such that* $||\mathbf{x}(t) - \mathbf{x}^*|| < \epsilon$ *for* $t > 0$ *whenever* $\mathbf{x}$ *is a solution to (A.2) and* $||\mathbf{x}(0) - \mathbf{x}^*|| < \delta$.

*ii. A locally stable equilibrium* $\mathbf{x}^*$ *is called* ***locally asymptotically stable*** *if and only if there exists some* $\delta > 0$ *such that* $x(t) \to \mathbf{x}^*$ *for* $t \to \infty$ *whenever* $\mathbf{x}$ *is a solution to (A.2) and* $||\mathbf{x}(0) - \mathbf{x}^*|| < \delta$.

*iii. An equilibrium is called unstable if and only if it is not locally stable, i.e., if and only if the following holds. There exists some* $\epsilon > 0$ *and a sequence* $\mathbf{x}_n$ *of solutions to (A.2) and a sequence* $t_n > 0$ *suchthat* $||\mathbf{x}_n(0) - \mathbf{x}^*|| \to 0, n \to \infty$, *but* $||\mathbf{x}(t_n) - \mathbf{x}^*|| > \epsilon$ *for all* $n \in \mathbb{N}$.

*iv. An equilibriumis called* ***globally stable*** *if it is stable for almost all initial conditions, not just those that are close to it.*

**Linearization of a Nonlinear System:** Consider a nonlinear dynamical system described in (A.2) and Let $\mathbf{x}^*$ be an equilibrium point of the system such that: $\mathbf{f}(\mathbf{x}^*) = 0$.

To approximate the behavior of the system near $\mathbf{x}^*$, let $\mathbf{x} = \mathbf{x}^* + \Delta\mathbf{x}$, where $\Delta\mathbf{x}$ is a small perturbation. Substituting this into the system and expanding $\mathbf{f}(\mathbf{x})$ using a first-order Taylor series around $\mathbf{x}^*$, we obtain:

$$\mathbf{f}(\mathbf{x}) \approx \mathbf{f}(\mathbf{x}^*) + \left.\frac{\partial \mathbf{f}}{\partial \mathbf{x}}\right|_{\mathbf{x}=\mathbf{x}^*} (\mathbf{x} - \mathbf{x}^*).$$

Since $\mathbf{f}(\mathbf{x}^*) = 0$, the system reduces to:

$$\frac{d\Delta\mathbf{x}}{dt} \approx \mathbf{J}\Delta\mathbf{x},$$

where $\mathbf{J}$ is the Jacobian matrix of $\mathbf{f}(\mathbf{x})$, evaluated at the equilibrium point $\mathbf{x}^*$, and is given by:

$$\mathbf{J} = \left.\frac{\partial \mathbf{f}}{\partial \mathbf{x}}\right|_{\mathbf{x}=\mathbf{x}^*} = \begin{bmatrix} \frac{\partial f_1}{\partial x_1} & \frac{\partial f_1}{\partial x_2} & \cdots & \frac{\partial f_1}{\partial x_n} \\ \frac{\partial f_2}{\partial x_1} & \frac{\partial f_2}{\partial x_2} & \cdots & \frac{\partial f_2}{\partial x_n} \\ \vdots & \vdots & \ddots & \vdots \\ \frac{\partial f_n}{\partial x_1} & \frac{\partial f_n}{\partial x_2} & \cdots & \frac{\partial f_n}{\partial x_n} \end{bmatrix}_{\mathbf{x}=\mathbf{x}^*}.$$

The resulting linearized system is given by

$$\frac{d\Delta\mathbf{x}}{dt} = \mathbf{J}\Delta\mathbf{x},$$

which represents a first-order approximation of the original nonlinear system in the vicinity of the equilibrium point $\mathbf{x}^*$. The stability of $\mathbf{x}^*$ can be assessed by analyzing the eigenvalues of the Jacobian matrix $\mathbf{J}$. The following theorem elucidates the stability conditions associated with the Jacobian matrix of the system.

**Definition A.1.8.** *Let* $\mathbf{x} = \mathbf{x}^*$ *be an equilibrium solution of (A.2),* $\mathbf{x}^*$ *is called a* ***hyperbolic*** *equilibrium point if none of the eigenvalues of* $Df(\mathbf{x}^*) = J$ *have zero real part. An equilibrium point that is not hyperbolic is called* ***non hyperblic*** *(Wiggins, 2003).*

**Theorem A.1.9.** *Suppose the system (A.2) has an equilibrium point at* $\mathbf{x}^*$ *and all of the eigenvalues of the linearized system (Jacobian Matrix) at* $\mathbf{x}^*$ *have negative real parts. Then* $\mathbf{x}^*$ *is* ***locally asymptotically stable****. (see, (Hirsch et al., 2013))*

**Remark A.1.10.** *i. If any eigenvalue of the Jacobain matrix has a positive real part, the equilibrium point is unstable.*

*ii. If eigenvalues of the Jacobain matrix have zero real parts, the stability requires further investigation.*

The characteristic polynomial for a higher-dimensional Jacobian matrix has a degree of three or greater. In this case, it is necessary to employ tools that provide necessary and sufficient conditions for the eigenvalues to possess negative real parts, thereby confirming the stability of the equilibrium point. These conditions are articulated by the **Routh–Hurwitz Criterion**, which is presented in (A.1.11).

**Theorem A.1.11 ( Routh–Hurwitz Criteria (Thieme, 2018)).** *Let the characteristic equation have the form*

$$\lambda^n + a_1\lambda^{n-1} + a_2\lambda^{n-2} + \ + a_{n-1}\lambda + a_n = 0.$$

*Consider the following expressions for characteristic equations with* $n \leq 4$*:*

$$\begin{aligned} n = 2 &: a_1, a_2; \\ n = 3 &: a_1, a_3, a_1a_2 - a_3; \\ n = 4 &: a_1, a_3, a_4, a_1a_2a_3 - a_3^2 - a_1^2a_4. \end{aligned}$$

*Then all zeros* $\lambda$ *have strictly negative real parts if all expressions are strictly positive. However, if at least one expression is strictly negative, then at least one root* $\lambda$ *has a strictly positive real part. (for more details, see (Martcheva, 2015)*

**Lyapunov function and Global stability:** For higher-dimensional systems, there are several techniques that could establish the global stability of an equilibrium. One of the most commonly used is the Lya punov function. Lyapunov functions are scalar functions that may be used to prove the global stability of an equilibrium.

**Definition A.1.12.** *A scalar function* $V(x)$ *such that* $V : \mathbb{R}^n \to \mathbb{R}$ *is called radially unbounded if*

$$V(x) \to \infty \quad if \quad ||\mathbf{x}|| \to \infty.$$

*One significant property of Lyapunov functions is that they are positive definite in the entire space.*

**Definition A.1.13.** *Let* $V$ *be a continuous scalar function, that is,* $V : \mathbb{R}^n \to \mathbb{R}$*. The function* $V$ *is called* ***positive definite*** *on the entire space if*

*i.* $V(\mathbf{x}^*) = 0$,

*ii.* $V(\mathbf{x}) > 0 \quad$ *for* $\mathbf{x} = \mathbf{x}^*$,

*where* $\mathbf{x}^*$ *is an equilibrium of the autonomous system* $\mathbf{x} = \mathbf{f}(\mathbf{x})$*. We define the derivative of* $V(x)$ *along the solutions of the system of differential equations as*

$$V'(\mathbf{x}) = \frac{d}{dt}V(\mathbf{x}(t)) = \frac{\partial V(\mathbf{x}(t))}{\partial(\mathbf{x}(t))}\frac{d\mathbf{x}}{dt}.$$

*Now we can state Lyapunov's theorem for global stability of the equilibrium* $\mathbf{x}^*$*. (see details in ((Chicone, 2006)))*

**Theorem A.1.14** ( **Lyapunov's Stability Theorem**)**.** *If a function* $V(x)$ *is globally positively definite and radially unbounded, and its time derivative is globally negative,*

$$V(\mathbf{x}) < 0 \quad \forall \mathbf{x} = \mathbf{x}^*,$$

*then the equilibrium* $\mathbf{x}^*$ *is globally stable.*

**Definition A.1.15.** *If a function* $V(\mathbf{x})$ *exists that satisfies the conditions of Theorem A.1.14, then this function is called a* ***Lyapunov function****.*

There are no established rules for finding a Lyapunov function, and often finding a Lyapunov function is tricky and computationally intensive. However, if a Lyapunov function is found, it can establish the global stability of an equilibrium. Lyapunov's Theorem requires that the derivative of a Lyapunov function with respect to t be strictly negative; however, we can often show only nonpositivity. In this case, an extension of Lyapunov's theorem was given by LaSalle (2012).

**Theorem A.1.16** (**Krasovkii–LaSalle Theorem (LaSalle, 2012)**)**.** *Consider the autonomous system* $\mathbf{x} = \mathbf{f}(\mathbf{x})$*,where* $\mathbf{x}^*$ *is an equilibrium, that is,* $\mathbf{f}(\mathbf{x}^*) = 0$*. Suppose there exists a continuously differentiable function* $V : \mathbb{R}^n \to \mathbb{R}$ *and that this function is positive definite on the entire space and radially unbounded and that it satisfies*

$$V(x) \leq 0 \quad \forall t \quad \textit{and} \quad \forall \mathbf{x} \in \mathbb{R}^n.$$

*Define the invariant set*

$$M = \{\mathbf{x} \in \mathbb{R}^n | V(\mathbf{x}) = 0\}.$$

*If* $M$ *contains only the equilibrium* $\mathbf{x}^*$*, then the equilibrium* $\mathbf{x}^*$ *is globally stable.*

**Definition A.1.17.** *The spectral radius of a matrix* $A$ *is defined as the maximum of the absolute values of the eigenvalues of* $A$*:*

$$\rho(A) = \sup\{|\lambda| : \lambda \in \sigma(A)\},$$

*where* $\sigma(A)$ *denotes the set of eigenvalues of* $A$*. It can be shown that* $V$ *is a nonsingular M-matrix.*

**Definition A.1.18** (**Basic reproduction number (ratio)**)**.** *The basic reproduction number,* $\mathcal{R}_0$*, is a key concept in infectious disease modeling, representing the average number of secondary infections caused by a single infectious individual in a fully susceptible population.*

The next-generation method is a systematic approach to compute $\mathcal{R}_0$ in deterministic compartmental models of infectious diseases and is widely used in epidemiological studies (see, e.g., (Van den Driessche et al., 2002)).

To compute $\mathcal{R}_0$ using this method, consider a compartmental model governed by a system of ordinary differential equations (ODEs) with assumption that there are $n$ infected compartments and $m$ non-infected compartments, so the entire ordinary differential equation model has $m + n$ dependent variables. Let $\mathbf{x}$ be the vector of dependent variables in the infected compartments, and let $\mathbf{y}$ be the vector of variables in the non-infected compartments. We have $\mathbf{x} \in \mathbb{R}^n$ and $\mathbf{y} \in \mathbb{R}^m$. The method below was introduced in (Van den Driessche et al., 2002). We then proceed with the following steps:

❶ First, we arrange the equations so that the first $n$ components of the ODE system correspond to the infected compartments. Thus, we write the original ODE system as:

$$\begin{aligned} x_i &= f_i(\mathbf{x}, \mathbf{y}), \\ y_j &= g_j(\mathbf{x}, \mathbf{y}), \quad for \quad i = 1, \ldots, n, j = 1, \ldots, m. \end{aligned} \tag{A.3}$$

❷ Second, we split the right-hand side in the infected compartments as follows:

$$x_i = \mathscr{F}_i(\mathbf{x}, \mathbf{y}) - \mathscr{V}_i(\mathbf{x}, \mathbf{y}), \quad y_j = g_j(\mathbf{x}, \mathbf{y}),$$

where $i = 1, \ldots, n$ and $j = 1, \ldots, m$,

- ➢ $\mathscr{F}_i(\mathbf{x}, \mathbf{y})$ is the rate of appearance of new infections in compartment $i$;
- ➢ $\mathscr{V}_i(\mathbf{x}, \mathbf{y})$ incorporates the remaining transitional terms, namely births, deaths, disease progression, and recovery.

❸ Assume that the disease-free system

$$y = g(0, \mathbf{y})$$

has a unique disease-free equilibrium $E_0 = (0, \mathbf{y}_0)$ such that all solutions with initial conditions of the form $(0, \mathbf{y})$ approach $(0, \mathbf{y}_0)$ as $t \to \infty$. Determine the disease-free equilibrium $E_0$.

❹ Determine the matrices $F$ and $V$ with components

$$F = \frac{\partial \mathscr{F}_i(0, \mathbf{y}_0)}{\partial x_j} \quad \text{and} \quad V = \frac{\partial \mathscr{V}_i(0, \mathbf{y}_0)}{\partial x_j}.$$

These matrices arise from the linearization of the system (A.3) around the disease-free equilibrium. It can be shown that

$$\frac{\partial \mathscr{F}_i(0, \mathbf{y}_0)}{\partial y_j} = \frac{\partial \mathscr{V}_i(0, \mathbf{y}_0)}{\partial y_j} = 0$$

for every pair $(i, j)$. This implies that the linearized equations for the infected compartments $\mathbf{x}$, computed at the disease-free equilibrium, are decoupled from the remaining equations. The linearized system for the infected compartments can be written as

$$\mathbf{x} = (F - V)\mathbf{x},$$

where the matrices $F$ and $V$ are defined above.

❺ The next-generation matrix is defined as

$$K = FV^{-1}$$

and

$$\mathcal{R}_0 = \rho(FV^{-1}),$$

where $\rho(A)$ denotes the spectral radius of $A$.

**Definition A.1.19.** *A matrix $A$ is called an M-matrix if:*

- *$A$ has the Z-pattern, that is, the off-diagonal elements of $A$ are nonpositive.*
- *The inverse of $A$ exists and has nonnegative elements: $A^{-1} \geq 0$.*

The value of $\mathcal{R}_0$ provides information about the potential for disease spread. If $\mathcal{R}_0 < 1$, the disease cannot invade or persist in the population and will eventually die out. Conversely, if $\mathcal{R}_0 > 1$, the disease can invade and persist, potentially leading to an epidemic. This method is particularly valuable for models with multiple infectious stages or host types, as it provides a rigorous framework for quantifying the transmission potential of infectious diseases. It has been widely employed in the literature to evaluate disease transmission dynamics and the impact of control strategies (see, e.g., (Van den Driessche et al., 2002)).

**Remark A.1.20.** *When we incorporate control measures into the model, such as vaccination, treatment, or quarantine, the term* ***basic reproduction number*** *is usually replaced by other terminology, such as the* ***control or effective reproduction number****. These terms account for the impact of interventions and represent the average number of secondary infections caused by a single infectious individual when control strategies are in place.*

## Bifurcation Theory

Bifurcation theory is a fundamental tool in the analysis of nonlinear dynamical systems, providing critical insights into the qualitative changes in system behavior as parameters vary (Van den Driessche et al., 2002). In the context of infectious disease modeling, bifurcation analysis is instrumental in identifying critical thresholds that dictate the long-term dynamics of disease transmission. Epidemiological models often exhibit multiple equilibrium states, and bifurcation theory offers a framework for understanding how these equilibria emerge, disappear, or change their stability as key parameters-such as transmission rates or recovery rates—are altered (Buonomo, 2015). In epidemic models, two phenomena, forward and backward bifurcations, usually arise de pending on the value of $\mathcal{R}_0$. Generally, a disease invades if the basic reproduction number is greater than unity ($\mathcal{R}_0 > 1$ ) and dies out if $\mathcal{R}_0 < 1$ (Van den Driessche et al., 2002). As the basic reproduction number in creases through 1, there is an exchange of stability between the disease-free equilibrium and endemic equilibrium at $\mathcal{R}_0 = 1$, which is called forward (or transcritical) bifurcation (Buonomo, 2015). In the case of a forward bifurcation, a disease can not spread if $\mathcal{R}_0 < 1$. However, in various complex epidemic models, a stable endemic equilibrium may also exist when the basic repro duction number is less than one ($\mathcal{R}_0 < 1$). In this situation, the system can tend to a stable endemic equilibrium state when the basic reproduction number is less than one ( $\mathcal{R}_0 < 1$). This phenomenon is called backward bifurcation. In the case of a forward bifurcation, it is su cient to reduce the basic reproduction number below one ($\mathcal{R}_0 < 1$) to eradicate a disease but $\mathcal{R}_0 < 1$ is not su cient, although necessary, to eradicate a disease in the case of the backward bifurcation. In epidemic models that exhibit the backward bifurcation phe nomenon, It is necessary to reduce $\mathcal{R}_0$ well below one to control the disease epidemic.

To determine the direction of the bifurcation at the critical value of a parameter, we can use the theorem by Castillo-Chavez and Song (Castillo-Chavez et al., 2004). The theorem is stated in Appendix (A.1.21).

**Theorem A.1.21 (Castillo-Chavez and Song (Castillo-Chavez et al., 2004)).** *Consider the following general system of ordinary differential equations (ODEs) with a parameter $\phi$:*

$$\frac{dx}{dt} = f(x, \phi), \quad f : \mathbb{R}^n \times \mathbb{R} \to \mathbb{R}^n, \quad f \in C^2(\mathbb{R}^n \times \mathbb{R}), \tag{A.4}$$

*where 0 is an equilibrium point of the system, that is, $f(0, \phi) \equiv 0$ for all $\phi$. Assume the following:*

*A1. Let $A = D_x f(0,0) = \left(\frac{\partial f_i}{\partial x_j}\right)_{(0,0)}$ be the linearization matrix of system (1) around the equilibrium 0 with $\phi$ evaluated at 0. Zero is a simple eigenvalue of $A$, and all other eigenvalues have negative real parts.*

*A2. The matrix $A$ has a nonnegative right eigenvector $w$ and a left eigenvector $v$, each corresponding to the zero eigenvalue. Let $f_k$ be the $k$-th component of $f$ and define:*

$$a = \sum_{k,i,j=1}^{n} v_k w_i w_j \frac{\partial^2 f_k}{\partial x_i \partial x_j}(0,0),$$

$$b = \sum_{k=1}^{n} v_k w_i \frac{\partial^2 f_k}{\partial x_i \partial \phi}(0,0).$$

*The local dynamics of the system around 0 are completely determined by the signs of $a$ and $b$:*

*(i) If $a > 0$ and $b > 0$: When $\phi < 0$ with $|\phi| \ll 1$, 0 is locally asymptotically stable, and there exists a positive unstable equilibrium; when $0 < \phi \ll 1$, 0 is unstable, and there exists a negative and locally asymptotically stable equilibrium.*

*(ii) If $a < 0$ and $b < 0$: When $\phi < 0$ with $|\phi| \ll 1$, 0 is unstable; when $0 < \phi \ll 1$, 0 is locally asymptotically stable, and there exists a positive unstable equilibrium.*

*(iii) If $a > 0$ and $b < 0$: When $\phi < 0$ with $|\phi| \ll 1$, 0 is unstable, and there exists a locally asymptotically stable negative equilibrium; when $0 < \phi \ll 1$, 0 is stable, and a positive unstable equilibrium appears.*

*(iv) If $a < 0$ and $b > 0$: When $\phi$ changes from negative to positive, 0 changes its stability from stable to unstable. Correspondingly, a negative unstable equilibrium becomes positive and locally asymptotically stable.*

*Particularly, if $a > 0$ and $b > 0$, then a backward bifurcation occurs at $\phi = 0$.*

## A.2 Epidemiological Preliminaries

① **Incidence Functions:** In mathematical epidemiology, the incidence function quantifies the rate of new infections in a population, playing a critical role in compartmental models such as the SIR (Susceptible-Infected-Recovered) model (Kermack et al., 1927). The interaction between susceptible and infectious hosts can be described using two primary types of transmission: frequency-dependent and density-dependent.

- ❍ **Frequency Dependent Transmission (Standard Incidence):** This incidence type assumes a fixed number of contacts per host, rendering the transmission rate independent of the total population size. It is mathematically represented as:

$$g(S, I) = \beta \frac{SI}{N}$$

where $\beta$ is the transmission rate, $S$ is the number of susceptible hosts, $I$ is the number of infectious hosts, and $N$ is the total population (Hethcote, 2000). This model is particularly useful in scenarios where contact rates are diluted across a large population.

- ❍ **Density Dependent Transmission (Mass action Incidence):** In contrast, this model relates the transmission rate directly to population size, typically characterized by the equation:

$$g(S, I) = \beta SI$$

This formulation reflects the "law of mass action" and is often applied in contexts such as livestock diseases, where herd size and farming practices significantly impact disease dynamics (Li, 2018; Brown, 2022).

To enhance density-dependent modeling, heterogeneous mixing terms can be introduced to better account for interactions among hosts, thus moving beyond the basic homogeneous model based on mean-field theory (Conlan et al., 2017). Other forms of incidence functions include:

An extension of the mass-action law of infection replaces the term $\beta SI$ with $\eta C(N)\frac{SI}{N}$ (Castillo-Chavez et al., 1989). Here, $C(N)$ represents the average number of contacts per individual in a population of size $N$, excluding deceased and quarantined individuals. The fraction $\frac{I}{N}$ indicates the probability of a contact occurring with an infectious individual, while $\eta$ represents the probability that such a contact results in infection.

The traditional mass-action model is recovered when $C(N)$ is proportional to $N$. If $C(N)$ is constant, this corresponds to standard incidence. Data suggest that $\frac{C(N)}{N}$ decreases with increasing $N$. (Dietz, 1982) proposes **a saturating contact rate**:

$$C(N) = \frac{\zeta N}{1 + \alpha N},$$

which is proportional to $N$ for small populations and nearly constant for large populations, bridging mass-action incidence and standard incidence.

Selecting the appropriate incidence function is crucial and should consider disease characteristics, population dynamics, and transmission assumptions, as these choices significantly influence disease control strategies and model predictions (Liu et al., 2023; Hethcote, 2000).

② **Latency (Incubation) Period:** The latency period is the period of time where a host is infected but is not infectious and/or detectable by diagnostic tests. For diseases that are considered to cause latent infection, calculating the latency period is important to understand the limits of testing for such a disease.

③ **Disease Equilibria:** As epidemic models are ODEs, their equilibria can be calculated as the equations turning points. Two equilibria can occur: the **Disease-Free Equilibrium (DFE)** and the **Endemic Equilibrium (EE)** (Costa et al., 2021). The DFE is where there are no infected hosts left in the population and the EE is when there is a stable proportion of infected hosts in the population. Calcu lating these equilibria can assist in studying the level at which a disease becomes endemic within a population and can provide an indication of how to improve disease managment. In particular, the DFE is useful as it can be used to create the next metric, the basic reproductive ratio.

④ **Spatial heterogeneity/ Metapopulations:** Spatial heterogeneity refers to variations in the landscape, climate, or other environmental factors that influence the dynamics of infectious diseases. It plays a crucial role in shaping the spread and persistence of infections, as populations are rarely homogeneously distributed across space. To account for this, metapopulation models are often employed. A metapopulation consists of multiple subpopulations, each with its own internal dynamics, but connected through the movement of individuals between them (Leibold et al., 2004; Keeling et al., 2011). These models allow for the incorporation of spatial heterogeneity by considering factors such as between-herd movements, contact in shared pastures, or environmental reservoirs, which are particularly relevant for diseases like peste des petits ruminants (PPR) (Fournié et al., 2018).

⑤ **Co-infection** is the simultaneous infection of a single host by two or more pathogens (e.g., viruses, bacteria, fungi) that may interact within the host to modify disease dynamics.

These interactions can alter pathogen load, clinical severity, transmission, diagnostic test performance, and treatment response (Derouin et al., 1998). For example, in cattle, Fasciola hepatica (liver fluke) can co-infect with Mycobacterium bovis; in small ruminants, bluetongue virus (BTV) is often accompanied by secondary bacterial pneumonia due to Mannheimia haemolytica or Pasteurella multocida.

## A.3 Optimal Control Theory in Epidemiology Models

Optimal control theory is one of optimization technique and a powerful Mathematical tool used to make decisions on how to control infectious animal disease like PPR viral disease in small ruminant, the main goal is to minimize the number of infected animals along with minimizing the cost of implementing control strategies (vaccination, biosecurity measures, supportive treatments, etc.). Optimal control theory is used to minimize investments in disease control, since financial resources are always limited (Dangelmayr et al., 2003). Quantitative methods are applied to optimize investments in the control of epidemiological diseases, to maximize the benefits of the affixed amount of financial resources (Rodrigues et al., 2012).

In a dynamical system, the optimal control problem for a system of ordinary differential equations is described by state equations in vector notation; we denote $\mathbf{u}(t)$ as the vector of control functions and $\mathbf{x}(t)$ as the vector of state variables. The state variables, $\mathbf{x}(t)$, satisfies the system ODE modeling the scenario. The control functions affects the state variables in the system ODE by

$$\begin{cases} \mathbf{x}'(t) = \mathbf{g}(t, \mathbf{x}(t), \mathbf{u}(t)) \\ \mathbf{x}(t_0) = \mathbf{x}_0 \end{cases} \tag{A.5}$$

Where $\mathbf{x}(t) = (x_1(t), x_2(t), ..., x_n(t))$, $\mathbf{u}(t) = (u_1(t), u_2(t), ..., u_m(t))$ (provide that $m < n$), $\mathbf{g} = (g_1(t, \mathbf{x}, \mathbf{u}), g_2(t, \mathbf{x}, \mathbf{u}), ..., g_n(t, \mathbf{x}, \mathbf{u}))$, and $\mathbf{x}_0 = (x_{10}, x_{20}, ..., x_{n0})$.

Note that the solution of the ODE (A.5) depends on the control variable $\mathbf{u}$ as well as on the the initial condition $\mathbf{x}_0$. Both $\mathbf{u}(t)$ and $\mathbf{x}(t)$ affect the goal, represented by the objective functional. The objective functional is typically an integral expression formulated terms of the state and control variables. We seek to find a vector of optimal control functions $\mathbf{u}^*$ and a vector corresponding to optimal state variables $\mathbf{x}^*$ that achieve the minimum of our objective functional. The optimal control problem may be stated as

$$J = \min_{\mathbf{u} \in \mathbf{U}} \int_0^T f(t, \mathbf{x}(t), \mathbf{u}(t)) dt, \quad t_0 = 0 \tag{A.6}$$

subject to

$$\mathbf{x}'(t) = \mathbf{g}(t, \mathbf{x}(t), \mathbf{u}(t)) \tag{A.7}$$

where

$$\mathbf{x}(0) = \mathbf{x}_0 \quad \text{and} \quad \mathbf{x}(T) \quad \text{is free} \tag{A.8}$$

We assume that our control set $\mathbf{U}$ is a Lebesgue-measurable function. A vector of optimal control, denoted by $\mathbf{u}^*(t) \in \mathbf{U}$, achieves maximum. Assuming that $f$ and $\mathbf{g}$ are continuously differentiable in their arguments. To show that an optimal control exists, we make use of the following theorem from Fleming and Rishel (Fleming et al., 2012).

**Theorem A.3.1** (**Existence of optimal control (Fleming et al., 2012)**). *Consider an optimal control problem (A.5) defined by the state equation and admissible controls. The following conditions must hold for the existence of an optimal control:*

① *The set of solutions for the state equation is non-empty; that is, there exists at least one pair* $(\mathbf{x}(t), \mathbf{u}(t))$ *that satisfies the state equations and adheres to the control constraints.*

② *The set of admissible controls* $\mathbf{U}$ *is convex and closed.*

③ *The function* $\mathbf{g}$*, which represents the right-hand side of the state equation (A.5), is continuous and bounded above by a function of the state and control variables:*

$$\mathbf{g}(t, \mathbf{x}(t), \mathbf{u}(t)) \leq c_1(1 + ||\mathbf{x}(t)|| + ||\mathbf{u}(t)||),$$

*for some constant* $c_1 > 0$*.*

④ *The function* $\mathbf{g}$ *can be expressed as a linear function of the control:*

$$\mathbf{g}(t, \mathbf{x}(t), \mathbf{u}(t)) = \phi(t, \mathbf{x}(t)) + \psi(t, \mathbf{x}(t))\mathbf{u},$$

*where* $\phi$ *and* $\psi$ *are suitable functions.*

⑤ *The function* $\boldsymbol{g}$ *satisfies the condition:*

$$||\mathbf{g}(t, x_1, \mathbf{u}) - \mathbf{g}(t, \mathbf{x}, \mathbf{u})|| \leq c_2||x_1 - x||(1 + ||\mathbf{u}||)$$

*for some constant* $c_2 > 0$*.*

⑥ *The integrand* $f(t, \mathbf{x}, \mathbf{u})$ *in the objective functional (A.6) is convex with respect to the control* $\mathbf{u}$ *and satisfies:*

$$f(t, \mathbf{x}, \mathbf{u}) \geq \alpha_1||u||^{\alpha} - \alpha_2$$

*for some fixed* $\alpha_1 > 0$*,* $\alpha_2 \in \mathbb{R}$ *and* $\alpha > 1$*.*

Condition (1) ensures that the problem is well-posed, making it meaningful to seek a minimum. Conditions (2) and (3) guarantee that solutions remain uniformly bounded for all $t$ in the interval $[0, T]$. Condition (4) requires the convexity of $\mathbf{g}(t, \mathbf{x}(t), \mathbf{u}(t))$ to ensure the existence of a minimum solution. If $\mathbf{g}(t, \mathbf{x}(t), \mathbf{u}(t))$ is not convex, a minimum may not exist. In condition (5), Lipschitz continuity ensures that the system has a unique solution.

### A.3.1 Characterization of Controls

If the optimal control exists, that is all conditions of Theorem (A.3.1) are satisfied, we use **Pontryagin's Maximum Principle** (Pontryagin, 1987) to obtain the characterization of the optimal control in terms of the state and adjoint variables. Pontryagin's Maximum Principle converts the minimization of the objective functional subject to the state system into pointwise minimization of Hamiltonian with respect to the control variable. The **Hamiltonian** $\mathcal{H}$ is defined as

$$\mathcal{H}(t, \mathbf{x}, \mathbf{u}, \boldsymbol{\lambda}) = f(t, \mathbf{x}, \mathbf{u}) + \boldsymbol{\lambda}(t).\mathbf{g}(t, \mathbf{x}, \mathbf{u}) \tag{A.9}$$

where $\boldsymbol{\lambda}$ is the adjoint variable associated with the state $\mathbf{x}$. Note that in the Hamiltonia $\mathcal{H}$, the first term denotes the integrand of the objective functional, while the adjoint variable $\boldsymbol{\lambda}$ is multiplied with the right-hand side of the associated state variable.

We can state the necessary first order conditions in the simplest form by Pontryagin's Maximum Principle (Pontryagin, 1987) as follows.

**Theorem A.3.2 (Pontryagin's Maximum Principle (Pontryagin, 1987)).** *Let* $\mathbf{u}^*$ *be a vector of optimal control functions and* $\mathbf{x}^*$ *be the vector of the corresponding optimal state variables for problem (A.6)-(A.8). With* $n$ *states, we will need* $n$ *adjoints, one for each state. Introduce a piecewise differentiable vector valued function* $\boldsymbol{\lambda}(t) = (\lambda_1(t), \lambda_2(t), ..., \lambda_n(t))$*, where each is the adjoint variable corresponding to state variable* $\mathbf{x}$*. One can generate the necessary conditions by maximizing* $H$ *with respect to* $\mathbf{u}(t)$ *at* $\mathbf{u}^*(t)$*. i.e.*

$$\mathcal{H}(t, \mathbf{x}^*(t), \mathbf{u}(t), \boldsymbol{\lambda}(t)) \leq \mathcal{H}(t, \mathbf{x}^*(t), \mathbf{u}^*(t), \boldsymbol{\lambda}(t)), \forall \mathbf{u}(t) \in \mathbf{U}$$

*at each time and* $\mathbf{u}^*(t), \mathbf{x}^*(t)$ *and* $\boldsymbol{\lambda}(t)$ *satisfy*

$$\begin{cases} x_i'(t) = \dfrac{\partial \mathcal{H}}{\partial \lambda_i} = g_i(t, \boldsymbol{x}, \boldsymbol{u}), x_i(t_0) = x_{i0}, \quad \textit{for} \quad i = 1, 2, ..., n, \\ \lambda_j'(t) = -\dfrac{\partial \mathcal{H}}{\partial x_j}, \quad \textit{for} \quad j = 1, 2, ..., n, \quad \textit{(adjoint equations)} \\ \lambda_j(T) = 0, \quad \textit{for} \quad j = 1, 2, ..., n, \quad \textit{(transversality condition)} \\ \dfrac{\partial \mathcal{H}}{\partial u_k} = 0 \quad \textit{at} \quad u_k^* \quad \textit{for} \quad k = 1, 2, ..., m, \textit{(optimality equations)} \end{cases} \tag{A.10}$$

*where*

$$\mathcal{H}(t, \mathbf{x}(t), \mathbf{u}(t), \boldsymbol{\lambda}(t)) = f(t, \mathbf{x}(t), \mathbf{u}(t)) + \sum_{i=1}^{n} \lambda_i(t) g_i(t, \mathbf{x}(t), \mathbf{u}(t))$$

**Theorem A.3.3** (**Sufficient Conditions (Mangasarian's Theorem (Lenhart et al., 2007)**)). *consider the standard end constrained problem (A.6)-(A.8) with* $\mathbf{U}$ *convex, and suppose that the partial derivatives* $\partial f/\partial u_j$ *and* $\partial g_i/\partial u_j$ *all exist and are continuous. If the pair* $(\boldsymbol{x}^*(t), \boldsymbol{u}^*(t))$ *satisfies all the necessary conditions in* ***Pontryagin's maximum principle*** *and if*

$$\mathcal{H}(t, \mathbf{x}(t), \mathbf{u}(t), \boldsymbol{\lambda}(t)) \quad \textit{is concave in } (\boldsymbol{x}(t), \boldsymbol{u}(t)) \textit{ for all } t \textit{ in } [0, T] \tag{A.11}$$

*then* $(\mathbf{x}^*(t), \mathbf{u}^*(t))$ *solves the problem.*
*If the function* $\mathcal{H}(t, \mathbf{x}(t), \mathbf{u}(t), \boldsymbol{\lambda}(t))$ *is strictly concave in* $(\mathbf{x}(t), \mathbf{u}(t))$,*then* $((\mathbf{x}^*(t), \mathbf{u}^*(t)))$ *is the unique solution to the problem.*

**Remark A.3.4.** *Since a sum of concave functions is concave, the concavity condition (A.11) is satisfied if* $f$ *and* $\lambda_1(t)g_1, ..., \lambda_n(t)g_n$ *are all concave in* $(\boldsymbol{x}(t), \boldsymbol{u}(t))$.

Frequently, when the control enters into the problem in a nonlinear way, we can set $H_{u_k}|_{u_k^*} = 0$ and solve for $\mathbf{u}^*$. This characterization of the optimal control will be in terms of $\mathbf{x}^*$ and $\boldsymbol{\lambda}$. In many biological or physical problems, the controls will have bounds imposed due to the specific application. Pontryagin's maximum principle (PMP) still holds when controls are restricted within the bounds $a_k \leq u_k(t) \leq b_k$.

### A.3.2 Numerical Solution of the Optimal Control Problem

We refer to the state and adjoint differential equations, along with control characterization, as an optimality system (A.10). In the optimality system (A.10), the state equation has initial condition $\mathbf{x}$, while the adjoint equation has terminal condition $\boldsymbol{\lambda}(T)$. A system of differential equations where some variables have initial conditions and other variables have terminal conditions is known as a two-point boundary value problem. Often, solutions of the optimality system cannot be solved explicitly, but can be approximated numerically (Neilan, 2009).

Then we use a Runge-Kutta method of fourth order **forward-backward sweep iterative method** (Lenhart et al., 2007) for solving the optimality system numerically. The algorithm to solve the optimality system (A.10) using forward-backward sweep method (Lenhart et al., 2007; Neilan, 2009) is as follows:

1. Initialize the control variable $\mathbf{u}$ with an initial guess.
2. Using the current value of $\mathbf{u}$, integrate the state equation forward in time using the initial condition.

❸ Using the current values of the state and control variables, integrate the adjoint equa tion backward in time using the terminal condition.

❹ Update the control variable value $\mathbf{u}$ by averaging the previous value and the new value arising from the control characterization.

❺ Repeat steps 1-4 until successive values of all states, adjoints, and control(s) are sufficiently close. The last step determining convergence requires the state, adjoint, and control values from two successive iterations to satisfy the relation

$$\frac{||v_i - v_{i-1}||}{||v_i||} \leq \epsilon$$

where $\epsilon$ is the accepted tolerance, $v_i$ is the vector (or matrix) (represents state ($\mathbf{x}$), adjoint ($\boldsymbol{\lambda}$), and control ($\mathbf{u}$) values ) of current values, $v_{i-1}$ is the vector (or matrix) from the previous iteration, and $||.||$ refers to the sum of the absolute value of the elements within $v$.

# Bibliography


Abraham, P. L., Kenfe, G., and Barrett, T. (1994). "PPR in Ethiopian goats". *Trop Anim Health Prod* 26, pp. 69–73.

Adam, H. D., Althubyani, M., Mirgani, S. M., and Saber, S. (2025). "An Application of Newton's Interpolation Polynomials to the Zoonotic Disease Transmission between Humans and Baboons System Based on a Time-Fractal Fractional Derivative with a Power-Law Kernel". *AIP Advances* 15.4.

Adedeji, A. J., Dashe, Y., Akanbi, O. B., Woma, T. Y., Jambol, A. R., Adole, J. A., Bolajoko, M. B., Chima, N., Asala, O., Tekki, I. S., et al. (2019). "Co-infection of peste des petits ruminants and goatpox in a mixed flock of sheep and goats in Kanam, North Central Nigeria". *Veterinary Medicine and Science* 5.3, pp. 412–418.

Aetiology, OIE Peste Des Petits Ruminants (2020). *Epidemiology Diagnosis Prevention and Control References; World Organisation for Animal Health: 2020*.

Ahaduzzaman, Md (2020). "Peste des Petits Ruminants (PPR) in Africa and Asia: A systematic review and meta-analysis of the prevalence in sheep and goats between 1969 and 2018". *Veterinary Medicine and Science* 6.4, pp. 813–833.

Alemu, B., Gari, G., Libeau, G., Kwiatek, O., Kidane, M., Belayneh, R., Siraw, B., Wieland, B., Asfaw, W., and Abdi, R. D. (2019). "Molecular detection and phylogenetic analysis of Peste des petits ruminants virus circulating in small ruminants in eastern Amhara region, Ethiopia". *BMC Veterinary Research* 15, pp. 1–9.

Alexander, M. E., Bowman, C., Moghadas, S. M., Summers, R., Gumel, A. B., and Sahai, B. M. (2004). "A vaccination model for transmission dynamics of influenza". *SIAM Journal on Applied Dynamical Systems* 3.4, pp. 503–524.

Aligaz, A. A. and Munganga, J. M. W. (2019). "Mathematical modelling of the transmission dynamics of contagious bovine pleuropneumonia with vaccination and antibiotic treatment". *Journal of Applied Mathematics* 2019.1, p. 2490313.

Althubyani, M. and Saber, S. (2025). "Hyers–Ulam Stability of Fractal–Fractional Computer Virus Models with the Atangana–Baleanu Operator". *Fractal and Fractional* 9.3, p. 158.

Altizer, S., Dobson, A., Hosseini, P., Hudson, P., Pascual, M., and Rohani, P. (2006). "Seasonality and the dynamics of infectious diseases". *Ecology Letters* 9.4, pp. 467–484.

Anderson, R. M. and May, R. M. (1991). *Infectious diseases of humans: dynamics and control*. Oxford University Press.

Balamurugan, V., Hemadri, D., Gajendragad, M.R., Singh, R. K., and Rahman, H. (2014). "Diagnosis and control of peste des petits ruminants: a comprehensive review". *Virusdisease* 25, pp. 39–56.

Berman, A. and Plemmons, R. J. (1994). *Nonnegative matrices in the mathematical sciences*. SIAM, p. 141.

Bernoulli, D. (1766). "A new analysis of the mortality caused by smallpox". *The History of Actuarial Science Vol VIII*. Routledge, pp. 1–38.

Bichara, D. and Iggidr, A. (2018). "Multi-patch and multi-group epidemic models: a new framework". *Journal of Mathematical Biology* 77.1, pp. 107–134.

Birindwa, B. A., George, G. C., Ntagereka, B. P., Christopher, O., and Lilly, B. C. (2017). "Mixed infection of peste-des-petits ruminants and Capripox in goats in South Kivu, Democratic Republic of Congo". *Journal of Advanced Veterinary and Animal Research* 4.4, pp. 348–355.

Bolatova, D., Kadyrov, S., and Kashkynbayev, A. (2024). "Mathematical modeling of infectious diseases and the impact of vaccination strategies". *Mathematical Biosciences and Engineering: MBE* 21.9, pp. 7103–7123.

Bonyah, E., Khan, M. A., Okosun, K. O., and Gómez-Aguilar, J. F. (2019). "Modelling the effects of heavy alcohol consumption on the transmission dynamics of gonorrhea with optimal control". *Mathematical Biosciences* 309, pp. 1–11.

Brown, E. (2022). "Mathematical Modelling for the Investigation of Bovine Tuberculosis in Northern Ireland". PhD thesis. Queen's University Belfast.

Buonomo, B. (2015). "A note on the direction of the transcritical bifurcation in epidemic models". *Nonlinear Analysis: Modelling and Control* 20.1, pp. 38–55.

Burton, J., Billings, L., Cummings, D. A. T., and Schwartz, I. B. (2012). "Disease persistence in epidemiological models: the interplay between vaccination and migration". *Mathematical Biosciences* 239.1, pp. 91–96.

Carr, J. (2012). *Applications of centre manifold theory*. Vol. 35. Springer Science & Business Media.

Castillo-Chavez, C., Hethcote, H. W., Andreasen, V., Levin, S. A., and Liu, W. M. (1989). "Epidemiological models with age structure, proportionate mixing, and cross-immunity". *Journal of Mathematical Biology* 27, pp. 233–258.

Castillo-Chavez, C. and Song, B. (2004). "Dynamical models of tuberculosis and their applications". *Mathematical Biosciences & Engineering* 1.2, pp. 361–404.

Chamchod, F. (2018). "Modeling the spread of capripoxvirus among livestock and optimal vaccination strategies". *Journal of Theoretical Biology* 437, pp. 179–186.

Chamchod, F., Cantrell, R. S., Cosner, C., Hassan, A. N., Beier, J. C., and Ruan, S. (2014). "A modeling approach to investigate epizootic outbreaks and enzootic maintenance of Rift Valley fever virus". *Bulletin of Mathematical Biology* 76.8, pp. 2052–2072.

Chicone, C. (2006). *Ordinary Differential Equations with Applications*. 2nd. Vol. 34. Texts in Applied Mathematics. New York: Springer.

Conlan, A. J. K., Webb, C., McKinley, T. J., Cunniffe, N., and Gaythorpe, K. (2017). *Mathematical Models for Infectious Disease Dynamics (Residential Course)*. Residential Course.

Costa, A., Pires, M. A., Resque, R. L., and Almeida, S. S. M. S. (2021). "Mathematical modeling of the infectious diseases: key concepts and applications". *Journal of Infectious Diseases and Epidemiology* 7.5, p. 209.

Couacy-Hymann, E., Bodjo, S. C., Danho, T., Koffi, M. Y., Libeau, G., and Diallo, A. (2007). "Early detection of viral excretion from experimentally infected goats with peste-des-petits ruminants virus". *Preventive Veterinary Medicine* 78.1, pp. 85–88.

(CSA), Central Statistical Agency (2021). *Agricultural Sample Survey. Volume II. Report on Livestock and Livestock Characteristics (Private Peasant Holdings)*. Statistical Bulletin, 589. Published by CSA. Addis Ababa.

Dangelmayr, G. and Kirby, M. (2003). *Mathematical modeling: a comprehensive introduction*. Fort Collins, CO: Colorado State University.

Derouin, F., Lacroix, C., Brun-Pascaud, M., Chau, F., Sinet, M., Maslo, C., and Girard, P. (1998). "Animal models of co-infection". *Clinical Microbiology and Infection* 4.10, pp. 559–562.

Dietz, K. (1982). "Overall population patterns in the transmission cycle of infectious disease agents". *Population Biology of Infectious Diseases: Report of the Dahlem Workshop on Population Biology of Infectious Disease Agents Berlin 1982, March 14–19*. Springer, pp. 87–102.

Dubie, T., Dagnew, B., Gelo, E., Negash, W., Hussein, F., and Woldehana, M. (2022). "Seroprevalence and associated risk factors of peste des petits ruminants among ovine and caprine in selected districts of Afar region, Ethiopia". *BMC Veterinary Research* 18.1, p. 429.

Ethiopia, FAO (2012). "Strategy for Progressive Control of PPR in Ethiopia". *Addis Ababa: Food and Agriculture Organization of the United Nations and Ethiopia*.

Fakri, F., Ghzal, F., Daouam, S., Elarkam, A., Douieb, L., Zouheir, Y., Tadlaoui, K., and Fassi-Fihri, O. (2015). "Development and field application of a new combined vaccine against Peste des Petits Ruminants and Sheep Pox". *Trials in Vaccinology* 4, pp. 33–37.

FAO, OIE (2015). "Global strategy for the control and eradication of PPR. 2015". *FAO and OIE International Conference for the Control and Eradication of peste des petits ruminants. Abidjan*.

Fathelrahman, E. M., Reeves, A., Mohamed, M. S., Ali, Y. M. E., El Awad, A. I., Bensalah, O. K., and Abdalla, A. A. (2021). "Epidemiology and cost of peste des petits ruminants (PPR) eradication in small ruminants in the United Arab Emirates—disease spread and control strategies simulations". *Animals* 11.9, p. 2649. DOI: 10.3390/ani11092649.

Fentie, T., Fenta, N., Leta, S., Molla, W., Ayele, B., Teshome, Y., Nigatu, S., and Assefa, A. (2017). "Sero-prevalence, risk factors and distribution of sheep and goat pox in Amhara Region, Ethiopia". *BMC Veterinary Research* 13, pp. 1–8.

Fentie, T., Teshome, Y., Ayele, B., Molla, W., Fenta, N., Nigatu, S., Assefa, A., and Leta, S. (2018). "Sero-epidemiological study of Peste des petits ruminants in small ruminants in Amahara region, Ethiopia". *Comparative Clinical Pathology* 27.4, pp. 1029–1036.

Fèvre, E. M., Bronsvoort, B. M. C., Hamilton, K. A., and Cleaveland, S. (2006). "Animal movements and the spread of infectious diseases". *Trends in Microbiology* 14.3, pp. 125–131.

Fleming, W. H. and Rishel, R. W. (2012). *Deterministic and stochastic optimal control*. Vol. 1. Springer Science & Business Media.

Fournié, G., Waret-Szkuta, A., Camacho, A., Yigezu, L. M., Pfeiffer, D.U., and Roger, F. (2018). "A dynamic model of transmission and elimination of peste des petits ruminants in Ethiopia". *Proceedings of the National Academy of Sciences* 115.33, pp. 8454–8459.

Freedman, H. I., Ruan, S., and Tang, M. (1994). "Uniform persistence and flows near a closed positively invariant set". *Journal of Dynamics and Differential Equations* 6, pp. 583–600.

Fulford, G. R., Roberts, M. G., and Heesterbeek, J. A. P. (2002). "The metapopulation dynamics of an infectious disease: tuberculosis in possums". *Theoretical Population Biology* 61.1, pp. 15–29.

Gopilo, A. (2005). "Epidemiology of peste des petits ruminants virus in Ethiopia and molecular studies on virulence". PhD thesis. INPT.

Gumel, A. B., McCluskey, C. C., and Watmough, J. (2006). "An SVEIR model for assessing potential impact of an imperfect anti-SARS vaccine". *Mathematical Biosciences and Engineering* 3.3, pp. 485–512.

Gupta, J., Dhar, J., and Sinha, P. (2022). "An eco-epidemic model with seasonal variability: a non-autonomous model". *Arabian Journal of Mathematics* 11.3, pp. 521–538.

Hammami, P., Lancelot, R., Domenech, J., and Lesnoff, M. (2018). "Ex-ante assessment of different vaccination-based control schedules against the peste des petits ruminants virus in sub-Saharan Africa". *Plos One* 13.1, e0190296.

Hethcote, H. W. (2000). "The mathematics of infectious diseases". *SIAM Review* 42.4, pp. 599–653.

Hirsch, M. W., Smale, S., and Devaney, R. L. (2013). *Differential equations, dynamical systems, and an introduction to chaos*. Academic Press.

Hugo, A., Makinde, O. D., Kumar, S., and Chibwana, F. F. (2017). "Optimal control and cost effectiveness analysis for Newcastle disease eco-epidemiological model in Tanzania". *Journal of Biological Dynamics* 11.1, pp. 190–209.

Jemberu, W. T., Knight-Jones, T. J. D, Gebru, A., Mekonnen, S. A., Yirga, A., Sibhatu, D., and Rushton, J. (2022). "Economic impact of a peste des petits ruminants outbreak and vaccination cost in northwest Ethiopia". *Transboundary and emerging diseases* 69.5, e2084–e2092.

Jilo, K. (2016). "Peste des petits ruminants (PPR): global and ethiopian aspects. a standard review". *Global Veterinaria* 17.2, pp. 142–153.

Jones, B. A., Rich, K. M., Mariner, J. C ., Anderson, J., Jeggo, M., Thevasagayam, S., Cai, Y., Peters, A. R., and Roeder, P. (2016). "The economic impact of eradicating peste des petits ruminants: a benefit-cost analysis". *PLoS One* 11.2, e0149982.

Keeling, M. J. and Rohani, P. (2011). *Modeling infectious diseases in humans and animals*. Princeton university press.

Kermack, W. O. and McKendrick, A. G. (1927). "A contribution to the mathematical theory of epidemics". *Proceedings of The Royal Society of London. Series A* 115.772, pp. 700–721.

Kgotlele, T., Chota, A., Chubwa, C. C., Nyasebwa, O., Lyimo, B., Torsson, E., Karimuribo, E., Kasanga, C. J., Wensman, J. J., Misinzo, G., et al. (2019). "Detection of peste des petits ruminants and concurrent secondary diseases in sheep and goats in Ngorongoro district, Tanzania". *Comparative Clinical Pathology* 28, pp. 755–759.

Khan, Z. A., Alaoui, A. L., Zeb, A., Tilioua, M., and Djilali, S. (2021). "Global dynamics of a SEI epidemic model with immigration and generalized nonlinear incidence functional". *Results in Physics* 27, p. 104477.

Kotchofa, P., Rich, K. M., Baltenweck, I., and Dione, M. M. (2021). "Macroeconomic impact assessment of peste des petits ruminants (PPR) in Ethiopia and Burkina Faso". *ILRI Research Brief*.

Kouidere, A., Balatif, O., and Rachik, M. (2021). "Analysis and optimal control of a mathematical modeling of the spread of African swine fever virus with a case study of South Korea and cost-effectiveness". *Chaos, Solitons & Fractals* 146, p. 110867.

Lakshmikantham, V., Leela, S., and Martynyuk, A. A. (1989). *Stability analysis of nonlinear systems*. Springer.

LaSalle, J. P. (2012). "The stability of dynamical systems, Regional Conference Series in Applied Mathematics, SIAM, Philadelphia, 1976". *Khalid Hattaf Department of Mathematics and Computer Science, Faculty of Sciences Ben M'sik, Hassan II University, PO Box* 7955.

Leibold, M. A., Holyoak, M., Mouquet, N., Amarasekare, P., Chase, J. M., Hoopes, M. F., Holt, R. D., Shurin, J. B., Law, R., Tilman, D., et al. (2004). "The metacommunity concept: a framework for multi-scale community ecology". *Ecology Letters* 7.7, pp. 601–613.

Lenhart, S. and Workman, J. T. (2007). *Optimal control applied to biological models*. Chapman and Hall/CRC.

Li, M. Y. (2018). *An introduction to mathematical modeling of infectious diseases*. Vol. 2. Springer.

Li, M. Y. and Shuai, Z. (2009). "Global stability of an epidemic model in a patchy environment". *Canadian Applied Mathematics Quarterly* 17.1, pp. 175–187.

Liu, M. and Li, Y. (2023). "Dynamics analysis of an SVEIR epidemic model in a patchy environment". *Mathematical Biosciences and Engineering* 20.9, pp. 16962–16977.

Makinde, Oluwole Daniel and Okosun, Kazeem O (2011). "Impact of chemo-therapy on optimal control of malaria disease with infected immigrants". *BioSystems* 104.1, pp. 32–41.

Malik, Y. S., Singh, D., Chandrashekar, K. M., Shukla, S., Sharma, K., Vaid, N., and Chakravarti, S. (2011). "Occurrence of dual infection of peste-des-petits-ruminants and goatpox in indigenous goats of central India". *Transboundary and Emerging Diseases* 58.3, pp. 268–273.

Mariner, J. C., McDermott, J., Heesterbeek, J. A. P., Catley, A., and Roeder, P. (2005). "A model of lineage-1 and lineage-2 rinderpest virus transmission in pastoral areas of East Africa". *Preventive Veterinary Medicine* 69.3-4, pp. 245–263.

Martcheva, M. (2015). *An introduction to mathematical epidemiology*. Vol. 61. Springer.

Meiss, J. D. (2007). *Differential dynamical systems*. SIAM.

Mekuriaw, Z., Harris-Coble, L., Duong, M. C., Nguyen-Viet, H., Grace, D., Ty, C., Sokchea, H., Sina, V., Young, M. F., Balehegn, M., et al. (2021). "Ethiopia's Livestock Systems: Overview and Areas of Inquiry".

Munir, M. (2013). *Mononegaviruses of veterinary importance, volume 1: pathobiology and molecular diagnosis*. Vol. 1. CABI.

Mushayabasa, S. and Bhunu, C. P. (2011a). "Modelling the effects of heavy alcohol consumption on the transmission dynamics of gonorrhea". *Nonlinear Dynamics* 66, pp. 695–706.

Mushayabasa, S., Bhunu, C. P., and Dhlamini, M. (2011b). "Impact of vaccination and culling on controlling foot and mouth disease: a mathematical modelling approach". *World Journal of vaccines* 1.4, pp. 156–161.

Neilan, R. L. M. (2009). "Optimal Control Applied to Population and Disease Models". PhD thesis. University of Tennessee, Knoxville.

Nepomuceno, E. G., Barbosa, A. M., Silva, M. X., and Perc, M. (2018). "Individual-based modelling and control of bovine brucellosis". *Royal Society Open Science* 5.5, p. 180200.

Njeumi, F., Ferrari, G., Raizman, E., Diallo, A., Domenech, J., Leboucq, N., and Munstermann, S. (2015). "Global Strategy for the Control and Eradication of PPR".

Nyerere, N., Luboobi, L. S., Mpeshe, S. C., and Shirima, G. M. (2020a). "Mathematical model for brucellosis transmission dynamics in livestock and human populations". Published by Communications in Mathematical Biology and Neuroscience.

Nyerere, N., Luboobi, L. S., Mpeshe, S. C., and Shirima, G. M. (2020b). "Optimal control strategies for the infectiology of brucellosis". *International Journal of Mathematics and Mathematical Sciences* 2020, pp. 1–17.

Osman, S., Otoo, D., Makinde, O. D., et al. (2020). "Modeling anthrax with optimal control and cost effectiveness analysis". *Applied Mathematics* 11.03, p. 255.

Ozmen, O., Kale, M., Haligur, M., and Yavru, S. (2009). "Pathological, serological, and virological findings in sheep infected simultaneously with Bluetongue, Peste-des-petits-ruminants, and Sheeppox viruses". *Tropical Animal Health and Production* 41, pp. 951–958.

Pontryagin, Lev S. (1987). *Mathematical theory of optimal processes*. CRC press.

Rahmayani, S. A, Aldila, D., and Handari, B. D. (2021). "Cost-effectiveness analysis on measles transmission with vaccination and treatment intervention". *AIMS Mathematics* 6.11, pp. 12491–12527.

Rodrigues, H. S., Monteiro, M. T. T., and Torres, D. F. M. (2012). "Modeling and optimal control applied to a vector borne disease". *arXiv preprint arXiv:1207.1949*.

Saber, S. and Solouma, E. (2025). "The Generalized Euler Method for Analyzing Zoonotic Disease Dynamics in Baboon–Human Populations". *Symmetry* 17.4. ISSN: 2073-8994.

Salmani, M. and van den Driessche, P. (2006). "A model for disease transmission in a patchy environment". *Discrete Contin. Dyn. Syst. Ser. B* 6, pp. 185–202.

Sanchez, M. A. and Blower, S. M. (1997). "Uncertainty and sensitivity analysis of the basic reproductive rate: tuberculosis as an example". *American Journal of Epidemiology* 145.12, pp. 1127–1137.

Savagar, B., Jones, B. A., Arnold, M., Walker, M., and Fournié, G. (2023). "Modelling flock heterogeneity in the transmission of peste des petits ruminants virus and its impact on the effectiveness of vaccination for eradication". *Epidemics* 45, p. 100725.

Sen, A., Saravanan, P., Balamurugan, V., Rajak, K. K., Sudhakar, S. B., Bhanuprakash, V., Parida, S., and Singh, R. K. (2010). "Vaccines against peste des petits ruminants virus". *Expert Review of Vaccines* 9.7, pp. 785–796.

Shim, E. (2004). "An epidemic model with immigration of infectives and vaccination". PhD thesis. University of British Columbia.

Sigdel, R. P. and McCluskey, C. C. (2014). "Global stability for an SEI model of infectious disease with immigration". *Applied Mathematics and Computation* 243, pp. 684–689.

Smith, C. A., Campbell, S. W., and Toomey, R. G. (2025). *A First Course in Differential Equations, Modeling, and Simulation*. CRC Press.

Sosoma, I., Mureithi, E., and N., Shaban M. (2025). "Mathematical Modeling Of Brucellosis Transmission Dynamics And Its Age-Specific Applications". *Abstract and Applied Analysis*. Vol. 2025. 1. Wiley Online Library, p. 6552487.

Sseguya, I., Mugisha, J. Y. T., and Nannyonga, B. (2022). "Outbreak and control of Foot and Mouth Disease within and across adjacent districts—A mathematical perspective". *Results in Control and Optimization* 6, p. 100074.

Strogatz, S. H. (2001). *Nonlinear Dynamics and Chaos: With Applications to Physics, Biology, Chemistry, and Engineering*. Vol. 1. Studies in Nonlinearity. Westview Press.

Stuart, A. and Humphries, A. R. (1998). *Dynamical systems and numerical analysis*. Vol. 2. Cambridge University Press.

Tadesse, B., Hamid, M., and Hamid, A. (2022). "Transmission dynamics and economic impacts of sheeppox and goatpox disease outbreak in Chifra district of Afar Region Ethiopia". *Heliyon* 8.6.

Thieme, H. R. (2018). *Mathematics in population biology*. Vol. 1. Princeton University Press.

Van den Driessche, P. and Watmough, J. (2002). "Reproduction numbers and sub-threshold endemic equilibria for compartmental models of disease transmission". *Mathematical biosciences* 180.1-2, pp. 29–48.

Walle, Y., Mugisha, J. Y. T., Melese, D., and Tessema, H. (2024). "Modeling the Peste des Petits Ruminants (PPR) disease transmission dynamics with impacts of vaccination and restocking in small ruminant population in Amhara region, Ethiopia". *Heliyon* 10.24.

Walle, Y., Mugisha, J. Y. T., Melese, D., and Tessema, H. (2025). "The impact of movement and vaccination on Peste des Petits Ruminants disease spread between two different agroecological zones". *Scientific African*, e02532.

Wang, X., Liu, Z., Wang, L., Guo, C., and Xiang, H. (2021). "An application of a novel geometric criterion to global-stability problems of a nonlinear SEIVS epidemic model". *Journal of Applied Mathematics and Computing* 67.1, pp. 707–730.

Waret-Szkuta, A., Roger, F., Chavernac, D., Yigezu, L., Libeau, G., Pfeiffer, D.U., and Guitián, J. (2008). "Peste des Petits Ruminants (PPR) in Ethiopia: Analysis of a national serological survey". *BMC Veterinary Research* 4, pp. 1–10.

Wieland, B., Dione, M. M., Jones, B. A., Campbell, Z., Ilboudo, G., Kotchofa, P., Rutto, E., Okoth, E., Haan, N. C., and Rich, K. M. (2020). "Epidemiology and Control of Peste des Petits Ruminants (ECo-PPR) Study Design and Toolbox: A suite of tools toward understanding epidemiology and socio-economic impact of peste des petits ruminants".

Wiggins, S. (2003). *Introduction to Applied Nonlinear Dynamical Systems and Chaos*. Vol. 2. Texts in Applied Mathematics. New York, NY: Springer.

WOAH (2020). *Peste des Petits Ruminants*. Accessed: 2025-06-19. URL: https://www.woah.org/fileadmin/Home/eng/Animal_Health_in_the_World/docs/pdf/Disease_cards/PESTE_DES_PETITS_RUMINANTS.pdf.

WOAH (2023). *World Animal Health Information System (WAHIS)*. Accessed: 2023-06-26. URL: https://wahis.woah.org/#/dashboards/qd-dashboard.

Wondimu, A., Tassew, H., Gelaye E.and Hagos, Y., Belay, A., Teshome, Y., Laiju, S., and Asebe, G. (2021). "Outbreak investigation and molecular detection of pox virus circulating in sheep and goats in selected districts of west Gojjam and Awi zones northwest, Ethiopia". *Veterinary Medicine: Research and Reports*, pp. 303–315.

World Organisation for Animal Health (WOAH) (2023). *Sheep and goat pox*. Accessed: 2025-02-29.

Wosu, L. O. (1989). "Management of clinical cases of peste des petits ruminants (PPR) disease in goats." *Beitrage zur Tropischen Landwirtschaft und Veterinarmedizin* 27.3, pp. 357–361.

Yang, X. (2002). "Generalized form of Hurwitz-Routh criterion and Hopf bifurcation of higher order". *Applied Mathematics Letters* 15.5, pp. 615–621.

Zewdie, G., Derese, G., Getachew, B., Belay, H., and Akalu, M. (2021). "Review of sheep and goat pox disease: current updates on epidemiology, diagnosis, prevention and control measures in Ethiopia". *Animal Diseases* 1.1, p. 28.

Zhang, D., Yang, B., Zhang, T., Shi, X., Shen, C., Zheng, H., Liu, X., and Zhang, K. (2021). "In vitro and in vivo analyses of co-infections with peste des petits ruminants and capripox vaccine strains". *Virology Journal* 18, pp. 1–12.

Zhao, H., Njeumi, F., Parida, S., and Benfield, C. T. (2021). "Progress towards eradication of peste des petits ruminants through vaccination". *Viruses* 13.1, p. 59.